Technische Universiteit Delft

Advancing sustainable transportation by charging EVs with PV power at the workplace

An optimal charging strategy

D.W. van der Meer

TU Delft

Advancing sustainable transportation by charging EVs with PV power at the workplace

An optimal charging strategy

by

D.W. van der Meer

to obtain the degree of Master of Science
at the Delft University of Technology,
to be defended publicly on Monday June 13, 2016 at 09:30 AM.

Student number:	1381458	
Project duration:	July 1, 2015 – June 13, 2016	
Thesis committee:	Prof. dr. ir. P. Bauer,	TU Delft, chair
	Dr. ir. L. M. Ramirez Elizondo,	TU Delft, university supervisor
	Dr. ir. M. Cvetkovic,	TU Delft, committee member
	Ir. G. R. Chandra Mouli,	TU Delft, advisor

An electronic version of this thesis is available at `http://repository.tudelft.nl/`.

TU Delft

Abstract

Arguably the most important challenge of our time is climate change. In The Netherlands in 2014, 30% and 21.5% of total CO_2 emissions were emitted by the electricity producing and transportation sector, respectively. Electric vehicles (EVs) have therefore gained interest as they do not emit carbon dioxide whilst driving and therefore do not pollute, at least directly. Nevertheless, when EVs are charged with electricity produced by a fossil-fuel power plant there are indirect emissions. Additionally, high penetration of EVs will inevitably lead to increased stress on the grid and consequently capital expenditure. A viable solution to mitigate both these disadvantages is by charging EVs at the workplace with locally produced PV power. The high level of coincidence between parking time and solar power paves way to charge EVs in a sustainable and cost-efficient manner.

The thesis work presents the design of an energy management system (EMS) capable of forecasting PV power production and optimizing power flows between PV system, grid and EVs at the workplace. The aim is to reduce energy demand on the grid by increasing PV self-consumption while minimizing charging costs and consequently increasing sustainability of the EV fleet. The developed EMS consists of two components: an autoregressive integrated moving average (ARIMA) model to predict PV power production and a mixed-integer linear programming (MILP) framework that optimally allocates power to minimize charging costs. The EMS is designed such that it can be implemented in practice and moreover, is versatile, implying that it can be utilized for alternative purposes as well. Additionally, the predictive quality of the system enables it to anticipate and act accordingly, rather than solely react. In order to perform sensitivity analyses, case studies will be formulated in which the effectiveness of the system can be ascertained.

The results show that the developed EMS is able to reduce charging costs significantly, while simultaneously increasing PV self-consumption and reducing energy demand from the grid. Furthermore, during a case study analogous to one repeatedly considered in literature, i.e. dynamic grid tariff and dynamic feed-in tariff (FIT), the EMS reduces charging costs by 118.44% and 427.45% in case of one and two charging points, respectively. Moreover, stress on the grid is alleviated through both load shifting and power injection during peak demand. In addition, the EMS proves that vehicle-to-grid (V2G) leads to optimality only in extraordinary cases. The optimization problem is modeled in GAMS, whereas the ARIMA process is modeled in Matlab and subsequently, the EMS is simulated in Matlab.

Acknowledgments

This thesis has been performed at the DC systems, Energy conversion & Storage (DCE&S) group, Technical University Delft. I would like to dedicate this page to express my gratitude to those that have aided me throughout this endeavor.

I would first like to extend my thanks to my thesis supervisor dr. ir. Laura Ramirez Elizondo of the DCE&S group at TU Delft. The door to her office was always open in case I had a question about my research or other affairs. I am also grateful for the recommendation letter she wrote, which allowed me to continue my academic career at Uppsala University, Sweden.

I would also like to thank ir. Gautham Ram Chandra Mouli for allowing me to participate in this particular project. He has been available throughout the entire project to exchange ideas with and to guide me. He had a clear vision of what he wanted to achieve with this research work and subtly led me into the right direction, without dictating what I should do and therefore allowing this thesis to be my own work. Further, I would like to thank dr. ir. Germán Morales España for his inspiring and passionate discussions about optimization, reviewing my model even though he was not a part of my thesis committee and the recommendation letter he wrote that led to my PhD position at Uppsala University. I also want to thank prof. Pavol Bauer and dr. ir. Milos Cvetkovic for consenting to be part of my thesis committee.

Finally, I must express my very profound gratitude to my parents, brother and sister for their unfailing support throughout my bachelor and master. Additionally, I would like to thank Antía Varela Souto for her continuous support during my research work, as she has provided me with valuable feedback and means to complete my thesis. This accomplishment would not have been possible without them. Thank you.

Contents

List of Figures

List of Tables

1

Introduction

In November 2015, the World Meteorological Organization (WMO) announced that the amount of greenhouse gases (GHGs) in the atmosphere had reached another record high in 2014, as can be seen in fig. 1.1. The WMO stated in their annual Greenhouse Gas Bulletin that the new record for CO_2 particles in the atmosphere amounted to 397.7±0.1 ppm and it is estimated that the global annual average is likely to surpass the symbolic 400 ppm barrier in 2016. In addition, other GHGs such as CH_4 (1833±0.1 ppb) and N_2O (327.1±0.1 ppb) together with CFC-12 and CFC-11 account for approximately 96% of radiative forcing due to Long-Lived GHGs (LLGHGs) [102]. Regarding the global CO_2 emissions, 25% was emitted by the energy producing sector and another 14% was due to transportation [50]. Moreover, fossil fuel is still responsible for 80% of total primary energy demand and more than 90% of energy-related emissions [48]. For the Netherlands, 30% of total CO_2 emissions was discharged by the energy producing sector and 21.5% by the transportation sector in 2014 [19].

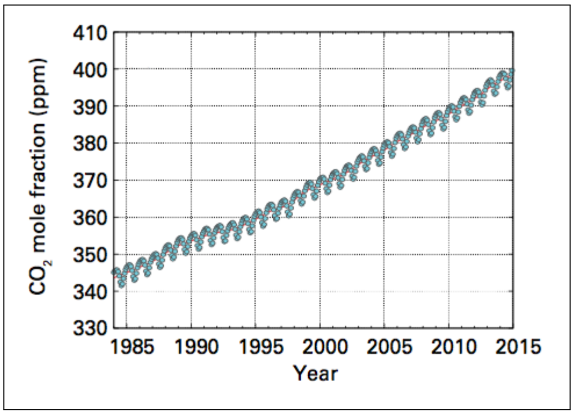

Figure 1.1: Rise of CO_2 mole fraction in the atmosphere. From [102].

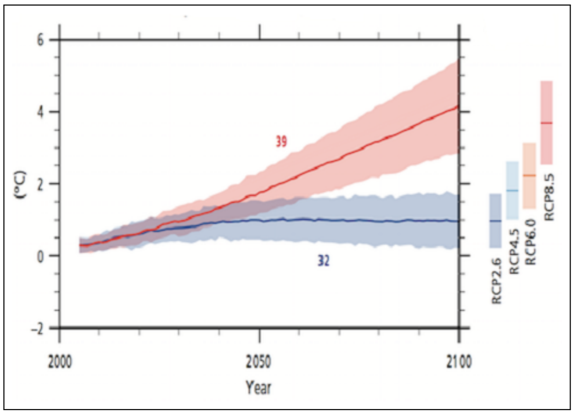

Figure 1.2: Rise in temperature under different scenarios. From [50].

Furthermore, the Intergovernmental Panel for Climate Change (IPCC) predicted that for four different future scenarios of CO_2 emissions, only the scenario with stringent mitigation efforts will likely keep the rise in average global temperature below 2°C by the end of this century [50]. The two scenarios with the highest level of CO_2 emissions, where the business-as-usual scenario sits in between, will likely cause an average increase in temperature by 2°C, as can be seen in fig. 1.2 [50]. In light of the upcoming Conference of Parties (COP21) in Paris, other studies were performed to estimate the global rise in temperature based on the Intended Nationally Determined Contributions (INDCs) submitted by large emitting countries. It was found by [67] that there is a 50% likelihood that temperature will have increased with 3.7°C by the end of this century. Another study showed that if conditional INDCs are fully implemented, the global average temperature increase will be less than 3-3.5°C by the end of this century, with more than 66% probability [95]. As a consequence, the global mean sea level will likely rise between 0.26m and 0.55m at the end of the 21^{st} century in the best-case scenario, as described in [50]. Even though it is generally accepted that global warming is caused by the emission of GHGs, the International Energy Agency (IEA) [49] calculated that according to the INDCs, investments in fossil fuels still top investments in more sustainable energy solutions, as can be seen in fig. 1.3.

An encouraging trend can be noticed though. According to the IEA, Renewable Energy Sources (RESs) are becoming more and more cost competitive and it is estimated that the RES generating capacity in 2014 has increased with 128GW, of which about a third was in the form of solar power. Moreover, it is projected that investments will to continue to rise, enabling even more installed capacity [48]. However, some reservations need to be made regarding high penetration of photovoltaic (PV) generation, since it poses a challenge as there is limited coincidence between PV generation and demand, which may result in curtailed PV generation [21]. Furthermore, a report by PBL Netherlands Environmental Assesment Agency concluded that the increase in CO_2 emission growth almost stalled to 0.5%, while the world's economy and population grew with 3% and 1%, respectively. The three largest emitting countries/regions were China (30%), United States (15%) and EU-28 (9.6%), accounting for 54% of total emissions. While China and the United States saw emissions increase with 0.9%, EU-28 realized a decrease of 5.4% during 2014. However, even though China is the world's largest emitter of CO_2, when per capita emissions are taken into consideration, the United States emit roughly twice the amount of China and EU-28, as can be seen in fig. 1.4 [73].

Another encouraging trend is the increase in electrification of the transportation sector. In a study performed by the Electric Power Research Institute (EPRI) it is estimated that in 2050, 62% of the entire vehicle fleet of the U.S.A. will consist of Plug-in Hybrid Electric Vehicles (PHEVs) [28]. PHEVs and Electric Vehicles (EVs) enable the possibility to reduce the carbon footprint of the transportation sector, although this strongly depends on the generation mix of the energy with which the PHEVs and EVs are charged [53]. Moreover, a high penetration of PHEVs and EVs also creates risks regarding the proper functioning of the electricity grid. Simulations from [24], performed in 2013, show that problems with grid reliability can already occur in 2015 in densely populated areas such as Amsterdam, even in the case of a relatively low penetration of EVs. However, it is also stated that measures such as vehicle to grid (V2G), price incentives and advances in smart grid technology can alleviate the stress on the grid and thus improve reliability of the grid [24], [68]. Furthermore, if the source and load are located relatively close together, it could reduce stress on the grid [99].

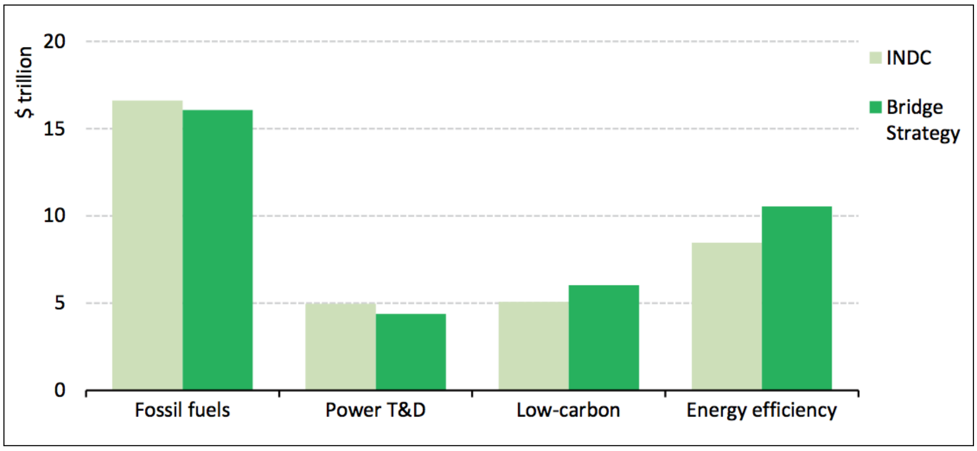

Figure 1.3: Cumulative investments from the world energy sector, by scenario. From[49]

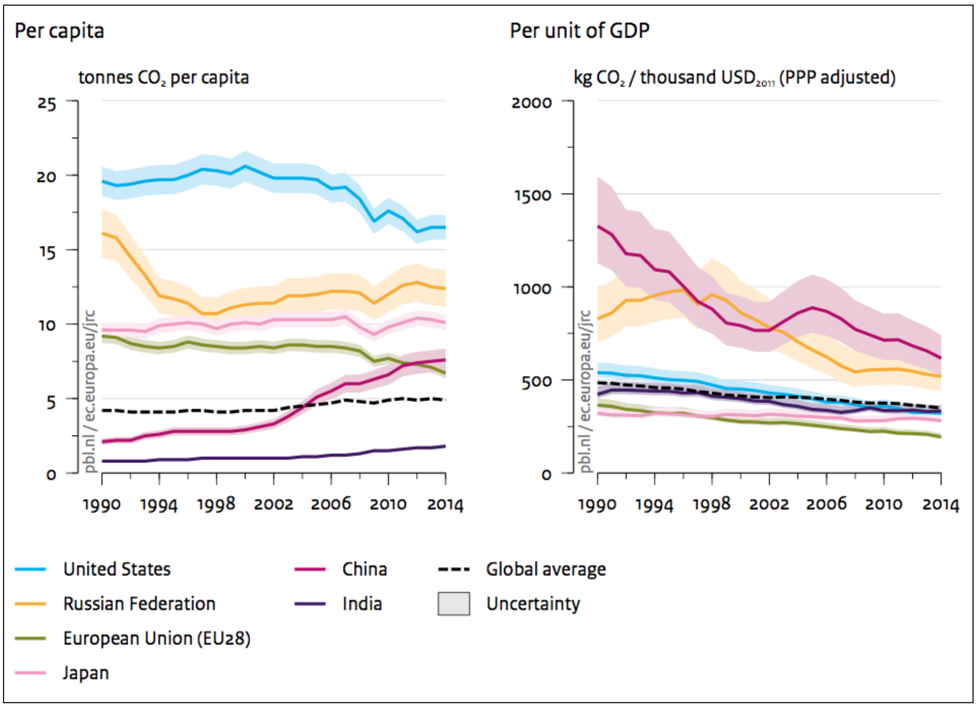

Figure 1.4: CO_2 emissions from fossil fuel use and cement production. From[73]

1.1. Project objectives

Taking the aforementioned into consideration, it appears to be of high importance to increase the electrification of the transportation sector, albeit under specific conditions. As stated before, uncontrolled charging, i.e. immediate charging upon arrival, can place significant stress upon the electricity grid. Combined with the low coincidence of PV output and demand, this conundrum demands a more sustainable and cost-effective solution. The long time cars are parked at the working place might just be such a solution. Since the average working day in the Netherlands is eight hours, this paves the way to investigate the possibility of charging EVs through PV at the working place.

The aim of this thesis is therefore to combine the aforementioned aspects. An energy management system (EMS) will be designed that optimally allocates power on an workplace parking lot between solar carports, EVs and grid. In general, optimal implies minimization of charging costs, which is found to be the main driver for consumers to transition to EVs [38]. However, sustainability plays an important role throughout this thesis and since a power plant producing one kWh emits 0.55 - 0.98 kg CO_2 for natural gas and coal respectively [97], the advantage of EVs as a sustainable form of transportation is reduced, as emissions become more localized. Therefore, although offering a financial incentive is the key objective that enables the aforementioned transition, PV self-consumption, i.e. consume what one's PV system generates, should be increased simultaneously. After all, PV power production entails zero green house gas emissions. Additionally, it is important to consider stress on the grid due to both uncontrolled charging and excessive PV power feed in, since this leads to congestion and consequentially efficiency losses, but also an increase of operational and capital expenditure to maintain and update the grid, respectively. In order to achieve these objectives, a mathematical framework will be designed. Nevertheless, such an EMS would not yet be satisfactory due to the fact that in case of real-time implementation, it could merely react to measured PV power generation. This would be unfavorable since the EMS cannot anticipate on future input and can therefore merely take uninformed decisions that lead to sub-optimal solutions. As a consequence, it is necessary to enable the EMS to forecast power generation of the PV system so that it can plan future power allocation in an optimal manner. In combination with a pricing mechanism that would represent peak and valley demand and enabling V2G, this will pave way for demand side management (DSM), e.g. through load shifting, and thus additional cost reductions combined with an increase in sustainability. How such a solar carport may look like is presented in fig. 1.5.

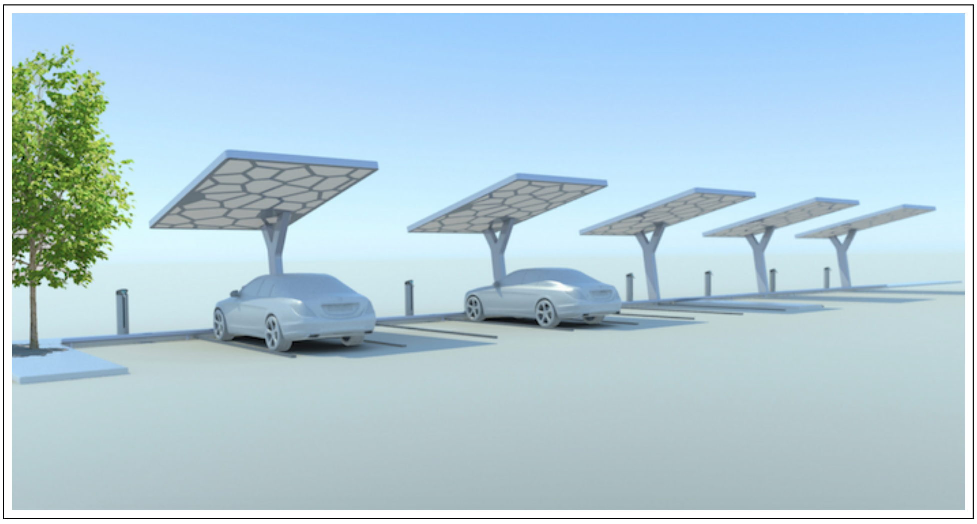

Figure 1.5: An impression of the charging station, reproduced from [59].

1.2. Research questions

In order to achieve the aforementioned goals, research questions are defined that will act as a guideline throughout the thesis. A total of seven research questions are formulated, of which the first three regard fundamental questions as to the design of the proposed EMS. These can be answered after the literature study, which is presented in the subsequent chapter. The latter four regard practical questions, i.e. results that are attained from the model and its effectiveness. Answering these questions will allow the reader to position the presented work in scientific literature. The research questions are presented below.

- Which optimization technique should be used that is able to include the required constraints so that reality is modeled in a satisfactory manner?
- Which available model should be utilized to forecast solar irradiance?
- As the forecast is made for a limited amount of time into the future, what methodology should be applied to provide the EMS with a predictive rather than reactive character?
- To what extent can the proposed EMS decrease the grid dependency?
- What would be the cost benefit if this EMS is implemented, when compared to uncontrolled ("dumb") charging?
- To what extent can the proposed EMS alleviate stress on the grid that otherwise would occur due to uncontrolled charging?
- To what extent is vehicle-to-grid (V2G) a viable concept?

These questions will be answered in section 6.3.

2

Literature review

This chapter is dedicated to explain some basics of EVs, PV and smart grids. An extensive literature study has been performed to assure the uniqueness of this thesis. Furthermore, an in-depth study has been carried out regarding battery technology, PV technology and smart grids in order to meet the standard of a master thesis conducted at the Technical University of Delft.

In section 2.1 a short introduction regarding EVs will be given, together with the potential and challenges of this technology. In addition, a brief overview of history, present day and future of EVs is presented. In section 2.2 a similar approach is applied. Even though the potential of PV power generation might be obvious, some challenges still need to be solved in case of high penetration into the power generating mix. Furthermore, a concise overview of history, present day and future is given. Moreover, subsection 2.2.3 elaborates upon existing methods to forecast solar irradiance.

In section 2.3, an introduction regarding smart grids and the potentials and challenges is given. Furthermore, an overview of the optimization methods is given and their abilities explained. Then, a summary is given of the papers that have been analyzed during the literature study for this thesis. Since this is an ongoing process, this chapter will likely be expanded in the near future. To conclude this chapter, the place in the literature and the justification of this thesis are explained. In addition, the contribution of this thesis to the academic community is discussed.

2.1. Electric vehicles

EVs have the possibility to reduce our carbon footprint, provided that they are charged with renewable energy. When looking at Well to Wheel (WHW) GHG emissions in 2035, EVs that are solely charged with renewable energy will only emit as much as 4 grams of CO_2 per kilometer. In contrast to this, Internal Combustion Engine Vehicles (ICEVs) will emit 117 grams of CO_2 per kilometer in this future scenario [26]. However, when EVs are charged with energy produced by non-renewable sources, the potential EVs have is almost nullified [53]. Therefore, if the desire is to reduce the carbon footprint of the transportation sector, it is imperative that EVs be charged with RESs. Moreover, a high level of penetration opens up the possibility for EVs to act as independent distributed energy sources and provide ancillary services such as frequency and voltage regulation [68]. Due to the fact that the battery of an EV does not have a significant ramp rate, it is able to respond very fast [58]. This quality make EVs particularly interesting as distributed energy sources.

2.1.1. Short history on EVs

The EV has been around since the second half of the 19th century when French and English inventors built the first practical EVs, although these were more like carriages. By that time, the electric form of transportation co-existed with other technologies such as gasoline and steam powered vehicles. Electric transportation offered some advantages over both gasoline and steam. EVs were not as noisy and smelly as gasoline vehicles and did not require as much start-up time as steam engines did, especially on cold days. However, the popularity of EVs decreased drastically when Ford released the Model T in 1908 at a price of only $650, as opposed to the $1,750 one had to pay for an EV. When oil was discovered in Texas by the 1920s and became readily available for all Americans, it meant the end of EVs, at least for the time being[1].

In 1997 the EV came back into the picture with the introduction of the Toyota Prius. This Hybrid Electric Vehicle (HEV) used a Nickel Metal Hydride (Ni-MH) battery which was charged upon braking and assisted the Internal Combustion Engine (ICE) during acceleration. Increasing fuel prices and growing awareness about CO_2 pollution and climate change made the Prius the best selling HEV of the past decade. During 2008, Tesla introduced the Roadster, which was a full EV and capable of driving 320 km with a single charge. In 2010, Chevrolet launched the first commercial PHEV with the capability of driving a short distance fully electric instead of merely assisting the ICE with accelerating.

2.1.2. Present day and future of EVs

The costs of the Li-ion battery pack are roughly 25% of the total costs of an EV, taking up a large portion of the price. However, between 2007 and 2014, battery costs have approximately declined with 14% per year, dropping from over $1000 per kWh to roughly $410 per kWh. Moreover, the costs of battery packs used by leading EV manufacturers are even lower, at $300 per kWh [71]. Furthermore, numerous countries such as the Netherlands, but also municipalities such as Amsterdam[2], have implemented subsidies on the purchase of EVs to help stimulate the technology, since EVs are still regarded as a niche product [71].

Even though the future of EVs is uncertain, it is estimated that the costs for batteries will decrease to $230 per kWh in 2017-2018. For the EV to become cost competitive with ICE vehicles, the price of battery packs should drop with another 33% to $150 per kWh [71]. Interestingly, at their Global Business Conference, the CEO of General Motors recently said[3] that for a battery cell, the company currently pays $145 per kWh, implying that battery costs are overestimated. New technologies will play an important role in the future of EVs. Research is being done to develop batteries that are not only cheaper, but also have a higher specific energy as can be seen in fig. 2.1.

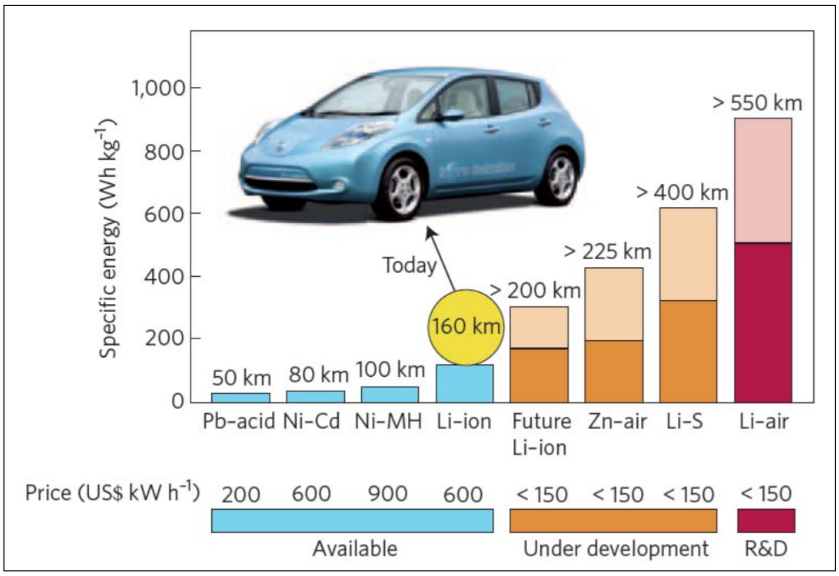

Figure 2.1: Battery energy density future outlook. From [12].

2.2. Photovoltaic power generation

PV power generation occurs when a semi-conductor material is exposed to electromagnetic radiation and as a consequence, a potential difference is generated. Electrons inside the semi-conductor material are excited

[1] U.S. Department of Energy [Internet] The History of the Electric Car [update 09/15/2015; cited 11/13/2015] Available from: <http://www.energy.gov/articles/history-electric-car>

[2] Gemeente Amsterdam [Internet] Subsidy Electric Vehicles [update 01/01/2015; cited 11/13/2015] Available from: <https://www.amsterdam.nl/parkeren-verkeer/luchtkwaliteit/slim-schoon-stad/stimuleringsregeling/subsidie-elektrische/>

[3] EV Obsession [Internet] $145 per kWh Battery Cell Costs At Chevy Bolt Launch, GM Says [update 10/04/2015; cited 05/19/2016] Available from: <http://evobsession.com/gm-145-kwh-battery-costs-bolt-ev-launch/>

by photons and consequently electron-hole pairs are created. When the charge carriers are collected at either end of the semi-conductor material by electrical contacts connected to an external circuit, a current can flow and power is generated. At the end of 2013, variable RESs such as wind and solar energy generated around 2.9% and 0.7% of global electricity production, respectively [79]. Contrary to wind energy, which usually requires large upfront investments, PV enables renewable power generation on a residential scale. Since 2000, the price of PV panels has dropped from around $4.6 per Wp to roughly $0.75 per Wp in 2014, boosting the widespread implementation of this technology, as can be seen in fig. 2.2. Moreover, large scale subsidies provided by governments have substantially contributed to the increase in installed capacity as well.

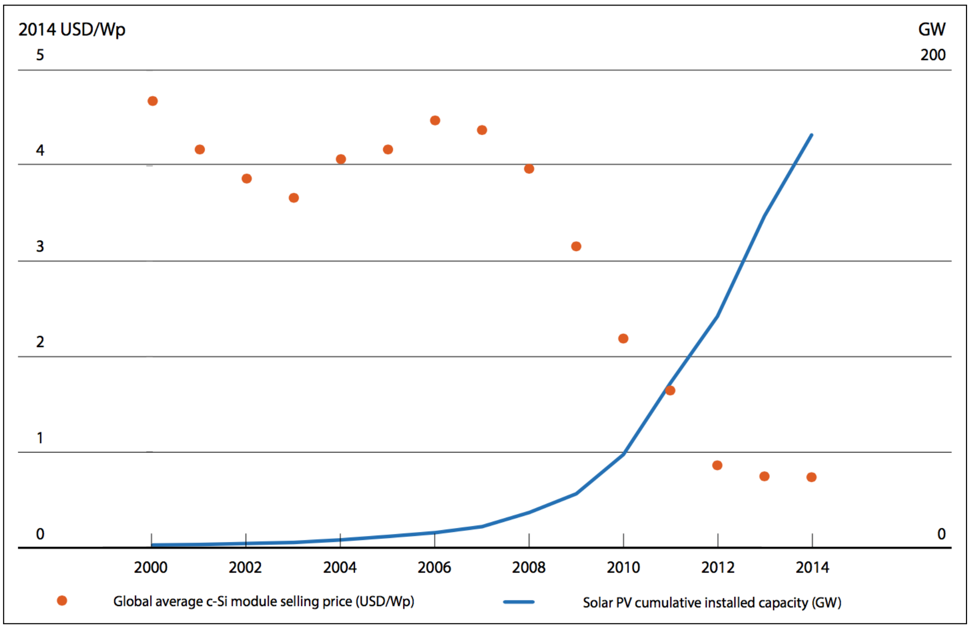

Figure 2.2: Cumulative global PV deployment and PV module prices. From [47].

However, there are some reservations to be made regarding high levels of renewable energy penetration. Due to the intermittent nature of RESs, and solar in particular, high penetration can cause disturbances in the grid and lead to curtailment, inefficiencies and decreased reliability [32]. Therefore, shifting demand such as charging EVs with PV power can smooth the intermittent nature of PV. Furthermore, EVs with V2G capability can provide ancillary services and act as support for RESs [36]. Moreover, accurate forecasting methods are required so that the optimal allocation of renewable energy can be accomplished.

2.2.1. Short history on PV

In 1839, the French scientist Edmond Becquerel discovered the photovoltaic effect. However, it was not until 1954 that the first silicon solar cell was developed which was able to produce enough power to run everyday electronic equipment. This solar cell was developed by Daryl Chapin, Calvin Fuller and Gerald Pearson at Bell Labs and had an efficiency of 4% [107]. In the following years, numerous solar arrays found their way into space related applications but availability to the public was not in question due to the pricing of around $100 per Watt. However, there were initiatives to show the potential of PV, such as by Paul MacCready, who built the first solar-powered aircraft in 1981, called the Solar Challenger. With this aircraft, he managed to cross the English Channel, flying from France to England [107].

Thin-film technology was first commercially available in 1986, released by ARCO Solar [107]. This technology has the benefit that it is cheaper and also flexible, paving the way for new applications of PV. However, current efficiency of a thin-film solar cell is still lower than that of silicon solar cells. Therefore, the latter have the advantage that less area is required for the same amount of installed capacity.

2.2.2. Present day and future of PV

Currently, the market share for crystalline silicon (c-Si) is roughly 90%, whereas thin-film accounts for the remaining 10%. Silver and aluminum are the most expensive non-silicon materials used in current c-Si solar cells. It is estimated that a reduction of 100 mg to 40 mg of silver per cell will be realized by 2025. Furthermore, an important loss mechanism in solar cells are the recombination losses. Due to advancements in process technology, it is expected that these losses will be reduced between 55% and 70% by 2025 [52].

Costs for a system larger than 100 kW are expected to show a gradual decrease. In 2025, total costs (excluding soft costs, e.g. installation costs) will have gone down with 35% as opposed to 2014. In addition, Levelized Cost Of Electricity (LCOE) for a specific yield of 1000 kWh/kWp is estimated to decrease from 0.103 $/kWh to 0.065 $/kWh in 2025 [52].

2.2.3. Forecasting methods of solar irradiance

Solar irradiance can have a highly intermittent character. To be able to plan the allocation of power produced by RESs, potential purchase of short-term power and perhaps incorporate backup power, it is important to use an accurate forecasting method. Generally speaking the distinction is made between statistical models and Numerical Weather Prediction (NWP) based models [100]. Statistical data can be used by time series models to forecast or predict. NWP relies on complex models that describe nature in an accurate way. Computation of these models requires powerful computers and are mainly used by meteorological institutes to forecast weather [76]. A classification based on temporal and spatial resolution is given in fig. 2.3.

To evaluate the accuracy of a model, different measures are used in literature. Commonly, Root Mean Square Error (RMSE), Mean Bias Error (MBE), Mean Absolute Error (MAE) and Mean Absolute Percentage Error (MAPE) are used, see e.g. [100], [76], [22]. These measures are mathematically represented in eqs. (2.2.1) to (2.2.4).

$$\mathrm{RMSE} = \sqrt{\frac{\sum_{t=1}^{n}\left(y_{\mathrm{predicted},t} - y_{\mathrm{observed},t}\right)^2}{n}} \tag{2.2.1}$$

$$\mathrm{MBE} = \frac{1}{n}\cdot\sum_{t=1}^{n}\left(y_{\mathrm{predicted},t} - y_{\mathrm{observed},t}\right)^2 \tag{2.2.2}$$

$$\mathrm{MAE} = \frac{1}{n}\cdot\sum_{t=1}^{n}\left|y_{\mathrm{predicted},t} - y_{\mathrm{observed},t}\right| \tag{2.2.3}$$

$$\mathrm{MAPE} = \frac{1}{n}\cdot\sum_{t=1}^{n}\left|\frac{y_{\mathrm{observed},t} - y_{\mathrm{predicted},t}}{y_{\mathrm{observed},t}}\right| \tag{2.2.4}$$

RMSE is the most common measure to quantify the error of the predicted variable. However, comparing this parameter is precarious since it mainly depends on the size and resolution of the system. Furthermore, MAPE is less difficult to interpret than MAE [76].

In addition, the coefficient of determination, R^2, is used to indicate to what extent the statistical model fits the data [74]. R^2 is mathematically formulated as follows

$$R^2 = 1 - \frac{\sum_t\left(y_{\mathrm{observed},t} - y_{\mathrm{predicted},t}\right)^2}{\sum_t\left(y_{\mathrm{observed},t} - \bar{y}\right)^2}. \tag{2.2.5}$$

Time series forecasting

A time series is composed of a set of measurements of a specific variable, taken at regular time intervals. Time series can be used to forecast this variable through different models. Examples of linear stationary methods are Autoregessive (AR), Moving Average (MA) and Autoregessive Moving Average (ARMA), while Autoregressive Integrated Moving Average (ARIMA) is considered to be a linear non-stationary method. These methods are widely used to forecast solar irradiance [76]. Artificial Neural Networks (ANN) based prediction models are among non-linear models, which can also be used to predict or forecast based on measured data [78].

In [74], the ARIMA model was outperformed by ANN but still provided satisfactory results. According to [22] and [78], the ARIMA model was found to produce the most accurate forecasts and [100] found that for intraday forecasting, ARIMA appears to be the most reliable and accurate model. Only for high time resolutions,

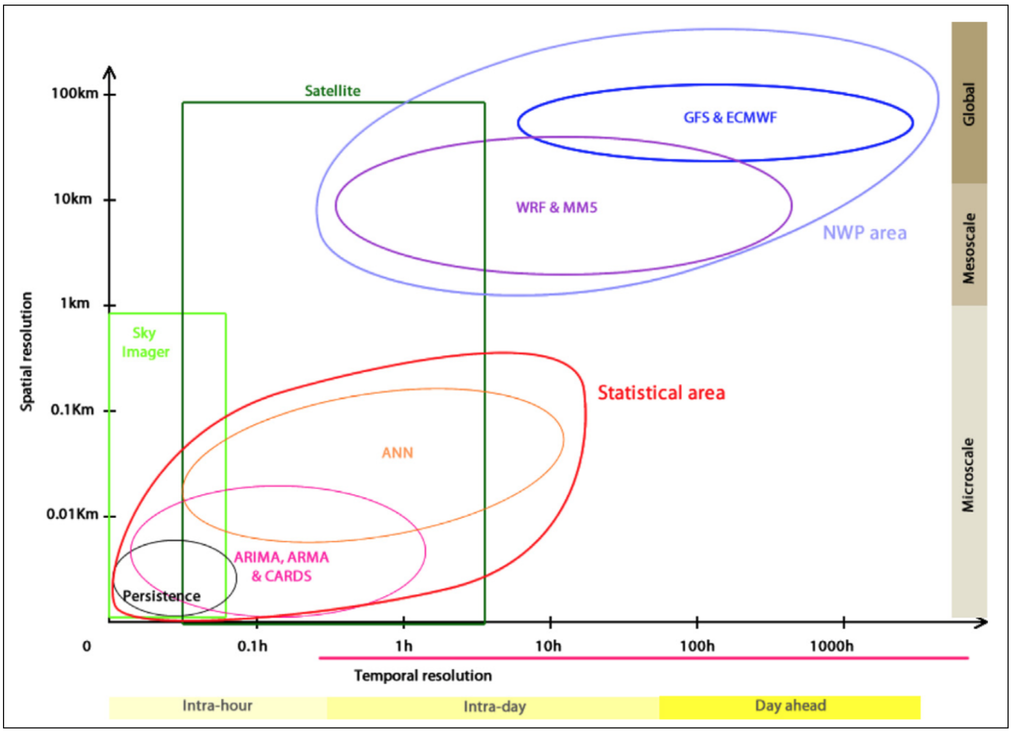

Figure 2.3: Classification of forecasting methods based on spatial and temporal resolution. From [22].

in the order of 5 minutes, the ARIMA was outperformed by ANN [78]. Typical time horizons for the ARIMA model are 5 minutes to 6 hours however, similar linear time series have also been used for day-ahead planning [76], [34]. A limitation of time series models is that, unlike NWP, physical properties are not taken into account. In case of the ARIMA model, one will have to incorporate physical behavior of solar irradiance such as sunrise and sunset [22].

However, this thesis will consider one day in summer and one day in winter. Due to the fact that this process fluctuates around a static mean, this can be considered as a stationary process. Consequently, it will not be necessary to use the non-stationary ARIMA model and accordingly, the stationary ARMA method should provide a good alternative. The reason for this is that the ARIMA model analyzes d differences and every dth difference is regarded as a stationary ARMA process [46].

Numerical Weather Prediction

As stated above, NWP is based on detailed knowledge of the instantaneous cloud field and is therefore difficult to use with respect to solar irradiance [100]. An advantage of NWP is that it can be used up to 15 days ahead and is therefore regularly used among weather stations [46]. Furthermore, NWP allows for the modeling of the aforementioned cloud field for locations for which no statistical data is gathered [46]. However, with a general temporal resolution of 1 hour, it is quite coarse. Moreover, the spatial resolution is generally 16-50 km, both considered to be a limitation of NWP [22]. Another limitation of NWP is its complexity and the consequent demand for high computational power [22].

2.2.4. Conclusion

The scope of this thesis is to design an energy management system for an industrial parking lot with high penetration of both PV and EVs, which can be regarded as a local problem. Furthermore, the temporal resolution is set to 1 minute to increase accuracy. Therefore, the potential model is required to provide precise forecasts intra-day and day-ahead. Furthermore, high spatial resolution is required. Combining these necessities leads to the conclusion that the ARMA model should provide satisfactory results.

2.3. Smart grids

Although opinions of what a smart grid exactly entails may vary, a clear description is given in [30]: "A smart grid is an electricity network that can intelligently integrate the actions of all users connected to it - generators, consumers and those that do both - in order to efficiently deliver sustainable, economic and secure electricity supplies." Furthermore, it has some key characteristics such as that it allows consumers to play a part in optimizing the operation of the system and provide them with greater information and choice of supply. In addition, a smart grid significantly reduces the environmental impact of the whole electricity supply system [30]. In order to achieve this, technology and ICT play a vital role. Software designed to efficiently or optimally allocate power is required to transform an ordinary grid into a smart grid. Finally, collaboration between the United States Department of Energy and the National Energy Technology Laboratory produced the Modern Grid Initiative. This initiative defines seven characteristics of a smart grid [96]:

- Self-healing
- Motivating and including the consumer
- Resisting attacks
- Increasing power quality
- Accommodating all generation and storage options
- Enabling markets
- Optimizing assets and operating efficiently

Large scale uncontrolled charging of EVs can pose a threat to the grid as it can cause overloads [24], increase peak loads significantly, decrease overall performance [17], increase emissions [93] and cause blackouts [57]. It was found in [32] that with a penetration of 50% EVs, around 200,000 units, the peak load can increase with 10% to 16%. Basically, there are two ways of dealing with these threats, namely the installation of extra generation capacity and load shifting [20]. Furthermore, high penetration of RESs, especially PV, can lead to curtailment in generation since the power output is highest when demand is moderate and power plants that generate base load are limited in flexibility [21]. Therefore, an interesting opportunity would be to charge EVs whilst the owner is at work, when supply and demand have optimal coincidence, consequently shifting the load from the evening to midday by using local produced energy. An impression of what this might look like is presented in fig. 2.4.

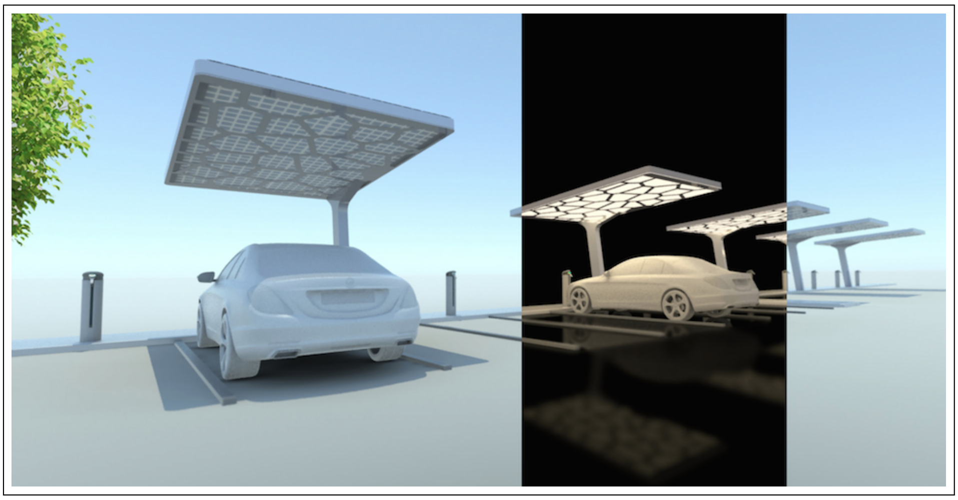

Figure 2.4: An impression of the charging station, reproduced from [59].

2.3.1. Energy management strategies: rule-based and optimization-based

In general a distinction can be made between rule-based and optimization based energy management strategies, as can be seen in fig. 2.5. Even though this figure gives an overview of energy management strategies *inside* HEVs, it goes without saying that these techniques can be generalized.

Rule-based energy management strategies

These energy management strategies are easy to implement and do not require much computational capacity and as a consequence, real-time energy management is possible. However, the main disadvantage is that the optimal strategy cannot be guaranteed. Furthermore, calibration and tuning of the parameters is required in order to improve performance [105].

Optimization-based energy management strategies

In case of optimization-based strategies, it can be said that there are two main categories, namely global optimization and real-time optimization.

Global optimization can in turn be divided into static and dynamic optimization, as can be seen in fig. 2.5. When performing static optimization, the parameters of a rule-based strategy are to be optimized through static optimization methods [105]. Of these methods, only Linear Programming (LP) and Mixed-Integer Linear Programming (MILP) will guarantee to provide a global optimum. These strategies can only be used when the objective function and constraints are linear. However, in order to perform the optimization, all necessary information is to be known before the start of the optimization and therefore it cannot be implemented directly as real-time control. Also, required computational capacity is higher than in case of rule-based strategies [105].

Other global optimization strategies have been widely applied, such as Particle Swarm Optimization (PSO) and Genetic Algorithm (GA), see e.g. [91], [83], [16] and [77]. The main advantage of these methods is that non-linear problems can be solved and due to the nature of these algorithms, they can do so in a relatively short amount of time. However, there are some disadvantages to these methods. Perhaps the most important one is that global optimality cannot be guaranteed. Moreover, it is easy for e.g. the PSO algorithm to get trapped in a local optimum and even though the optimization is done in a relatively short amount of time, real-time application is not possible [105].

Dynamic optimization, also called optimal control, minimizes or maximizes an objective function over a period of time. This in contrast with static optimization, where an objective function is optimized for one instance in time, e.g. a day. Dynamic Programming (DP), found to be the most-used form of dynamic optimization in the literature, was proposed by Bellman in 1957 to solve non-linear, dynamical problems by solving sub-problems per time interval in a backwards manner. However, DP requires huge computational capacity and is not suitable for real-time optimization [105]. Furthermore, global optimality cannot be guaranteed.

As stated before, static optimization cannot be used for real-time applications. For this, real-time optimization is necessary. However, the implemented strategy should be simple enough to avoid huge computational requirements and memory resources [105]. Due to this disadvantage and the fact that for this thesis day-ahead optimization is considered, real-time optimization will not be considered.

Conclusion

As stated before, this thesis considers day-ahead optimization. Furthermore, in order to attain the optimal solution to the objective function while respecting the constraints, LP is found to be the most promising method to solve the optimization problem.

2.3.2. Prior studies

In order to assure the uniqueness of this thesis, an extensive literature study has been performed about work that has been done until the moment of writing. Many papers are dedicated to control or optimize charging of PHEVs and/or EVs, sometimes with RESs and each with their own objective(s).

In [65], the researchers performed an analysis on charging electric bikes by means of two objectives, namely that the electric bike should be charged when the user wants to leave and that energy provided by PV is used as much as possible. Three strategies were used; dump charging, time-controlled charging and charging based on weather forecast. It was concluded that the latter two methods provided similar results. However, due to poor accuracy of the forecasts on clouded and rainy days, it was decided that research would continue with time-controlled charging. A similar study was performed in [23], however, a more refined scheduling

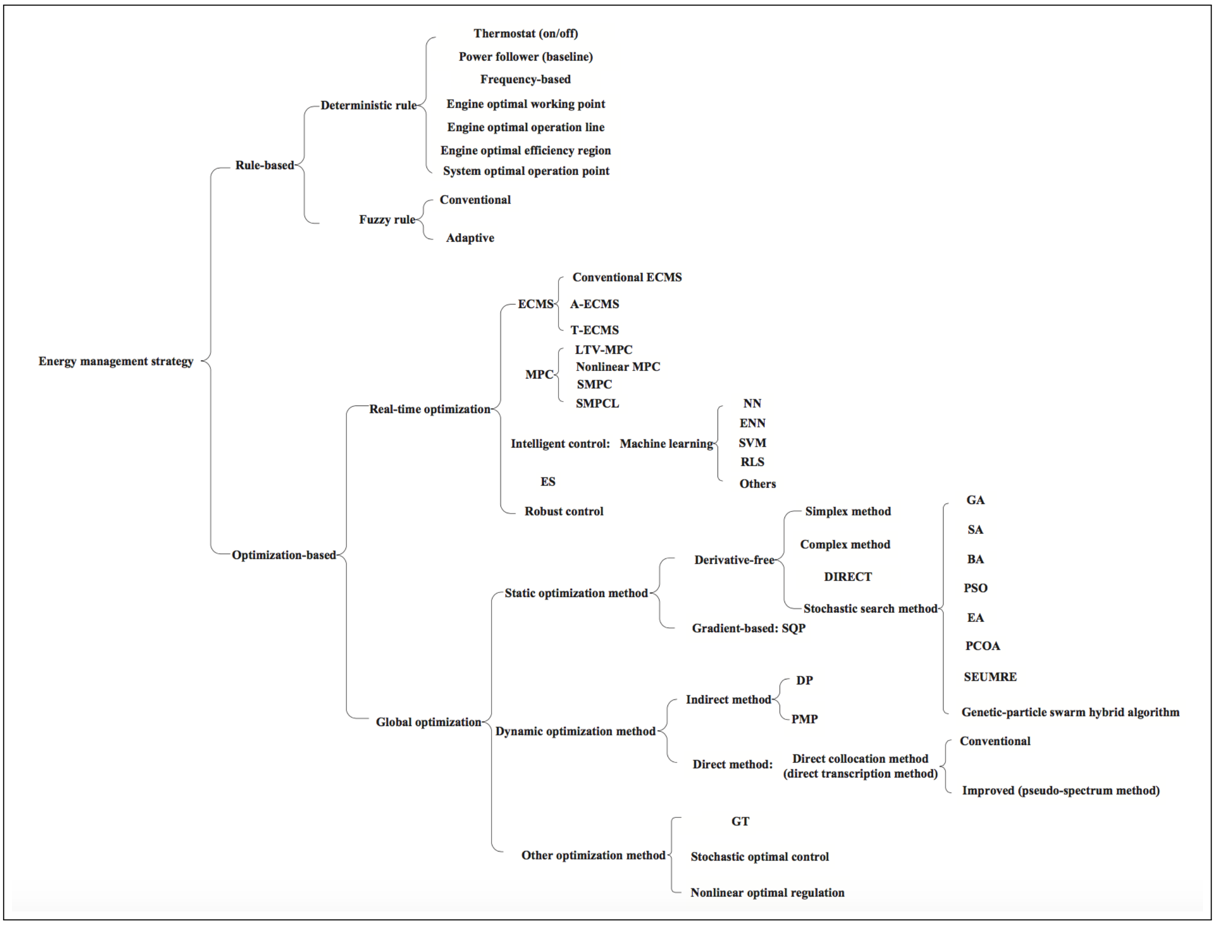

Figure 2.5: Overview of optimization techniques. From [105].

method was used.

It was found in [93] that charging EVs at the workplace with a PV based charging station has economic benefits when compared to home charging. These benefits are to such an extent that the costs of the PV installation will break even within the lifetime of said PV installation. Furthermore, when a carbon tax would be implemented, the benefits of such a charging station would increase further. Moreover, it was concluded that such charging stations would have other advantages such as alleviating stress on the grid, increasing penetration of RESs in the transportation sector and encouraging people to buy an EV even though they are not able to charge them at home.
This study was elaborated upon by the same authors in [94], through the addition of stochastic variables using Probability Density Functions (PDFs). It was demonstrated by a back-of-the-envelope calculation that in case of an average irradiation of 4 kWh/m^2/day, one parking spot covered with PV panels with an efficiency of 12% could produce enough energy to charge an EV such that it would be able to drive 40 miles per day. Regarding the stochastic variables, the PDF representing PV output was derived from satellite data and presented in a graph through box plots for every hour of the day. Furthermore, parking statistics were used to derive PDFs for the number of vehicles arriving and parking time. A Gaussian distribution was utilized to represent the number of arriving vehicles during each time interval. Since a workplace parking lot was considered, mean values during the morning were set to a high value with a relatively large variance. Consequently, the PDFs were used to calculate the number of vehicles entering during each time interval over the course of 1 year. DP was used to maximize self-consumption while satisfying energy demand.
This study considered four cases: nighttime home charging, daytime charging without PV, daytime charging with PV but without DP and daytime charging with PV and DP. As a result, each EV would save roughly 0.6 tons of CO_2 per year, which implied 55% less emissions when compared to the first case. It should be noted

that this reduction was high due to the coal-fired power plants producing electricity for the grid. Finally, the authors noted that the studied algorithm does not have much effect on the payback period of the parking garage but again, when a carbon tax would be implemented, this would benefit the profitability of such a PV based charging station.

According to [20], there are two ways to cope with increased loads at peak demand; by increasing generating capacity and by load shifting. To this end, Time-Of-Use (TOU) rates, which is an incentive for users to use electricity when demand and thus price is low, were considered. Furthermore, a control algorithm was designed for a solar carport with the following objectives: ensuring all EVs were charged as much as possible upon departure while paying the least amount of money for electricity as possible and that excess solar energy is fed back into the grid. Even though no optimization was performed, it was still found that the control algorithm was capable to charge EVs in an economical and efficient way.

In [81], EV charging at home through PV is simulated for commuters in both summer and winter. It was found that in July, 70% of the energy produced by PV was used for the monthly energy needs when using a 5 kWp PV installation and an EV with a battery capacity of 29 kWh. In January, the grid supplied more than 90% of the energy requirements. Furthermore, the simulations showed that for short distance commuters and a 5 kWp PV installation, 42% of their energy demand for mobility could be provided by said PV installation, without major losses in mobility. Moreover, a household using EV and PV could save between €100 and €180 a year with this configuration, according to the legal situation in Germany is 2011.

An interesting case study, performed in [98], investigated the behavior of a micro grid with the aim to increase self-consumption of PV power to charge EVs. The micro grid consisted of a 31 kWp PV installation, several uncontrollable loads and two EVs. Three algorithms were proposed for a simulation period of one year; by using real-time information, real-time information with V2G and linear optimization where the latter used predictions for PV generation and V2G, both at a temporal resolution of 15 minutes. Regarding LP, the authors considered two scenarios for PV output; perfect information and uncertainties. The latter was executed with predicted values and evaluated with real values. Furthermore, the fact that EVs charge slower when reaching 100% State-Of-Charge (SOC) was not included in this study since this constraint would be non-linear. It was found that EVs can significantly contribute to the balance between supply and demand. In addition, it was concluded that the LP algorithms provided the best results on self-consumption and relative peak reduction. The self-consumption increased from 49% to between 62% and 87%, depending on the selected strategy. Moreover, LP decreased the impact on battery lifetime, which can be negatively influenced by V2G because of the higher energy throughput. It was found that average charging power was lowest in case of LP. In addition, the average SOC had a value of around 50%, which according to [40] is ideal for battery lifetime.
This study shows similarities to the study presented in this thesis. However, the study in [98] had the objective to increase self-consumption whereas this thesis shall minimize the costs for the end user under varying circumstances. Second, LP was considered which was possible due to the fact that two EVs with two charging points were considered. In this thesis however, multiple charging points with multiple EVs linked to each of these charging points will be considered. To avoid simultaneous V2G and G2V and charging multiple EVs at once [84], MILP will be used. Finally, the two EVs were used for car sharing, meaning that each EV would make on average three trips per week, with a minimum of 20 kilometers and a maximum of the total EV range, per trip.

The authors of [69] designed a Smart Home Energy Management System (SHEMS), controlled by Fuzzy Logic. The SHEMS was designed to control a colony consisting of 40 smart homes with 2.5 kWp PV, home storage batteries and EVs. Every home storage battery has an energy capacity of 10 kWh whereas the EV batteries have an energy capacity of 16 kWh each. Fuzzy Logic control was chosen because of its flexibility and adaptive nature. The results show that node voltage changes from 1.1 p.u. - 0.82 p.u. to 1.05 p.u. - 0.95 p.u., thus decreasing the voltage drop and shaving the peak demand.

Research conducted in [32] combined PV and EVs with an open source linear optimization model named EVLS. In this study, 100 different combinations of PV and EV penetration levels were considered for Northern Italy. Around 500,000 people live in this region, owning a total of 400,000 vehicles. Notably, the authors point out that the combination of EV and PV has not yet been fully analyzed, since most research focuses on combining EVs and wind energy. The objective of this research was to investigate the impact of uncontrolled and smart charging strategies with different levels of PV and EV penetration. Furthermore, perfect information was studied. The results led to the conclusion that for 50% penetration of EVs, peak demand can increase with 10% to 16%. In case of uncontrolled charging, usually in the evening, demand of the EVs has to be satisfied by non-PV capacity. Smart charging can therefore add flexibility to a system where power is mostly generated by power plants with large ramp rates. Furthermore, V2G has shown to be able to reduce peak demand by 35% in case of high penetration of both EV and PV.

In [36], the authors proposed an optimal charging strategy for the combination of EVs and PV. PV generation was predicted using the ARMA model, EVs were classified upon driving patterns using Fuzzy C-means and uncertainties in PV output and driving patterns were described by Monte Carlo simulation (MCS). Furthermore, a PSO algorithm was designed to optimally make use of the V2G capabilities of EVs. Finally, a cost-benefit analysis was performed to evaluate the economic feasibility of V2G for PV power integration. The revenues that could be made from V2G were calculated using real-time prices. The costs included capital costs and cost of energy discharged through V2G, such as battery degradation. Regarding energy produced by PV, production tax credit is considered. In addition, penalty factors are assigned in case the predicted and actual PV output fall outside a certain bandwith. The objective of this research was to minimize the penalty costs, while satisfying the constraints. The research considered 12 MW of PV and 424 EVs. It was found that by using this strategy, PV power utilization increased from 71.6% to 97.34% when enabling V2G. However, the cost-benefit analysis showed that V2G revenues alone cannot sustain the costs of V2G, unless other possible services due to V2G are considered, such as fast-response reserve capacity. Moreover, with increasing forecasting error, the proposed method reduced the penalty cost.

The authors of [103] analyzed the electrical energy balance of a household with PV and an EV, taking into account Vehicle-To-Home (V2H). Four different control schedules were considered; PV only charging, weekend fill-up, every-night fill-up and weather dependent charging. The latter one considered weather forecasts, e.g. if the next day would be clouded, then the EV would be charged during the night. Regarding the economic evaluation, day- and nighttime tariffs were used. Furthermore, potential revenues from the sale of excess PV power were not taken into consideration. Bearing in mind that no optimization occurred, the results showed that the electricity costs and CO_2 emissions were reduced while self-consumption of PV power increased. Weather dependent charging in combination with V2H provided the best performance. Moreover, the simulation showed that the system benefited from the V2H service in case PV power was insufficient.

An intelligent Energy Management System (iEMS) was presented in [57], which was designed to allocate power to charge PHEVs at a municipal parking deck in a smart way. This was done by real-time monitoring and control. The system took user preferences such as charge time and rate of charge into account in order to dynamically manage power flows. Furthermore, data such as initial SOC, capacity, electricity prices and charge time was used by the iEMS, which allocated power periodically or in case of a trigger due to a special event, e.g. when a new car plugged in. Moreover, an extensive model of a battery was used, which incorporated factors such as aging, internal resistance and charge acceptance. Optimization was performed although the the kind of optimization was not specified. The results showed that the constraints were not properly implemented, since for the first simulation the maximum power was exceeded. Furthermore, during the second simulation the time of completion was more than was specified. Finally, the authors developed a Graphical User Interface (GUI) with Labview.
The co-author of [57] elaborated on the findings from [91]. Again, a municipal parking deck was considered where the objective was to maximize the average SOC of all plugged in PHEVs. The Degrees Of Freedom (DOFs) were SOC, charging time and energy price. The battery was modeled as a capacitor circuit because "a simple linear model cannot reflect the highly non-linear battery dynamics". Furthermore, a truncated normal distribution was used to represent the parking time and a log-normal distribution characterized the initial SOC. The optimization was done by both Estimation of Distribution Algorithm (EDA) and PSO for >3000 PHEVs, and their results were compared. The authors concluded that EDA can reach the near-optimal at a reasonable convergence rate while providing a better overall fitness value than PSO. Moreover, EDA proved to be more immune to local minima than PSO. Concluding, with a computation time of 2.98 s, using EDA would make near real-time near-optimal control possible.

In [83], a smart grid with PHEVs capable of V2G and PV was considered. This study aimed to minimize emissions and costs by integrating 50,000 PHEVs into the grid, together with 40 MW PV, 25.5 MW wind and traditional thermal power plants. By using Unit Commitment (UC), the authors were able to commit and decommit generating power in order to minimize emission-costs, under uncertain conditions. Due to the parabolic nature of the fuel costs, the objective function was non-linear. Therefore, the authors selected PSO to perform the optimization. Furthermore, start-up costs and spinning reserves were taken into account although ramp rates of the thermal generation units were not. Energy prices for V2G were not included. Results showed that during off-peak hours, PHEVs were used to store excess renewable energy and acted as sources during peak hours. Because of this, thermal generation units could be decommited, saving 6503.55 tons of emissions per day without taking the emissions savings by replacing all mechanical vehicles by PHEVs into account. Furthermore, the smart grid saved at least $219,940.2 per day, taking both RESs and PHEVs into account. The execution time of the algorithm was 1275.44 s, when taking all scenarios into account, which was said to be tolerable for offline applications.

The authors of [60] study the impact of PHEV integration in a smart grid, combined with RESs and conventional energy sources. To address the intermittent nature of RESs and random behavior of PHEV owners, a stochastic optimization framework was proposed to minimize the total power cost. A composite random variable was introduced which contained all scenarios defined over the event space. Furthermore, the stochastic optimization problem was transformed into a Deterministic Equivalent Formulation (DEF), so that the optimization can be executed by traditional software. For example; to model the randomness of the wind power, the authors defined six output levels. Moreover, a penalty factor was introduced for every wasted unit of energy produced by RESs. The authors concluded from the results that the PHEV fleet can be used to store excess renewable energy. In addition, when there would be a shortage of energy, the PHEV fleet could provide the difference.

Research conducted in [16] aimed to find a way to optimally integrate PHEVs in Micro Grids (MGs), with the objective to minimize costs and to find the optimal amount of parking numbers. Uncertainties about PV power production, daily driven distances by PHEVs, electricity market prices, other MG loads and short-term scheduling were taken into account while performing this study. Furthermore, the economic impact of PHEVs on the MG was assessed. Energy production was a mix of PV, Fuel Cells (FCs) and micro turbines. The Energy Management System (EMS) should optimally allocate power production while minimizing total cost. In addition, PV power forecasting was done by the Radial Basis Function Network (RBFN) which, for sunny days, predicted with a MAPE of 11.36%. It should be noted that the authors claim this method is a relatively common one. However, this was the only time during this literature study this method was come across. Daily energy requirements and initial SOC of the PHEVs were acquired through MCS. Since the authors aimed to find the optimal amount of parking numbers, daily PHEV infrastructure costs were taken into account, depending on the size of the PHEV fleet. Furthermore, the authors considered this as an UC problem, however, without considering ramp rates for the production units. To solve the optimization problem, the authors used the GA tool from MATLAB. The results showed that for this problem the optimal number of PHEV charging stations was 9. Furthermore, the Distributed Generators (DGs), including PHEVs, were producing near their respective upper limits to sell energy to the main grid, when electricity prices were high.

In [63], the authors proposed an intelligent workplace parking garage for PHEVs. The system consists of a 75 kW PV array, smart charging controller, DC distribution bus and a link to the main grid. Furthermore, besides V2G, also V2V charging/discharging was considered. In addition, PHEVs were classified among their energy requirements and time left for the energy to be fed to the PHEV. Because of non-linearity the authors chose a fuzzy logic based controller. The objective of this controller was to limit the impact on the main grid while maximizing self-consumption. Based on the Central Limit Theorem, the authors presented the distribution of arrival and departure time. By subtracting the Probability Density Functions (PDFs), they were able to find the PDF of the average parking time. Furthermore, log normal distributions were used to represent the daily traveled distance and power required by the PHEVs. To predict PV output, the authors utilized the ARX model, regenerated from [5]. For the working place garage, around 180 PHEVs were considered. Since a fuzzy logic controller was used, real-time control was possible and information would be updated every 6 minutes. When one PHEV was randomly selected to investigate, it was found that due to its long parking time, it was awarded with a low classification. Therefore, when the electricity price was high, this PHEV was used for V2V. Furthermore, it was shown that the voltage drop decreased from a minimum of 0.75 p.u. without smart control to 0.95 p.u. with smart control. It is worth noting that this study considered control and as a consequence, the title is incorrect since optimization was not performed.

The authors of [61] proposed a heuristic operation strategy for commercial building MGs in order to improve self-consumption of PV power and reduce impact on the grid of charging EVs. The proposed strategy can be split into three parts: the model representing the feasible charging region of the EV, dynamic event triggering and the real-time power allocating algorithm. However, the authors did not take EV demand or PV output forecasting into consideration in order to reduce computational demand. In this study, 60 EVs, 240 kWp PV power and a peak load of 500 kW were considered. Furthermore, the initial SOCs and arrival times were randomly generated. To attain results, the authors performed 5 case studies. The two of main interest: the comparison between the proposed model and the case where feasible charging region of the EV, dynamic event triggering and PSO were combined. After comparison, it was concluded that the proposed strategy proved to be the most reasonable. Moreover, the proposed strategy showed to be most efficient in terms of calculation time, with around 0.432 s per calculation as opposed to 55.3 s per calculation for the strategy with PSO.
The same authors proposed a heuristic charging strategy for the real-time operation of a PV-based charging station for EVs in [17]. This study made use of the same model representing the feasible charging region, which limits the search area for the optimization algorithm. Although interesting, this paper did not provide any new insights with respect to the former paper.
In [77], the same authors studied the PV-based charging station again, but this time with real-time prices incorporated. Historical data of energy prices were used to forecast energy prices by means of the wavelet neural network algorithm, for a period of 24 hours. It was concluded that the total charging costs with the proposed strategy would save about 16.5% compared to uncontrolled charging.

The study conducted in [43] focused on the optimization of a PHEV charging station with RESs, additional battery storage units, connection to the grid and real-time electricity prices. To evaluate the optimization results, they were compared with an analysis where uncertainty was introduced. Furthermore, since the constraints and objective function were linear, the minimization of the cost of the station could be performed by LP and thus attaining a global optimum. The input for the optimization consisted of historical data, which for one case study was complemented with 20% noise to mimic uncertainties. The results showed that compared with no optimization, optimization with perfect information reduced the cost of electricity from $42.51 per MWh to $16.70 per MWh. Due to the uncertainties the electricity price increased to $22.14 per MWh, which was still a satisfying result compared to the case of no optimization.

An extensive literature review on V2G and RESs integration in smart grids was done in [68]. The authors found that EVs can act as distributed energy sources and therefore have the potential to enter the electricity market. Furthermore, it was stated that due to the possibility of sharing information between smart grids and EVs, this combination would be perfect for state-of-the-art power systems. In addition, the literature study revealed that an algorithm aiming to optimize the utilization of the EV in a smart grid setting would be crucial. For example, the authors found in [64] that by optimizing the profit for owners of EVs when participating in V2G, 10% could be saved for drivers with flexible charging schemes. Furthermore, peak demand was reduced by 56%. Another interesting example given by the authors was the analysis in [6]. Here, the potential of PV on public parking lots in the Swiss city of Frauenfeld was studied. It was concluded that 15% to 40% of future energy demand by EVs could be satisfied by these PV powered public parking lots. Furthermore, the authors pointed to an international company called Better Place. This company pursues the electrification of the transportation sector by introducing battery switching stations. At such a station, it would be possible to swap the battery of ones EV within 5 minutes.
However, the study also revealed that even though many studies were dedicated to V2G, EV manufacturers had not yet introduced many V2G enabled EVs. The authors claimed that this is mainly due to potential EV owners, since they would have to decide whether or not to participate in the energy market through V2G. For example, when a manufacturer decides to introduce an V2G enabled EV, it should also build a model without this possibility for people who would not want to make use of this feature. The authors claimed this might divide market share, which would not benefit EV penetration. In conclusion, it was also pointed out that perhaps the most important challenge still lies in battery wear due to frequent charging/discharging because of V2G.

In [54] the authors proposed an optimal charging strategy for V2G enabled EVs. Furthermore, this study took uncertainties into account by incorporating stochastic EV connection to the smart grid. This was done by a so-called event-triggering scheme. The events were described as connection to the grid and unexpected disconnection from the grid. Due to this scheme, the authors utilized DP to minimize the power load variance over the course of a day, which was divided into 15 minute time slots. To protect the batteries, minimum and maximum SOC were set to 0.2 and 0.8 for all connected EVs, respectively. Furthermore, the authors noted that maximum charging power was limited to 4 kW and additionally stated that slow discharging (3.3 kW) would be preferable for V2G operation. Moreover, initial and demanded SOC and battery capacity follow uniform distributions, with initial SOC between 0.3 and 0.6, demanded SOC between 0.4 and 0.7 and battery capacity between 12 kWh and 20 kWh. The arrival times were assumed to follow a Chi-square distribution and total parking time was represented by a normal distribution. The results clearly show that the V2G event-triggering scheme effectively flattened the resulting load curves. Moreover, the time to solve a single model with 300 EVs was 5 s, which the authors deemed satisfactory taking into consideration that one time slot was 15 minutes.

A multi-objective algorithm to minimize the overall energy cost of a 45-bus distribution network was proposed in [25]. Renewable energy from PV and wind were considered, combined with diesel generators and PHEVs. The algorithm was designed to determine the number, locations and sizes of the RESs and parking lots. The optimization was done using Artificial Bee Colony (ABC). Due to the size of the 45-bus distribution network, an important aspect was the cost of energy transportation losses in the network. In addition, costs of importing energy from the grid, costs of energy supplied by the Distributed Generators (DGs) and costs of battery discharging were taken into account. The problem became non-linear because of the cost-function for the diesel generator and grid electricity. Furthermore, minimum and maximum SOC were set to 0.25 and 0.90, respectively, while initial SOCs were fixed to either 0.30, 0.45 or 0.70. All PHEVs were assumed to have a battery of 16 kWh and their charge/discharge power was considered to be 2.3 kW. A comparison was made between the proposed algorithm and a similar one, based on PSO. The results showed that the voltage drop decreased for both cases with the addition of DGs. Interestingly enough, it was concluded that ABC provided a better voltage profile than PSO. As a consequence, the energy loss decreased with 4% and 10% for PSO and ABC, respectively. Furthermore, the amount of power imported from the grid decreased with 42% and 66% for PSO and ABC, respectively.

The authors proposed a stochastic energy scheduling method for MGs with RESs in [89]. The method consisted of two stages where the first stage was used to make an optimal decision on the day-ahead energy transaction. The second stage was designed to simulate real-time operations. This strategy was chosen because of the fact that the initial MINLP problem would be difficult to solve. Interestingly, decisions made during the first stage do not vary across the scenarios in the second stage. These scenarios were used to model the uncertainties due to RESs. A total of 100 scenarios were considered, each with a 0.01 probability. Furthermore, the authors pointed out that frequent charging/discharging negatively affects the lifetime of batteries. Therefore, the relationship between lead-acid battery cycle life and Depth Of Discharge (DOD) was expressed as a linear function. The resulting cost function was also linear. The cost function for the considered non-renewable DGs was non-linear. As stated before, the initial problem was decomposed into two problems: the master energy scheduling problem and the power flow sub problem. The first stage solved the problem without taking the constraints on power flows into consideration. During the next stage, the possible solutions were checked to see whether the power flow constraints were satisfied. Due to this method, the algorithm should converge to at least a local optimum. The output of the model involves the decision on the day-ahead energy transactions and which DG units were committed. Because of the two applied strategies, the stochastic approach provided better results when compared to the deterministic approach. The controlled charging via the stochastic approach resulted in total costs of $22,276 versus $23,500 with the deterministic approach. Furthermore, energy losses were reduced by approximately 5% due to the stochastic approach.

In [84], the authors designed an energy management system which optimally allocated V2G, G2V and V2V energy exchanges between multiple Electric Vehicle Charging Points (EVCPs). The proposed model minimized the difference between full SOC and actual SOC upon departure, by using MILP. The authors noted this method should be used in order to in order to prevent simultaneous V2G and G2V operations. Furthermore, individual battery characteristics, charging/discharging status, PHEV and EV plug-in patterns, hourly energy prices and the negative impact of DOD were taken into account. Interestingly, the minimum SOC value was set to 0.7 to preserve battery life. As stated before, the objective function minimized the difference between full SOC and actual SOC upon departure, by penalizing the difference in terms of money. Furthermore, costs of G2V, profits from V2G and costs from V2V were included into the objective function. To differentiate be-

tween sale price for V2G and purchase price for G2V, the authors assumed the purchase price to be 10% less than that of the sale price. Input data regarding mobility patterns were taken from previous studies. To obtain results, the authors compared the proposed model to uncontrolled charging. It was found that the proposed model mainly charged PHEVs and EVs through G2V. In addition, V2V was used more often than V2G in order to reduce energy cost. The authors noted that when sale price for V2G would be equal or higher than purchase price for G2V, the comparison results would likely be opposite. Furthermore, it was concluded that costs were reduced by 33%, 10% and 20% for the household case, commercial case and mixed case, respectively, when compared to uncontrolled charging. These costs were mainly reduced by shifting peak demand to valley price periods. A sensitivity analysis with respect to the minimum SOC value resulted in the conclusion that if no minimum would be applied, i.e. minimum SOC = 0, the average price would be reduced by 5.5% when compared to a minimum SOC of 1.
The same main author continued upon the research done in [84] by introducing stochastic programming in [85]. Similar to [89], the proposed model consisted of two stages. The first stage decisions determined the day-ahead energy transactions whereas the second stage would reflect the intraday markets and vehicle staying patterns. Interestingly, the batteries of the studied EVs were assumed to have a linear degradation performance per kWh. The objective function consisted of five elements, where elements 2, 4 and 5 were particularly interesting. In these elements, a probability factor α was introduced, representing scenario probability. Furthermore, three combinations, with 50%, 30% and 20% probability, of hourly arrival and departure rates were utilized. In addition, profiles of the selling and purchasing energy prices for day-ahead and intraday were attained from the Spanish service operator. The penalties per non-supplied kWh to the EVs were fixed to €1 and €3, to account for possible inconvenience generated. The results showed that cost reduction was realized by shifting the load to a period with valley prices. The cost reduction amounted to 15%, 10% and 10% for the household and commercial and mixed patterns, respectively. Furthermore, the authors noted that the stochastic average cost can be seen as a relevant measure of the uncertainty regarding the energy cost. Moreover, sensitivity analysis regarding the minimum SOC value showed that decreasing the minimum SOC value would increase profitability, even when extra battery wear occurred.

Research in [99] was conducted to assess the self sustaining capacity of the island of Flores, in terms of energy, and the potential EVs could have in such a system. The island of Flores currently utilizes of hydropower, wind power and diesel generators to satisfy energy demand. Due to the lack of data, some assumptions were made. As details regarding driving patterns were insufficient, data from the Netherlands was used. Furthermore, wind data was not readily available and therefore Danish data was taken into account, although the authors noted that this should not have a significant impact on the study. In addition, baseload was assumed to be covered by hydropower whereas the remaining fluctuating demand should ideally be satisfied by wind power. The research question of the paper is therefore to what extent can EVs assist in smoothing the remainder of the fluctuations. Regarding the cost function, the authors noted that demand was to be met by mainly RESs, which practically have zero marginal costs. Power shortage should therefore be priced based on the fact that economically spoken something becomes more valuable when it is scarce. The objective of this research was to minimize the charge costs while satisfying constraints. One of the constraints was that it would be unsatisfactory if transportation needs could not be met. The optimization was performed through DP. Furthermore, the tariff for G2V and V2G were taken to be equal although for the latter, battery degradation costs were subtracted from the revenue. Battery degradation costs were assumed to have a constant value of $0.042 per kWh, which the authors attained from [75]. Characteristics such as battery energy and charging/discharging power were modeled using a Gaussian distribution, where $E_{battery}$ = 24 kWh, P_{max} = 3 kW and P_{min} = -1 kW were used as averages. The results indicated that when 1000 EVs (i.e. 50% of vehicle fleet) were considered, fluctuations in demand were decreased significantly although capacity due to EVs was not sufficient to prevent thermal generation from being necessary. Furthermore, even though demand increased drastically in case of uncontrolled charging, still less back-up generating capacity was required than in the case without EVs. In addition, the effect on emissions were studied. One of the conclusions was that the total reduction of CO_2 emissions amounted to roughly 80% when electricity was produced by hydropower and wind power, with diesel as back-up, as opposed to the case when total energy demand was satisfied by diesel, including ICEVs. Furthermore, controlled charging in case of 100% EVs and RESs with diesel back-up provided a reduction of 50% CO_2 emissions when compared to uncontrolled charging. In addition, it was concluded that in terms of CO_2 emissions, it would hardly make a difference whether EVs or ICEVs were deployed. Finally, the authors noted that when price incentives which include capital costs will be implemented, the degradation costs of EV batteries through V2G will not be a real obstacle.

In [88], a day-ahead resource scheduling method was proposed which included demand response for EVs in combination with V2G. Regarding demand response, the authors proposed two methods to influence demand of EV users. The first method was to offer a financial incentive for the users if they were to reduce their travel necessities, also called trip reducing demand response. The second method was to try and shift the demand from EV users. A total of 2000 EVs were implemented into the model. Due to the constraints imposed by the authors the optimization problem became non-linear and MINLP was chosen to perform the optimization. Furthermore, a comparison was made with PSO to assess the computational performance of both algorithms. According to the results, almost all EVs would participate in reducing their travel necessities, as was computed by both algorithms. In addition, 110 EVs would shift their trip to another period of the day. Finally it was stated that computational performance with PSO was faster than MINLP: 30 to 34 s versus 85,475 to 97,416 s, respectively. Moreover, the difference between objective function when comparing both cases ranged from 0% to 3%.

Two smart energy control strategies were presented in [66], and compared to a business-as-usual scenario. The first strategy was controlled the charging of one PHEV, whereas the second strategy was based on information of 150 homes. Furthermore, optimization was done through quadratic programming. Even though no V2G or RESs were incorporated, some interesting conclusions were drawn. In the business-as-usual scenario, a 30% PHEV penetration led to an increase in peak demand of almost 1.5 times. Furthermore, again for a 30% PHEV penetration level but controlled on a local level resulted in a reduction of peak demand of 26%.. The second strategy showed to reduce peak demand with an extra 4%.

The authors of [33] designed an intelligent optimization algorithm using GA, which consisted of multiple steps. As a first step, the authors optimized the size and location of DG system while considering power loss minimization. Then, in order to satisfy the size of the DG system, a so-called on-grid Hybrid Renewable Energy System (HRES) was chosen. Further, to minimize energy costs, an optimal sizing of the HRES was performed while also attaining the best number of decision variables, for this case the number of system components. Finally, charging rate optimization was executed for the PHEVs while taking demand uncertainties of PHEV parking patterns into consideration. Interestingly, as RESs, not only PV but also a relatively small 10 kW wind turbine was chosen. Furthermore, to model statistical arrival times, the authors used an exponential PDF for 1 - 8 AM and a 3-parameter Weibull PDF for 9 AM - 24 PM. The results showed that optimal DG size would be 550 kW and 450 kW, implying two DG systems however, with a total diesel generating capacity of 520 kW the system was far from sustainable. In addition, the power loss was reduced by 0.267 MW.

In [104], the authors proposed a cooperative algorithm for a charging station, taking into account dynamic pricing. V2G was not utilized however, V2V was used in order to minimize total social costs. To differentiate between charging, discharging and idle, the authors found that the objective function and its constraints should be considered as MILP. Due to one of the imposed constraints, which basically implied that the sum of all charging power should be lower than the load limit of the charging station and therefore coupled all EVs, the authors stated that the objective function should be decomposed to increase efficiency. This was done by first utilizing dual decomposition, after which decentralized Benders decomposition was used to improve computational performance. The results showed that a 2.6% reduction in total social costs was realized. Furthermore, the computational performance of this algorithm showed to be very promising as opposed to centralized Benders decomposition, e.g. for 9 EVs a reduction of a factor 1000 in computation time was realized. However, temporal resolution of this research was quite poor, since only four time periods were taken into account. In addition, a deterministic approach was taken and no RESs were considered. Even though the results in this study indicate much time can be won on the computation aspect, this thesis shall impose a lower limit on the number of EVs per charging point. Therefore, the proposed approach will not be necessary since computational efficiency will be inherently higher than that of the presented scenario in [104], with centralized Benders decomposition.

In order to preserve battery lifetime, it is important to charge and discharge it properly [40], especially when V2G is considered. By discharging 20% to 30% of the battery capacity before recharging, instead of completely discharging, the number of cycles can be extended significantly. As a rule of thumb one can equal 5 to 10 shallow discharges to one full discharge. Furthermore, keeping the battery fully charged and charging it to its full capacity will shorten its lifetime as well. By charging the battery to 85% instead of 100 %, capacity fading over a large number of cycles is reduced, as can be seen in fig. 2.6 where a 4.1 V float voltage and 4.2 V float voltage represent 85% and 100% capacity utilization, respectively. Finally, high charge and discharge currents can reduce cycle life, although chemistries such as Li-ion manganese and Li-ion phosphate are better able to cope with high currents.

The authors of [10] proposed and Energy Management System (EMS) based on Model Predictive Control (MPC), aimed to minimize operating costs and CO_2 emissions. Their proposed EMS was applied to the comprehensive test-bed facility of the University of Genova, consisting of micro gas turbines, PV, Concentrating Solar Power (CSP), batteries, EV charging stations and an absorption chiller. MPC has the advantage that a optimization horizon can be set and thus it is not necessary to optimize over the entire period of interest, thereby increasing computational performance. The authors point out that the model is nonlinear, concluding that a global optimum cannot be attained. Regarding computational performance, each optimization run takes 10 seconds. The results show that the proposed EMS saves 15% in costs and 8% in CO_2 emissions.

In [4], a MILP model was developed to optimize power exchange in both a conventional AC micro grid and a hybrid AC-DC micro grid with power generation by wind, PV, diesel generator and PHEVs. The objective was to minimize overall operating costs over the entire scheduling period, which was 24 hours. An interesting feature of the proposed model was the different charging rates implemented, depending on the SoC of the PHEV. Furthermore, binary constraints were imposed to avoid simultaneous charging and discharging. A total of 6 binary constraints were utilized. The PHEV batteries had a capacity of 5 kWh and the study used 25 kW PV, 25 kW wind and a 40 kW DG unit based on fossil fuel. The results showed that during high grid tariffs, power generated by the DC sources was transferred to the main grid and vice versa when grid tariffs were low. Furthermore, the PHEVs were found to be utilized more effectively although it should be noted here that the authors did not consider battery degradation. It could very well be the case that PHEV utilization would be lower due to this. In addition, the proposed model showed a reduction of 11.9% in energy drawn from the grid for the hybrid micro grid and a 7.6% increase in energy fed to the grid. Finally, the overall costs for the hybrid micro grid decreased by 23.8% although it is not clear how much of this was due to extra input of the diesel generator.

The study performed in [41] aimed to create an energy resources management model for a micro grid consisting of micro turbines, fuel cells, commercial and residential loads, RESs and a parking lot with EVs. The proposed model was in the form of MILP. Constraints due to technology, renewable power forecasting errors, spinning reserves and EV owner satisfaction were considered. The latter comprised desired charging/discharging price limits, parking time, and the battery life of the EV. To forecast the solar and wind output a time series model was used although it was not specified which model exactly. The objective of the proposed day-ahead energy management model was to minimize total operation costs and reserve capacity was taken into consideration to cope with the intermittent nature of RESs. An interesting feature of the proposed model was that EVs were, depending on their age, limited in the amount of times they could switch between charging and discharging. Further, all EVs were considered to be the same model and temporal resolution was 1 hour. The results showed that cost reduction lied between 1.6 - 8.4% and that EVs would sell energy back to the grid during high tariffs.

The authors of [37] proposed a framework maximize the revenue of a parking deck with on-site renewable energy generation and EVs. The authors used a stochastic approach by defining a number of scenarios for solar output and adding uncertainty to arrival and departure times and SoC upon arrival. The electricity prices utilized were flat-tariff. Furthermore, the authors investigated three methods of charging: uncontrolled charging, constrained charging and smart charging, where during constrained charging the energy was equally distributed over the day. In addition, the authors assumed that each EV would connect to its own charger once a day. The results showed that stochastic optimization provides more feasible results than deterministic optimization but further interesting conclusions were not drawn.

Conclusion

During the literature study a wide variety of control and optimization strategies came to light, as can be seen in section 2.3.2 and table 2.1. It can be seen in table 2.1 that a similar study has not yet been performed. Some of the papers with most similarities will be briefly touched upon once more here. In [98] a LP algorithm was

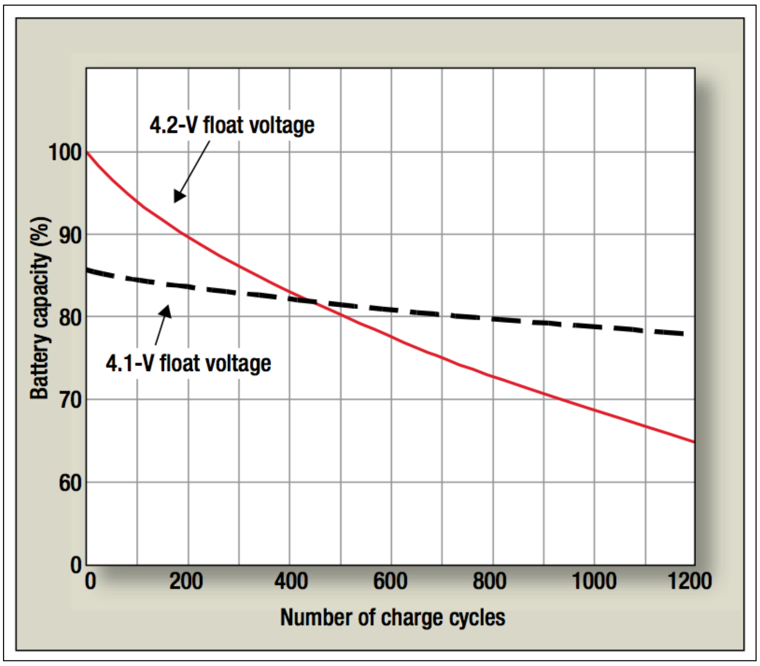

Figure 2.6: Impact of float voltage on battery capacity and cycle life. Reproduced from [40].

implemented in maximize self-consumption of PV power however, forecasting was not taken into account. Furthermore, the study considered only two cars and two chargers whereas in this study multiple chargers will be implemented and to each of them, multiple cars can be connected and as a consequence, MILP has to be utilized [84]. A more detailed description of this method will be given in 2.5 and the complete mathematical representation will be given in chapter 3

On the other hand, the authors of [36] and [16] did use a forecasting method to predict PV output however, due to the utilization of PSO and GA, respectively, as optimizing algorithms, the global optimum could not have been attained.
The study performed in [63] showed some coincidence with this thesis such as the fact that ARX was used as forecasting method and that a workplace parking garage powered by PV was considered. However, since fuzzy logic was utilized no optimization was performed.

In conclusion, to the best of the author his knowledge, the proposed strategy in this thesis will be unique. The strategy will be elaborated upon in section 2.5 and chapter 3.

2.4. Optimization

Imagine having class at 9.00 a.m. and one would like to stay in bed for as long as possible, thus aiming to maximize the hours of sleep. There are several modes of transport, such as public transportation or the bike, where the former costs money but may be quicker and the latter is free but less comfortable, e.g. during winter. These are considered to be the variables of the morning conundrum. There are also some conditions or constraints that need to be considered, such as the time it takes to have breakfast or to take a shower. For example, it may take at least 5 minutes to take a shower and 15 minutes to have breakfast, drastically influencing time that can be spent in bed. These constraints define the domain in which one can seek the maximum amount of time he or she is able to sleep.

Optimization is a process that is encountered in everyday life and usually comprises of finding the best possible solution under a set of constraints that need to be satisfied. However, while the aforementioned example can be solved using intuition, experience and adding and subtracting, engineering problems usually have far more constraints and optimization variables and are therefore more complex. To this end, mathematical programming can be utilized. Depending on the constraints and objective function, an optimization problem

Table 2.1: Overview of approaches from previous studies.

Overview						
Authors	**Objective**	**Optimization technique**	**Forecasting method**	**V2G**	**EVs**	**RESs**
Ghofrani et al. [36]	Minimize penalty costs	PSO	ARMA	Yes	Yes	Yes
Chen and Duan [16]	Minimize costs	GA	RBFN	Yes	Yes	Yes
Honarmand et al. [41]	Minimize operating costs	MILP	Time series	Yes	Yes	Yes
van der Kam and van Sark [98]	Maximize self-consumption	LP	(-)	Yes	Yes	Yes
Fattori et al. [32]	Study impact of PV and EV on grid	EVLS	(-)	Yes	Yes	Yes
Verzijlbergh et al. [99]	Minimize charge costs	DP	(-)	Yes	Yes	Yes
Saber and Venayagamoorthy [83]	Minimize emissions and costs	UC PSO	(-)	Yes	Yes	Yes
Baboli et al. [4]	Minimize operating costs	MILP	(-)	Yes	Yes	Yes
Guo et al. [37]	Maximize revenue	Stochastic Programming	(-)	No	Yes	Yes
Ma and Mohammed [63]	Increase self-consumption	(-)	ARX	Yes	Yes	Yes
Bracco et al. [10]	Minimize operating costs	MPC	Not specified	Yes	Yes	Yes
Sánchez-Martín et al. [84]	Minimize difference between full SOC and actual SOC	MILP	(-)	Yes	Yes	No
Sanchez-Martin et al. [85]	Minimize penalty costs	Stochastic Programming	(-)	Yes	Yes	No
Jian et al. [54]	Minimize power load variance	DP	(-)	Yes	Yes	No
Soares et al. [88]	Minimize EV usage by owners	MINLP	(-)	Yes	Yes	No
Tulpule et al. [94]	Maximize self-consumption	DP	(-)	No	Yes	Yes
Li et al. [60]	Minimize total power costs	Stochastic Programming	(-)	No	Yes	Yes
Liu et al. [61]	Increase self-consumption	PSO	(-)	No	Yes	Yes
El-Zonkoly [25]	Minimize overall energy costs	ABC	(-)	No	Yes	Yes
You et al. [104]	Minimize total social costs	MILP	(-)	No	Yes	No
Su and Chow [91]	Maximize avg. SOC of all PHEVs	PSO and EDA	(-)	No	Yes	No
Su et al. [89]	Minimize costs	MINLP	(-)	No	No	Yes
Huang et al. [43]	Minimize cost of PHEV charging station	LP	(-)	No	No	Yes
Cutler et al. [20]	Charge EVs as much as possible	(-)	(-)	No	Yes	Yes
Yoshimi et al. [103]	Increase self-consumption	(-)	(-)	No	Yes	Yes

can be among others linear, integer, mixed integer or nonlinear and these are subsequently called linear programming (LP), integer programming (IP), mixed integer programming (MIP) and nonlinear programming (NLP). As stated before, if an optimal solution can be found this would be a global optimum in the case of LP, IP and MILP whereas NLP and MINLP could produce a local optimum. The focus of the rest of this thesis shall lie on (MI)LP.

Linear programming is generally formulated in canonical form with optimization variables, the objective function and constraints as follows:

$$\text{maximize} \quad \mathbf{c}^{\mathrm{T}}\mathbf{x} \tag{2.4.1}$$

$$\text{subject to} \quad \mathrm{A}\mathbf{x} \leq \mathbf{b} \tag{2.4.2}$$

$$\text{and} \quad \mathbf{x} \geq 0 \tag{2.4.3}$$

where vector **x** contains the optimization variables, **c** and **b** are vectors of known coefficients and A is a matrix of known coefficients. However, when considering a MILP problem, some of the optimization variables in vector **x** are constrained to integer values.

The optimization variables, as the name implies, represent the variables that can be altered in order to find the optimal solution. From this it becomes clear that optimization becomes impossible to solve by hand when there are more than three optimization variables.

The constraints can be divided into equality and inequality constraints and define the feasible region, i.e. the region where the solution can be found. If an equality constraint is present, the feasible region will be represented by the equation defining the equality constraint. In contrast, the inequality constraints define the area in which the optimal solution should be found. Moreover, if an optimal solution exists, this solution will lie on the boundary of the feasible area. The constraint on which the optimal solution is found is called an active constraint. Therefore, equality constraints are invariably active constraints.

The objective function represents the function that is required to be minimized or maximized. This can range from minimizing costs or maximizing welfare. Further, the optimal solution is always a scalar, implying that the solution found is one that is the total of the studied time period. Note that when considering LP or MILP, minimizing is identical to maximizing the objective function when multiplied with -1.

Consider an example to illustrate the aforementioned in a more graphical manner. Suppose there are two power plants, capable of generating a variable output. The output of the two power plants should equal the demand and the output is constrained due to technical properties. Further, both plants have a certain marginal cost. The typical formulation of such a problem would be as follows:

Optimization variables:

$$P_{G_1} \text{ and } P_{G_2}. \tag{2.4.4}$$

Constraints:

$$P_{G_1} + P_{G_2} = \mathrm{P}_{\text{demand}} \tag{2.4.5}$$
$$\mathrm{P}_{G_1}^{\min} \leq P_{G_1} \leq \mathrm{P}_{G_1}^{\max} \tag{2.4.6}$$
$$\mathrm{P}_{G_2}^{\min} \leq \mathrm{P}_{G_2} \leq \mathrm{P}_{G_2}^{\max}. \tag{2.4.7}$$

Objective function:

$$\text{minimize } \left(\lambda_{G_1} \cdot P_{G_1} + \lambda_{G_2} \cdot P_{G_2}\right) \tag{2.4.8}$$

where λ_{G_1} and λ_{G_2} are the marginal costs for generating unit one and two, respectively.

The data belonging to the aforementioned equations are: $\mathrm{P}_{\text{demand}} = 400$ MW, $\mathrm{P}_{G_1}^{\min} = 25$ MW, $\mathrm{P}_{G_1}^{\max} = 250$ MW, $\mathrm{P}_{G_2}^{\min} = 50$ MW, $\mathrm{P}_{G_2}^{\max} = 350$ MW, $\lambda_{G_1} = 2$ €/MWh and $\lambda_{G_2} = 3$ €/MWh. Using this data, it is possible to generate fig. 2.7.

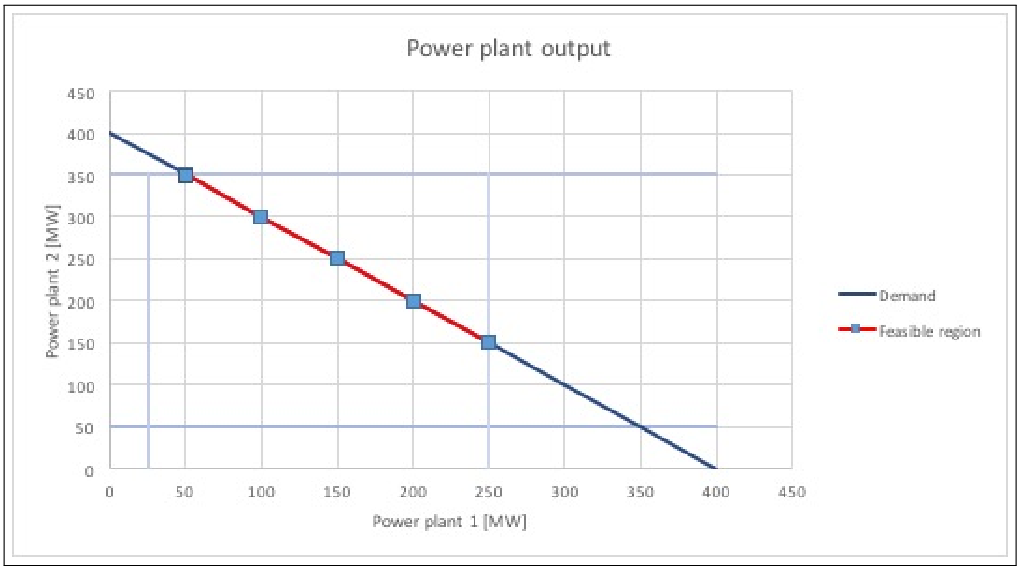

Figure 2.7: Basic optimization problem.

From fig. 2.7 it can clearly be seen that the feasible area is determined by the inequality constraints, i.e. the horizontal and vertical lines. As stated before, equality constraint eq. (2.4.6) is by definition an active constraint and one can therefore find the optimal solution on this line. The feasible region is determined by combining the equality and inequality constraints. Since by definition the optimal solution lies on the edge of the feasible region, it is straightforward to see that the upper and lower squares are both candidates for the optimal solution. By plugging the coordinates into eq. (2.4.8), it can be determined that the costs would be €1150 and €950 for the upper and lower square, respectively. Since the aim of this example was to minimize costs, the latter solution is the global optimum.

This was an example that could be solved by hand. However, it is not hard to imagine that if more degrees of freedom are added it will become impossible to apply a similar analysis. Furthermore, adding integer or binary variables to the optimization problem will greatly increase the complexity further and therefore it is impossible to solve such problems without algorithms such as the simplex method, which was proposed by George Dantzig in 1947. Explanation of this method is beyond the scope of this thesis however, it is considered to be an efficient algorithm for solving large (MI)LP problems.

2.5. Thesis motivation

Optimal power allocation is a well-studied topic in the literature. It is therefore important to have conducted a thorough literature study to ensure this thesis uniqueness. The proposed energy management system (EMS) in this thesis aims to provide an optimal day-ahead and intra-day power allocating schedule. The objective of this EMS is to minimize costs incurred through G2V charging, while V2G discharging is enabled to further decrease costs if this would be optimal. This will offer a financial incentive to EV owners to become better aware of the advantages, in terms of both cost and sustainability, that RESs are able to provide. Simultaneously, the EMS should reduce stress on the grid and increase PV self-consumption, so as to increase sustainability of the transportation sector. In addition, minimization of energy exchange with the grid is considered to ascertain the performance of the former objective in terms of self-consumption. To achieve minimal costs, a PV-based charging station at an industrial parking lot will be studied, which provides three benefits:

- Supply and demand have maximal coincidence,
- Decouple the transportation sector from fossil fuels by increasing electrification, while avoiding charging EVs with electricity produced by fossil fuels
- Apart from initial capital costs, the produced energy is less expensive than energy from the grid.

Furthermore, output of the PV system will be predicted using the ARIMA model, based on historical data. This has clear advantages, e.g. it allows the EMS to anticipate on future power input and plan accordingly, rather than merely react to input. Such a feature would enable real-life implementation of the EMS, in contrast to creating a purely abstract model. In addition, flat as well as dynamic tariffs from the utility, together with battery degradation due to V2G operation will be included to study the effect on the costs. Arrival and departure times of EVs will be based on historical data, as this has an unmistakable repetitive character. Additionally, energy demand from the EVs will be selected in such a way that it is substantially more than what is likely to be expected, so as to ascertain the performance of the EMS.

In order to attain *global* optimality, MILP will be used and solved with the CPLEX Optimizer in General Algebraic Modeling System (GAMS).

The main contributions of this thesis are therefore: To minimize EV charging costs via a PV-based charging station at the workplace with a grid connection, computed with high temporal resolution to improve accuracy, while taking battery degradation and dynamic price tariffs into consideration. As stated before, output of the PV system will be predicted by means of an ARIMA model, which would enable real-life implementation where power allocation needs to be planned. Except for PV power, a deterministic approach will be taken, which can be justified by realizing that driving patterns of commuters are very constant and recurring in their nature, as can be seen in figure 4.29 [39]. In addition, capital expenditure for the PV charging station will be taken into account as marginal cost. Binary variables are utilized to prevent simultaneous V2G discharging and G2V charging [84], but also to avoid charging of multiple EVs at the same charging point at a specific point in time. Moreover, a strategy to benefit from the full potential of the EMS will be proposed.

3

Problem definition: A mathematical approach

Nomenclature

Italic letters are used for denoting variables and indexes, whereas regular letters denote parameters and sets.

Indexes and Sets

c	Charging points, running from 1 to C.
i	Electric vehicle, running from 1 to N.
t	Time, running from 1 to T minutes.

System parameters

η_{inv}	Inverter efficiency [-].
η_{MPPT}	DC-DC converter efficiency [-].
λ_{G2V_t}	Marginal buying price of utility energy during time period t [€/kWh].
λ_{FIT_t}	Marginal selling price of utility energy during time period t [€/kWh].
λ_{PV_t}	Marginal price of PV energy during time period t [€/kWh].
$\mathrm{C_{ch}}$	Charging costs [€].
$\mathrm{E_{grid}}$	Energy exchange with the grid [kWh].
$\mathrm{P}^{+,\mathrm{max}}_{\mathrm{grid}_{i,c}}$	Maximum power transfer from the grid to the ith EV at the cth charging point [kW].
$\mathrm{P}^{-,\mathrm{max}}_{\mathrm{grid}_{i,c}}$	Maximum power transfer to the grid to the ith EV at the cth charging point [kW].
$\mathrm{P}^{\mathrm{max}}_{\mathrm{PV}_t}$	Maximum PV power during time period t [kW].
$\mathrm{R_{dis}}$	Revenues from discharging [€].
TC	Total costs incurred from the charging/discharging process [€].

Electric vehicle parameters

η_{ch} EV charging efficiency [-].

η_{dis} EV discharging efficiency [-].

λ_{deg} Degradation costs of EV's battery [€/kWh].

$\text{EC}_{i,c}^{\text{arrival}}$ Energy content of the ith EV at the cth charging point upon arrival [kWh].

$\text{EC}_{i,c}^{\text{departure}}$ Energy content of the ith EV at the cth charging point upon departure [kWh].

$\text{EC}_{i,c}^{\text{max}}$ Maximum energy content of the ith EV at the cth charging point for all time periods t [kWh].

N^{max} Maximum initiations of charging and discharging process [-].

$\text{P}_{\text{ch}_{i,c}}^{\text{max}}$ Maximum power transfer to the ith EV at the cth charging point [kW].

$\text{P}_{\text{V2G}_{i,c}}^{\text{max}}$ Maximum power transfer from the ith EV at the cth charging point [kW].

Decision variables

$D_{i,c,t}^{\text{ch},+}$ Positive difference between on and off state of binary variable $u_{i,c,t}$ [-].

$D_{i,c,t}^{\text{ch},-}$ Negative difference between on and off state of binary variable $u_{i,c,t}$ [-].

$D_{i,c,t}^{\text{dis},+}$ Positive difference between on and off state of binary variable $v_{i,c,t}$ [-].

$D_{i,c,t}^{\text{dis},-}$ Negative difference between on and off state of binary variable $v_{i,c,t}$ [-].

$EC_{i,c,t}$ Energy content of the battery of the ith EV at the cth charging point during time period t [kWh].

$P_{\text{V2G}_{i,c,t}}$ Power transfer from the ith EV at the cth charging point during time period t [kW].

$P_{\text{ch}_{i,c,t}}$ Power transfer to the ith EV at the cth charging point during time period t [kW].

$P_{\text{grid}_{i,c,t}}^{+}$ Power transfer from the grid to the ith EV at the cth charging point during time period t [kW].

$P_{\text{grid}_{i,c,t}}^{-}$ Power transfer to the grid from the ith EV at the cth charging point during time period t [kW].

$P_{\text{PV-EV}_{i,c,t}}$ Power transfer from the PV system to the ith EV at the cth charging point during time period t [kW].

$P_{\text{PV-grid}_t}$ Power transfer from the PV system to the grid during time period t [kW].

Binary variables

$s_{i,c,t}$ Binary variable that prevents feeding power into the grid while drawing power from the grid [-].

$u_{i,c,t}$ Binary variable that determines whether the ith EV at the cth charging point during time period t is available for charging (1) or not (0) [-].

$v_{i,c,t}$ Binary variable that determines whether the ith EV at the cth charging point during time period t is discharging (1) or not (0) [-].

3.1. Introduction

In order to translate the physical world to a model, mathematics need to be applied. This chapter presents the model in mathematical terms and is organized as follows: section 3.2 presents an overview of the specifications of the project and a schematic figure representing the solar carport. Then, section 3.3 presents the translation of the specifications to the mathematical model. First to be specified are the constraints regarding the EVs, after which constraints involving the grid and PV will follow. In addition, the objective functions will be formulated in section 3.3.4. Moreover, underlying assumptions will be elaborated upon and equations will be justified. Finally, at the end of the chapter an overview is given of all optimization variables, constraints and objective functions.

3.2. Project specifications

As in any real-life situation, bounds are imposed on physical phenomena, either explicit or implicit. The goal of this section is to determine these, to ensure that the mathematical model describes the physical problem as accurately as possible. Explicit constraints may be imposed by the manufacturer of the EV, such as a maximum on the charging power or a minimum on the level until the battery may be discharged. Regarding implicit constraints, one might think of irradiation, the amount of $\mathrm{kWh/m^2}$ that is received at a certain location on Earth. An overview of the imposed constraints is presented in table 3.1.

The maximum charging and discharging power is 10 kW and -10 kW, respectively. These are imposed on the charging station and therefore do not directly relate to the EV. Evidently, when an EV is bounded by a lower maximum charging power, that limit would apply. Further, each charging station is equipped with a PV system, which is rated at 10 $\mathrm{kW_p}$. Additionally, a maximum of four EVs can be connected to a single charging point. The reason for this is understandable since the PV system produces a limited amount of energy due to its power constraint. In order to charge the connected EVs to satisfy their energy demand, the number of EVs needs to be limited so that energy demand can always be satisfied. However, the number of EVs that are allowed to connect to a single charging point can vary based upon e.g. the size of the PV array.

Another constraint will be placed upon the minimum energy content of the battery in order to protect it against overdischarging, since that will reduce cycle life [40]. In this thesis a minimum of 20% of the maximum energy content of the battery will be applied, adapted from [94]. Furthermore, overcharging the battery should likewise be prevented. Therefore, a limit on the energy content of the battery, $\mathrm{EC}_{i,c}^{\max}$, is considered, which is specific to every available EV.

Finally, simultaneous charging and discharging of a single EV is not possible [84]. In addition, it is physically impossible to charge multiple EVs at the same charging point and during the same time period with different charging power. Consequently, binary variables will be introduced so that the model acts accordingly.

Table 3.1: Overview of constraints.

Constraints	
Maximum charging power	10 kW
Maximum discharging power	-10 kW
PV system	10 $\mathrm{kW_p}$
Minimum energy content of the battery	$0.2 \cdot \mathrm{EC}_{i,c}^{\max}$
Maximum energy content of the battery	$\mathrm{EC}_{i,c}^{\max}$
Maximum amount of EVs connected to one charging point	4
Simultaneous charging or discharging	1 EV per charging point

3.3. Mathematical model

The present section is dedicated to the mathematical framework of the model. As stated before, a division is made according to the overview presented in fig. 3.1. This entails that constraints concerning EVs, the PV system and the grid will be treated separately in sections 3.3.1 to 3.3.3, respectively. Finally, section 3.3.4 will present the objective functions.

3.3.1. The electric vehicles

The table 3.1 presents constraints to which the EVs are submitted. However, other practical constraints need to be implemented as well, e.g. the fact that the charging power should be zero in case there is no EV to charge. This section will clarify the constraints imposed on the model by such real-life occurrences.

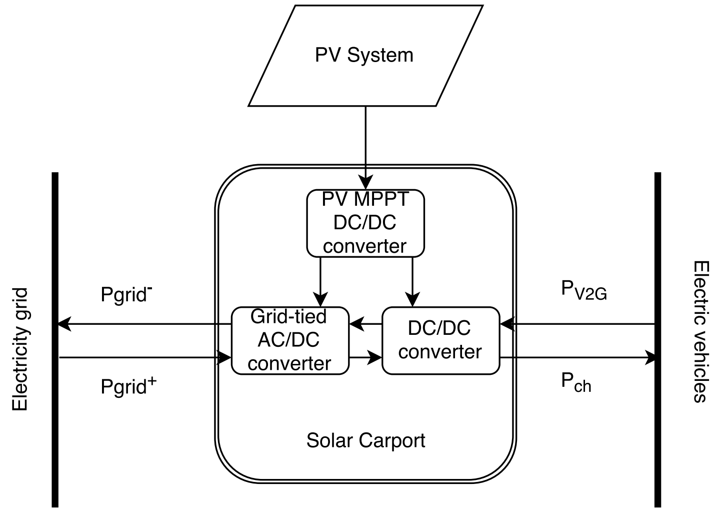

Figure 3.1: Schematic representation of the solar carport.

First, each charging point is physically limited to a charge and discharge power up to 10 kW. Further, a single EV cannot simultaneously charge and discharge. It is also physically not possible to charge two EVs at the same charging point at the same time with different charging rates. In order to model the aforementioned, binary variables need to be implemented as follows

$$0 \le P_{\mathrm{ch}_{i,c,t}} \le u_{i,c,t} \cdot \mathrm{P}^{\max}_{\mathrm{ch}_{i,c}} \qquad \forall i, c, t \tag{3.3.1}$$

$$0 \le P_{\mathrm{V2G}_{i,c,t}} \le v_{i,c,t} \cdot \mathrm{P}^{\max}_{\mathrm{V2G}_{i,c}} \qquad \forall i, c, t \tag{3.3.2}$$

$$\sum_{i=1}^{\mathrm{N}} u_{i,c,t} + \sum_{i=1}^{\mathrm{N}} v_{i,c,t} \le 1 \qquad \forall c, t. \tag{3.3.3}$$

The eqs. (3.3.1) and (3.3.2) determine whether the ith EV at the cth charging point can either charge or discharge, respectively. Simultaneously, these equations ensure that charging power $P_{\mathrm{ch}_{i,c,t}}$ and discharging power $P_{\mathrm{V2G}_{i,c,t}}$ remain within their respective bounds. Furthermore, to avoid simultaneous charging or simultaneous discharging of multiple EVs at the same charging point, eq. (3.3.3) is imposed on the model. As can be seen from this equation, for every charging point there can only be one EV charging or discharging and never more than one, or none of them. It should be noted that the maximum charging power of an EV can differ from $\mathrm{P}^{\max}_{\mathrm{ch}_{i,c}}$, but as will be explained in section 4.1.5, this parameter is limited by the charging point and not the EVs.

It is said in literature that intermittent charging and discharging will lead to faster capacity fade, ultimately leading to reduced battery life [75]. In addition, constant power charging is preferred over constant current charging for fast charging processes [106]. Therefore, in order inhibit the amount of charging or discharging initiations, the following constraints are imposed on the energy management system

$$u_{i,c,t} - u_{i,c,t-1} = D^{\mathrm{ch},+}_{i,c,t} - D^{\mathrm{ch},-}_{i,c,t} \qquad \forall i, c, t \tag{3.3.4}$$

$$v_{i,c,t} - v_{i,c,t-1} = D^{\mathrm{dis},+}_{i,c,t} - D^{\mathrm{dis},-}_{i,c,t} \qquad \forall i, c, t \tag{3.3.5}$$

$$\sum_{t=1}^{\mathrm{T}} \left(D^{\mathrm{ch},+}_{i,c,t} + D^{\mathrm{ch},-}_{i,c,t} \right) \le \mathrm{N}^{\max} \qquad \forall i, c \tag{3.3.6}$$

$$\sum_{t=1}^{\mathrm{T}} \left(D^{\mathrm{dis},+}_{i,c,t} + D^{\mathrm{dis},-}_{i,c,t} \right) \le \mathrm{N}^{\max} \qquad \forall i, c \tag{3.3.7}$$

Subject to

$$D^{\text{ch},+}_{i,c,t}, D^{\text{dis},+}_{i,c,t} \geq 0 \qquad \forall i,c,t$$
$$D^{\text{ch},-}_{i,c,t}, D^{\text{dis},-}_{i,c,t} \geq 0 \qquad \forall i,c,t.$$

The eqs. (3.3.4) and (3.3.5) calculate the difference between the attained value of decision variable $u_{i,c,t}$ and $v_{i,c,t}$ respectively and its previous value, which can be 1, 0 or -1. For example, if an EV is charging in period t while it was not yet charging in period $t-1$, it clearly initiated a charging process and therefore $u_{i,c,t} - u_{i,c,t-1} = 1$. Subsequently, a value of 1 is stored in $D^{\text{ch},+}_{i,c,t}$ and -1 in $D^{\text{ch},-}_{i,c,t}$, where the latter represents the case in which a charging process is terminated. The following step is to add these vectors over time, unique for each EV at all charging points, and constrain this to N^{max}. An appropriate value for N^{max} is found to be 8, according to [41].

Subsequently, before the arrival time or after the departure time of the ith EV at charging point c, a safeguard needs to be implemented so that there can be neither charging or discharging. This is accomplished by the following equations

$$u_{i,c,t} = 0, \qquad \text{if } t < t_{\text{arrival}_i} \text{ or } t > t_{\text{departure}_i}\ \forall i,c \tag{3.3.8}$$
$$v_{i,c,t} = 0, \qquad \text{if } t < t_{\text{arrival}_i} \text{ or } t > t_{\text{departure}_i}\ \forall i,c. \tag{3.3.9}$$

Third, realizing that $P_{\text{V2G}_{i,c,t}}$ and $P_{\text{ch}_{i,c,t}}$ represent the power from and to the EV from the chargers' point of view, one can see that the efficiency of the charging/discharging process is not yet taken into account, which is necessary for the power balance, described with eq. (3.3.23). Therefore, an extra variable $P_{\text{EV}_{i,c,t}}$ is introduced so that

$$P_{\text{EV}_{i,c,t}} = \eta_{\text{ch}} \cdot P_{\text{ch}_{i,c,t}} - \frac{1}{\eta_{\text{dis}}} \cdot P_{\text{V2G}_{i,c,t}} \qquad \forall i,c,t \tag{3.3.10}$$

Subject to

$$P_{\text{ch}_{i,c,t}} \geq 0 \qquad \forall i,c,t$$
$$P_{\text{V2G}_{i,c,t}} \geq 0 \qquad \forall i,c,t.$$

where η_{ch} and η_{dis} are the charging and discharging efficiency, respectively. Charging and discharging efficiency comprise of battery and charger efficiency. Although it has been shows that charging efficiency is not constant but increases in a logarithmic manner with increasing charging power [45],, for the sake of simplicity it is assumed that it is constant. Moreover, this is in accordance with scientific literature. Further, the round trip efficiency for the Tesla Powerwall is found to be 92% [92], which is considered to be a valid assumption for the battery efficiency used in this thesis. Then, charging and discharging efficiencies are $\sqrt{0.92} = 0.96$. Regarding the charger efficiency, the ABB Terra 23 charging station is considered [2]. The charging efficiency is 94% however, there is no mention of efficiency for V2G operation. Therefore, it is assumed that this is also 94%. Having acquired the necessary data, charging and discharging efficiency η_{ch} and η_{dis} are found to be $0.96 \cdot 0.94 = 0.90$, thus $\eta_{\text{ch}} = \eta_{\text{dis}} = 0.90$. The efficiencies are presented in table 3.2.

Finally, the energy content of the battery of the ith EV at the cth charging point needs to be assessed and constrained within certain bounds. When one is aiming to charge a battery, power is added over a period time and thus providing energy to said battery. From this, a basic equation in physics arises relating energy, power and time as follows

$$\text{E} = \int_0^{\text{T}} P(t)\,\text{d}t. \tag{3.3.11}$$

Since the problem at hand is discrete, eq. (3.3.11) can be transformed into a Riemann sum for which the following basic equation exists

$$\text{E} = \sum_{t=1}^{\text{T}} P_t \cdot \Delta t \tag{3.3.12}$$

where Δt determines the time scale and thus the accuracy of the result.

Therefore, to calculate energy content $EC_{i,c,t}$ of the ith EV at the cth charging point, one has to add $P_{\mathrm{EV}_{i,c,t}}$ to the previous level of energy content under the condition that the energy content is zero when the specific EV has not yet arrived, as follows

$$EC_{i,c,t} = \begin{cases} EC_{i,c,t-1} + P_{\mathrm{EV}_{i,c,t}} \cdot \Delta t, & \text{if } t_{\mathrm{arrival}_i} < t < t_{\mathrm{departure}_i} \ \forall i,c \\ \mathrm{EC}_{i,c}^{\mathrm{departure}} & \text{if } t > t_{\mathrm{departure}_i} \ \forall i,c \\ 0, & \text{if } t < t_{\mathrm{arrival}_i} \ \forall i,c \end{cases} \tag{3.3.13}$$

with $P_{\mathrm{EV}_{i,c,t}}$ as defined in eq. (3.3.10).

Further, the battery should not be charged beyond its maximum energy rating, which is specific for each EV, to protect the battery from overcharging nor discharged below 20% of its maximum energy rating [98] in order to protect the battery from overdischarging. However, this can be changed based on user requirements. The energy content for each EV will therefore be constrained as follows

$$0.2 \cdot \mathrm{EC}_{i,c}^{\max} \leq EC_{i,c,t} \leq \mathrm{EC}_{i,c}^{\max} \qquad \forall i,c,t \tag{3.3.14}$$

where it should be noted that the aforementioned equation always holds, as will be elaborated upon in section 4.1.5. In addition, the energy content of the battery of the ith EV at the cth charging point upon arrival and departure needs to be specified. The exact process behind this will also be explained in section 4.1.5, however, the mathematical formulation will be given here and is as follows

$$EC_{i,c,t} = \mathrm{EC}_{i,c}^{\mathrm{arrival}} \qquad \text{if } t = t_{\mathrm{arrival}_i} \qquad \forall i,c \tag{3.3.15}$$

$$EC_{i,c,t} = \mathrm{EC}_{i,c}^{\mathrm{departure}} \qquad \text{if } t = t_{\mathrm{departure}_i} \qquad \forall i,c. \tag{3.3.16}$$

3.3.2. The PV system

Each solar carport is equipped with a 10 $\mathrm{kW_p}$ PV system. Further, the accompanying DC/DC converter is equipped with a Maximum Power Point Tracker (MPPT). The DC/DC converter considered in this thesis is developed by SMA and has a European efficiency of $\eta_{\mathrm{MPPT}} = 0.98$ [87]. In addition, the energy produced by the solar carport is not necessarily free, as will be explained in section 4.1.6. As the energy is not free, it is required to determine the quantity that is supplied to the EVs and the grid separately in order to establish a fair division of the incurred costs. Furthermore, as dynamic prices will be introduced, it may be possible that energy from the grid costs less than energy produced by the PV system. In this case, it is not desirable to force the PV energy to either the EVs or grid, as this would lead to a sub-optimal solution. As a consequence, it should be possible to curtail PV production. To achieve both these aspects, the following equation is introduced

$$\sum_{c=1}^{\mathrm{C}} \sum_{i=1}^{\mathrm{N}} \frac{1}{\eta_{\mathrm{MPPT}}} \cdot P_{\mathrm{PV\text{-}EV}_{i,c,t}} + \frac{1}{\eta_{\mathrm{MPPT}} \cdot \eta_{\mathrm{inv}}} \cdot P_{\mathrm{PV\text{-}grid}_t} \leq \mathrm{P}_{\mathrm{PV}_t}^{\max} \qquad \forall t \tag{3.3.17}$$

Subject to

$$P_{\mathrm{PV\text{-}EV}_{i,c,t}} \geq 0 \ \text{ if } t_{\mathrm{arrival}_i} < t < t_{\mathrm{departure}_i} \text{ and} \qquad \forall i,c$$

$$P_{\mathrm{PV\text{-}EV}_{i,c,t}} = 0 \ \text{ if } t < t_{\mathrm{arrival}_i} \text{or} \, t > t_{\mathrm{departure}_i} \text{ and} \qquad \forall i,c$$

$$P_{\mathrm{PV\text{-}grid}_t} \geq 0 \qquad \forall i,c,t.$$

In eq. (3.3.17), $P_{\mathrm{PV\text{-}grid}_t}$ is multiplied with both the inverse of η_{MPPT} and η_{inv}. The reason for this is that this variable does not occur in the power balance, which will be explained in the following section. In addition to this, details regarding η_{inv} will be given as well.

3.3.3. The grid

Similarly as in section 3.3.1, it is necessary to impose constraints upon the maximum power fed to and drawn from the grid. As presented in table 3.1, this too is limited to 10 kW. Further, since charging and discharging power are already constrained by binary variables it is not necessary to impose these on power exchange with the grid. Therefore, the equations governing the aforementioned requirements are formulated as follows

$$0 \leq P^{+}_{\text{grid}_{i,c,t}} \leq s_{i,c,t} \cdot \mathrm{P}^{+,\max}_{\text{grid}_{i,c}} \qquad \forall i,c,t \tag{3.3.18}$$

$$0 \leq P^{-}_{\text{grid}_{i,c,t}} \leq \mathrm{P}^{-,\max}_{\text{grid}_{i,c}} \qquad \forall i,c,t \tag{3.3.19}$$

where grid power is divided into two decision variables $P^{+}_{\text{grid}_{i,c,t}}$ and $P^{-}_{\text{grid}_{i,c,t}}$, which will be elucidated in section 3.3.4. The implication of binary variable $s_{i,c,t}$ in eq. (3.3.18) will be elaborated upon after the introduction of eq. (3.3.21). Further, to rule out the possibility that the energy management system draws power from the grid without EVs present to charge, a constraint needs to be imposed that equates positive grid power to zero during the period that EVs absent.

$$P^{+}_{\text{grid}_{i,c,t}} = 0, \qquad \text{if } t < t_{\text{arrival}_i} \text{ or } t > t_{\text{departure}_i} \ \forall i,c \tag{3.3.20}$$

where eq. (3.3.20) ensures that there will be no power drawn from the grid while there is no EV available. Note that $P^{-}_{\text{grid}_{i,c,t,}}$ can always attain a value, due to the fact that PV power can be fed into the grid when no EVs are present and $P^{-}_{\text{grid}_{i,c,t,}}$ is therefore not equated to zero at any time. Additionally, it is necessary to constrain the sum of power feeds to the grid, i.e. $P^{-}_{\text{grid}_{i,c,t,}}$ and $P_{\text{PV-grid}_t}$ to the maximum that the converter is designed for, i.e. $\mathrm{P}^{-,\max}_{\text{grid}_{i,c}}$. This is formulated as follows

$$P^{-}_{\text{grid}_{i,c,t}} + P_{\text{PV-grid}_t} \leq \left(1 - s_{i,c,t}\right) \cdot \mathrm{P}^{-,\max}_{\text{grid}_{i,c}} \qquad \forall i,c,t. \tag{3.3.21}$$

The binary variable $s_{i,c,t}$ introduced in eqs. (3.3.18) and (3.3.21) is imposed on the system to avoid arbitrage, e.g. in case when the feed-in tariff is higher than the dynamic purchase tariff.

Finally, the power balance can be introduced to guarantee that the energy management system cannot consume or produce more power than is actually available. This equation balances grid power and PV system generation for charging all EVs and will be in the form of

$$\sum P_{\text{in}} = \sum P_{\text{out}} + \sum P_{\text{losses}} \ \forall t. \tag{3.3.22}$$

After plugging in all the aforementioned variables, eq. (3.3.22) can be written in a more complete form as follows

$$\sum_{c=1}^{\mathrm{C}} \sum_{i=1}^{\mathrm{N}} \left(P_{\text{ch}_{i,c,t}} - P_{\text{V2G}_{i,c,t}}\right) = \sum_{c}^{\mathrm{C}} \sum_{i}^{\mathrm{N}} P_{\text{PV-EV}_{i,c,t}} + \sum_{c=1}^{\mathrm{C}} \sum_{i=1}^{\mathrm{N}} \left(\eta_{\text{inv}} \cdot P^{+}_{\text{grid}_{i,c,t}} - \frac{1}{\eta_{\text{inv}}} \cdot P^{-}_{\text{grid}_{i,c,t}}\right) \qquad \forall t \tag{3.3.23}$$

where η_{inv} is the grid-tied inverter efficiency. The value for the efficiency of a grid-tied inverter very much depends on the selected topology, however, a reasonable value is found to be 98% [51], thus $\eta_{\text{inv}} = 0.98$.

Note that this equation is applied at the charging point and consequently, the efficiency for the charging process and battery pack are not included as these are relevant only from the charging point to the EV. Therefore, the efficiencies were included in eq. (3.3.10). Furthermore, $P_{\text{PV-grid}_t}$ does not appear directly in this equation. The reason for this is twofold. First, it does appear, albeit implicitly because of eq. (3.3.17). Since $P_{\text{PV-grid}_t}$ does not participate in the charging of EVs, it need not be directly in the power balance. Second, if the aforementioned variable were to appear as positive on the right hand side in eq. (3.3.23), this would lead to an unwanted solution when minimizing costs. The reason for this is that $P_{\text{PV-grid}_t}$ is also present in eq. (3.3.37), but then as a negative variable since one can sell it and subsequently deduct it from the total costs. Due to the fact that minimizing a negative variable is the same as maximizing the variable, this would imply that an optimal solution would be attained by letting variable $P_{\text{PV-EV}_{i,c,t}}$ be zero for all time and variable $P_{\text{PV-grid}_t}$ not, while actually still charging the EVs with PV power as they would be considered equal. On the other hand, if $P_{\text{PV-grid}_t}$ were to appear as negative on the right hand side in eq. (3.3.23), it would not be correct from a mathematical point of view due to the fact that the variable for power transfer to the grid is subject to $P^{-}_{\text{grid}_{i,c,t}} \geq 0$ during the entire day.

3.3.4. Objective function

The aim of any optimization program is to find the optimal solution of the objective function, either a maximum or a minimum. To this end, different scenarios can be thought of for which the objective function of interest might vary. For example, one could aim to minimize the energy exchange with the main electricity grid and rely more upon the PV system. The objective function for this case study would differ from when one would e.g. like to maximize profit by selling energy to the grid. The case studies of interest for this thesis will be elaborated upon in chapter 4. In the present section, the mathematical representation of the case studies will be introduced.

1. Minimize energy exchange

The first case aims to minimize the energy exchanged with the grid for time horizon T. Since the aim is to minimize the energy exchange with the grid, $P_{\text{grid}_{i,c,t}}$ is to be multiplied with the amount of time over which the minimization ought to take place, as stated in eq. (3.3.12). Furthermore, realizing that $P_{\text{grid}_{i,c,t}}$ can be both positive and negative and the fact that minimizing a negative number would yield an undesired solution, the objective function is to be formulated as follows

$$\text{minimize } \mathrm{E}_{\text{grid}} = \sum_{t=1}^{\mathrm{T}} \sum_{c=1}^{\mathrm{C}} \sum_{i=1}^{\mathrm{N}} \left| P_{\text{grid}_{i,c,t}} \right| \cdot \Delta t + \sum_{t=1}^{\mathrm{T}} P_{\text{PV-grid}_t} \cdot \Delta t. \tag{3.3.24}$$

However, an absolute value would create a non-linear problem as can be seen in eq. (3.3.25)

$$\left| P_{\text{grid}_{i,c,t}} \right| = \sqrt{\left(P_{\text{grid}_{i,c,t}} \right)^2} \tag{3.3.25}$$

and thus $\left| P_{\text{grid}_{i,c,t}} \right|$ needs to be reformulated such that it is possible to find a solution using linear programming. The solution to this problem is to define two positive variables $P^+_{\text{grid}_{i,c,t}}$ and $P^-_{\text{grid}_{i,c,t}}$ such that

$$\begin{aligned}
& P_{\text{grid}_{i,c,t}} = P^+_{\text{grid}_{i,c,t}} - P^-_{\text{grid}_{i,c,t}} && \forall i, c, t \qquad (3.3.26)\\
& \text{Subject to} && \\
& P^+_{\text{grid}_{i,c,t}} \geq 0 && \forall i, c, t \\
& P^-_{\text{grid}_{i,c,t}} \geq 0 && \forall i, c, t
\end{aligned}$$

where it should noted that in this case the efficiency is not incorporated, since this was already done in eq. (3.3.23).

Since the aim is to minimize the energy exchanged with the grid as defined in eq. (3.3.24), this can be formulated as follows

$$\text{minimize } \sum_{t=1}^{\mathrm{T}} \sum_{c=1}^{\mathrm{C}} \sum_{i=1}^{\mathrm{N}} P^+_{\text{grid}_{i,c,t}} \cdot \Delta t \text{ and} \tag{3.3.27}$$

$$\text{minimize } \sum_{t=1}^{\mathrm{T}} \sum_{c=1}^{\mathrm{C}} \sum_{i=1}^{\mathrm{N}} P^-_{\text{grid}_{i,c,t}} \cdot \Delta t \tag{3.3.28}$$

where the latter term in eq. (3.3.24) remains.

By combining eqs. (3.3.27) and (3.3.28), the objective function becomes

$$\text{minimize } \mathrm{E}_{\text{grid}} = \sum_{t=1}^{\mathrm{T}} \sum_{c=1}^{\mathrm{C}} \sum_{i=1}^{\mathrm{N}} \left(P^+_{\text{grid}_{i,c,t}} + P^-_{\text{grid}_{i,c,t}} \right) \cdot \Delta t + \sum_{t=1}^{\mathrm{T}} P_{\text{PV-grid}_t} \cdot \Delta t. \tag{3.3.29}$$

Moreover, as a consequence of eq. (3.3.29), another interesting outcome can be observed. Reformulating eq. (3.3.23) yields

$$\sum_{c=1}^{C}\sum_{i=1}^{N}\left(\eta_{\text{inv}}\cdot P^{+}_{\text{grid}_{i,c,t}}-\frac{1}{\eta_{\text{inv}}}\cdot P^{-}_{\text{grid}_{i,c,t}}\right)=\sum_{c=1}^{C}\sum_{i=1}^{N}\left(P_{\text{ch}_{i,c,t}}-P_{\text{V2G}_{i,c,t}}\right)-\sum_{c=1}^{C}\sum_{i=1}^{N}\eta_{\text{MPPT}}\cdot P_{\text{PV-EV}_{i,c,t}}\,\forall t. \tag{3.3.30}$$

It can be seen that by minimizing the absolute power exchange with the main electricity grid one implicitly minimizes the absolute power exchange with the EVs while maximizing PV self-consumption, since minimizing a negative objective is similar to maximizing the objective. Further clarification of this can be achieved by plugging eq. (3.3.30) into eq. (3.3.29), which results in

$$\text{minimize } \mathrm{E}_{\text{grid}}=\sum_{t=1}^{T}\sum_{c=1}^{C}\sum_{i=1}^{N}\left(P_{\text{ch}_{i,c,t}}+P_{\text{V2G}_{i,c,t}}-P_{\text{PV-EV}_{i,c,t}}\right)\cdot\Delta t+\sum_{t=1}^{T}P_{\text{PV-grid}_t}\cdot\Delta t \tag{3.3.31}$$

where $P_{\text{ch}_{i,c,t}}$ and $P_{\text{V2G}_{i,c,t}}$ are added to each other, similar as in eq. (3.3.29).

Essentially, eq. (3.3.31) minimizes the difference between the energy used by the EVs and the output of the PV system, while simultaneously minimizing the PV energy feed into the grid, basically curtailing $P_{\text{PV-grid}_t}$. As a conclusion, it can be stated that minimizing the energy exchange with the grid has the implication that PV self-consumption is maximized.

2. Minimize total costs

According to a study performed by IBM Institute for Business Value, 48% of the consumers stated that sustainability concerns are the primary driver for the transition from ICE vehicles to EVs. However, 71% of the consumers found that the primary driver was the possibility of innovative pricing models and lower overall costs [38]. Therefore, if EV owners would have the possibility of charging their EVs with virtually free PV power and perhaps even sell some energy back through V2G when the price is high enough, this would drive down overall costs further and as a consequence EV ownership would become more appealing. Therefore, it is interesting to examine the case where charging costs are minimized.

First, it is necessary to define charging costs C_{ch} and discharging revenues R_{dis}. When fig. 3.1 and eq. (3.3.23) are examined in detail, the factors that directly influence C_{ch} and R_{dis} can be deduced. However, perhaps an illustrative example might assist in a better understanding. Suppose $P_{\text{PV-EV}_{1,1,12}}$ = 3 kW there is but one EV available for charging, at the first charging point. Assume the EV will be available for exactly 1 hour, requires 7 kWh and Δt is 1 hour. The latter implies that the energy output of the PV system is 3 kWh and $P_{\text{ch}_{1,1,12}}$ = 7 kW. Plugging these values into eq. (3.3.23) and, for the sake of simplicity, assuming no losses would yield

$$\begin{aligned}P_{\text{ch}_{1,1,12}}-P_{\text{V2G}_{1,1,12}}&=P_{\text{PV-EV}_{1,1,12}}+P^{+}_{\text{grid}_{1,1,12}}-P^{-}_{\text{grid}_{1,1,12}}\\ 7\text{kW}&=3\text{kW}+P^{+}_{\text{grid}_{1,1,12}}\\ P^{+}_{\text{grid}_{1,1,12}}&=4\text{kW}.\end{aligned} \tag{3.3.32}$$

Therefore, when considering charging costs C_{ch} it is necessary to look at $P^{+}_{\text{grid}_{i,c,t}}$ and $P_{\text{PV-EV}_{i,c,t}}$ separately since their marginal costs will not be the same. Furthermore, a division needs to be made between PV power fed to the grid or EVs, as specified in eq. (3.3.17).

Suppose now that instead, the same EV has 1 kWh to spare and could sell that to the grid through V2G, while all other data remains the same as in the example above. However, due to the fact that there is a surplus of energy, Then, the power balance will look as follows

$$\begin{aligned}P_{\text{ch}_{1,1,12}}-P_{\text{V2G}_{1,1,12}}&=P_{\text{PV-EV}_{1,1,12}}+P^{+}_{\text{grid}_{1,1,12}}-P^{-}_{\text{grid}_{1,1,12}}\\ -1\text{kW}&=0\text{kW}-P^{-}_{\text{grid}_{1,1,12}}\\ P^{-}_{\text{grid}_{1,1,12}}&=1\text{kW}.\end{aligned} \tag{3.3.33}$$

Thus, when one wants to calculate the revenues made by selling back to the grid from the perspective of the EV owners, $P^{-}_{\text{grid}_{i,c,t}}$ has to be considered, since eq. (3.3.17) will take into account the surplus of PV energy being sold to the grid. Another important remark regarding V2G operation is battery degradation. According to a study, the capacity lost per normalized Wh was found to be rather low: -6.0 · 10^{-3}% for driving tasks and -2.7 · 10^{-3}% for V2G tasks [75]. However, as a final remark the authors pointed out that if V2G is more intermittent in its nature, the lost capacity might be significantly higher. Degradation costs used in this thesis are adapted from [99], which in turn based its findings on [75], where it is assumed that these costs are constant and amount to \$0.042 per kWh, or 0.038 €/kWh. Additionally, a similar value can be deduced from [72], where linear regression was applied on data describing the relation between battery life and the number of cycles. Furthermore, the author formulated the degradation cost equation as a function of a charge and discharge cycle of χ kWh: $\mathrm{C}^{\chi} = \left|\frac{k}{100}\right| \frac{\chi}{\mathrm{B}} \mathrm{C}^{\mathrm{B}}$ where k represents the slope of the linear regression, B the battery capacity and C^{B} the battery pack cost. It should be noted that degradation costs are denoted by λ_{deg}.

In order to calculate total costs (TC) incurred from the charging and discharging processes, the revenues made through V2G minus battery degradation costs need to be subtracted from the costs related to energy taken from the grid and PV system as follows

$$\mathrm{C}_{\text{ch}} = \sum_{t=1}^{\mathrm{T}} \sum_{c=1}^{\mathrm{C}} \sum_{i=1}^{\mathrm{N}} \lambda_{\text{G2V}_t} \cdot P^{+}_{\text{grid}_{i,c,t}} \cdot \Delta t + \sum_{t=1}^{\mathrm{T}} \sum_{c=1}^{\mathrm{C}} \sum_{i=1}^{\mathrm{N}} \lambda_{\text{PV}_t} \cdot P_{\text{PV-EV}_{i,c,t}} \cdot \Delta t \tag{3.3.34}$$

$$\mathrm{R}_{\text{dis}} = \sum_{t=1}^{\mathrm{T}} \sum_{c=1}^{\mathrm{C}} \sum_{i=1}^{\mathrm{N}} \left(\lambda_{\text{FIT}_t} - \lambda_{\text{deg}}\right) \cdot P^{-}_{\text{grid}_{i,c,t}} \cdot \Delta t \tag{3.3.35}$$

where λ_{G2V_t}, λ_{FIT_t} and λ_{PV_t} represent the marginal cost of energy bought from the grid, energy sold to the grid (feed-in tariff) and energy bought from the PV system, respectively.

Suppose the solar carport that the employees use to charge their EVs is owned by the company for which the employees work. In that case, it could be argued that to promote EV ownership, the revenues made by selling energy to the grid produced by the PV system could be added to the revenues made by V2G operation to drive charging costs down further. The subsequent equation for the revenues can be formulated as follows

$$\mathrm{R}_{\text{dis}} = \sum_{t=1}^{\mathrm{T}} \sum_{c=1}^{\mathrm{C}} \sum_{i=1}^{\mathrm{N}} \left(\lambda_{\text{FIT}_t} - \lambda_{\text{deg}}\right) \cdot P^{-}_{\text{grid}_{i,c,t}} \cdot \Delta t + \sum_{t=1}^{\mathrm{T}} \left(\lambda_{\text{FIT}_t} - \lambda_{\text{PV}_t}\right) \cdot P_{\text{PV-grid}_t} \cdot \Delta t. \tag{3.3.36}$$

Finally, the objective function will then become

$$\begin{aligned} &\text{minimize TC} = \mathrm{C}_{\text{ch}} - \mathrm{R}_{\text{dis}} \\ &\text{minimize TC} = \sum_{t=1}^{\mathrm{T}} \sum_{c=1}^{\mathrm{C}} \sum_{i=1}^{\mathrm{N}} \lambda_{\text{G2V}_t} \cdot P^{+}_{\text{grid}_{i,c,t}} \cdot \Delta t + \sum_{t=1}^{\mathrm{T}} \sum_{c=1}^{\mathrm{C}} \sum_{i=1}^{\mathrm{N}} \lambda_{\text{PV}_t} \cdot P_{\text{PV-EV}_{i,c,t}} \cdot \Delta t + \ldots \\ &- \sum_{t=1}^{\mathrm{T}} \sum_{c=1}^{\mathrm{C}} \sum_{i=1}^{\mathrm{N}} \left(\lambda_{\text{FIT}_t} - \lambda_{\text{deg}}\right) \cdot P^{-}_{\text{grid}_{i,c,t}} - \sum_{t=1}^{\mathrm{T}} \left(\lambda_{\text{FIT}_t} - \lambda_{\text{PV}_t}\right) \cdot P_{\text{PV-grid}_t} \cdot \Delta t. \end{aligned} \tag{3.3.37}$$

The table 3.2 presents the values related to efficiencies η and marginal prices λ. The marginal prices will be further elaborated upon in chapter 4.

3.4. Conclusion

Defining the optimization variables, constraints and objective functions is perhaps the most challenging part of this thesis. Applying constraints can have far-reaching implications that one might not immediately consider. The goal of this chapter was therefore to shine light upon the presented mathematical framework describing the solar carport and its underlying assumptions. A final remark should be made here since any charging process is non-linear, i.e. when the battery is approaching its full capacity, the charging rate is lowered. However, regarding the charging process as linear is generally accepted in scientific literature. The functioning of the EMS is depicted in the flowchart below, fig. 3.2, from which it can be observed that a feedback loop has been implemented. More specifically, the EMS will be updated every fifteen minutes so that the

Table 3.2: Overview of parameter values.

Parameter	Value
η_{ch}	0.90
η_{dis}	0.90
η_{MPPT}	0.98
η_{inv}	0.98
λ_{deg}	€0.038 per kWh
λ_{G2V_t}	Scenario dependent
λ_{FIT_t}	Scenario dependent
$\lambda_{\text{PV-EV}_t}$	€0.097 per kWh [13]
$\lambda_{\text{PV-grid}_t}$	€0.097 per kWh [13]

accuracy of the solar power forecast is improved and consequently the accuracy of the optimization will be improved. In addition, an overview of all defined optimization variables, constraints and objective functions is given.

Optimization variables

$$
\begin{aligned}
&u_{i,c,t} && \forall i,c,t\\
&v_{i,c,t} && \forall i,c,t\\
&D^{\text{ch},+}_{i,c,t} && \forall i,c,t\\
&D^{\text{ch},-}_{i,c,t} && \forall i,c,t\\
&D^{\text{dis},+}_{i,c,t} && \forall i,c,t\\
&D^{\text{dis},-}_{i,c,t} && \forall i,c,t\\
&P_{\text{V2G}_{i,c,t}} && \forall i,c,t\\
&P_{\text{ch}_{i,c,t}} && \forall i,c,t\\
&P^{+}_{\text{grid}_{i,c,t}} && \forall i,c,t\\
&P^{-}_{\text{grid}_{i,c,t,}} && \forall i,c,t\\
&P_{\text{PV-EV}_{i,c,t}} && \forall i,c,t\\
&P_{\text{PV-grid}_t} && \forall t
\end{aligned}
$$

Constraints

$$
\begin{aligned}
&0 \le P_{\text{ch}_{i,c,t}} \le u_{i,c,t} \cdot \mathrm{P}^{\max}_{\text{ch}_{i,c}} && \forall i,c,t\\
&0 \le P_{\text{V2G}_{i,c,t}} \le v_{i,c,t} \cdot \mathrm{P}^{\max}_{\text{V2G}_{i,c}} && \forall i,c,t\\
&\sum_{i=1}^{\mathrm{N}} u_{i,c,t} + \sum_{i=1}^{\mathrm{N}} v_{i,c,t} \le 1 && \forall c,t\\
&u_{i,c,t} - u_{i,c,t-1} = D^{\text{ch},+}_{i,c,t} - D^{\text{ch},-}_{i,c,t} && \forall i,c,t
\end{aligned}
$$

$$v_{i,c,t} - v_{i,c,t-1} = D^{\text{dis},+}_{i,c,t} - D^{\text{dis},-}_{i,c,t} \qquad \forall i,c,t$$

$$\sum_{t=1}^{T} \left(D^{\text{ch},+}_{i,c,t} + D^{\text{ch},-}_{i,c,t} \right) \leq \mathrm{N}^{\max} \qquad \forall i,c$$

$$\sum_{t=1}^{T} \left(D^{\text{dis},+}_{i,c,t} + D^{\text{dis},-}_{i,c,t} \right) \leq \mathrm{N}^{\max} \qquad \forall i,c$$

$$u_{i,c,t} = 0, \text{if } t < t_{\text{arrival}_i} \text{ or } t > t_{\text{departure}_i} \qquad \forall i,c$$

$$v_{i,c,t} = 0, \text{if } t < t_{\text{arrival}_i} \text{ or } t > t_{\text{departure}_i} \qquad \forall i,c$$

$$P_{\text{EV}_{i,c,t}} = \eta_{\text{ch}} \cdot P_{\text{ch}_{i,c,t}} - \frac{1}{\eta_{\text{dis}}} \cdot P_{\text{V2G}_{i,c,t}} \qquad \forall i,c,t$$

$$EC_{i,c,t} = \begin{cases} EC_{i,c,t-1} + P_{\text{EV}_{i,c,t}}, \text{if } t_{\text{arrival}_i} < t < t_{\text{departure}_i} \ \forall i,c \\ \mathrm{EC}^{\text{departure}}_{i,c} \text{if } t > t_{\text{departure}_i} \ \forall i,c \\ 0, \text{if } t < t_{\text{arrival}_i} \ \forall i,c \end{cases}$$

$$0.2 \cdot \mathrm{EC}^{\max}_{i,c} \leq EC_{i,c,t} \leq \mathrm{EC}^{\max}_{i,c} \qquad \forall i,c,t$$

$$EC_{i,c,t} = \mathrm{EC}^{\text{arrival}}_{i,c} \text{ if } t = t_{\text{arrival}_i} \qquad \forall i,c$$

$$EC_{i,c,t} = \mathrm{EC}^{\text{departure}}_{i,c} \text{ if } t = t_{\text{departure}_i} \qquad \forall i,c$$

$$\sum_{c=1}^{C} \sum_{i=1}^{N} \frac{1}{\eta_{\text{MPPT}}} \cdot P_{\text{PV-EV}_{i,c,t}} + \frac{1}{\eta_{\text{MPPT}} \cdot \eta_{\text{inv}}} \cdot P_{\text{PV-grid}_t} \leq \mathrm{P}^{\max}_{\text{PV}_t} \qquad \forall t$$

$$P_{\text{PV-EV}_{i,c,t}} \geq 0 \ \text{ if } t_{\text{arrival}_i} < t < t_{\text{departure}_i} \qquad \forall i,c$$

$$P_{\text{PV-EV}_{i,c,t}} = 0 \ \text{ if } t < t_{\text{arrival}_i} \text{or} t > t_{\text{departure}_i} \qquad \forall i,c$$

$$P_{\text{PV-grid}_t} \geq 0 \qquad \forall i,c,t$$

$$0 \leq P^{+}_{\text{grid}_{i,c,t}} \leq s_{i,c,t} \cdot \mathrm{P}^{+,\max}_{\text{grid}_{i,c}} \qquad \forall i,c,t$$

$$0 \leq P^{-}_{\text{grid}_{i,c,t}} \leq \mathrm{P}^{-,\max}_{\text{grid}_{i,c}} \qquad \forall i,c,t$$

$$P^{+}_{\text{grid}_{i,c,t}} = 0, \text{if } t < t_{\text{arrival}_i} \text{ or } t > t_{\text{departure}_i} \qquad \forall i,c$$

$$P^{-}_{\text{grid}_{i,c,t}} + P_{\text{PV-grid}_t} \leq \left(1 - s_{i,c,t}\right) \cdot \mathrm{P}^{-,\max}_{\text{grid}_{i,c}} \qquad \forall i,c,t$$

$$\sum_{c=1}^{C} \sum_{i=1}^{N} \left(P_{\text{ch}_{i,c,t}} - P_{\text{V2G}_{i,c,t}} \right) = \sum_{c}^{C} \sum_{i}^{N} P_{\text{PV-EV}_{i,c,t}} + \sum_{c=1}^{C} \sum_{i=1}^{N} \left(\eta_{\text{inv}} \cdot P^{+}_{\text{grid}_{i,c,t}} - \frac{1}{\eta_{\text{inv}}} \cdot P^{-}_{\text{grid}_{i,c,t}} \right) \qquad \forall t$$

$$P_{\text{grid}_{i,c,t}} = P^{+}_{\text{grid}_{i,c,t}} - P^{-}_{\text{grid}_{i,c,t}} \qquad \forall i,c,t$$

Objective functions

$$\text{minimize } \mathrm{E}_{\text{grid}} = \sum_{t=1}^{T} \sum_{c=1}^{C} \sum_{i=1}^{N} \left(P^{+}_{\text{grid}_{i,c,t}} + P^{-}_{\text{grid}_{i,c,t}} \right) \cdot \Delta t + \sum_{t=1}^{T} P_{\text{PV-grid}_t} \cdot \Delta t$$

$$\text{minimize } \mathrm{TC} = \sum_{t=1}^{T} \sum_{c=1}^{C} \sum_{i=1}^{N} \lambda_{\text{G2V}_t} \cdot P^{+}_{\text{grid}_{i,c,t}} \cdot \Delta t + \sum_{t=1}^{T} \sum_{c=1}^{C} \sum_{i=1}^{N} \lambda_{\text{PV}_t} \cdot P_{\text{PV-EV}_{i,c,t}} \cdot \Delta t + \ldots$$

$$- \sum_{t=1}^{T} \sum_{c=1}^{C} \sum_{i=1}^{N} \left(\lambda_{\text{FIT}_t} - \lambda_{\text{deg}} \right) \cdot P^{-}_{\text{grid}_{i,c,t}} - \sum_{t=1}^{T} \left(\lambda_{\text{FIT}_t} - \lambda_{\text{PV}_t} \right) \cdot P_{\text{PV-grid}_t} \cdot \Delta t$$

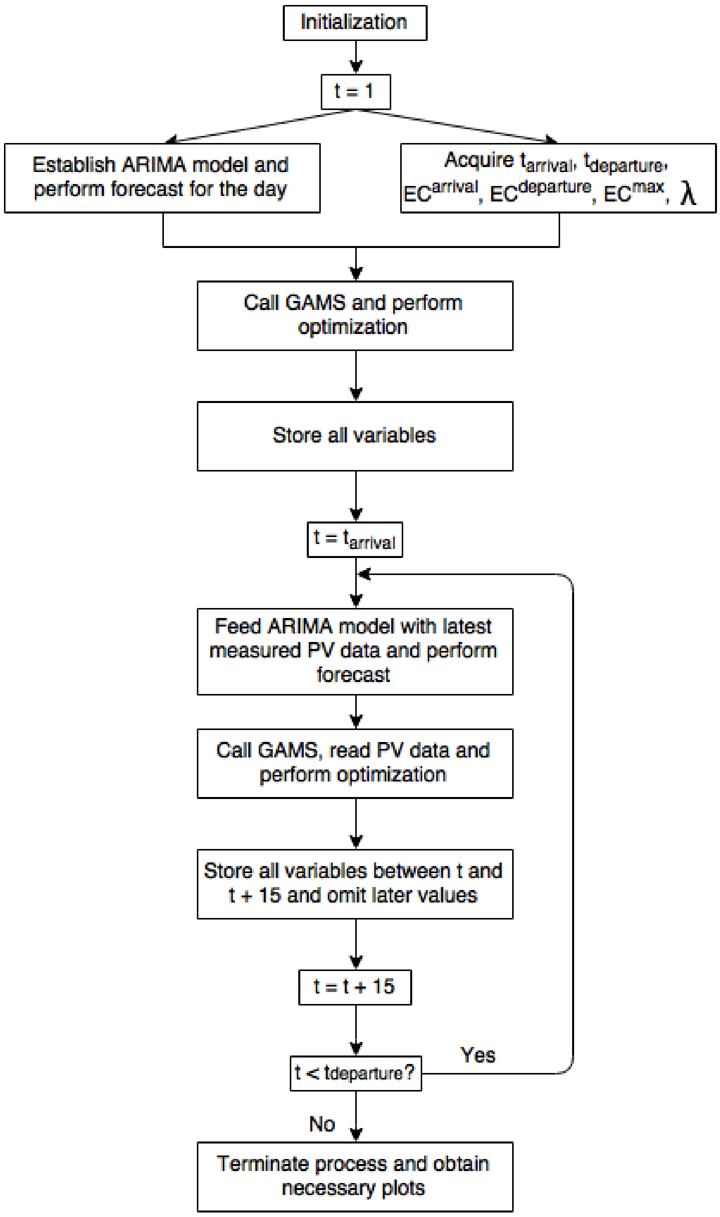

Figure 3.2: Flowchart representing the functioning of the EMS.

4

Data acquisition and scenarios

In order to simulate real-life scenarios, corresponding realistic data regarding driving patterns, EVs and available solar energy have to be obtained. Further, to be able to investigate the proposed energy management system, it is important to e.g. compare it against other means of charging or compare the behavior of the system during summer and winter. Therefore, scenarios are necessary so that the effectiveness can be examined and quantified. This chapter presents the manner in which data is acquired and will justify its accuracy. In addition, different scenarios such as uncontrolled and optimal charging will be elaborated upon and justified.

The present chapter is organized as follows: section 4.1 will be used to go into detail on how the acquisition of data is done. This section is further divided into four subsections, where section 4.1.1 covers data regarding PV, section 4.1.4 examines driving patterns, section 4.1.5 will consist of input data regarding the EVs and finally section 4.1.6 will elaborate upon the energy prices utilized. Then in section 4.2, the different scenarios emulating real-life will be presented. Finally, the conclusions regarding this chapter will be drawn in section 4.3.

4.1. Data acquisition

For this thesis, several input data will be used. These input parameters constitute the basis upon which the energy management system will make its decisions. In order to try and provide a realistic energy management system, forecasting upon historical data will be used instead of deterministic data. The goal of this is to create a more versatile system which could be used for real-life situations. Driving patterns such as arrival time are important to consider as it will describe how much time the energy management system has to charge the available EVs. Further, specifications related to EVs purchased in the Netherlands have to be known, in order to replicate the configuration of e.g. battery capacity and maximum charging power that might be encountered by the solar carport. In addition, as stated in section 3.3.4.2, one of the objectives is to minimize total costs. In order to do this, the price of energy from different sources needs to be known so that available energy can be optimally allocated. How the data is attained will be elaborated upon in the following subsections.

4.1.1. Solar power modeling

In order to increase realism in the proposed energy management system and to allow for possible real-life implementation, it is decided to include forecasting capability. In the literature study it became clear that a model from the Autoregressive Integrated Moving Average (ARIMA) class will be utilized. This class was introduced in 1970 by G. Box and G. Jenkins with the aim of finding the best fit of a time series model to a historical time series. The time series can be of any kind although it has to meet certain requirements, which will be explained later in this section. The modeling approach proposed by Box and Jenkins consists of three steps and the whole process can be regarded as an iterative process. The three steps are as follows

1. Model identification

2. Model estimation

3. Diagnostic checking.

If in the final step the conclusion is drawn that e.g. the residuals of the attained model are not normally distributed, one should go back to either step 1 or 2 in order to pre-process the original time series or assess the validity of the estimated parameters. In order to arrive at a satisfactory model, references [15], [62], [35], [3], [46] and [8] will be used as guidelines throughout this section.

The ARIMA class

Nevertheless, it is fitting to begin with an introduction to the topic for a basic understanding. The ARIMA model consists of three parts, the Auto Regressive (AR), Integrated (I) and Moving Average (MA) models. The former model is a method to describe the state of a process based on its previous states and a stochastic term. The AR model is said to be of order p, that is the number of previous time steps that are taken into account plus a random shock. This can be mathematically represented as follows

$$X_t = \sum_{i=1}^{\mathrm{p}} \phi_i \cdot X_{t-i} + \epsilon_t. \tag{4.1.1}$$

From eq. (4.1.1) it can be seen that the larger the order p, the more previous data is taken into consideration. Therefore, careful fitting is required so that not too much previous data is used as that could compromise the linearity of the acquired relationship as described in eq. (4.1.1) [42]. Further, a polynomial notation is often used to describe the AR(p) model. For this, a backward shift operator b first needs to be introduced as follows

$$b^{-1} X_t = X_{t-1} \text{ or} \tag{4.1.2}$$

$$b^{-k} X_t = X_{t-k} \tag{4.1.3}$$

Then, the summation in eq. (4.1.1) can be expressed in polynomial form as

$$\phi(b) X_t = \epsilon_t \tag{4.1.4}$$

in which ([15])

$$\phi(b) = \sum_{k=0}^{\mathrm{p}} \phi_k \cdot b^{-k}. \tag{4.1.5}$$

Before continuing with the MA model, two things are important to note. First, for the model to be dynamically stable, the roots of the characteristic equation of eq. (4.1.1) should lie outside the unit circle, i.e. larger than one [46]. The characteristic equation looks as follows

$$1 - \phi_1 z - \phi_2 z^2 - ... - \phi_{\mathrm{p}} z^{\mathrm{p}} = 0. \tag{4.1.6}$$

Stationarity can be readily assessed by the requirement that $|\phi_1 + ... + \phi_{\mathrm{p}}| < 1$ [62]. This can be understood by looking at eq. (4.1.1), where $\phi_i > 1$ would yield an explosive series and therefore would not be stationary [15]. Furthermore, in the case that $|\phi_1 + ... + \phi_{\mathrm{p}}| = 1$, the process is said to have a unit root, implying that the the series should be integrated, or differenced, once, which will be explained later in this section. Second, the shock term ϵ_t influences the outcome infinitely far into the future. This is especially clear when one takes a closer look at eq. (4.1.4). It can be seen that every value of X_t depends on ϵ_t. Since X_{t+1} depends on X_t, such a one-time shock will be visible in all future values of X_t although if the process is stationary, the effect tends to zero in the limit.

In order to assess the stationarity of a time series, the autocorrelation function is often used. A time series is said to be stationary if the mean and covariance are finite and independent of time. Mathematically, this can be formulated as follows

$$E[X_t] = \mu \tag{4.1.7}$$
$$cov[X_t, X_{t+l}] = E[(X_t - \mu)(X_{t+l} - \mu)] = \gamma_l \;\; \forall t \tag{4.1.8}$$

where the latter equation is the autocovariance function with γ_0 equals the variance σ^2. Subsequently, the autocovariance function can be standardized to produce the autocorrelation function (ACF) in terms of its coefficients, as can be seen in eq. (4.1.9).

$$\rho_l = \frac{\gamma_l}{\gamma_0}. \tag{4.1.9}$$

A stationary series exhibits a clear pattern in its ACF, either by displaying decreasing exponentially or damped sine or cosine waves [15].

The MA model can be interpreted as a linear regression that depends on white noise or shocks from the previous time steps, depending on the order q. This can be mathematically represented as follows

$$X_t = \sum_{j=1}^{\mathrm{q}} \theta_j \epsilon_{t-j} \tag{4.1.10}$$

where ϵ_t the white noise or shock with zero mean and variance σ_t^2. It can be observed from eq. (4.1.10) that the outcome of the MA model depends directly upon the white noise or shock, whereas the AR model is indirectly influenced by this. Further, these shocks only affect values of X in the current period and q periods in the future, whereas in the AR model this effect can be noticed infinitely far into the future, as stated before.

Using the backward shift operator defined in eq. (4.1.3), it is possible to define eq. (4.1.10) in polynomial form as follows

$$X_t = \theta(b)\epsilon_t \tag{4.1.11}$$

in which ([15])

$$\theta(b) = \sum_{k=0}^{\mathrm{q}} \theta_k b^{-k}. \tag{4.1.12}$$

In contrast to the AR process, the MA process is always stationary [46]. However, a similar constraint on the coefficients is imposed as with the AR process to guarantee the uniqueness of the solution, called the invertibility condition. This is due to the fact that two identical MA(1) processes with θ and θ^{-1} will have exactly the same ACF [15]. Therefore, the coefficients are constrained by $|\theta_1 + ... + \theta_{\mathrm{q}}| < 1$.

Finally, the ARMA model can be constructed. The standard form is presented in eq. (4.1.13) and the polynomial form is presented in eq. (4.1.14).

$$X_t = \sum_{i=1}^{\mathrm{p}} \phi_i \cdot X_{t-i} + \sum_{j=1}^{\mathrm{q}} \theta_j \epsilon_{t-j} + \epsilon_t \tag{4.1.13}$$
$$\phi(b) X_t = \theta(b)\epsilon_t \tag{4.1.14}$$

where the mean of the ARMA process is assumed to be zero or an appropriate transformation is applied.

However, it can occur that the time series of interest is non-stationary. In fact, most time series are non-stationary in one way or another [15] and as a consequence, the aforementioned processes cannot be directly applied. There are several methods to make a non-stationary series stationary and one of these is so-called differencing, implying that instead of looking at X_t, one looks at the difference between X_t and X_{t-1}. In terms of the backward shift operator, this can be formulated as follows

$$X_t - X_{t-1} = (1-b)X_t. \tag{4.1.15}$$

This can be applied several times if necessary, ultimately leading to d differences. The ARIMA(p,d,q) model is presented in its polynomial form in eq. (4.1.16).

$$\phi(b)(1-b)^{\mathrm{d}} X_t = \theta(b)\epsilon_t \tag{4.1.16}$$

where d is the order of differencing. From the equation above it is possible to see that if b were replaced with variable x, the left hand side would have d unit roots, which was the reason for differencing in the first place.

As stated before, a stationary series exhibits a clear pattern in its ACF, either by displaying decreasing exponentially or damped sine or cosine waves. In case differencing is applied to make the time series stationary, it is good practice to perform unit root tests. However, often one applies as many orders of differencing needed until the ACF comes down to zero 'quickly' [15].

Finally, there is the possibility of seasonality or periodicity, i.e. recurring events such as a peak in sales during the holiday season. Solar power is regarded as a recurring event since it possesses diurnal periodicity. Therefore, to model such a recurring event a seasonality term can be added to the ARIMA model which accounts for such periodicity. Reexamining eq. (4.1.3) leads to the conclusion that a similar approach can be utilized to perform seasonal difference to the time series. In this case, the backward shift operator $b^{-\mathrm{s}}X_t = X_{t-\mathrm{s}}$ can be applied, where s is the number of time periods in the considered period, e.g. 12 for the number of months in between each holiday season. Accordingly, eq. (4.1.15) can be reformulated as $X_t - X_{t-\mathrm{s}} = (1-b^{\mathrm{s}})X_t$ to describe the seasonal differencing term. The seasonal ARIMA, or SARIMA, has non-seasonal terms (p, d, q), equivalent to the ARIMA model, and seasonal terms (P, D, Q) and is noted as SARIMA(p, d, q) × (P, D, Q)$_{\mathrm{S}}$ [15]. The polynomial form is presented in eq. (4.1.17).

$$\phi(b)\Phi(b^s)\left(1-b\right)^{\mathrm{d}}\left(1-b^{\mathrm{s}}\right)^{\mathrm{D}} X_t = \theta(b)\Theta(b^{\mathrm{s}})\epsilon_t. \tag{4.1.17}$$

4.1.2. Modeling procedure during a day with high irradiation

Step 1: Model identification

Upon establishing a basic understanding of the ARIMA class models, it is necessary to acquire the data to be modeled. To this end, the website of the Royal Dutch Meteorological Institute (KNMI) is consulted where data regarding irradiance is available with a 1 minute temporal resolution [56]. Further, it is necessary to use the acquired data and simulate the output of a 10 $\mathrm{kW_p}$ system, which is done for three days during May 2012, giving a total of 4320 data points [14]. The result is depicted in fig. 4.1.

It can be seen that the actual power output does not reach the rated power of the PV system. In fact, a recent study showed that one could utilize a converter of 70% of the rated PV power and lose only 3.2% annual yield for a location in the Netherlands, due to the fact that the converter will not shut down in such an event, but produce the power it was rated for [14].

The next step is to difference the time series for seasonality, since it displays diurnal periodicity. To assess the stationarity of the seasonal differenced time series, the ACF and partial ACF (PACF) presented in fig. 4.2 are examined. The PACF shows the partial autocorrelation, i.e. the correlation between e.g. X_t and X_{t-2} corrected for the fact that X_t and X_{t-2} are indirectly correlated through X_{t-1}. It can be observed that the ACF remains significant for a large number of lags, indicative for a non-stationary time series. Therefore, non-seasonal differencing needs to be applied. The resulting ACF and PACF are presented in fig. 4.3, from which it can be seen that except for some significant spikes at lower lags, stationarity is achieved for higher lags. In addition, it is worth noting that the ACF and PACF together display a so-called MA(q) signature, i.e. a cut-off in the ACF and a gradual decay in the PACF. Finally, from fig. 4.4 it can be seen that a seasonal MA(Q) term needs to be included in order to compensate for the seasonal difference. As a conclusion, a SARIMA(p, 1, q) × (0, 1, 1)$_{1440}$ model will suffice, where the remaining orders p and q and accompanying parameters will be estimated in the following section.

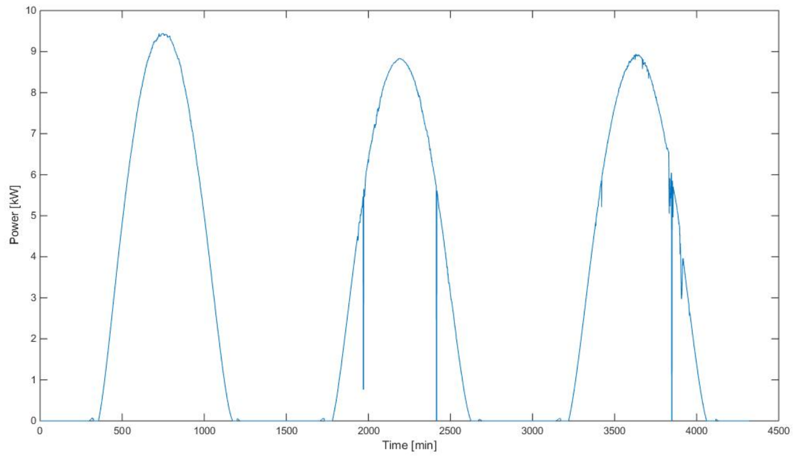

Figure 4.1: Power output of a 10 kW_p PV system during three days in May with a 1 minute temporal resolution.

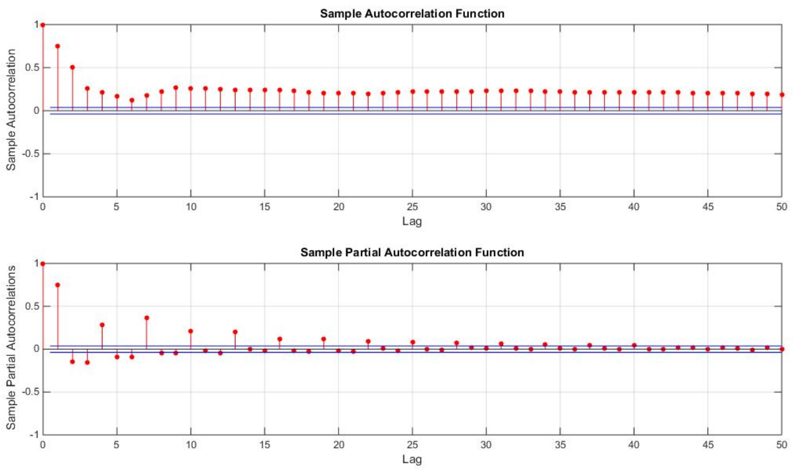

Figure 4.2: ACF and PACF of the seasonally differenced time series.

Step 2: Model estimation

In this section the order of p and q will be determined, after which parameters ϕ_i, θ_j and Θ can be estimated. Each geographical location has its unique amount of parameters and the accompanying values [44]. In order to find the amount of aforementioned parameters, the Bayesian information criterion (BIC) or Schwarz criterion is applied, proposed by Gideon Schwarz in 1978 [86]. This criterion can be applied to select the proper dimensions of a model that fits the observed data without over dimensioning it, which would lead to overfitting. The latter implies that one would develop a model that describes the noise instead of the underlying relationship. The BIC avoids overfitting by introducing a penalty term for the number of parameters in the model, thus ensuring that the minimum amount of parameters will be selected. The BIC is defined in eq. (4.1.18).

$$\text{BIC} = -2 \cdot \ln\left(L\right) + k \cdot \ln\left(n\right) \tag{4.1.18}$$

where L is the likelihood, k the number of parameters to be estimated and n the the size of the time series. The results are a measure of the goodness of fit relative to the other tested models and the best result is therefore not an absolute best. Further, the model with the lowest result is considered to be the best. It should be noted that the details of the BIC are beyond the scope of this thesis. This criterion can easily be implemented

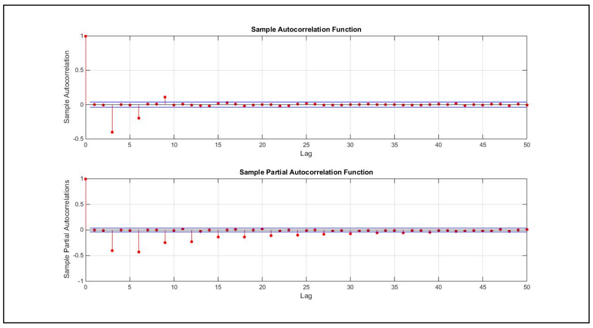

Figure 4.3: ACF and PACF of the seasonal and non-seasonal differenced time series.

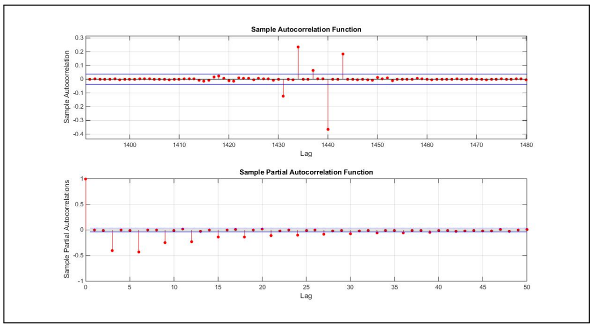

Figure 4.4: ACF and PACF of the seasonal and non-seasonal differenced time series, zoomed in at lag 1440.

Table 4.1: Results of Bayesian information criteria, May.

q	1	2	3	4
p				
1	-1954.3922	-1303.9528	**-3730.2015**	-1289.0756
2	-1303.9512	-1296.6128	-3723.6114	-1281.9904
3	-2674.0734	-2667.8040	-3717.0863	-2652.1147
4	-1289.0757	-1281.9904	-3708.0601	-1269.3426

Table 4.2: Parameters of the SARIMA$(1,1,3)\times(0,1,1)_{1440}$ *model.*

Parameter	**Value**
ϕ_1	0.0130
θ_1	-0.0220
θ_2	$8.94 \cdot 10^{-5}$
θ_3	-0.859
Θ	-0.970
Mean	$7.93 \cdot 10^{-9}$
Variance	0.0244

in Matlab[1] to find the appropriate amount of parameters.

The results are presented in table 4.1. From the results it becomes apparent that the optimal combination would be p = 1 and q = 3. It should be noted that during the subsequent stage an eye should be kept on the possibility of unit root, i.e. $|\phi_1 + ... + \phi_p| < 1$, as BIC does not include this. If $|\phi_1 + ... + \phi_p| \geq 1$ or even very close to unity, it might be better to difference the time series once more. Obviously, the BIC should be applied to the updated time series so as to make an informed decision about the order of p and q.

As the order of the model is determined, it is possible to ascertain the parameters belonging to the respective models, which can be done by the `estimate` function present in Matlab[2]. This function is a maximum likelihood estimator, which is an ordinary least squares estimator under the assumption that the residuals are normally distributed. The Gauss-Markov Theorem states that the ordinary least squares estimate is the best linear unbiased estimator as long as the residuals have constant variance, mean zero and are uncorrelated. The following section will analyze if these requirements are satisfied. The parameters are presented in table 4.2, where it can be seen that no unit root exists and that the mean is close to zero, which is one of the requirements. Therefore, this model can be passed on to the next step.

[1]Mathworks [Internet] Akaike or Bayesian information criteria [update 01/01/2016; visited 03/15/2016] Available from: <http://nl.mathworks.com//help/econ/aicbic.html>

[2]Mathworks [Internet] Estimate ARIMA or ARIMAX model parameters [update 01/01/2016; visited 04/04/2016] Available from: <http://nl.mathworks.com/help/econ/arima.estimate.html>

Step 3: Diagnostic checking

A model of the ARIMA class can be seen as a filter which separates the signal from white noise. The white noise, or error terms, needs to meet the aforementioned requirements, otherwise it can be that the model describes the time series in addition to remaining residuals. In the present section a series of tests will be performed to ascertain the validity of the model. The first way to assess the model is through the graph presented in fig. 4.5. This figure presents several tests, beginning with the standardized residuals. From this particular figure it can be seen that it seems the requirement of constant variance of the residuals is not satisfied. This is a possible sign of heteroscedasticity or non-constant variance, which will be elaborated upon later in this section. Next is the quantile-quantile plot (Q-Q plot), which presents the distribution of the residuals versus a normal distribution. As can be seen, the residuals do not show perfect normal distribution however, it is assumed that this still is acceptable. Finally, the ACF and PACF show no serial correlation in the residuals. To be certain about this statement, the Ljung-Box test is applied which tests for the null hypothesis that the residuals are serially uncorrelated. The results are presented in fig. 4.6, where it can be seen that the Ljung-Box test fails to reject the null hypothesis with high p-values for lags 1 to 40. The conclusion is therefore that the selected model fits the time series well, although there is still a sign of variable variance which needs to be examined. This can be done by plotting the autocorrelation function of the squared residuals and by performing the Ljung-Box and Engle's autoregressive conditional heteroscedasticity (ARCH) tests on the squared residuals [62]. From fig. 4.7 it can be seen that there is no significant peak, revealing that there appears to be no serial correlation. Furthermore, figs. 4.8 and 4.9 show that the null hypothesis of serial uncorrelated squared residuals and no conditional heteroscedasticity respectively, should not be rejected.

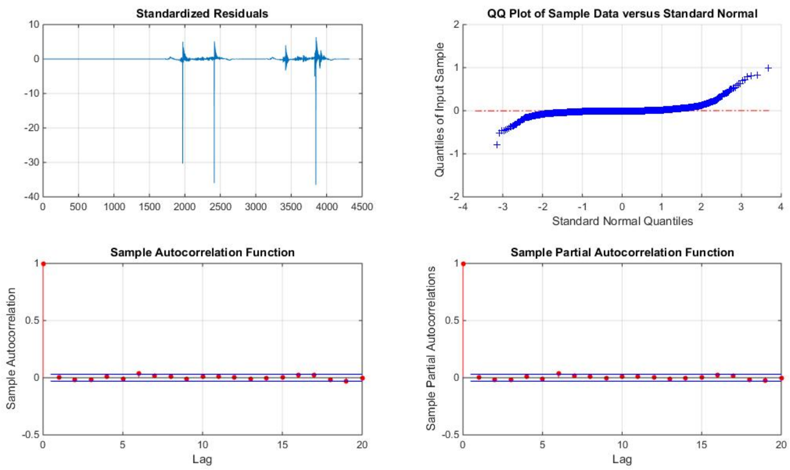

Figure 4.5: Residuals testing of the SARIMA$(1,1,3)\times(0,1,1)_{1440}$ *model.*

Out of sample forecasting

Since it is now valid to say that the developed model describes the time series presented in fig. 4.1 well, it is possible to perform an exemplary "out of sample" forecast. This is done using the `forecast` function in Matlab[3] and the resulting graph is presented in fig. 4.10. At least two points of interest can be noticed from this figure. First, before noon there is quite some variability in the measure PV data, which the forecast fails to incorporate. This can be explained by the fact that the model is trained with relatively smooth days and since it is not updated during the forecast, it has no way of knowing that such variability exists. Second, the 95% confidence interval seem to widen over time. A closer look at the standard deviation, depicted in fig. 4.11, shows that it does increase over time. The RMSE for this forecast is found to be 0.502 kW, whereas the coefficient of determination, R^2, is found to be 0.978. The aforementioned conclusion paves way to assume that short-term forecasts would yield better accuracy, which was also found in [78]. This conclusion justifies the methodology aimed for in this thesis, where the forecast is regularly updated with the latest data so as to

[3]Mathworks [Internet] Forecast ARIMA or ARIMAX process [update 01/01/2016; visited 04/05/2016] Available from: <http://nl.mathworks.com/help/econ/arima.forecast.html>

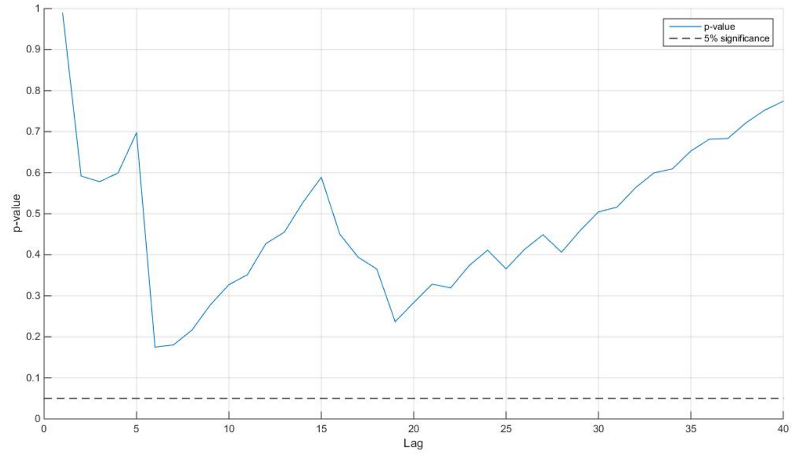

Figure 4.6: Ljung-Box test for serial correlation of the residuals.

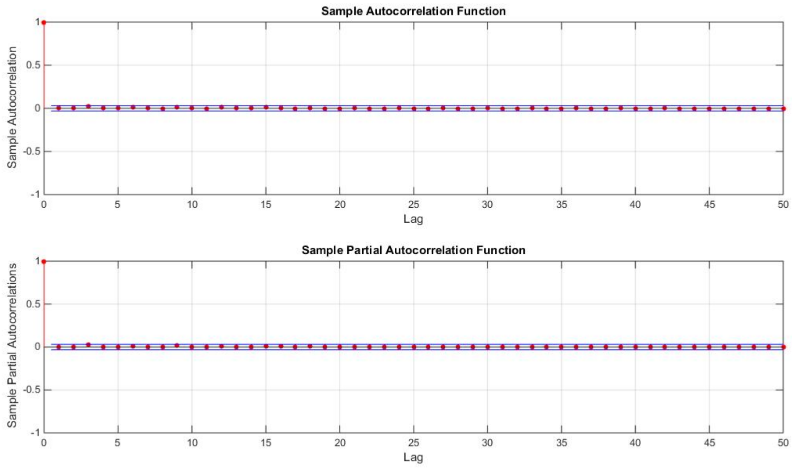

Figure 4.7: ACF and PACF of the squared residuals.

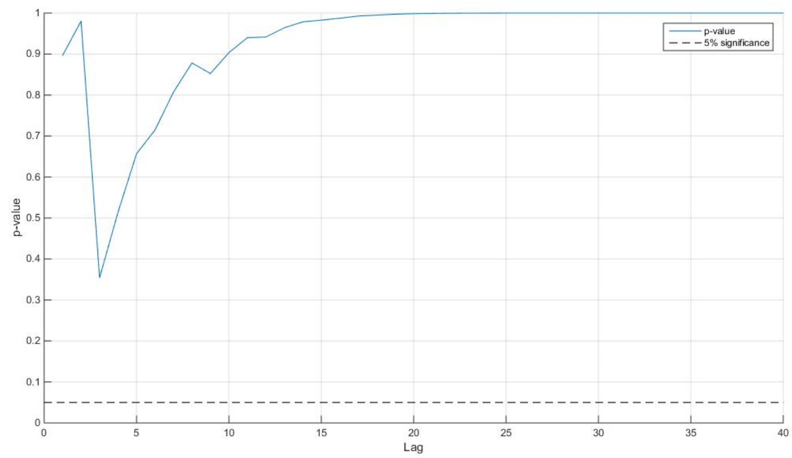

Figure 4.8: Ljung-Box test for the serial correlation of the squared residuals.

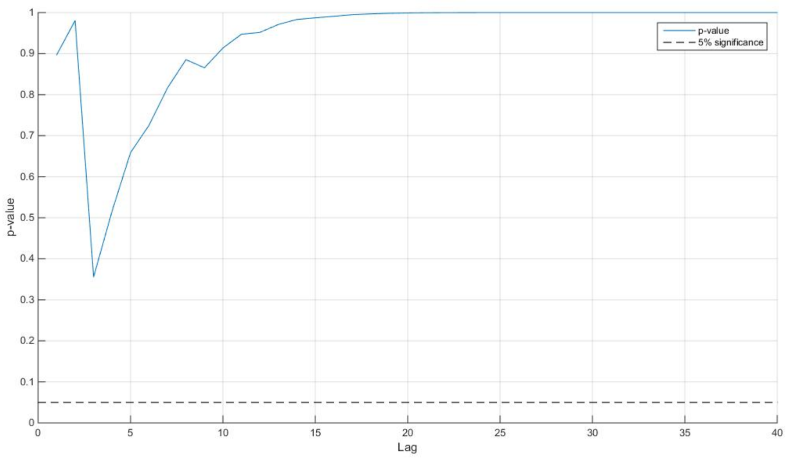

Figure 4.9: Engle's ARCH test for the squared residuals.

acquire an accurate PV power input into GAMS.

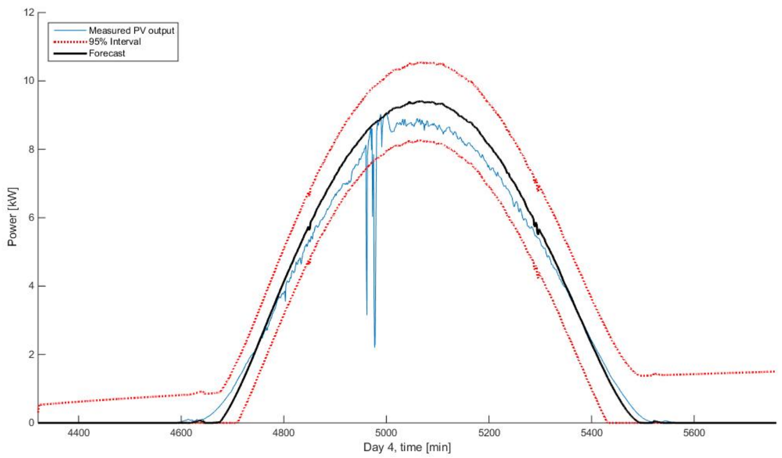

Figure 4.10: Out of sample one day ahead forecast.

To support the above conclusion, an out of sample forecast is also performed with a forecast horizon of 15 datapoints and consequently 15 minutes. Furthermore, the accompanying standard error is also plotted. The figs. 4.12 and 4.13 present the results. From the first graph it can be seen that the forecast and actual PV output are very close. In fact, R^2, is improved to 0.986, whereas the RMSE is reduced to 0.395 kW, which can be regarded as satisfactory results. Also, the period of variability before noon is now captured and incorporated by the model. In addition, the 95% confidence intervals seem to remain closer to the actual forecast which is supported by the result in the second graph. Two interesting points can be noticed from this graph. First, the absolute value of the standard error has decreased from 0.77 kW to 0.27 kW, a decrease of roughly 65%. Second, after each forecast horizon the standard error repeats itself, implying that indeed the low standard error is maintained throughout the entire day and the forecast has improved in terms of accuracy.

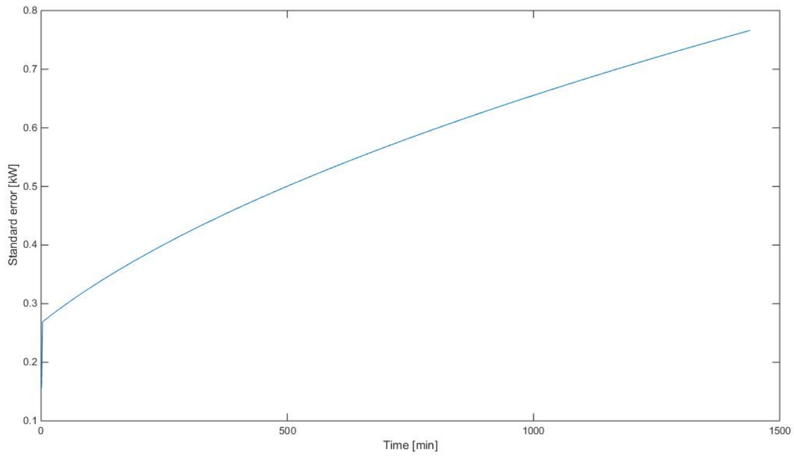

Figure 4.11: Standard deviation of the one day ahead forecast.

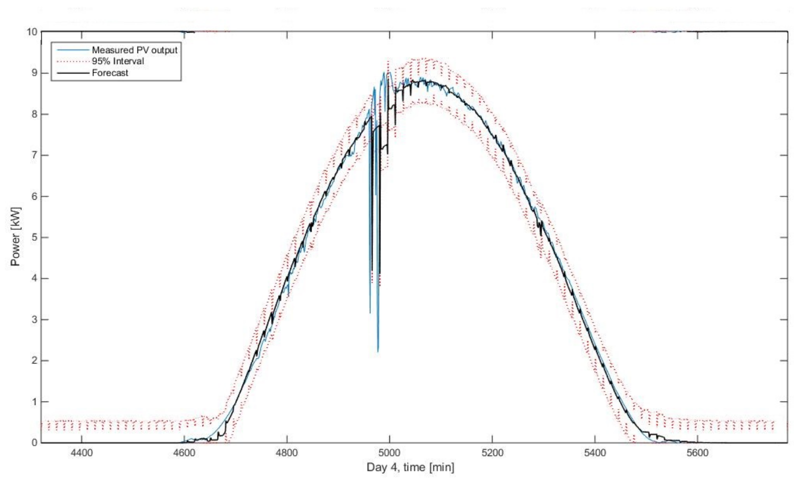

Figure 4.12: Out of sample forecast with forecast horizon of 15 minutes.

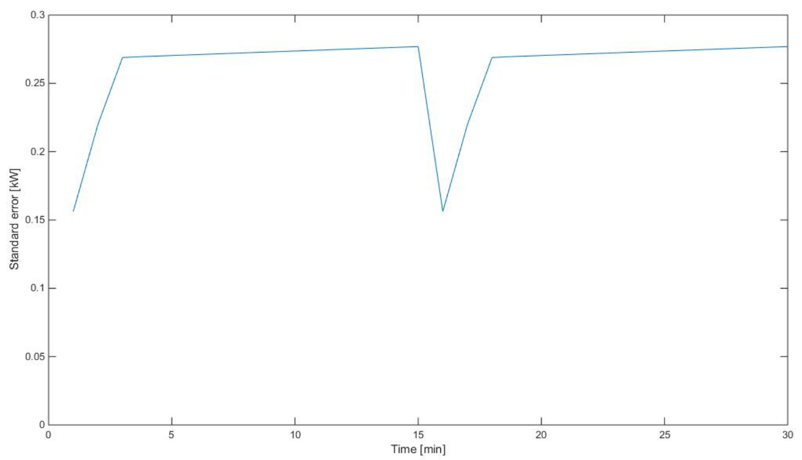

Figure 4.13: Standard deviation of the 15 minute ahead out of sample forecast.

4.1.3. Modeling procedure during a day with low irradiation

Step 1: Model identification

Similar to section 4.1.2, a model of the ARIMA class can be fitted to data of three days in January, of which the graph is presented in fig. 4.14. Again, data is taken from the KNMI [56]. It can be seen that the PV power shows more variability during the day as well as in terms of absolute power between days. With such high temporal resolution, this complicates the fitting procedure as it becomes more likely to attain non-constant variance and non-normal residuals. If this appears to be the case, it will be concluded during diagnostic checking.

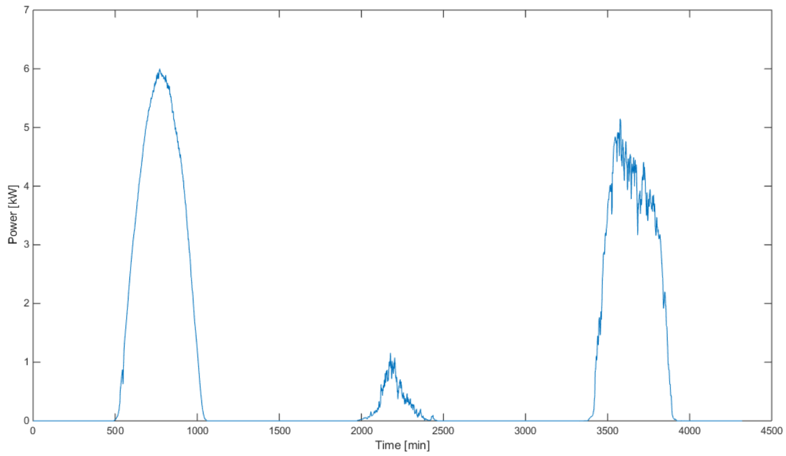

Figure 4.14: Power output of a 10 kW_p PV system during three days in January with a 1 minute temporal resolution.

The fig. 4.15 presents the ACF and PACF, from which it can be seen that the time series is non-stationary. In addition, it can be deduced from the PACF graph that a unit root exists, since the partial autocorrelation at lag 1 equals unity. Due to the higher variability in the current time series than that of May, it is found to be more appropriate to apply two non-seasonal differences instead of one non-seasonal and one seasonal difference, which was done in section 4.1.2. This is supported by results found in another study, in which seasonal differencing resulted in larger errors than non-seasonal differencing for high temporal resolutions [78]. The ACF and PACF of the resulting time series are depicted in fig. 4.16, from which it can clearly be seen that MA terms are required to compensate for the non-seasonal differencing, although the signature less characteristic than that of fig. 4.3. As a result, an ARIMA(p, 2, q) will be utilized, where p and q will be calculated in the subsequent section.

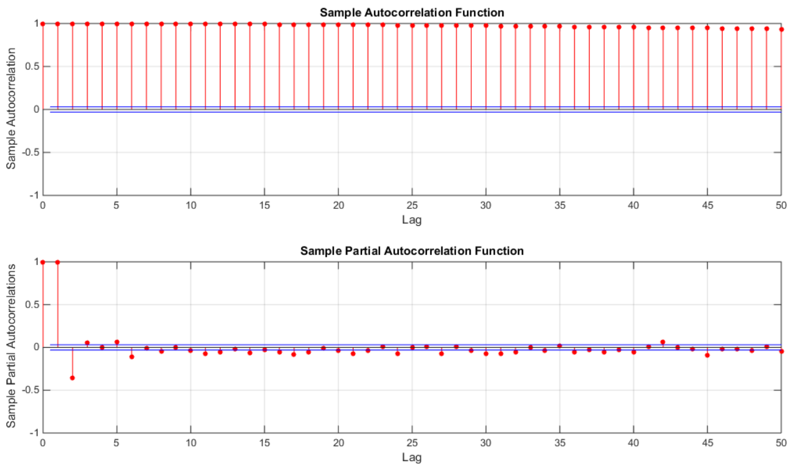

Figure 4.15: ACF and PACF of the January time series.

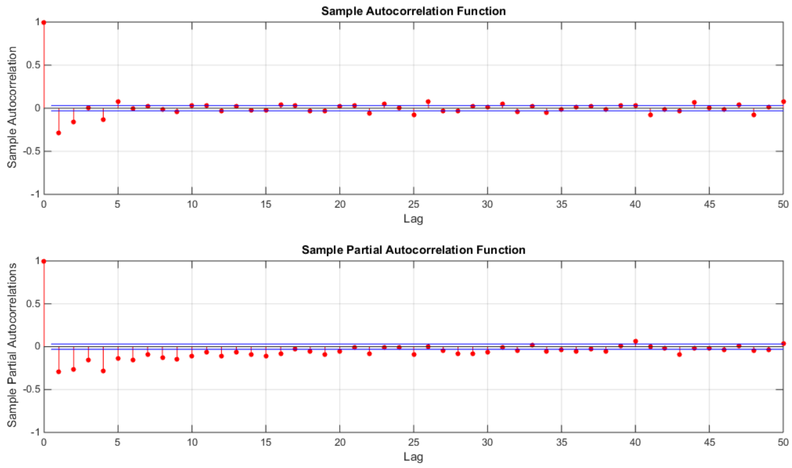

Figure 4.16: ACF and PACF of the non-seasonal differenced time series.

Table 4.3: Results of Bayesian information criteria, January.

q	1	2	3	4
p				
1	-16915.7926	-16944.2143	-16956.5910	-16961.1533
2	-16949.1021	-16959.2867	-16954.4013	-16967.8354
3	-16951.0126	-16959.0738	**-17033.5926**	-17001.9792
4	-17011.9837	-17021.0024	-17026.2637	-17024.1832

Step 2: Model estimation

The order of p and q are determined by the Bayesian information criterion (BIC), explained in section 4.1.2 and formulated in eq. (4.1.18). The results are shown in table 4.3 from which it can be deduced that the optimal combination would be an ARIMA(3,2,3) model. Subsequently, the parameters can be estimated using the `estimate` function in Matlab, which are presented in table 4.4. The results show that there is no unit root present since $|\phi_1 + \phi_2 + \phi_3| < 1$. In addition, $|\theta_1 + \theta_2 + \theta_3| \approx 0.99$, which implies that the estimated parameters are valid since the MA process is unconditionally stable [46]. Therefore, the acquired model can be checked for validity in the following section.

Step 3: Diagnostic checking

In order to assess whether the model obtained in the previous section describes the actual time series and not white noise, a series of diagnostic checks are performed. The fig. 4.17 presents the standardized residuals, Q-Q plot of the residuals versus the standard normal distribution and ACF and PACF of the residuals. Since the days in the time series presented in section 4.1.2 were quite long, it was not necessary to delete the residuals during night time. However, since it is redundant to check the residuals during nighttime, the error terms in the present time series are removed, similar as in [78]. This is done because the days in January are significantly shorter than in May, resulting in greater errors during nighttime.

Table 4.4: Parameters of the ARIMA$(3,2,3)$ model.

Parameter	Value
ϕ_1	0.386
ϕ_2	0.663
ϕ_3	-0.238
θ_1	-1.05
θ_2	-0.746
θ_3	0.803
Mean	$-7.82 \cdot 10^{-10}$
Variance	0.00112

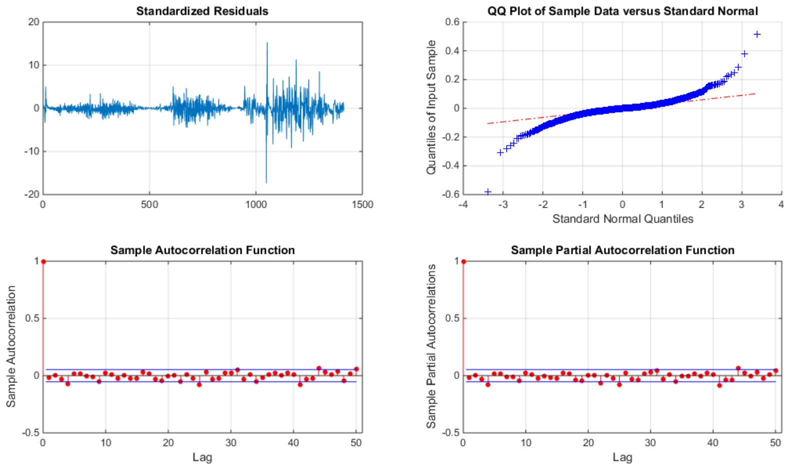

Figure 4.17: Residuals testing of the ARIMA(3,2,3) model.

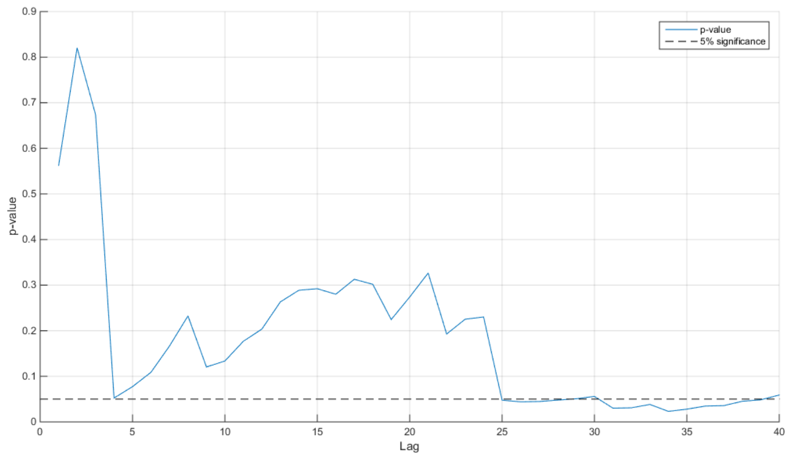

Figure 4.18: Ljung-Box test for serial correlation of the residuals.

The fig. 4.17 shows clear heteroscedasticity of the residuals, violating one of the requirements for the maximum likelihood estimator to provide reliable parameters, according to the Gauss-Markov theorem. As briefly touched upon in section 4.1.2, this can be dealt with by means of an autoregressive conditional heteroscedasticity (ARCH(q)) model, first proposed by Robert Engle in 1982 [27]. However, like the ARMA model being a more general extension of the AR model, Tim Bollerslev proposed the generalized autoregressive conditional heteroscedasticity (GARCH(p,q)) model in 1986 [9]. Remembering that ϵ_t is defined as a white noise process with zero mean and variance σ_t^2, the GARCH(p,q) model can be utilized to model the non-constant variance. This can be formulated as follows [27]

$$\sigma_t^2 = \alpha_0 + \sum_{i=1}^{q} \alpha_i \epsilon_{t-i}^2 + \sum_{i=1}^{p} \beta_i \sigma_{t-1}^2 \tag{4.1.19}$$

Subject to

$\mathrm{p} \geq 0,\ \mathrm{q} > 0$

$\alpha_0 > 0,\ \alpha_i \geq 0$

$\beta_i \geq 0$

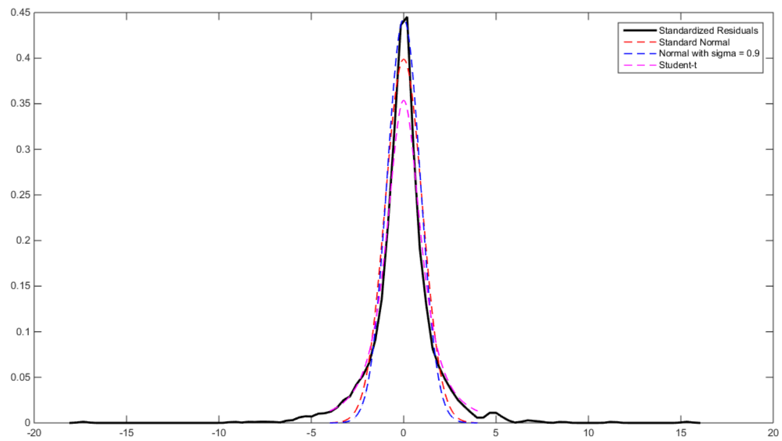

Figure 4.19: Comparison between the distribution of the residuals and several others.

where, in case p is equal to zero, the aforementioned reduces to an ARCH(q) model.

In addition, fig. 4.17 shows the Q-Q plot. It can be seen that the residual distribution shows outliers on both sides than the standard normal distribution, which is also a sign of heteroscedasticity [62]. To support this conclusion, a kernel smoothing estimation is performed on the residuals and compared with a student-t distribution and normal distribution with $\sigma = 0.9$. The result presented in fig. 4.19 shows that the distribution of the residuals encompass features of both and therefore it is assumed that the normality assumption is still valid, albeit that heteroscedasticity needs to be addressed.

Finally from fig. 4.17 it can be seen that there is no serial autocorrelation of the residuals, although there appears to be slight significant autocorrelation at lag 4. However, upon assessing the Ljung-Box test presented in fig. 4.18, it is valid to say that the p-value is still lies above the 5% significance boundary. Furthermore, even though there is a dip in the p-values for lags between 30 and 40, it is assumed that this should pose no problem to the forecasting capabilities of the model.

The subsequent step is to check if incorporating the GARCH(p,q) model is necessary, i.e. if the residuals have non-constant variance. This can be assessed by plotting the ACF and PACF of the squared residuals, performing the Ljung-Box test on the squared residuals and ARCH test on the residuals. The results are presented in figs. 4.20 to 4.22, respectively. As can be seen from fig. 4.20, there is clearly significant autocorrelation in lower lags. In addition, figs. 4.21 and 4.22 show that both the Ljung-Box and Engle's ARCH tests reject the null hypothesis of no ARCH effect. To assess the order of the GARCH(p,q) model, a similar approach as with selecting the order of the ARIMA(p,q) model is utilized, implying that the decision will be based upon the Bayesian information criteria (BIC). It should be noted that in case of a GARCH model, the conditional distribution upon which it can be superimposed can also be selected. The distribution to be selected can be normal or student-t, and several options are presented in table 4.5. The results from the BIC show that GARCH(1,1) with a student-t distribution superimposed is most preferable, which was expected since fig. 4.19 showed that the tails of the residual distribution resembled those of a student-t distribution. The parameters are presented in table 4.6.

To see whether the proposed GARCH(1,1) model is effective in describing the non-constant variance, the foregoing tests are repeated in addition to the Q-Q plot of the residuals versus standard-t distribution. The results are presented in figs. 4.23 to 4.25 and clearly show that the GARCH(1,1) model describes the residuals well. Therefore, the model can be used to forecast, which will be done in the following section.

Out of sample forecasting

Since all the previous steps have been completed and the ARIMA(3,2,3)-GARCH(1,1) model passed all the necessary tests, it can be utilized to forecast. The forecast will cover 15 time steps, i.e. 15 minutes, into the

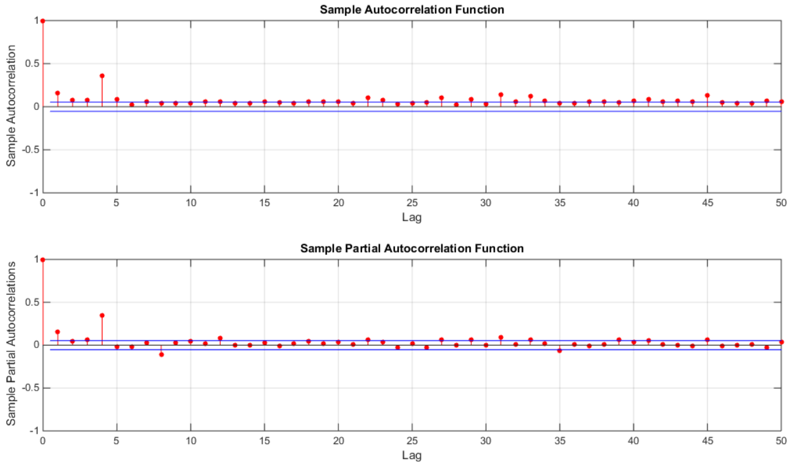

Figure 4.20: ACF and PACF of the squared residuals.

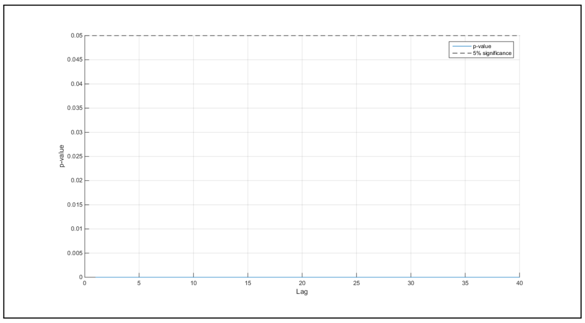

Figure 4.21: Ljung-Box test of squared residuals.

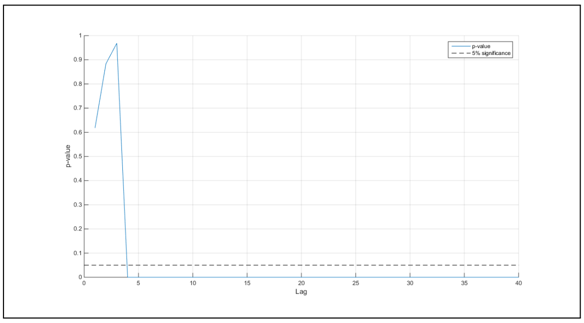

Figure 4.22: Engle's ARCH test of squared residuals.

Table 4.5: Results of Bayesian information criteria for several GARCH models, January.

Model	BIC student-t	BIC normal
GARCH(0,1)	-4974.4931	-4390.4490
GARCH(0,2)	-5095.8639	-4482.1586
GARCH(0,3)	-5165.0378	-4618.3006
GARCH(0,4)	-5232.5317	-4671.0963
GARCH(1,1)	**-5401.4777**	-5053.9764
GARCH(1,2)	-5345.5661	-5053.9764
GARCH(1,3)	-53210925	-5047.9347
GARCH(1,4)	-5303.2414	-5061.3069

Table 4.6: Parameters of the GARCH$(1,1)$ model.

Parameter	Value
α_1	0.152
β_1	0.848
Mean	$2.53 \cdot 10^{-6}$
DoF	6.36

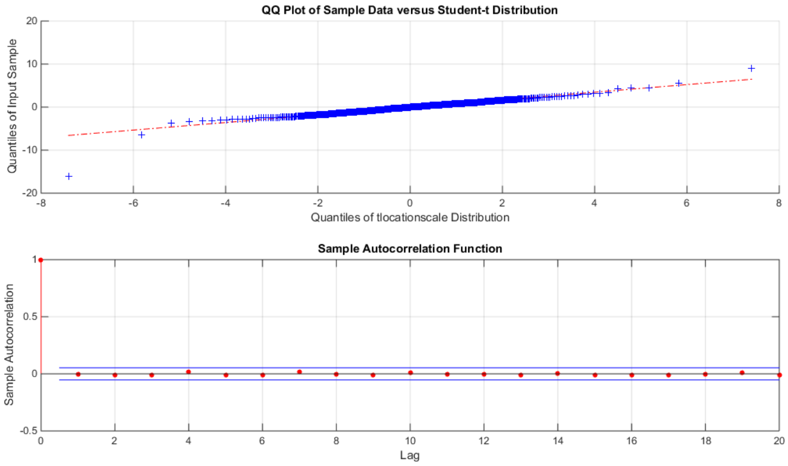

Figure 4.23: ACF and PACF of the squared residuals.

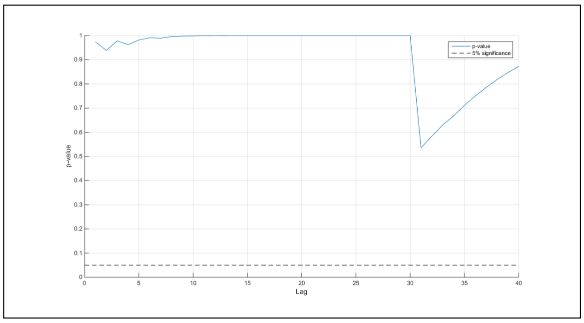

Figure 4.24: Ljung-Box test of the squared residuals.

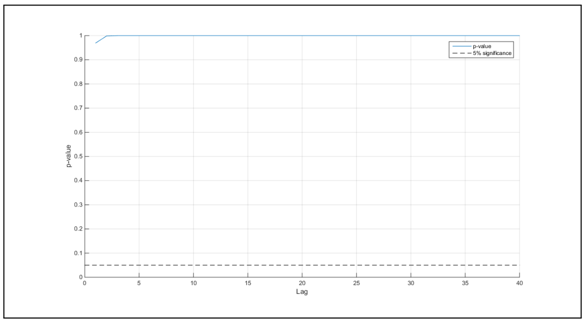

Figure 4.25: Engle's ARCH test for the squared residuals.

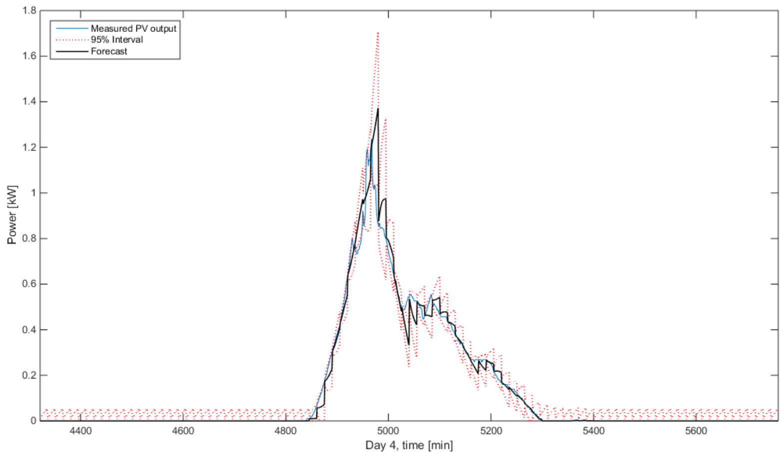

Figure 4.26: Out of sample forecast with forecast horizon of 15 minutes.

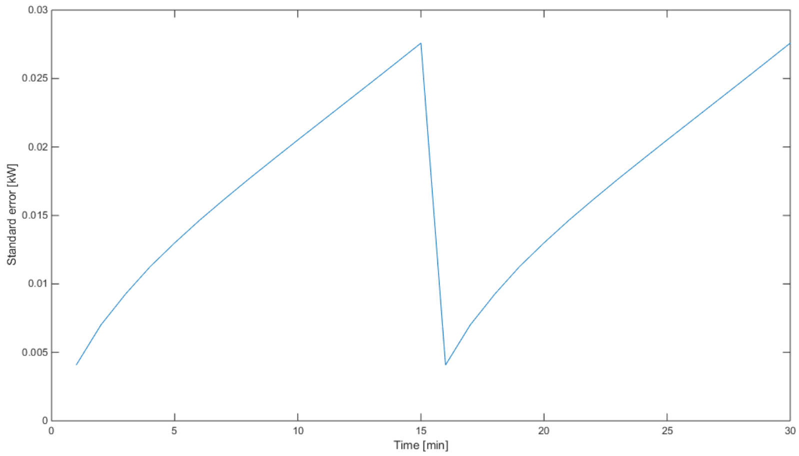

Figure 4.27: Standard deviation of the 15 minute ahead out of sample forecast.

future and will then be compared to the observed data in order to calculate the RMSE and R^2. The forecast and the standard deviation are depicted in figs. 4.26 and 4.27. From the first figure it becomes apparent that the power output during that day is rather low and quite variable, however, the proposed model shows good forecasting properties. The RMSE is calculated to be 0.0429 kW, which is significantly lower than the RMSE calculated in section 4.1.2. However, this is mainly due to the fact that the overall output of the PV system is lower in January. The coefficient of determination, R^2, is found to be 0.970, which is regarded as a satisfactory result. Finally, fig. 4.27 shows the standard deviation of the forecast. In terms of absolute value it is again lower than that of the forecast in May, however, the relative increase from beginning to the end of the forecasting period is significantly larger. This implies that this model would be unfit to forecast for longer horizons, i.e. 2 hours.

4.1.4. Driving patterns

In contrast to real-time PV output, driving behavior is often less difficult to predict as this has a steady, recurring character. The author of [39] used data provided by the Dutch mobility survey (MON) and simulated driving patterns for an average day, as can be seen in fig. 4.28. This figure clearly indicates two peaks during the morning and afternoon commute, at 8 a.m. and 6 p.m. respectively. Further, the author touched upon the fact that with the occurrence of such peaks and a high penetration of EVs, it is possible to estimate when a peak in electricity demand would arise.

The aforementioned results reflect the Dutch motorists and take all vehicles into account. A recent study performed at a North American university campus over a period of 166 weeks focused on driving patterns and charging behavior of EVs, both PHEVs and BEVs. The authors revealed a similar trend regarding driving patterns as specified above, although the arrival and departure times do vary somewhat. It was found that there is a significant peak in the number of arrivals at 10 a.m. and a significant drop of available EVs after 6 p.m., indicating departure time [7]. This is probably due to the fact that the start and finish of a day at a university differ from that of a company. Further, the authors of this study also emphasized the opportunity of charging EVs with local generated PV power. The latter observation provides one of the keystones of this thesis and justifies the investigation of a solar carport at the workplace. The data from these studies will be used for this thesis.

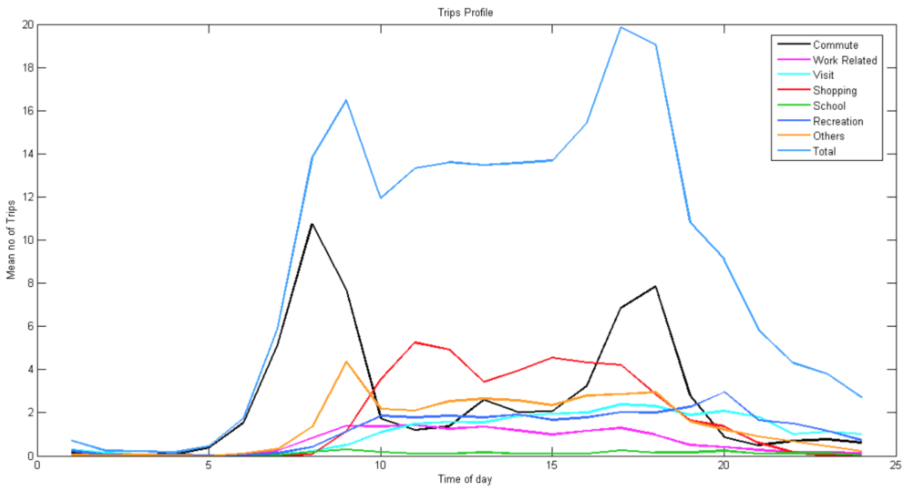

Figure 4.28: Hourly driving patterns, reproduced from [39].

In addition, the author of [39] did a similar analysis for an average week, as can be seen in fig. 4.29. It can be observed that commuting intensity decreases while the week progresses, although the peak during the morning and afternoon commute are still clearly visible. Therefore, it can be established from this figure that the time span of morning and afternoon commute remain constant throughout the week. This conclusion is shared by the study performed in [7], where it was found that the number of EV arrivals at the university campus remains highly constant throughout the week.

When taking the aforementioned data into consideration and assuming a high penetration of EVs, it becomes clear that it is important to develop an energy management system which optimally allocates energy to charge EVs. Even in the case when RESs would not be considered, it is not difficult to imagine that uncontrolled charging could have severe consequences on the stability of the grid [17], [24], [57]. Further, since most EVs are idle between the peaks and the fact that PV output, if any, will be maximum in between these peaks, another keystone of this thesis is provided.

In conclusion, it can be deduced from figs. 4.28 and 4.29 that on average, EVs are available for charging between 8.30 a.m. and 5.30 p.m., which is in accordance with a typical working day in the Netherlands. Further, this is comparable to data found in [63], where the standard deviation of arrival and departure time were taken as 1.1 hour, which will therefore be utilized. The data regarding arrival and departure time are pre-

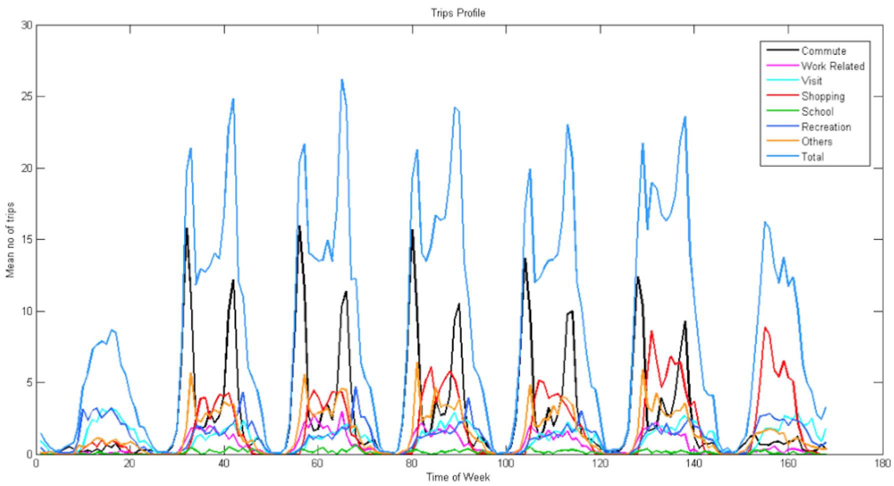

Figure 4.29: Weekly driving patterns, reproduced from [39].

Table 4.7: Arrival and departure time of Dutch motorists.

	Arrival	**Departure**
Average [h]	8.30 a.m.	5.30 p.m.
Standard deviation [h]	1.1	1.1

sented in table 4.7 and will be used as realistic input parameters for this study.

4.1.5. EV data

The Dutch government has expressed the ambition to have 200.000 EVs on the road by 2020 [80]. It should be noted that this figure includes bot BEVs and PHEVs, whereas this thesis makes the distinction between EVs and PHEVs. Currently, there are around 10.000 EVs and roughly 78.000 PHEVs registered in the Netherlands. Further, the three EVs most sold in the Netherlands are: Tesla Model S, Nissan Leaf and Renault Zoe [82]. An overview of the specifications, retrieved from the respective EV manufacturers' websites, is given in table 4.8. As can be deduced from the aforementioned table, 64.3% of the three most sold EVs is a Tesla, 19.4% a Nissan and 16.3% a Renault.

As stated before, the study performed in [7] has accumulated vast amounts of data regarding driving patterns and charging behavior of EVs on a North American university campus. Data regarding driving patterns was elaborated upon in section 4.1.4. However, perhaps even more interesting was the data acquired regarding energy demand of the investigated EVs. It was found that 90.1% of the EVs required between 0 - 16 kWh of energy to charge the battery. In addition, the average energy transfer was 8.53 kWh with a standard deviation of 6.49 kWh. It was concluded that since the size of mainstream batteries lies between 16 - 85 kWh, the parking lots were mainly used by EV owners to extend the range of the EVs.

Table 4.8: Overview of EV specifications.

	Tesla Model S	**Nissan Leaf**	**Renault Zoe**
Battery capacity [kWh]	90	30	22
Energy consumption [kWh/km]	0.164	0.120	0.092
Range [km]	550	250	240
Maximum charging power [kW]	120	50	43
Amount registered [-]	4469	1345	1135

Other important parameters which need to be considered are the energy content of the battery upon arrival and departure. There is little data available regarding energy content upon arrival since this depends upon many variables. In scientific literature however, deterministic values [4] or probability distribution functions are commonly used to represent a range of possible values, ranging from a uniform distribution [54], [61] to a log-normal distribution [90]. For this study the energy content upon arrival and departure shall be represented by a uniform distribution. Further, when taking the aforementioned statistics into consideration and since a maximum of four EVs per charging point applies, it would be reasonable to assume that each EV out of the top three presented in table 4.8 would appear at said charging point and it is decided that the medium sized EV appears twice. As a consequence, if the results found in [7] are to be respected, the boundaries of the uniform distribution need to be selected carefully as the batteries of the EVs in table 4.8 show a large variation in size. The uniform distribution for the energy content upon arrival shall lie between $0.3 \cdot \mathrm{EC}_{i,c}^{\max}$ and $0.5 \cdot \mathrm{EC}_{i,c}^{\max}$. The required energy stored in the battery upon departure will lie between $0.6 \cdot \mathrm{EC}_{i,c}^{\max}$ and $0.8 \cdot \mathrm{EC}_{i,c}^{\max}$. In this way, the maximum energy demanded by a single EV, a Tesla, will be $(0.8 - 0.3) \cdot 90$ kWh = 45 kWh and the minimum energy demanded by a single EV, a Renault, will be $(0.6 - 0.5) \cdot 22$ kWh = 2.2 kWh. As a result, the proposed energy management system will always have to cope with the energy demand specified in [7] and likely more, so that it can be proven that the model can perform not only in case of normal demand, but also in case of high demand.

4.1.6. Marginal costs of energy

In the Netherlands there are currently two possibilities regarding utility energy prices, from the perspective of the consumer. Many houses are still equipped with so-called single meters and therefore always pay the same tariff. The second option is a double meter, which is able to make a distinction between tariffs, e.g. day- and night-time tariff. This implies that during night-time, the consumer pays less than during the day. The reason for this is due to the configuration of the current energy generation system. Electricity producing plants, in the Netherlands these are usually coal plants, are often not flexible and therefore provide the base load for a relatively low tariff, whereas gas plants are used for peak demand at a relatively higher tariff. This is possible since ramp rates of gas power plants are significantly higher than those of coal power plants and can therefore be activated when demand is expected to increase. However, it should be noted that the difference between day- and night tariff in the Netherlands is between 0.02-0.03 €/kWh [29] and may seem trivial. Moreover, since this thesis merely studies day-time charging and discharging, a single tariff will be taken into consideration. Furthermore, the tariff that one receives for feeding electricity back to the grid is the same as the supply price, which is an average of 0.23 €/kWh. Finally, it should be noted that the Netherlands does not utilize a Feed-In Tariff (FIT), but rather a system where the aforementioned meter runs backwards when one is producing more electricity than using. This method is called 'netting' (Dutch: salderen) and at the end of the month consumers pay for consumed minus produced electricity.

Countries such as Germany make use of Feed-In Tariffs (FITs) in order to promote the transition to RESs. The FITs in Germany decrease as levelized costs of electricity by PV decrease, due to a phenomenon called economies of scale. This phenomenon occurs when a market grows and matures, whereby fixed costs can be spread out over more units and production costs decrease. A fact sheet written by the Fraunhofer Institute for Solar Energy Systems specified that currently the average FIT is 0.33 €/kWh, which is for all built PV systems; residential and commercial. Further, it was stated that the current FIT level lies between 0.085 and 0.123 €/kWh, depending on the power output [101]. Unfortunately, no specifications were given regarding the exact FIT and the corresponding power output. Therefore it is assumed that FIT increases proportionally to the size of the PV system and consequently it is assumed that the second FIT is 0.09 €/kWh.

Regarding dynamic tariffs, It should be noted that to enable dynamic tariffs, legislation needs to be adapted. Since 2015, the Dutch government facilitated the possibility for a small scale real-life experiment by changing legislation [55]. Key to this is the fact that operators of local projects will be able to determine their own tariffs. Further, transmission system operators (TSOs) plea to allow variable pricing in order to decrease capital and operational expenditure by increasing local consumption and thus relieving stress on the grid [70]. As dynamic tariffs are not yet implemented, another method to acquire such data is used. The APX group provides a platform in the Netherlands, United Kingdom and Belgium on which the wholesale market can trade power. Information regarding market clearing prices, intra-day and day-ahead hourly energy prices and volumes are readily available online, as can be seen in fig. 4.30[1]. The average energy price, represented by the red line, is 27.86 €/MWh.

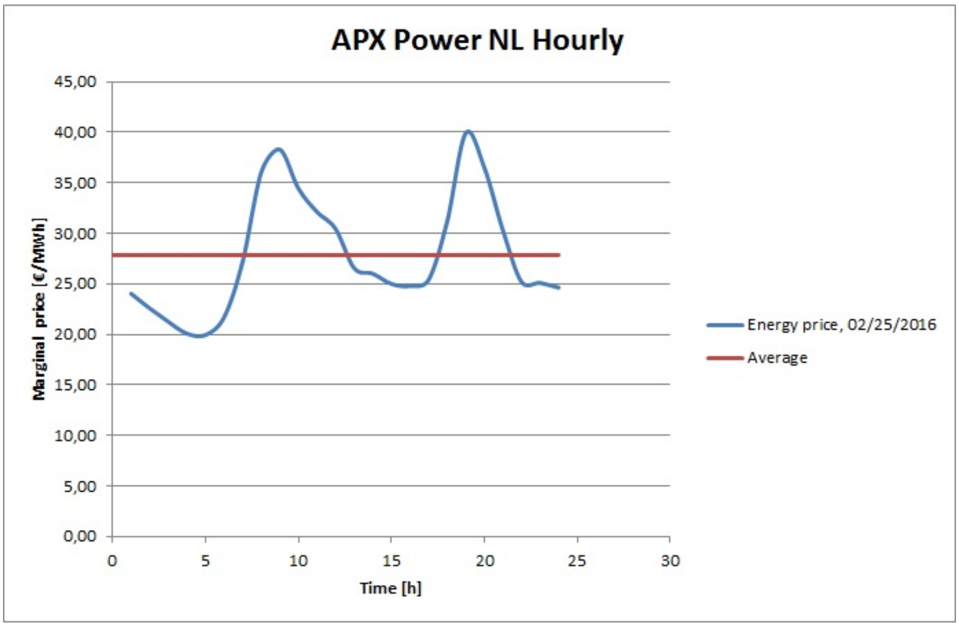

Figure 4.30: Hourly energy prices, data from APX.

However, as can be deduced from the values and units in fig. 4.30, this data cannot be utilized directly in the proposed model. First, division by 1000 is necessary to convert MWh to kWh. Second, the prices presented in the aforementioned figure represent prices on the wholesale market, i.e. without VAT, energy tax, transmission and distribution costs, operation and maintenance costs etc., and therefore need to be adjusted to the average price level. Since the average price in the Netherlands is 0.23 €/kWh, the average of the values seen in fig. 4.30 need to amount to 0.23. This can be done by converting the data to the consumer price level and calculate the average price accordingly. This method is essentially a vertical translation of the graph depicted in fig. 4.30. The resulting dynamic tariff is presented in fig. 4.31.

The marginal costs of the PV system due to capital and operational expenditure is to be considered. In recent studies this aspect is often, either deliberately or not, not taken into account. However, a recent study showed that these costs are far from negligible. While investigating irradiance and capital expenditure in the Netherlands with respect to rooftop PV and a solar carport, the authors found that the marginal costs would be 0.097 and 0.28 €/kWh, respectively [13]. As can be seen in fig. 4.31, this implies that for a substantial part of the day, energy generated by the solar carport is actually more expensive than energy from the grid. Therefore, it is imperative that such costs are incorporated if one is trying to minimize total costs. It should be noted that the marginal costs of the PV system depends strongly on the irradiance and therefore varies per country. In addition it should be noted that in this study a marginal cost of 0.097 €/kWh will be utilized. The reason for this is understandable, since the high costs are due to the construction of the solar carport which are sunk costs and are not directly relevant for the energy calculation. Moreover, all scenarios will also be considered without marginal cost for PV for the same reason.

Finally, battery degradation costs are considered during this study. In section 3.3.4.2, it was stated that the capacity lost per normalized Wh was found to be rather low: $-6.0 \cdot 10^{-3}$% for driving tasks and $-2.7 \cdot 10^{-3}$% for V2G tasks [75]. However, the authors also pointed out that in case of intermittent V2G, lost capacity might be significantly higher. Degradation costs are adapted from [99] and amount to 0.038 €/kWh.

4.2. Scenarios

As can be seen in the previous sections, several variables arise which can be exploited to analyze the effectiveness of the proposed model. The present section is therefore dedicated to examining which scenarios are possible with the aforementioned variable inputs. The outcome will be scenarios that can be used in the

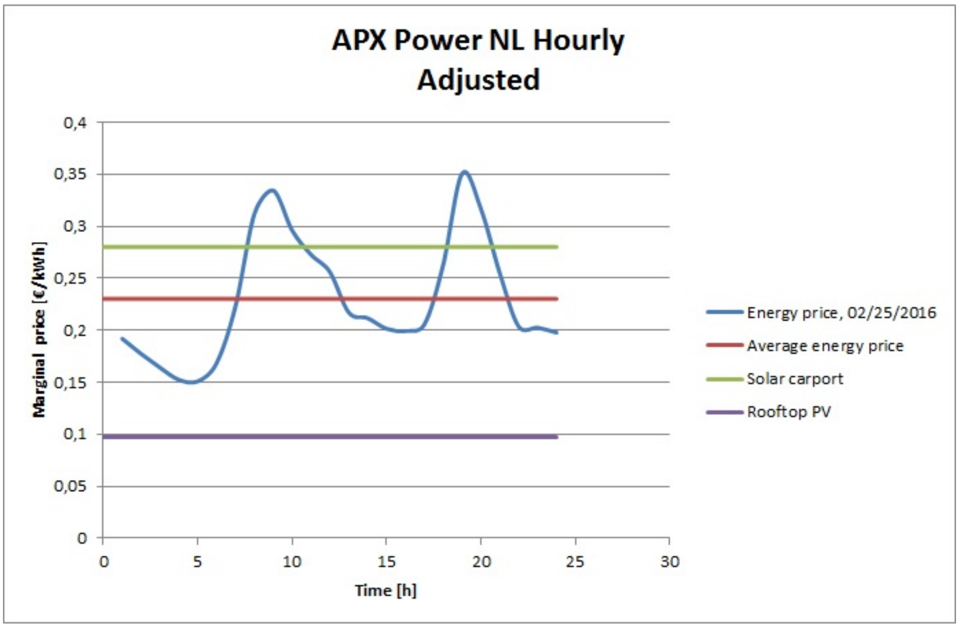

Figure 4.31: Marginal costs, from [13] and hourly energy prices, data from APX (adjusted).

subsequent chapter. Identical scenarios will be constructed for summer and winter and the results will be compared to see to what extent the energy management system is able to maintain its overall performance.

4.2.1. Summer/Winter

The difference between summer and winter might not always be obvious, as it depends on the latitude one lives. The farther away one is located from the equator, the larger this difference becomes. The Netherlands is located on 52° latitude, which implies that the variation between summer and winter irradiation is relatively large. For example, during January the average irradiation is 1.23 kWh/m^2/day, whereas in May this is 5.31 kWh/m^2/day [31]. Therefore, it is interesting to investigate these two possibilities as the base cases over which the other scenarios will be analyzed and ultimately compared. The PV output of a 10 kW$_p$ system during a day in May and January are presented in figs. 4.1 and 4.14, where the difference can clearly be seen. However, this is mainly to give a general idea of what the difference entails, the actual PV data will be attained as explained in section 4.1.1. Further, another observation that can be made from the aforementioned figures is the intermittent nature of PV output, even in a seemingly sunny day in May. This is important to realize if one aims to increase self-consumption, as the charging power will hardly ever be constant.

4.2.2. Charging strategies

Perhaps the most important distinction that can be made is between uncontrolled charging and smart charging, where the latter is optimized by the energy management system. The mathematics regarding the energy management system have been elaborated upon in chapter 3. Uncontrolled charging however does not require any mathematics since the EVs are charged immediately upon connection to the grid. It is obvious that this method of charging will not lead to an optimal solution, however, it is interesting to quantify the difference. It should be noted that uncontrolled charging will comprise of grid power, supplemented with PV power when that is possible.

4.2.3. Tariffs

Another interesting manner to compare the proposed model is through different forms of pricing. These were already elaborated upon in section 4.1.6, where it was established that currently there are two different electricity pricing schemes in the Netherlands: single- and double tariff, where the latter makes the distinction between day and night. As stated before, the latter will be ignored since night-time charging is not of interest for this study. The first scenario regarding tariffs will therefore be the case where the consumer can buy and sell energy from and to the grid for the same price. The flat tariff will be 0.23 €/kWh. The second scenario will include a FIT of 0.09 €/kWh, currently in effect in Germany and is specified here as the double flat tariff.

In addition, the potential of dynamic pricing will be investigated. As can be seen in figure 4.31, several possibilities arise for this scenario. For example, it might be interesting to examine what would happen if the purchase and sell price are the same or if the purchase price is averaged at 0.23 €/kWh and the sell price is averaged at 0.09 €/kWh. Another possibility would be to consider the case where the purchase tariff is dynamic but the sell tariff is flat, or the other way around. However, to avoid too many scenarios, 48 scenarios are selected that are considered to be realistic. As stated before, dynamic or real-time prices are currently being experimented with in the Netherlands. In addition, several utilities [18] in the United States have already implemented such tariffs, where the price has the possibility to become negative, i.e. in case of overcapacity. Further, real-time FITs are hardly considered as of yet and since PV power has reached grid-parity in several countries such as Germany (2011), the FIT has steadily been decreased accordingly [101]. Therefore, the fifth and sixth scenarios will encompass a dynamic purchase tariff with an average of 0.23 €/kWh and a FIT of 0.23 €/kWh and 0.09 €/kWh, respectively.

The aforementioned scenarios regarding tariffs are an estimate of what might happen in the future, as there is much uncertainty on this topic as of yet. Furthermore, during each of these scenarios the marginal costs of the solar carport will remain 0.097 €/kWh while also examining the case of zero marginal costs of PV, as discussed in section 4.1.6.

4.2.4. Final scenarios

The scenarios that have been established in the previous sections will be linked to each other in this section. Further, table 4.9 will give an overview of these scenarios. Note that uncontrolled charging does not include V2G service and therefore only a single and double flat tariff will be investigated in this case. All scenarios will be repeated for summer and winter, in which two main cases are examined: one fully occupied charging point. i.e. four EVs, and two charging points where the second is only half occupied. This is done to examine if there will be energy transfer between the charging points, which theoretically is possible. Furthermore, it is the authors' conviction that if these two cases are examined, this can easily be extrapolated to systems of larger sizes, e.g. 10 solar carports. As a result, a total of 48 scenarios will be studied. In addition, data regarding EVs and driving patterns will be randomly selected once and then remain constant as it would be problematic to compare the results of the scenarios if these would be different for each scenario.

Table 4.9: Overview of scenarios.

	Summer/Winter					
	Uncontrolled charging	**Smart charging**	**Flat tariff**	**Double flat tariff**	**Dynamic purchase tariff 0.23 €/kWh flat sell tariff**	**Dynamic purchase tariff 0.09 €/kWh flat sell tariff**
Scenario 1	x	-	x	-	-	-
Scenario 2	x	-	-	x	-	-
Scenario 3	-	x	x	-	-	-
Scenario 4	-	x	-	x	-	-
Scenario 5	-	x	-	-	x	-
Scenario 6	-	x	-	-	-	x

4.3. Conclusion

This chapter specified details regarding the inputs required by the EMS; more specifically PV power, driving patterns, EV specifications and marginal costs of energy, ultimately combining these into scenarios with which the behavior of the EMS can be studied. Of the aforementioned inputs, PV power is considered to be variable throughout this thesis, whereas the other inputs are seen as parameters, i.e. fixed. This can be justified on account of the fact that, especially in The Netherlands, irradiation is highly variable over the course of e.g. a year, whereas driving patterns are definitely not. While it is true that dynamic grid tariff vary, depending on the day of the week and/or season, a day-ahead market exists and therefore this can be considered as a parameter. Additionally, EV specifications can vary as well, as it is difficult to predict which exact EV will connect which charging point. However, the EMS does not have to take decisions on power allocation while there is no EV connected and when an EV is connected, the system can ascertain the necessary details.

Power produced by a PV system can be forecasted using several different methodologies, as was explained during the literature study. For this thesis, time-series were selected, more specifically an ARIMA class model. The section 4.1.1 elaborated on the Box-Jenkins approach to model and forecast PV power. First, a model had to be identified, specific to the time-series at hand. Subsequently, the parameters of the identified model were estimated, after which the ascertained models were subjected to several statistical analyses. In case the models failed the tests, one was meant to go back to the first or second step, making this an iterative process. If the model was satisfactory, it would be used to perform a forecast with a horizon of 15 minutes. It was shown that for the day with high irradiation, the model achieved a coefficient of determination, R^2, of 0.986. In addition, the RMSE was found to be 0.395 kW, and both were concluded to be satisfactory. Regarding the day during which there was low irradiation, modeling the time series proved more challenging. However, after many iterations, an appropriate model was established with $R^2 = 0.970$ and RMSE = 0.0429 kW. It should be noted that although PV power is considered to be variable, two forecasts were made, summer and winter, and these will be kept constant throughout the following chapter so as to be able to compare the behavior. This applies for the subsequent parameters as well.

Driving patterns have been documented extensively by the Dutch mobility survey, of which the results have been examined further in [39]. This study clearly showed the patterns of commuters throughout the week, after which it was concluded that since these patterns are extremely repetitive, this pattern can be assumed constant. In addition, arrival and departure times showed normal behavior, i.e. with fixed mean and standard deviation. Therefore it was decided in section 4.1.4 to represent arrival time at the workplace as a normal distribution with mean 8.30 a.m. and departure time with mean 5.30 p.m., both with 1.1 hour standard deviation [63].

Selection of the EVs considered in this thesis was done in section 4.1.5 and were based on sales data of EVs in The Netherlands, each with its specific battery capacity and maximum charging power. Furthermore, the results of [7] were taken into account, where a long term study at a North American university campus showed that the average energy transfer at their charging points was 8.53 kWh with a standard deviation of 6.49 kWh. Consequently, a uniform distribution was utilized to randomly select energy content upon arrival and departure, where the former was chosen to lie between $0.3 \cdot \mathrm{EC}_{i,c}^{\max}$ and $0.5 \cdot \mathrm{EC}_{i,c}^{\max}$, while the latter would lie between $0.6 \cdot \mathrm{EC}_{i,c}^{\max}$ and $0.8 \cdot \mathrm{EC}_{i,c}^{\max}$. Because of the selected intervals, the minimum energy demand by a single EV will be 2.2 kWh, while maximum demand by one EV will be 45 kWh.

The final input to be established were the marginal costs of energy, e.g. for PV energy. It was found that several price mechanisms should be considered so that the improvements by the EMS could be compared to uncontrolled charging, but also to other studies. To purchase energy from the grid, two options were selected. First, a flat tariff of 0.23 €/kWh, which is the marginal cost of electricity in The Netherlands and the current purchase mechanism on the retail market. Second, a dynamic tariff, acquired from the day-ahead auction established by APX and adjusted to an average of 0.23 €/kWh, which is a future scenario that, in combination with an intelligent EMS, could alleviate stress on the grid by shifting demand away to off-peak periods. To sell energy to the grid, either directly through the PV system or through V2G, two flat tariffs were selected, depending on the scenario. The first FIT is 0.23 €/kWh, which, in combination with a purchase tariff of 0.23 €/kWh, is the current price mechanism in The Netherlands, although netting occurs over the entire year whereas this particular mechanism will be applied instantaneously. Second, it was decided to incorporate a FIT of 0.09 €/kWh, which is the current level in Germany. In addition, a marginal cost for the production of energy by the PV system of 0.097 €/kWh [13] will be taken into account as this allows for more realistic results, although this is not common in the field of optimization. All case studies will be performed without these costs as well, so as to be able to make a fair comparison regarding the results. Finally, battery degradation costs are taken into consideration, where it was concluded in section 3.3.4.2 that 0.038 €/kWh would be fitting.

The aforementioned inputs were combined in section 4.2 to form several scenarios so that sensitivity analyses can be performed in the subsequent chapter, so as to ascertain the performance of the proposed EMS. A total of 48 scenarios arose that were presented in table 4.9.

5
Results

This chapter is dedicated to displaying and explaining the results from the model, established in chapter 3, and scenarios, established in chapter 4. The arrival and departure times are selected once, with a normal distribution with mean 8.30 a.m. and 5.30 p.m., respectively and a standard deviation of 1.1 hour. The initial and departure energy content of the ith EV are selected via a uniform distribution, also once, and these parameters remain fixed throughout the present chapter so as to make comparison more straightforward. The results are shown in table 5.1. The final input will be the PV power, which was covered extensively in section 4.1.1. In addition, a base scenario will be established in the form of uncontrolled charging, which entails that the EVs start charging upon arrival, indicated as scenario 1 and 2 and defined in section 4.2. Scenario 3 and 4 are developed for direct comparison with scenario 1 and 2, whereas scenario 5 and 6 show the potential of dynamic tariffs with flat FITs. The latter scenarios will be compared to scenario 3 and 4 respectively, and therefore, if the results from scenario 5 and 6 show improvements over scenario 3 and 4, this implies that in comparison to uncontrolled charging, the effectiveness of the EMS is even further improved due to the dynamic purchase tariff. It should be noted that simultaneous charging in this case is also not possible and therefore the second EV starts charging when the first EV is done, until the final EV is charged. However, in the future this will be possible if the corresponding hardware is available. In section 5.1 the results of a day with high irradiation are presented, whereas section 5.2 will cover the behavior of the model during a day with low irradiation. In addition, at the end of each section an overview is presented with the results of each scenario for easy comparison. It should be noted that since there are ample graphs per scenario, the remaining graphs are placed in appendix A.

Table 5.1: Input parameters.

	$t_{arrival}$ (a.m.)	$t_{departure}$ (p.m.)	$EC_{arrival}$ [kWh]	$EC_{departure}$ [kWh]
EV 1	7.31	6.19	29.7	70.2
EV 2	8.37	7.23	13.8	21.9
EV 3	7.54	5.17	10.6	17.4
EV 4	8.50	3.09	10.8	21.3
EV 5	7.50	4.35	37.5	64.5
EV 6	9.02	6.59	10.3	23.3

5.1. Summer

The section 5.1.1 will investigate to what extent a single charging point is capable of supplying energy to the EVs connected to it, of which the specifications were presented in tables 4.8 and 5.1. In addition, the improvements that the proposed energy management system can deliver in terms of charging costs and stress alleviation on the grid will be examined. However, first two base scenarios will be established in which uncontrolled charging are studied to ascertain the impact on the grid and costs incurred. Furthermore, a scenario where the objective is to minimize the energy exchange with the grid is studied which will act as a benchmark to ascertain the maximum amount of PV self-consumption. The section 5.1.2 will investigate to what extent there will be cooperation between the charging points, e.g. by feeding a surplus of PV power to the charging point that would otherwise draw it from the grid.

5.1.1. One charging point - four EVs

Scenario 1 and 2

The current section presents the results for uncontrolled charging with λ_{FIT_t} = 0.23 €/kWh and λ_{FIT_t} = 0.09 €/kWh for scenario 1 and 2 respectively, although it should be noted that applying different pricing mechanisms will not affect the graphs for this particular form of charging, but merely the numerical results. Therefore, only one scenario is presented in term of a figure, whereas section 5.1.1.7 presents the various numerical results. These scenarios will act as a benchmark to which scenarios 3 and 4 can be compared, depending on λ_{FIT_t}. The power distribution is presented in fig. 5.1 from which it can be seen that the first EV starts charging immediately upon arrival. In addition to this, the power that cannot be supplied by the PV system is supplemented with power from the grid and is presented here as the inverse of the PV power. Furthermore, this graph shows the potential of EV charging with PV power at the workplace since the coincidence between supply and demand is unmistakable. As soon as the last EV is done charging, the remainder of the PV power is fed into the grid. It should be noted that uncontrolled charging in combination with a low FIT and marginal costs for PV power can prove disadvantageous for the penetration of PV in the electricity generation mix, since it one can lose money if the FIT is too low or marginal cost too high. The numerical results are tabulated in tables 5.2 and 5.3, from which it can be seen that the observation about the coincidence between supply and demand is supported by the relatively high 73.33% PV self-consumption. The appendix A.1.1.1 presents additional figs. A.1 to A.3 that provide more insight into the charging process. For example, the latter figure shows a zoom-in of the charging of EV 1 and how the grid power supplements PV power. In addition, key aspects of uncontrolled charging are listed below:

- No possibility to take solar power forecast and prices into account
- Tendency to add to morning peak demand and feed PV power into grid during afternoon
- Power exchange highly fluctuating due to dependency on PV power
- Easy to implement
- High FIT required to reduce payback time

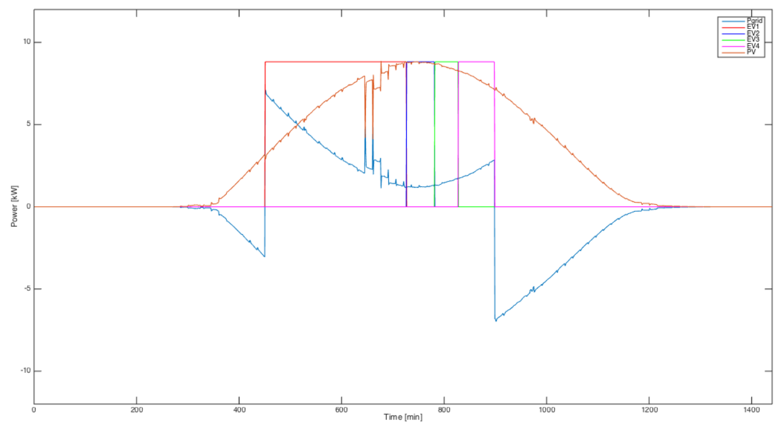

Figure 5.1: Power allocation during uncontrolled charging of 4 EVs with λ_{PV_t} = 0.097 €/kWh.

Scenario 3

The present section presents the results of scenario 3, in which λ_{FIT_t} = 0.23 €/kWh. The power exchanges over the course of one day are presented in figs. 5.2 and 5.3, where the former includes the sunk costs of the PV system. Immediately it can be seen that the proposed energy management system increases PV self-consumption, more specifically to 95.80% for both λ_{PV_t} = 0.097 €/kWh and λ_{PV_t} = 0 €/kWh. Due to the fact that PV power is less expensive than grid power, the EMS will only draw power from the grid to assist the PV system since there is not enough insolation throughout the day to charge the EVs solely with PV energy.

Furthermore, upon observing figs. 5.2 and 5.3, it can be seen that the graphs are identical. This conclusion is supported by the results in The tables 5.2 and 5.3. The fact that these are identical is logical, as $\lambda_{\mathrm{FIT}_t} > \lambda_{\mathrm{PV}_t}$ in both cases and therefore it is always beneficial to feed the surplus to the grid. In addition, since there is no financial incentive such as a dynamic tariff, other than low or zero marginal costs for PV, it is preferred to maximize $E_{\text{PV-EV}}$, i.e. PV self-consumption. Consequently, power allocation remains equal during these case studies. In addition, figs. A.4 to A.9 provide a deeper understanding of the charging processes. It should be noted that in these figures, a distinction is made between V2G power to the grid, i.e. 'grid', and PV power to the grid, i.e. 'PV-grid'. This distinction is a consequence of the particular way in which the power balance in chapter 3 was formulated.

The tables 5.2 and 5.3 present the results of the two studied cases. In the case study where marginal costs of PV are taken into consideration, charging costs are reduced by 3.56% when compared to uncontrolled charging. In addition to this, PV self-consumption is increased from 73.65% to 95.80%, which was expected since energy from the PV system is less expensive than energy from the grid which consequently decreases charging costs. In addition, this is found to be the maximum achievable self-consumption for these specific input parameters, as will be further elaborated upon when the objective is to minimize energy exchange with the grid. Furthermore, another beneficial consequence of the increased PV self-consumption is the fact that the energy exchange with the grid has been reduced by 79.83%, thus reducing stress and potentially leading to a decrease in capital expenditure in the future.

The second case study in which the marginal costs are considered to be zero, charging costs are reduced by 23.49% when compared to uncontrolled charging. Expressed in absolute values, the reduction in costs is similar as in the previous case but since charging costs in this scenario are significantly lower, the percentage reduction is substantial. Other results are, as stated before, identical to the previous case study.

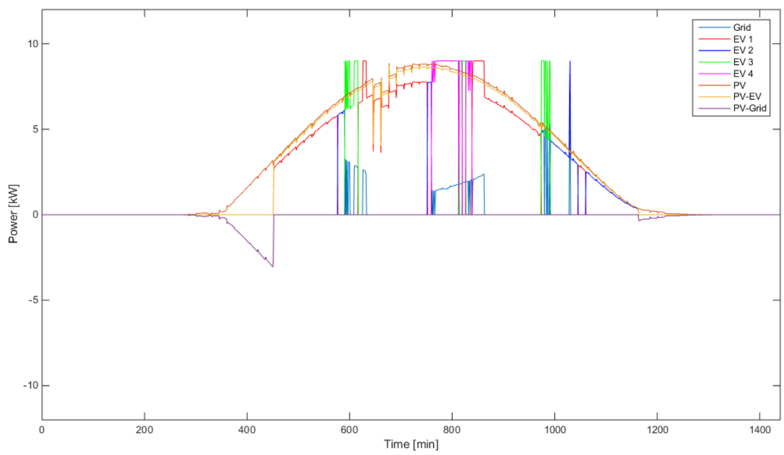

Figure 5.2: Power allocation during scenario 3 with 4 EVs and λ_{PV_t} = 0.097 €/kWh.

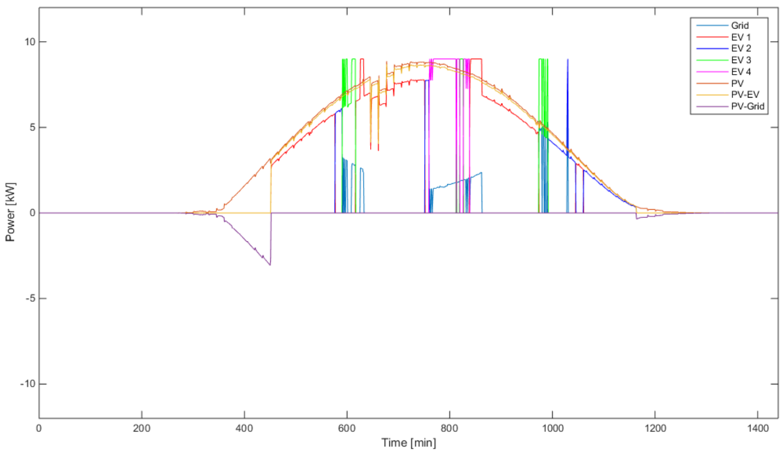

Figure 5.3: Power allocation during scenario 3 with 4 EVs and λ_{PV_t} = 0 €/kWh.

Scenario 4

This section presents the results of scenario 4, in which λ_{FIT_t} = 0.09 €/kWh. This feed-in tariff can be compared to the current situation in Germany, where this figure has been steadily reduced over the last years. For the case where λ_{PV_t} = 0.097 €/kWh, it can immediately be seen that feeding PV power to the grid would cost rather than yield money. This is the very reason eq. (3.3.17) was introduced, since this equation allows curtailment of PV so that the surplus does not have to be sold against a loss and consequently a non-optimal solution is avoided. The power exchanges during one day are presented in figs. 5.4 and 5.5, where it can be observed from the former figure that the EMS indeed prefers to curtail PV power rather than sell the surplus produced before arrival and after departure, to the grid. In both cases, PV self-consumption amounts to 95.80%, which was found to be the maximum achievable, as stated in the previous section. In case λ_{PV_t} = 0 €/kWh, there is an incentive to feed the surplus of PV power back to the grid, for the FIT is higher than the marginal costs, whereas this is not the case when λ_{PV_t} = 0.097 €/kWh. Both cases show an increase in power drawn from the grid near the departure time of EV 2. However, this will not contribute significantly to increase peak demand since this takes place around 8 p.m. in the Netherlands [98]. Furthermore, as will be explained in the subsequent section, dynamic tariffs offer the possibility to decrease peak demand due to the fact that grid prices and demand are correlated. The figs. A.10 to A.15 provide a deeper understanding of the charging processes.

While λ_{PV_t} = 0.097 €/kWh, the proposed EMS will reduce costs by 23.49% when compared to scenario 2, which can be deduced from table 5.2. Further, even though the FIT has decreased by 60.87% when compared to scenario 3, the costs have risen with a mere 5.18%. This proves that the EMS reduces the sensitivity to fluctuations in such subsidies. Finally, the energy exchange with the grid has decreased by 87.24% when compared to scenario 2, although it should be noted that the additional reduction in comparison to scenario 3 is achieved due to the fact that the EMS does not feed energy to the grid. However, due to this it is possible to observe to what extent the proposed EMS is able to decrease grid dependency. It is concluded that the EMS is able to plan the energy allocation in such a way that only 7.67% of the total energy requirements needs to be supplied by the grid.

During the second case study, without marginal costs for PV energy, charging costs are reduced by 72.75% in comparison to scenario 2, which can be seen from table 5.3. The reason this reduction supersedes the result seen in scenario 3 with the same case study is that the FIT is lower and since PV self-consumption is relatively low during uncontrolled charging, the effectiveness of the EMS is enhanced. In addition, the energy exchange with the grid is slightly higher than in the previous case, when λ_{PV_t} = 0.097 €/kWh, which is mainly due to the fact that in that particular case it was not optimal to feed energy into the grid. However, the energy exchange with the grid is still reduced by 79.84% when compared to uncontrolled charging, which can be considered satisfactory.

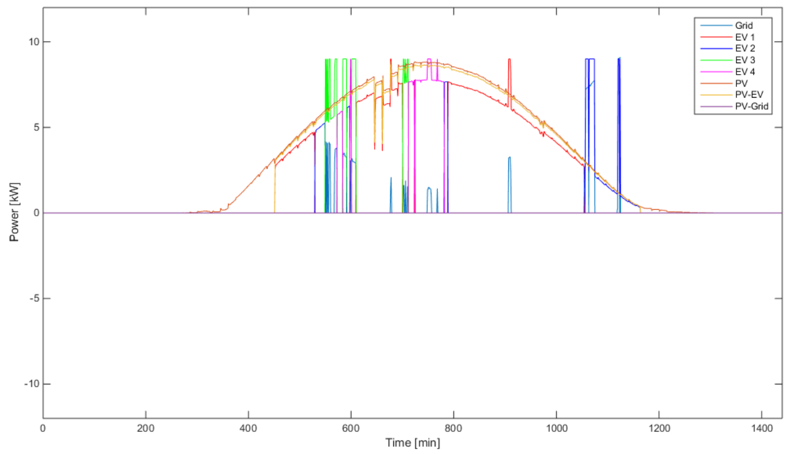

Figure 5.4: Power allocation during scenario 4 with 4 EVs and λ_{PV_t} = 0.097 €/kWh.

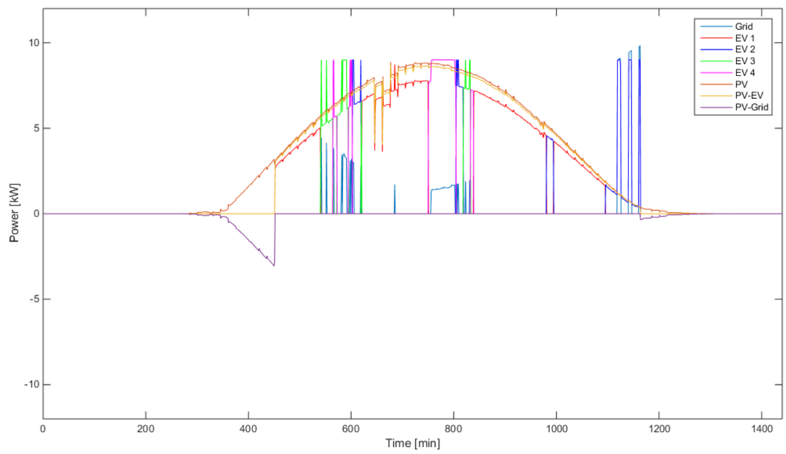

Figure 5.5: Power allocation during scenario 4 with 4 EVs and λ_{PV_t} = 0 €/kWh.

Scenario 5

The present section will elaborate on the results from scenario 5 in which a dynamic tariff is imposed, as was explained in section 4.1.6, while λ_{FIT_t} = 0.23 €/kWh. Since a dynamic tariff is correlated with demand, it can be used as a tool for demand side management, i.e. load shifting, in combination with an EMS that aims to minimize charging costs. The figs. 5.6 and 5.7 present the resulting power exchanges, whereas figs. A.16 to A.19 and figs. A.20 to A.23 provide an in-depth view of the charging processes in the respective case studies. From these figures it can be seen that during the morning peak in purchase tariff, the EMS switches between feeding power produced by the PV system into the grid and charging EVs with this power. This can be seen as beneficial, due to the fact that a dynamic tariff is correlated to demand, as stated before. Additionally, the EMS draws power from the grid during the period when the purchase tariff is relatively low, which implies that the load has shifted from peak demand to off-peak hours. This suggests that such a price mechanism can be a powerful tool in demand side management. As a consequence, PV self-consumption is lower than during scenario 3 and 4 however, the reason for this is advantageous for the grid operator.

The previous sections established that the EMS is effective at lowering charging costs. From table 5.2 it can be seen that the EMS is even more effective in combination with a dynamic pricing mechanism, due to the fact that the dynamic tariff allows it to postpone charging until the price is favorable so as to decrease costs further. When λ_{PV_t} = 0.097 €/kWh, the costs are further reduced by 4.28% when compared to scenario 3. In addition, when compared to uncontrolled charging, sustainability of the solar carport has increased due to the fact that self-consumption has increased to 82.30% while also supporting the grid in terms of a power feed.

In case of free PV energy, it can be seen from table 5.3 that the EMS can significantly reduce charging costs, more specifically with 58.13% when compared to scenario 3, while the energy exchange with the grid shows a similar pattern as was the case when λ_{PV_t} = 0.097 €/kWh. The significant cost reduction is achieved mainly due to the fact that the lion's share of energy demand is covered by PV power that is now considered to be free.

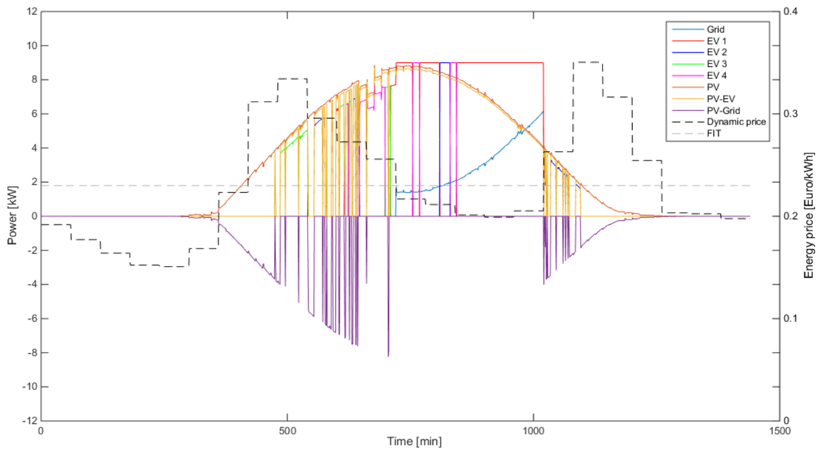

Figure 5.6: Power allocation during scenario 5 with 4 EVs and λ_{PV_t} = 0.097 €/kWh.

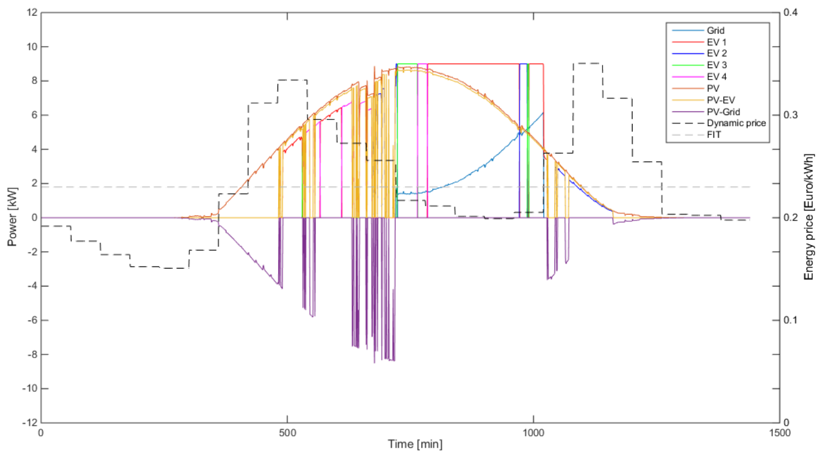

Figure 5.7: Power allocation during scenario 5 with 4 EVs and λ_{PV_t} = 0 €/kWh.

Scenario 6

The present section examines the results of the EMS in combination with λ_{FIT_t} = 0.09 €/kWh. Similarly as in scenario 4, when λ_{PV_t} = 0.097 €/kWh, the surplus of PV energy will be curtailed since it would cost more to produce than it would yield when fed into the grid, which can be seen in fig. 5.8. Furthermore, in both fig. 5.8 and fig. 5.9 the EMS refrains from drawing power from the grid until the absolute valley period is reached, where grid power is only utilized to supplement PV power. The figs. A.24 to A.27 and figs. A.28 to A.31 provide extra information regarding the charging process. It should be noted that the EMS, in combination with the present price mechanism and both case studies, achieves 95.80% PV self-consumption and therefore it can be concluded that low λ_{FIT_t} and λ_{PV_t} effectively increase self-consumption.

In the case study when λ_{PV_t} = 0.097 €/kWh, the EMS further reduces costs by 1.94% when compared to scenario 4. This supports the statement made before that the EMS will reduce costs while increasing PV self-consumption and simultaneously decreasing stress on the grid. Therefore, a separate objective function as presented in the following section will not be necessary when the right price mechanism is in place. As can be seen from table 5.2, PV self-consumption is at the maximum level of 95.80% and energy demand from the grid is 5.05 kWh, which is drawn at the valley period of demand. In addition, it is interesting to note the similarities between scenarios 4 and 6. These are identical except for the charging costs, which is due to the dynamic price of grid energy. The difference mainly lies in the power withdrawal from the grid. For the present scenario, this occurs only when the grid price is relatively low, whereas it can be seen from fig. 5.4 that power withdrawal occurs randomly throughout the day since the grid price is constant.

In the next case study, i.e. when λ_{PV_t} = 0 €/kWh, power allocation shows a similar trend, as can be seen in fig. 5.9. However, the surplus of PV energy is fed back into the grid as this aides in decreasing charging costs. The EMS achieves a cost reduction of 17.02% when compared to scenario 4. The reduction when compared to scenario 4 can be ascribed to the fact that the EMS postpones drawing power from the grid until valley prices are reached in the current scenario, whereas this is not possible during scenario 4. This is supported by the results in table 5.3 where scenario 4 and 6 exhibit similar behavior.

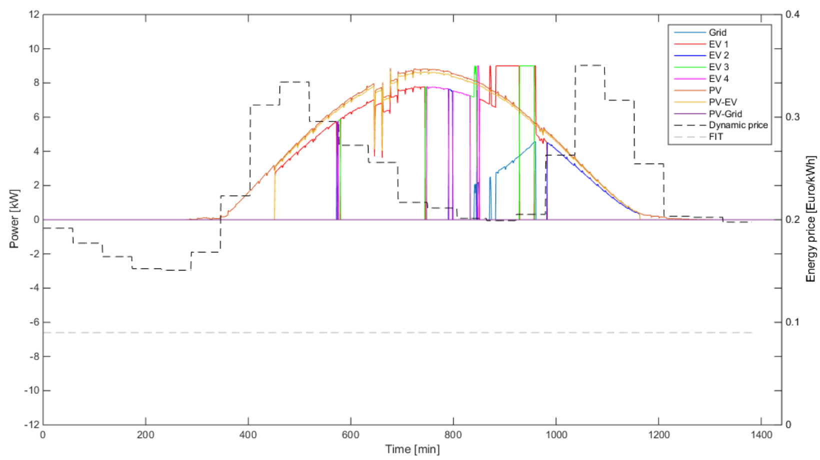

Figure 5.8: Power allocation during scenario 6 with 4 EVs and λ_{PV_t} = 0.097 €/kWh.

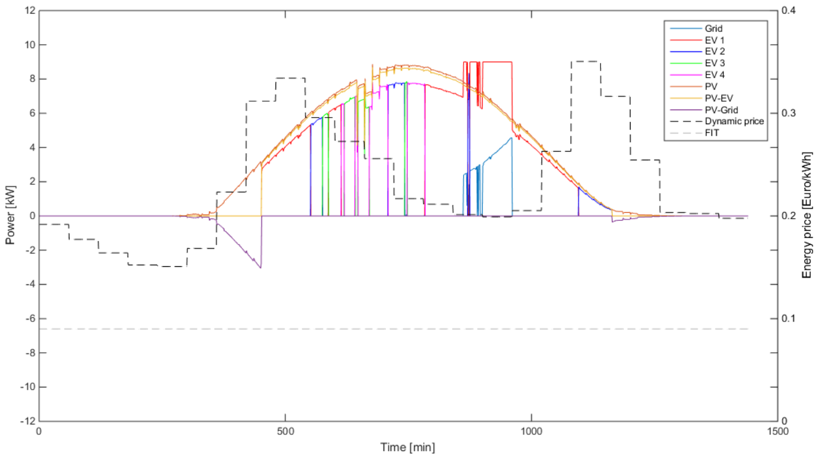

Figure 5.9: Power allocation during scenario 6 with 4 EVs and λ_{PV_t} = 0 €/kWh.

Minimize energy exchange with the grid

In order to assess to what extent the proposed EMS can decrease grid dependency, the objective function to be minimized will be as defined in section 3.3.4.1. This is important because only then can the effect of the different price mechanisms be put into perspective, since otherwise one would not know what the maximum level of e.g. PV self-consumption would be. It should be noted that price mechanisms or marginal costs of PV do not influence the current optimization itself, only the outcome in terms of charging costs, which can be seen in tables 5.2 and 5.3. The fig. 5.10 and figs. A.32 to A.34 present the results. It can be seen that PV power is curtailed when there is no EV to charge. Furthermore, $\lambda_{\mathrm{G2V}_t} = 0.23$ €/kWh in this case, and charging costs amount to €7.92 and €1.16 for $\lambda_{\mathrm{PV}_t} = 0.097$ €/kWh and $\lambda_{\mathrm{PV}_t} = 0$ €/kWh respectively, although this case should not be compared to scenario 1 through 6 in terms of costs since the objective functions are different. Finally, it can be concluded that the maximum amount of PV self-consumption with this PV profile is 95.80% and therefore it can be stated that scenario 3, 4 and 6 perform identical and, consequently, satisfactory with both $\lambda_{\mathrm{PV}_t} = 0.097$ €/kWh and $\lambda_{\mathrm{PV}_t} = 0$ €/kWh. In addition, scenario 5 will reduce the PV self-consumption significantly which was elaborated upon before.

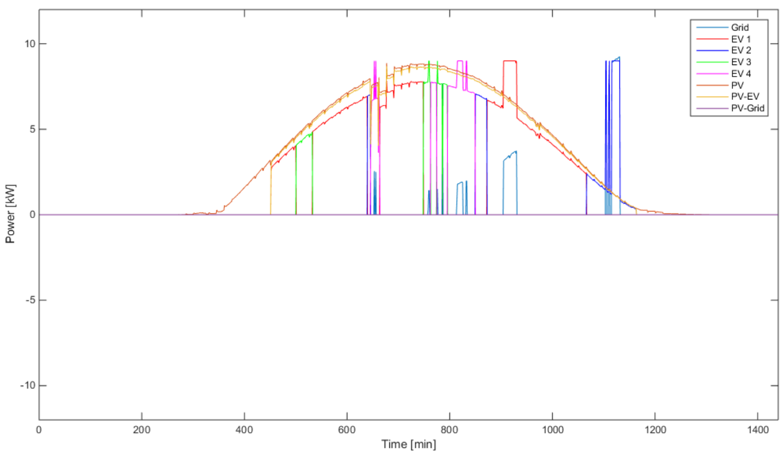

Figure 5.10: Power allocation during minimization of energy exchange with grid, with 4 EVs.

Overview of results

Table 5.2: Results of the scenarios with 4 EVs and λ_{PV_t} = 0.097 €/kWh.

	$E_{PV\text{-}EV}$ [kWh]	E_{PV} [kWh]	PV self-consumption [-]	Total costs [€]	E_{grid} [kWh]
Scenario 1	53.56	72.72	0.7365	7.807	39.61
Scenario 2	53.56	72.72	0.7365	10.35	39.61
Scenario 3	69.66	72.72	0.9580	7.530	7.986
Scenario 4	69.66	72.72	0.9580	7.920	5.053
Scenario 5	59.85	72.72	0.8230	7.208	27.22
Scenario 6	69.66	72.72	0.9580	7.767	5.053
min E_{grid}	69.66	72.72	0.9580	7.920	5.053

Table 5.3: Results of the scenarios with 4 EVs and λ_{PV_t} = 0 €/kWh.

	$E_{PV\text{-}EV}$ [kWh]	E_{PV} [kWh]	PV self-consumption [-]	Total costs [€]	E_{grid} [kWh]
Scenario 1	53.56	72.72	0.7365	0.7538	39.61
Scenario 2	53.56	72.72	0.7365	3.297	39.61
Scenario 3	69.66	72.72	0.9580	0.4877	7.986
Scenario 4	69.66	72.72	0.9580	0.8983	7.986
Scenario 5	59.85	72.72	0.8230	0.2042	27.22
Scenario 6	69.66	72.72	0.9580	0.7454	7.986
min E_{grid}	69.66	72.72	0.9580	1.162	5.053

5.1.2. Two charging points - six EVs

The present sections examines the behavior of the EMS when 6 EVs are connected to two charging points, i.e. 4 EVs at the first and 2 EVs at the second. In case there is a surplus of PV energy, which is likely in this case since the second charging point is occupied for 50%, there should be cooperation between the charging points so as to decrease the energy drawn from the grid. Furthermore, it is stressed that the results from the two case studies, i.e. one and two charging points, can be used to assess the effect of incorporating more charging points. It should be noted that EV 1 through EV 4 are connected to the first charging point, whereas EV 5 and EV 6 are connected to the second charging point.

Scenario 1 and 2

In order to establish a benchmark, first uncontrolled charging will be examined, similar as in section 5.1.1. Two case studies will be investigated, where λ_{PV_t} = 0.097 €/kWh and λ_{PV_t} = 0 €/kWh, although this solely influences the total charging costs. The resulting power exchange is presented in fig. 5.11, combined with additional graphs presented in figs. A.32 to A.34. To enhance clarity, the two charging stations are displayed in the same graph and PV power production is multiplied with two. In addition, in this case the lines representing the charging process of the EVs at the second charging point are dashed for clarity. Furthermore, the 10 kW charging/discharging constraint still applies, which is a constraint specific to each separate charging point. However, the car park as a whole will trade power with the grid, hence the grid power is able to exceed 10 kW and is actually limited to 20 kW in case of two charging points.

A similar pattern exists as with uncontrolled charging at one charging point. The EVs are charged one at a time upon arrival, until the last EV is done and the surplus is fed into the grid at either 0.23 €/kWh or 0.09 €/kWh for scenario 1 and 2 respectively. From this figure it can be deduced that charging power during early morning will be multiplied with the number of charging points and thus significantly add to peak demand. Where peak demand during uncontrolled charging by a single charging point in the previous section was around 7 kW, this has now doubled to around 14 kW. In addition, the EVs finish charging at around 3 p.m. which is more or less when the dynamic tariff reaches its minimum. Hence, PV power is fed into the grid at a time at which there is already low demand and possibly overproduction.

The results, presented in tables 5.4 and 5.5, show that with 58.00%, PV self-consumption is relatively low. As a result, the energy exchange with the grid more than doubled when compared to one charging point implying that stress on the grid is increased significantly. Charging costs do not show similar increase, precisely because of low PV self-consumption. Charging costs amount to €8.96 and €17.09 for scenario 1 and 2 respectively, when λ_{PV_t} = 0.097 €/kWh. When λ_{PV_t} = 0 €/kWh, scenario 1 generates a profit of €5.15 and scenario 2 generates a loss of €2.98. The reason for these results is straightforward: since there is a significant amount of irradiation, the marginal costs of PV energy play an important role in the result.

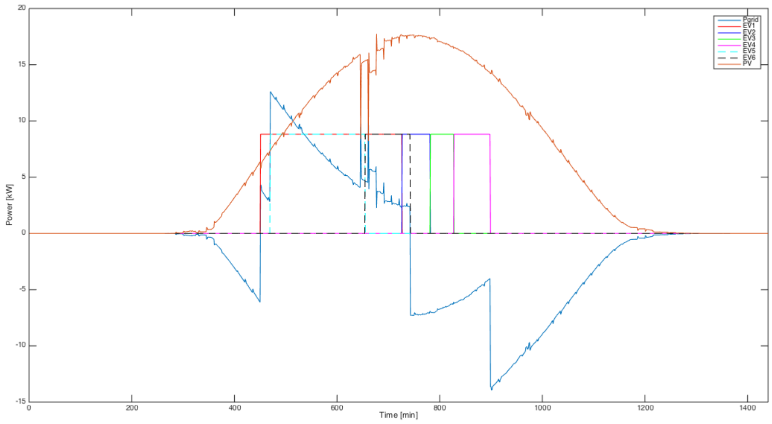

Figure 5.11: Power allocation during uncontrolled charging of 6 EVs with λ_{PV_t} = 0.097 €/kWh.

Scenario 3

The present section elaborates on the results of scenario 3, both with λ_{PV_t} = 0.097 €/kWh and λ_{PV_t} = 0 €/kWh. The power allocation for both cases is presented in figs. 5.12 and 5.13, whereas figs. A.38 to A.43 provide more background information about the charging processes. For example, from fig. A.40 it can be seen that at no point in time two EVs that are connected to the same charging point are simultaneously charging, whereas it does occur that two EVs at different charging points are charged simultaneously. From the graphs below it can be concluded that in both cases, the EMS is able to feed a significant amount of power into the grid, which may not come as a surprise since there is also a significant surplus of PV energy. Furthermore, figs. A.39 and A.42 show that there is no power drawn from the grid. Due to the fact that there is no price incentive, the EMS draws this power early in the morning and therefore adds to peak demand, albeit not significant. Another point of interest are the white areas in vertical direction between $E_{\text{EV-PV}}$ and P_{EV}. These differences are caused by losses due to the efficiencies.

The results presented in table 5.4 show that charging costs are reduced with 6.97%. in comparison to scenario 1, partly due to the increased revenues, which in turn is a consequence of the surplus of PV energy. Furthermore, the table shows that the maximum achievable PV self-consumption is 83.27%, which occurs when the objective is to minimize energy exchange with the grid. Therefore, it can be concluded that since self-consumption in this particular case amounts to 82.56%, the EMS performs close to optimal without an extra price incentive. The reason for this is unmistakably the fact that energy produced by the PV system is less expensive than energy from the grid.

Regarding the second case, table 5.5 shows that the profit is increased with 10.50% from the profit achieved in scenario 1. In addition, the PV self-consumption and energy exchange with the grid are identical to the results when λ_{PV_t} = 0.097 €/kWh and are therefore considered to be satisfactory.

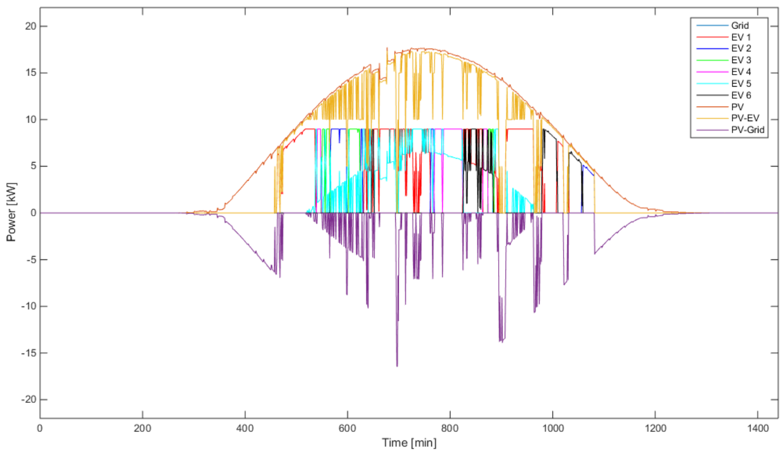

Figure 5.12: Power allocation during scenario 3 with 6 EVs and λ_{PV_t} = 0.097 €/kWh.

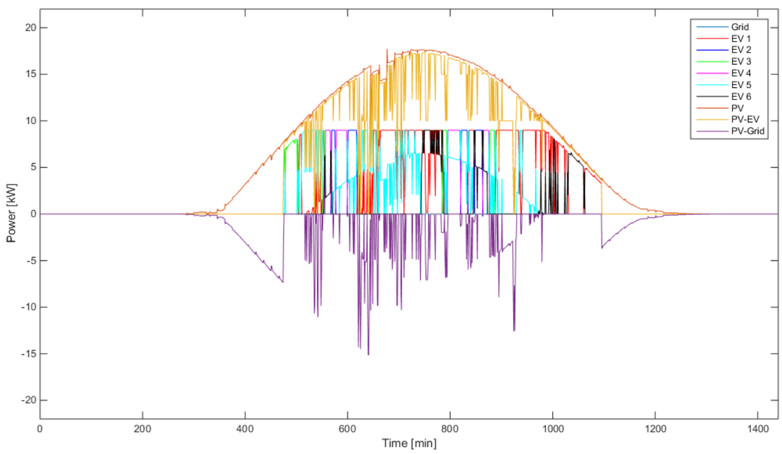

Figure 5.13: Power allocation during scenario 3 with 6 EVs and λ_{PV_t} = 0 €/kWh.

Scenario 4

The present scenario, in which λ_{FIT_t} = 0.09 €/kWh, is featured by the difference in outcome due to the two case studies, λ_{PV_t} = 0.097 €/kWh and λ_{PV_t} = 0 €/kWh. Hence, PV power is curtailed in fig. 5.14, whereas this is not the case in fig. 5.15. What can be observed from these figures and figs. A.44 to A.49 is that the EMS is capable of making the two charging points work together in such a manner that the entire system is autonomous, similarly as in the previous scenario. Another point of interest is the intermittent nature of the charging process. Even though eqs. (3.3.4) and (3.3.5) were imposed on the system, avoiding the highly variable character of the charging process has been succeeded only in part. The reason for this lies in eqs. (3.3.1) and (3.3.2), where the solver is allowed to set $P_{\mathrm{ch}_{i,c,t}}$ and $P_{\mathrm{V2G}_{i,c,t}}$ to zero as well. Several solutions such as ramping constraints on $P_{\mathrm{ch}_{i,c,t}}$ and $P_{\mathrm{V2G}_{i,c,t}}$ or providing a lower limit to the aforementioned decision variables larger than 0 kW can be implemented to overcome this. However, no concrete evidence has been found to support such measures, In fact, a study aimed to do the exact opposite, namely to use the EV battery to filter the intermittent nature of PV power so that a smooth power flow could be fed into the grid [11]. However, the latter aspect is not considered here, although this might be interesting for future work. Furthermore, apart from the power flow from the PV system to the grid, it should be noted that the case studies show high resemblance.

The EMS has achieves a cost reduction of 32.19% when λ_{PV_t} = 0.097 €/kWh when compared to scenario 2, as can be deduced from table 5.4, without feeding energy into or drawing energy from the grid and thus working autonomously. This can also be seen from the PV self-consumption, which approaches the value attained while minimizing energy exchange with the grid.

When λ_{PV_t} = 0 €/kWh, the EMS is able to reduce costs by an notable 171.43% which is due to the fact that the free PV energy is utilized much more efficiently than in scenario 2. Self-consumption is identical to that found when λ_{PV_t} = 0.097 €/kWh and is therefore a satisfactory result.

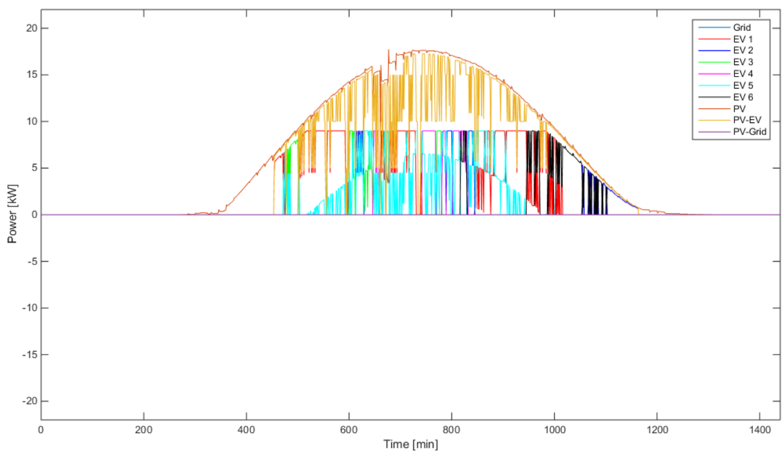

Figure 5.14: Power allocation during scenario 4 with 6 EVs and λ_{PV_t} = 0.097 €/kWh.

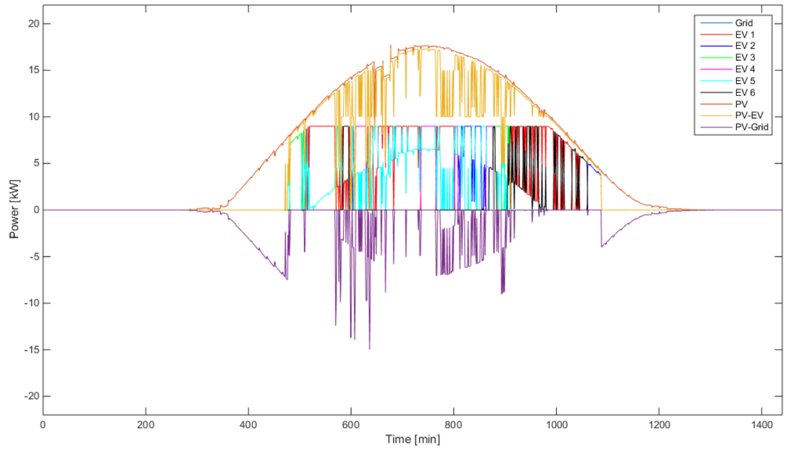

Figure 5.15: Power allocation during scenario 4 with 6 EVs and λ_{PV_t} = 0 €/kWh.

Scenario 5

The current section examines the behavior of the EMS when it minimizes costs while a dynamic tariff is imposed, combined with λ_{FIT_t} = 0.23 €/kWh. The results are depicted in figs. 5.16 and 5.17 whereas detailed graphs are presented in figs. A.50 to A.53 and figs. A.54 to A.57. Immediately a similar pattern as observed in scenario 5 with one charging point arises. The EMS charges the EVs with PV energy during the first part of the day, while also feeding a surplus back to the grid. It does this due to the fact that it knows energy prices will drop below λ_{FIT_t} during the afternoon. When that occurs, the EMS uses grid power to supplement PV power and charge the EVs accordingly. It was established in the previous sections that the EMS is capable of functioning autonomously but due to the high FIT and low purchase tariff, the EMS is motivated to feed PV power into the grid during the period with relatively high purchase tariff, whereas power is drawn during a valley in purchase tariff. Similarly as established in the case with one charging point, the EMS will actively aid to load shifting, while feeding power into the grid during peak demand. It can be seen in tables 5.4 and 5.5 that energy exchange with the grid is quite high, but this is considered to be advantageous. Furthermore, a dynamic FIT would provide extra motivation for the EMS to feed power into the grid while the price, and consequently demand, is high. This will be shown in section 5.3. In addition, the EMS is able to reduce costs further by 6.86% in case λ_{PV_t} = 0.097 €/kWh and increase profit further by 8.37% when λ_{PV_t} = 0 €/kWh, when compared to scenario 3.

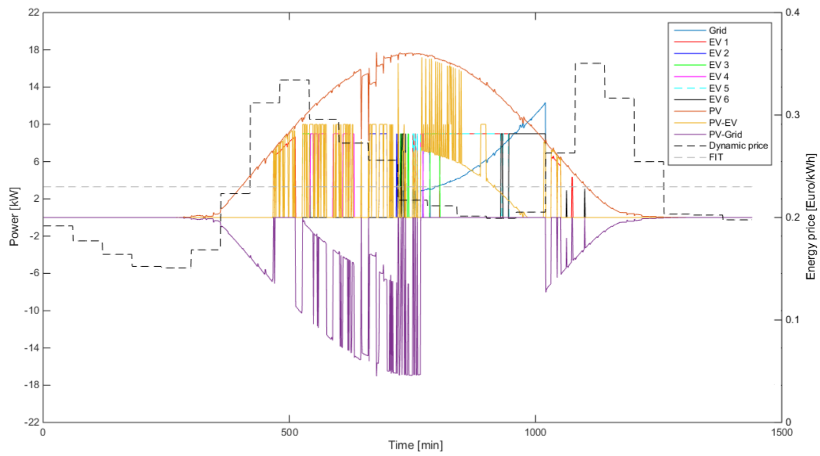

Figure 5.16: Power allocation during scenario 5 with 6 EVs and λ_{PV_t} = 0.097 €/kWh.

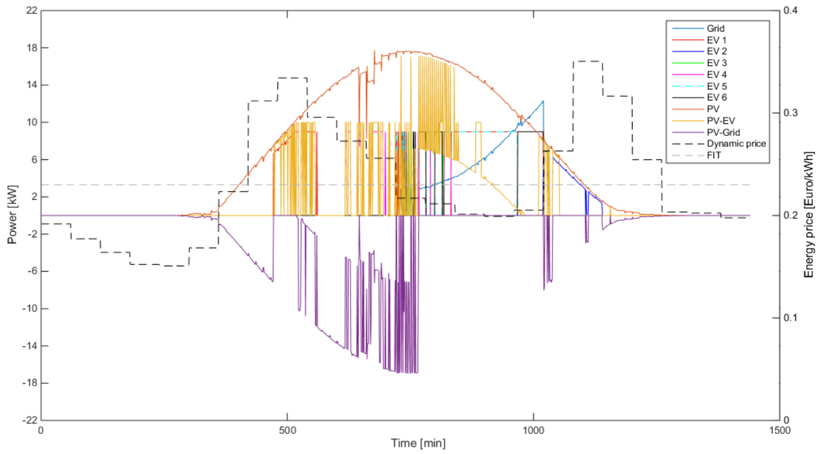

Figure 5.17: Power allocation during scenario 5 with 6 EVs and λ_{PV_t} = 0 €/kWh.

Scenario 6

The present section considers a dynamic tariff combined with a FIT of 0.09 €/kWh, which proved to be a well-founded financial incentive to increase self-consumption, as was concluded from scenario 4 and the case study which considered one charging point. Furthermore, since $\lambda_{\mathrm{PV}_t} > \lambda_{\mathrm{FIT}_t}$ for the first case study, it is expected that PV energy will be curtailed when the EVs are not charging, similarly as in scenario 4 when λ_{PV_t} = 0.097 €/kWh. This is indeed what the EMS proves to be optimal, as can be seen in fig. 5.18, figs. A.58 to A.61 and figs. A.62 to A.65. It is proven that the system can work autonomous in the current setting, with results exactly the same as in scenario 4 when λ_{PV_t} = 0.097 €/kWh. Therefore, no further cost reduction is achieved, which can also be seen in table 5.4. The reason for this is that, as stated before, the system can work autonomously and is not dependent on varying grid prices. Consequently, the costs incurred are solely due to the marginal costs of the PV system.

For the second case, the EMS does sell PV power back, owing to the fact that currently there are no costs attached to producing it. However, the same reasoning applies to this case as it did for the previous case. Specifically, the result is exactly the same as in scenario 4 which is due to the fact that the EMS can work autonomously, see table 5.5. In addition, since the grid price is dynamic but the FIT is constant, there is no improvement to be made by e.g. charging EVs extra and consequently postponing selling energy to the grid.

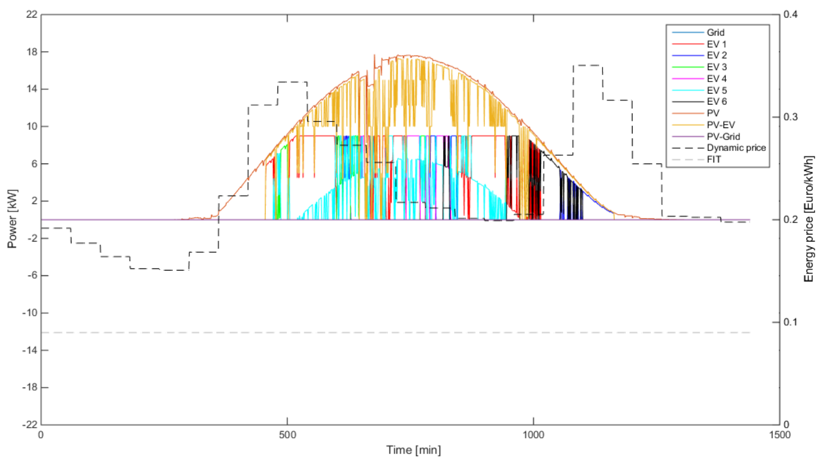

Figure 5.18: Power allocation during scenario 6 with 6 EVs and λ_{PV_t} = 0.097 €/kWh.

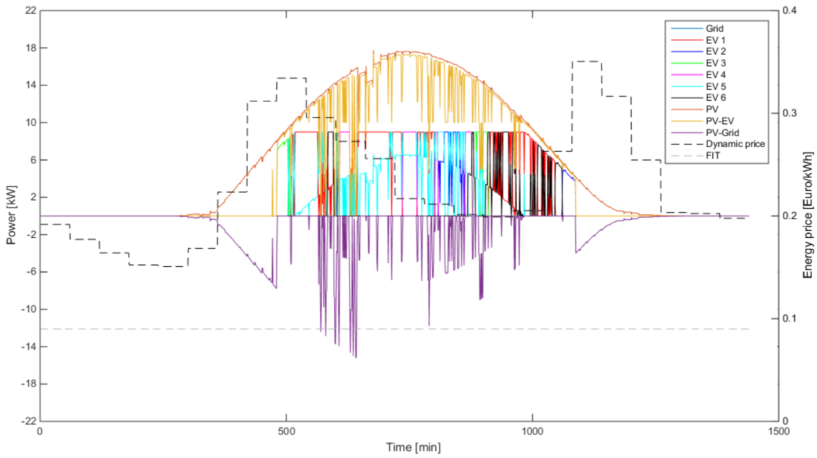

Figure 5.19: Power allocation during scenario 6 with 6 EVs and λ_{PV_t} = 0 €/kWh.

Minimize energy exchange with the grid

As was observed in the previous sections, the EMS can work autonomously when the second charging point is occupied for 50%. It is stressed that in contrast to the previous case studies, costs do not play a role in this case study. Therefore, the total costs solely depend on λ_{PV_t} and the graphs for both case studies will consequently be the same. The fig. 5.20 presents the resulting power allocation which the EMS proved to be optimal. It can be observed that there is no interaction with the grid, which is supported by the results in tables 5.4 and 5.5. However, an interesting phenomena occurs, which is shown in more detail in figs. A.66 to A.68. The EMS decides to charge EV 6, parked at the second charging point, beyond its required energy content upon departure since there is a surplus of energy production at that particular charging point. In contrast, a single charging point is not able to work autonomously as was concluded from section 5.1.1. In addition to this, even though the charging points share PV energy, the charging power per EV is still constrained to 10 kW and consequently there is not enough time to charge the four EVs connected to the first charging point solely with PV energy. Therefore the EMS stores a surplus of energy produced at the second charging point in EV 6 so as to charge EV 1 at a later moment, supplemented with PV energy.

Evidently, losses that are accompanied with such a strategy may be undesirable from a technical point of view, nor desirable from a financial point of view. More specifically, since the energy requirements of the EVs is constant throughout this thesis, it can be deduced that the current strategy, also known as vehicle to vehicle (V2V), increases $E_{\text{EV-PV}}$ with 1 kWh, which is in fact the loss due to extra battery charging/discharging. However, as stated before, these factors do not play a role in this particular case study. Similarly as was the case with one charging point, this section and objective function in particular, is designed to assess the maximum amount of self-consumption achievable by minimizing energy exchange with the grid. The results show that in this specific case, the maximum lies at 83.27%.

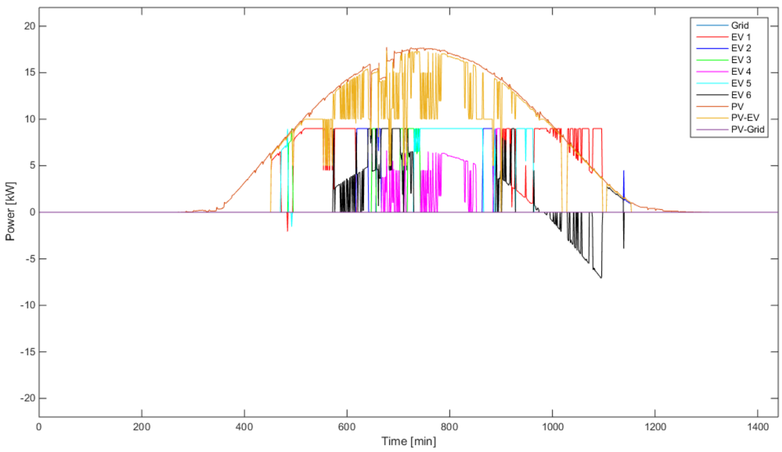

Figure 5.20: Power allocation during minimization of energy exchange with grid, with 6 EVs.

Overview of results

Table 5.4: Results of the scenarios with 6 EVs and λ_{PV_t} = 0.097 €/kWh.

	$E_{\text{PV-EV}}$ [kWh]	E_{PV} [kWh]	PV self-consumption [-]	Total costs [€]	E_{grid} [kWh]
Scenario 1	84.40	145.4	0.5804	9.037	94.24
Scenario 2	84.40	145.4	0.5804	17.18	94.24
Scenario 3	120.1	145.4	0.8256	8.407	24.36
Scenario 4	120.1	145.4	0.8256	11.65	0
Scenario 5	91.92	145.4	0.6322	7.830	79.53
Scenario 6	120.1	145.4	0.8256	11.65	0
min E_{grid}	121.1	145.4	0.8327	11.75	0

Table 5.5: Results of the scenarios with 6 EVs and λ_{PV_t} = 0 €/kWh.

	$E_{PV\text{-}EV}$ [kWh]	E_{PV} [kWh]	PV self-consumption [-]	Total costs [€]	E_{grid} [kWh]
Scenario 1	84.40	145.4	0.5804	-5.071	94.24
Scenario 2	84.40	145.4	0.5804	3.069	94.24
Scenario 3	120.1	145.4	0.8256	-5.603	24.36
Scenario 4	120.1	145.4	0.8256	-2.193	24.36
Scenario 5	91.92	145.4	0.6322	-6.072	79.53
Scenario 6	120.1	145.4	0.8256	-2.193	24.36
min E_{grid}	121.1	145.4	0.8327	0	0

5.2. Winter

The present section will elaborates on the performance of the proposed EMS during a day in winter, with very low irradiation which enables the PV system to produce 3.16 kWh over the entire day. In addition to this, the day is considerably shorter. Therefore, it will be far more challenging for the EMS to achieve cost reduction since the overlap between total parking time extends beyond the amount of daylight. In that respect, this case study will act as a "worst-case scenario". First, two base scenarios in which uncontrolled charging occurs will be examined in order to assess the performance of the EMS during winter, depending on different scenarios.

5.2.1. One charging point - four EVs

Scenario 1 and 2

The current scenarios will investigate the costs incurred when uncontrolled charging is in place, both with λ_{PV_t} = 0.097 €/kWh and λ_{PV_t} = 0 €/kWh, although this nor the FIT make a difference for the figures. The power allocation is presented in fig. 5.21 whereas figs. A.69 to A.71 provide extra information regarding the charging process. It can be seen that EV 1 immediately starts charging upon arrival while there is no PV energy production. This implies that 10 kW is drawn from the grid at 7.31 a.m., amidst peak demand during morning. However, it seems unlikely that the EMS in combination with a flat tariff will decide significantly different, as there is no financial incentive to do so. Furthermore, the numerical results are presented in tables 5.6 and 5.7, from which several interesting points can be noticed. First, as was expected, PV self-consumption is with 96.26% significant. Second, for scenario 1 and 2 and with both λ_{PV_t} = 0.097 €/kWh and λ_{PV_t} = 0 €/kWh, total costs are barely influenced by the tariff in place. This can be ascribed to the fact that only 3.03 kWh out of the total 65.90 kWh required to charge the four EVs is produced by the PV system, whereas self-consumption is high and consequently only 0.13 kWh is fed into the grid. Since this is a small quantity compared to the total energy requirements, λ_{PV_t} and to an even lesser extentλ_{FIT_t} hardly play a role in terms of total costs.

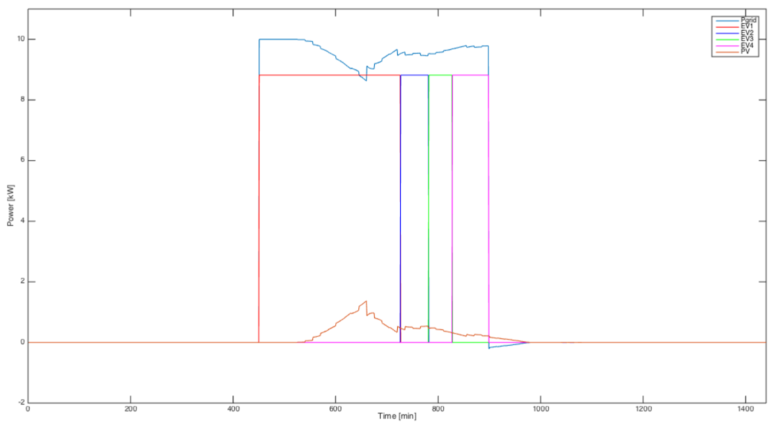

Figure 5.21: Power allocation during uncontrolled charging of 4 EVs with λ_{PV_t} = 0.097 €/kWh.

Scenario 3

The results for the present scenario are presented in figs. 5.22 and 5.23 and more detailed in figs. A.72 to A.77. At least two interesting points can be noticed after studying these figures. First, the charging process is spread out over the entire parking time of the EVs, rather than in sequence. Consequently, it appears that all available PV energy has been utilized for the charging process, which can be verified with help of tables 5.6 and 5.7. Second, due to the fact that there is no dynamic tariff in place, the EMS is not motivated to postpone charging and therefore, similarly as in uncontrolled charging, it starts charging right away at 7.31 a.m., thus contributing to morning peak demand.

Furthermore, the EMS did manage to decrease charging costs with 0.39% and 0.40% for λ_{PV_t} = 0.097 €/kWh and λ_{PV_t} = 0 €/kWh, respectively, when compared to scenario 1. Even though this is marginal, it does prove that the EMS is beneficial, even in a worst-case scenario.

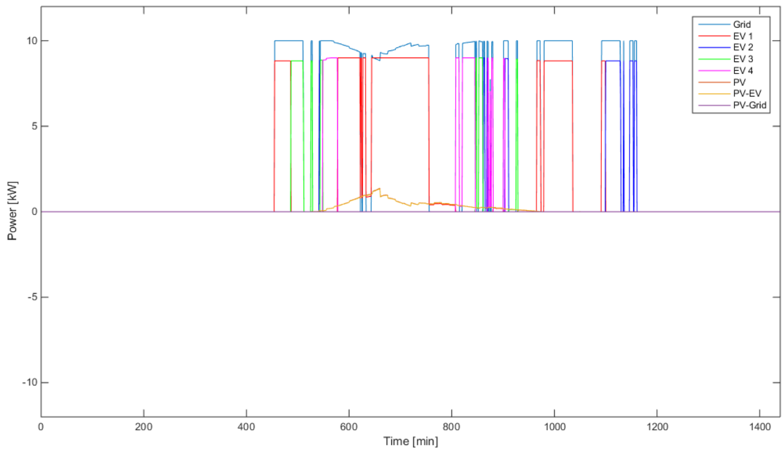

Figure 5.22: Power allocation during scenario 3 with 4 EVs and λ_{PV_t} = 0.097 €/kWh.

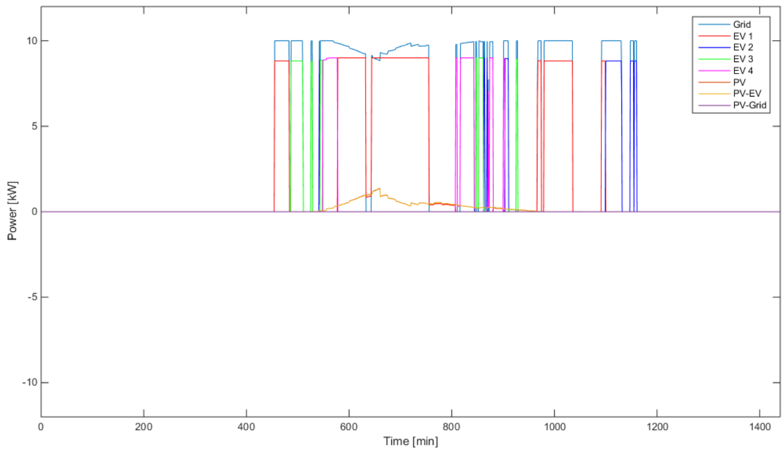

Figure 5.23: Power allocation during scenario 3 with 4 EVs and λ_{PV_t} = 0 €/kWh.

Scenario 4

The present section considers scenario 4, in which λ_{FIT_t} = 0.09 €/kWh. However, the previous section already showed that even with λ_{FIT_t} = 0.23 €/kWh, the EMS proved it to be non-optimal to feed energy back into the grid. Therefore, as can be seen in figs. 5.24 and 5.25 as well, this will not occur here either, especially since $\lambda_{\text{PV}_t} > \lambda_{\text{FIT}_t}$. In addition, these figures and figs. A.78 to A.83 are nearly identical to those of the previous section, as are the results in tables 5.6 and 5.7, and will therefore not be further explained.

Further cost reduction amounts to 0.49% and 0.50% for λ_{PV_t} = 0.097 €/kWh and λ_{PV_t} = 0 €/kWh, respectively, in comparison to scenario 2. The reason that this is higher than in scenario 3 is due to decrease in λ_{FIT_t} and since scenario 1 and 2 rely on feeding energy back into the grid to bring costs down, the FIT makes a, albeit relatively small, difference.

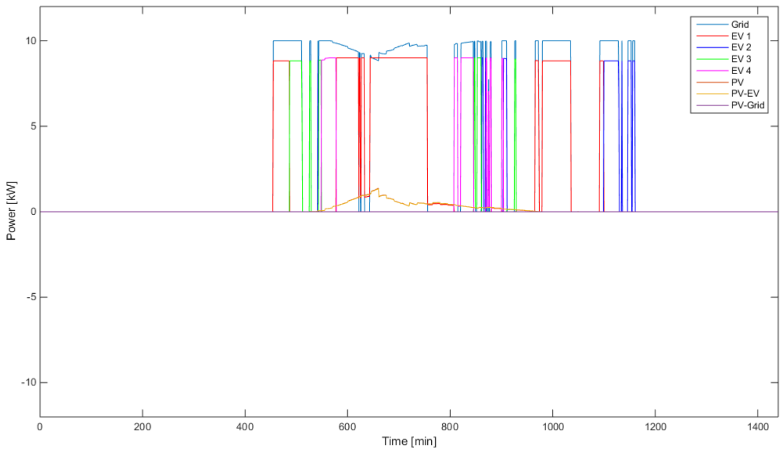

Figure 5.24: Power allocation during scenario 4 with 4 EVs and λ_{PV_t} = 0.097 €/kWh.

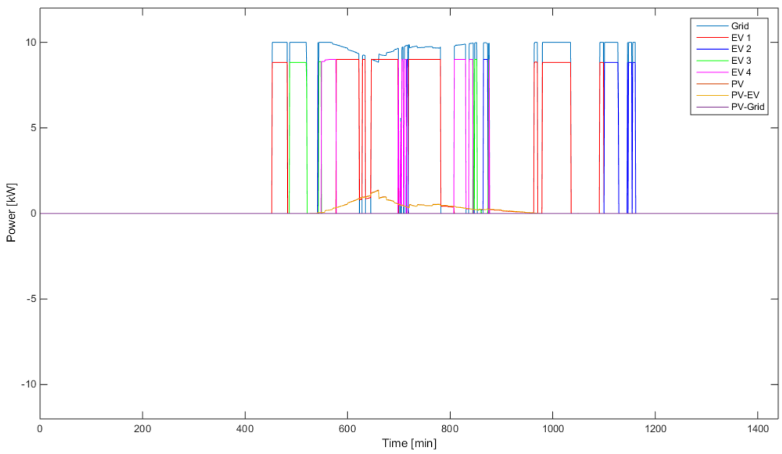

Figure 5.25: Power allocation during scenario 4 with 4 EVs and λ_{PV_t} = 0 €/kWh.

Scenario 5

The present section will investigate, on the basis of two case studies, how the EMS behaves when a dynamic tariff is in place, combined with a FIT of 0.23 €/kWh. The results are presented in figs. 5.26 and 5.27, figs. A.84 to A.87 and figs. A.88 to A.91. Since the pattern in both case studies is clearly similar, apart from some minor details, the case studies will be discussed as one.

Similarly as during summer, the EMS postpones drawing power from the grid until the price is well below its peak value, attained during the morning. During that time, one EV is charged with PV power. When the price has significantly lowered, the EMS decides to charge the EVs with a combination of PV and grid power. Unlike during summer, the EMS does not attempt to feed PV power into the grid, simply because there is no PV power generated during the morning peak in price. In addition, the EMS ensures that charging is complete before the peak in grid tariff occurs during the evening. The tables also show that costs are further reduced, by 2.80% and 2.86% for $\lambda_{\mathrm{PV}_t} = 0.097$ €/kWh and $\lambda_{\mathrm{PV}_t} = 0$ €/kWh, respectively, when compared to scenario 3. These results clearly show the potential of the EMS in combination with a dynamic purchase tariff, even in case of negligible PV power generation, as it reduces stress on the grid by postponing charging to off-peak hours and consequently reducing costs.

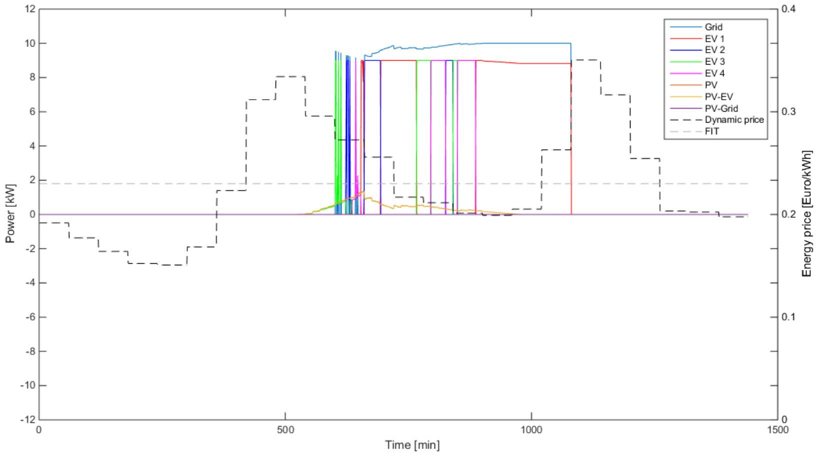

Figure 5.26: Power allocation during scenario 5 with 4 EVs and $\lambda_{PV_t} = 0.097$ €/kWh.

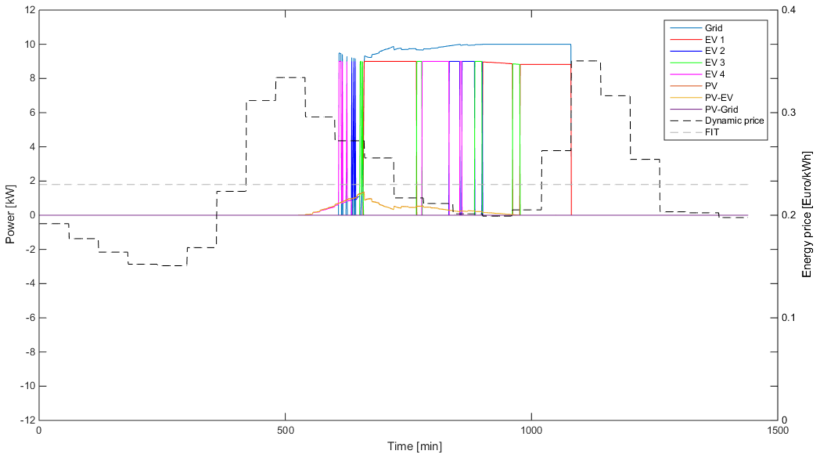

Figure 5.27: Power allocation during scenario 5 with 4 EVs and $\lambda_{PV_t} = 0$ €/kWh.

Scenario 6

A similar pattern arises as in the previous section, although currently the EMS utilizes all energy produced by the PV system to charge the EVs, as can be seen in figs. 5.28 and 5.29, figs. A.92 to A.95 and figs. A.96 to A.99.

Again, a dynamic tariff with low FIT proves it forces the EMS to act as a multi-objective optimization program: costs are minimized, which is the objective, while PV self-consumption is optimal or near the optimum and demand is shifted from peak price, i.e. peak demand, to valley price, i.e. valley demand. The tables 5.6 and 5.7 show that, in comparison to scenario 4, costs have been further reduced by 2.78% and 2.83% for $\lambda_{\mathrm{PV}_t} = 0.097$ €/kWh and $\lambda_{\mathrm{PV}_t} = 0$ €/kWh, respectively. In addition, results acquired in scenario 5 and 6 are almost the same which can be explained by the fact that λ_{PV_t} nor λ_{FIT_t} hardly play a role during such level of irradiation.

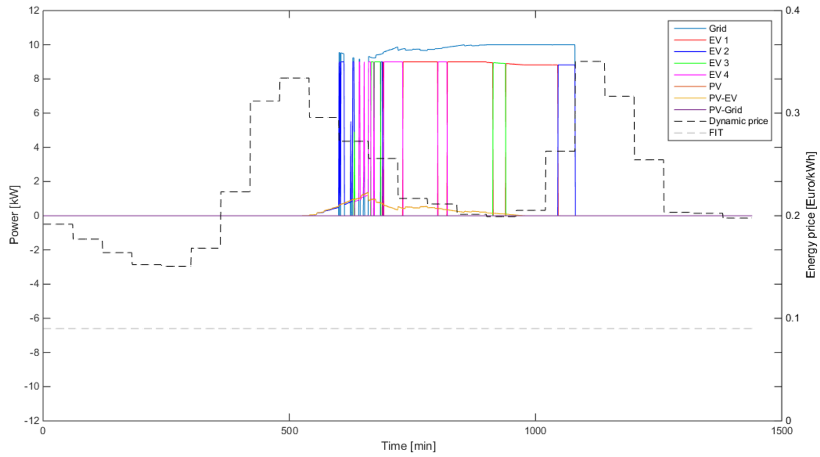

Figure 5.28: Power allocation during scenario 6 with 4 EVs and λ_{PV_t} = 0.097 €/kWh.

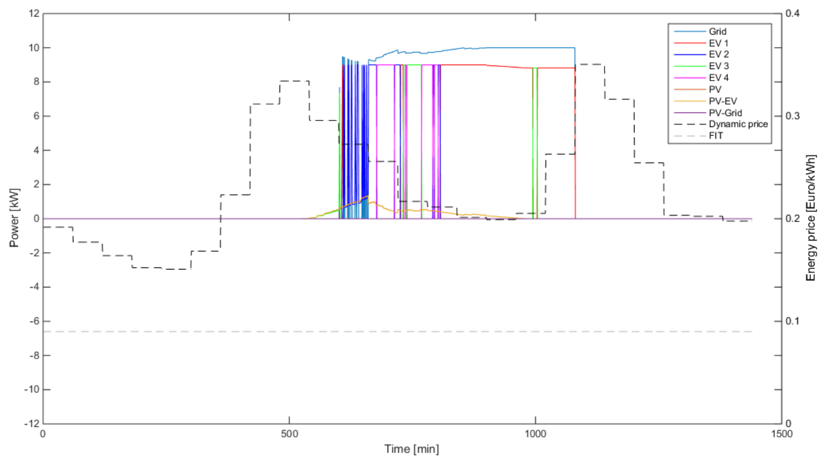

Figure 5.29: Power allocation during scenario 6 with 4 EVs and λ_{PV_t} = 0 €/kWh.

Minimize energy exchange with the grid

Finally, there is case study in which the maximum PV self-consumption can be ascertained, as discussed in section 3.3.4.1. However, it should come as no surprise that the maximum is 100%, a value that has been attained by most previous scenarios. As a consequence, charging costs incurred are exactly those incurred during scenario 3 and 4, taking into consideration which λ_{PV_t} was applicable. In addition, figs. 5.30 and A.100 to A.102 show exactly the same results as well.

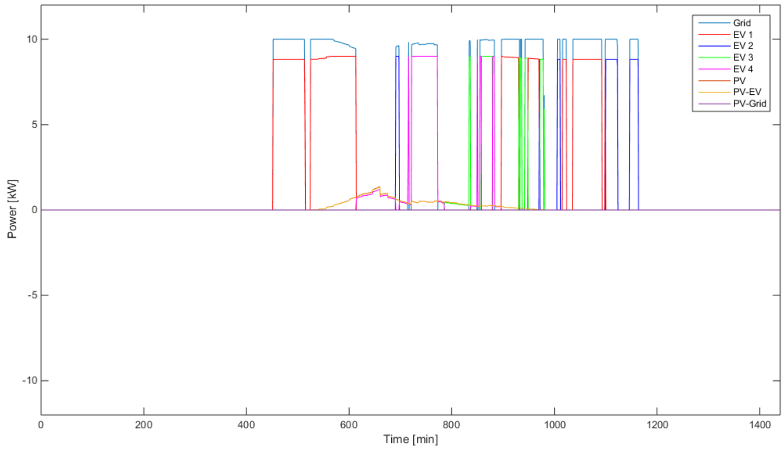

Figure 5.30: Power allocation during minimization of energy exchange with grid, with 4 EVs.

Overview of results

The results achieved by the EMS in scenario 3 and 4, presented in the tables below, are identical due to the fact that self-consumption is 100%, which implies that equal amounts of energy for the same tariff had to be drawn from the grid in order to satisfy demand.

Table 5.6: Results of the scenarios with 4 EVs and λ_{PV_t} = 0.097 €/kWh.

	$E_{PV\text{-}EV}$ [kWh]	E_{PV} [kWh]	PV self-consumption [-]	Total costs [€]	E_{grid} [kWh]
Scenario 1	3.038	3.155	0.9626	16.83	72.08
Scenario 2	3.038	3.155	0.9626	16.85	72.08
Scenario 3	3.155	3.155	1	16.77	71.56
Scenario 4	3.155	3.155	1	16.77	71.56
Scenario 5	3.155	3.155	1	16.30	71.56
Scenario 6	3.155	3.155	1	16.30	71.56
min E_{grid}	3.155	3.155	1	16.77	71.56

Table 5.7: Results of the scenarios with 4 EVs and λ_{PV_t} = 0 €/kWh.

	$E_{PV\text{-}EV}$ [kWh]	E_{PV} [kWh]	PV self-consumption [-]	Total costs [€]	E_{grid} [kWh]
Scenario 1	3.038	3.155	0.9626	16.53	72.08
Scenario 2	3.038	3.155	0.9626	16.54	72.08
Scenario 3	3.155	3.155	1	16.46	71.56
Scenario 4	3.155	3.155	1	16.46	71.56
Scenario 5	3.155	3.155	1	15.99	71.56
Scenario 6	3.155	3.155	1	15.99	71.56
min E_{grid}	3.155	3.155	1	16.46	71.56

5.2.2. Two charging points - six EVs

Scenario 1 and 2

Similarly as before, the present section will provide a basis with which the performance of the EMS during future scenarios can be compared. The resulting graphs are depicted in fig. 5.31 and figs. A.103 to A.105. The graphs show the significant power withdrawal early in the morning, contributing to peak demand in that period. It should be noted that this pattern adds with every charging point installed and thus will increase substantially with increasing penetration of EVs at the workplace.

The results in tables 5.8 and 5.9 show charging costs amount to €26.89 and €27.04 for λ_{PV_t} = 0.097 €/kWh and λ_{PV_t} = 0 €/kWh, respectively. In addition, similarly as with one charging point, the difference between the scenarios in terms of absolute energy exchange does not appear to be significant. This is mainly due to the fact that the EVs have fixed energy requirements and since irradiation is low, this will not contribute significantly to the charging process. In addition it should be noted that the graphs for scenario 1 and 2 are exactly the same.

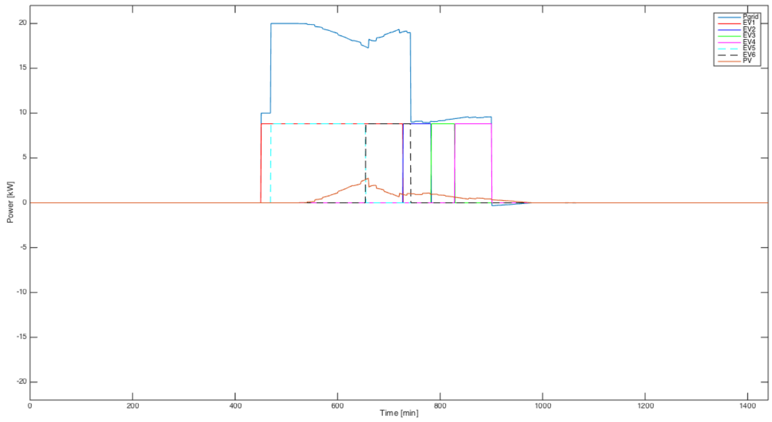

Figure 5.31: Power allocation during uncontrolled charging of 6 EVs with λ_{PV_t} = 0.097 €/kWh.

Scenario 3

The present section examines the performance of the EMS when a price mechanism is imposed similar to netting, as currently is the case in The Netherlands. The results are presented in figs. 5.32 and 5.33 and figs. A.106 to A.111. From the aforementioned figures it can be seen that the EMS behaves in a similar fashion during both case studies, which is supported by the results presented in tables 5.8 and 5.9.

The charging process as a consequence of the present scenario shows similarities to the charging process shown in scenario 1 and 2, albeit that available PV energy is better utilized and the entire process is spread out over the day. However, the current scenario will still contribute significantly to peak demand during morning, an obstacle that can, with the proposed EMS, be mitigated by imposing a dynamic tariff that reflects peak demand in terms of marginal costs. As explained during the winter case study examining one charging point, the EMS is not able to make a significant difference in terms of reducing the absolute power exchange with the grid due to low irradiation. Nevertheless, the EMS increases PV self-consumption to 100%, a result that was also achieved in case of one charging point. In comparison to scenario 1, charging costs have been reduced by 0.41% and 0.42% when λ_{PV_t} = 0.097 €/kWh and λ_{PV_t} = 0 €/kWh, respectively.

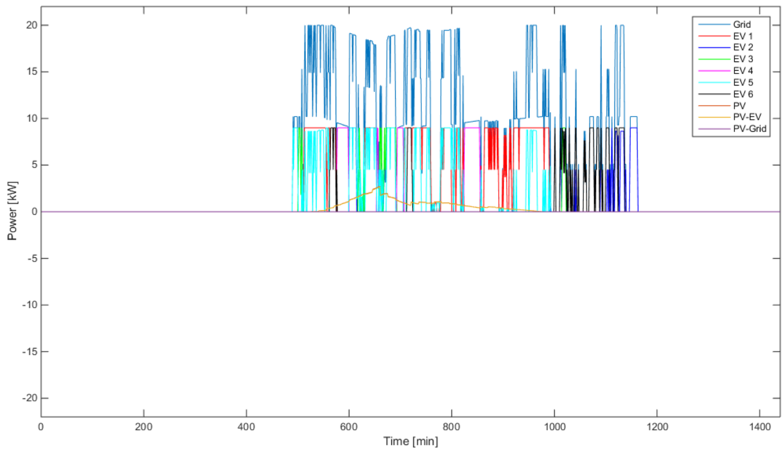

Figure 5.32: Power allocation during scenario 3 with 6 EVs and λ_{PV_t} = 0.097 €/kWh.

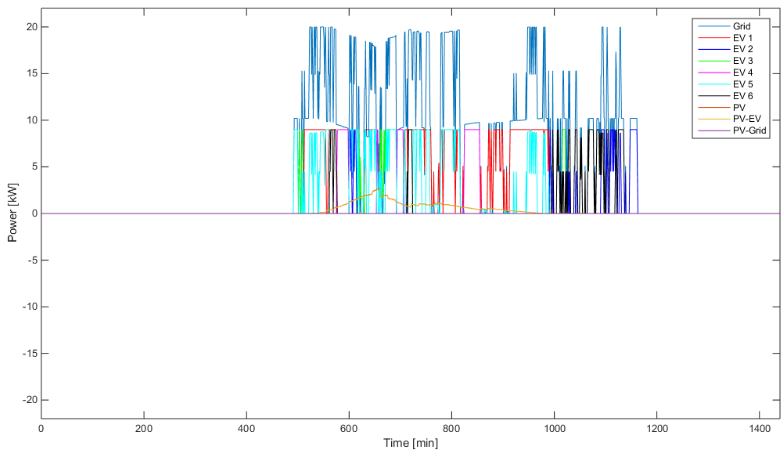

Figure 5.33: Power allocation during scenario 3 with 6 EVs and λ_{PV_t} = 0 €/kWh.

Scenario 4

The results of the present scenario are presented in figs. 5.34 and 5.35 and figs. A.112 to A.117. In addition, tables 5.8 and 5.9 show the obtained numerical results. As can be seen from the figures and tables, the behavior of the EMS in this case study is similar to that of scenario 3. Therefore, the same conclusions regarding the results apply. However, in terms of cost reduction the present scenario shows an improvement due to the fact that the FIT has been lowered. This results a cost reduction of 0.99% and 1.02% when λ_{PV_t} = 0.097 €/kWh and λ_{PV_t} = 0 €/kWh, respectively, in comparison to scenario 2.

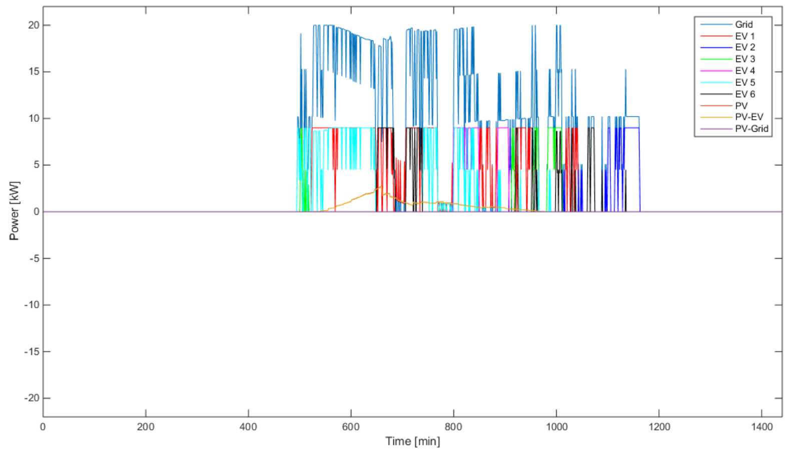

Figure 5.34: Power allocation during scenario 4 with 6 EVs and λ_{PV_t} = 0.097 €/kWh.

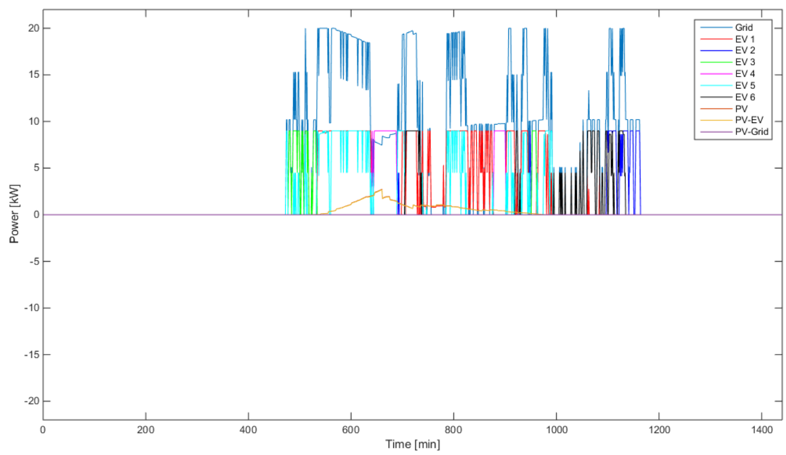

Figure 5.35: Power allocation during scenario 4 with 6 EVs and λ_{PV_t} = 0 €/kWh.

Scenario 5

The present section investigates what the potential is of a dynamic price mechanism. As results of previous similar case studies have shown, such a grid tariff proved to be effective in both further reducing costs and shifting demand from a peak to valley period, although the FIT needs to be carefully considered. A comparable charging strategy is initiated by the EMS here as well, as can be seen from figs. 5.36 and 5.37, figs. A.118 to A.121 and figs. A.122 to A.125. Since the results for $\lambda_{\mathrm{PV}_t} = 0.097$ €/kWh and $\lambda_{\mathrm{PV}_t} = 0$ €/kWh are analogous, both case studies will be discussed simultaneously.

Apart from the suspected behavior, i.e. shifting demand, the EMS proves it is optimal to discharge EV 5, parked at the second charging point, in order to charge EVs parked at the first charging point. This was not the case during summer, essentially due to the fact that during the early morning, the EMS was able to allocate PV power to the EVs rather than drawing power from the grid or other EVs. However, since currently this is not the case, the EMS has to decide either to charge the EVs with expensive grid power or to draw energy from an EV at the second charging point, knowing that the grid price will significantly decrease during the afternoon after which that specific EV can still meet its energy requirements. In addition, the figures show that the EMS already utilizes the entire period in which the price is relatively low and therefore the only viable solution is the one currently performed. Obviously, such a strategy is costly, in terms of efficiency losses but also battery degradation. As stated before however, discharging the battery does not degrade it more than normal driving patters due to the fact that less power is drawn and as a consequence, there is less strain on the battery. In fact, the lost capacity per normalized Wh is found to be $-6.0 \cdot 10^{-3}$% for discharging to support driving while that is $-2.7 \cdot 10^{-3}$% for discharging to support V2G [75].

Comparable to the other case studies in which scenario 5 was examined, PV self-consumption is quite low. Nevertheless, tables 5.8 and 5.9 show that the current scenario does allow the EMS to decrease costs further by 5.90% and 5.89% for $\lambda_{\mathrm{PV}_t} = 0.097$ €/kWh and $\lambda_{\mathrm{PV}_t} = 0$ €/kWh, respectively, when compared to scenario 3. It is also interesting to note that energy exchange with the grid is slightly higher than other scenarios, which is due to the efficiency losses during additional charging/discharging processes.

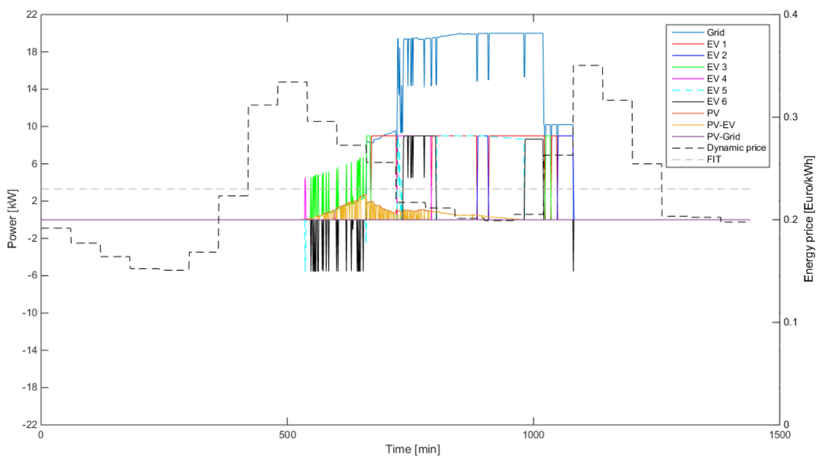

Figure 5.36: Power allocation during scenario 5 with 6 EVs and $\lambda_{PV_t} = 0.097$ €/kWh.

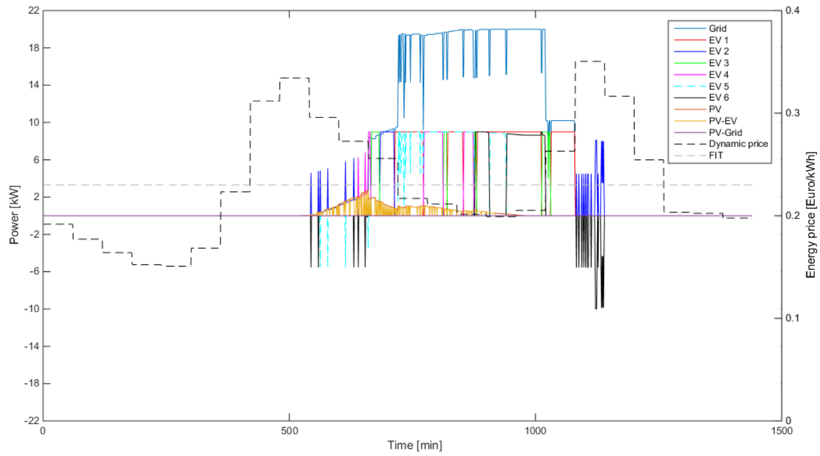

Figure 5.37: Power allocation during scenario 5 with 6 EVs and λ_{PV_t} = 0 €/kWh.

Scenario 6

Similarly as in scenario 4 of this particular case study, the results of the present scenario are analogous to the results attained in the previous scenario although PV energy is not fed into the grid since $\lambda_{\mathrm{PV}_t} > \lambda_{\mathrm{FIT}_t}$. That the results are analogous can be seen in figs. 5.38 and 5.39, figs. A.126 to A.129 and figs. A.130 to A.133, in addition to tables 5.8 and 5.9. Therefore, the same reasoning regarding the operation of the EMS applies. Furthermore, the EMS shows to have reduced charging costs further by 5.88% and 6.05% for λ_{PV_t} = 0.097 €/kWh and λ_{PV_t} = 0 €/kWh, respectively, in comparison to scenario 4, while maximizing PV self-consumption to 100%.

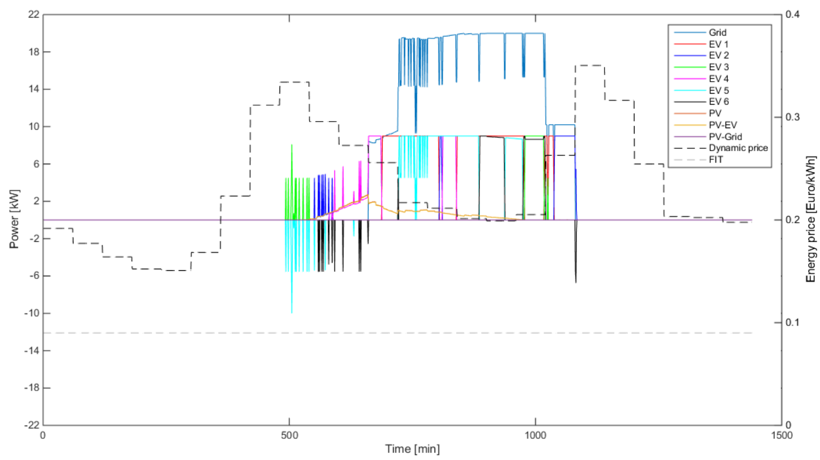

Figure 5.38: Power allocation during scenario 6 with 6 EVs and λ_{PV_t} = 0.097 €/kWh.

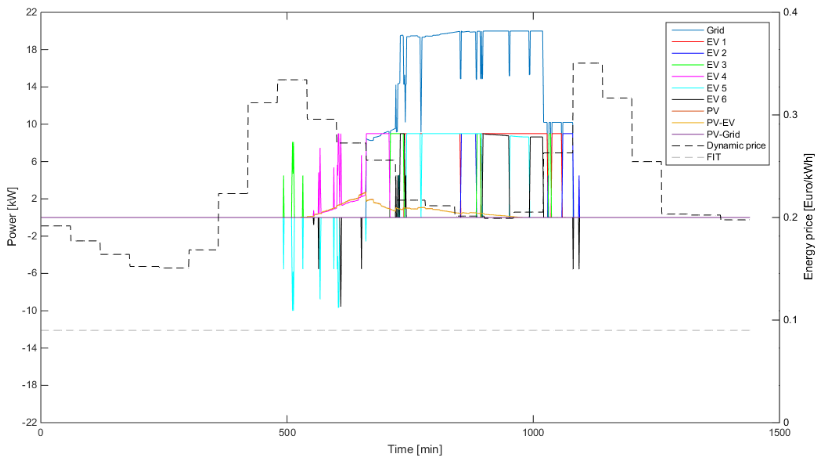

Figure 5.39: Power allocation during scenario 6 with 6 EVs and λ_{PV_t} = 0 €/kWh.

Minimize energy exchange with the grid

It was already established throughout this entire section that the EMS was able to reach 100% PV self-consumption during scenario 3, 4 and 6 and the present section might therefore be considered trivial. The reason that self-consumption can be 100% is due to the fact that the hours of daylight are actually less than the parking time, as was established before. As a result, the tables 5.8 and 5.9 show that total charging costs are identical to those during scenario 3 and 4, whereas the EMS managed to reduce charging costs during scenario 5 and 6 due to the specific price mechanism imposed. The figs. 5.40 and A.134 to A.136 present the charging process in more detail, from which it can be seen that although the final results are the same, the power allocation varies from that seen in figs. 5.32 to 5.35. From the point of view of the grid, the current result may be considered more favorable since power withdrawal is more spread out over the day, with the gravity of energy withdrawal during midday rather than during the morning. However, it should be noted that there is no stimulus for the EMS to do this, other than the fact the objective function has changed. In that sense, the EMS can allocate power as it calculates to be optimal, as long as the constraints and objective function are satisfied.

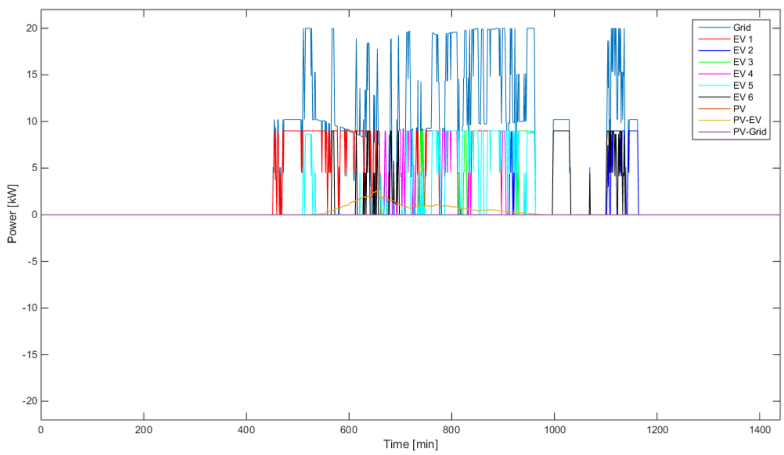

Figure 5.40: Power allocation during minimization of energy exchange with grid, with 6 EVs.

Overview of results

Table 5.8: Results of the scenarios with 6 EVs and λ_{PV_t} = 0.097 €/kWh.

	$\mathbf{E_{PV\text{-}EV}}$ **[kWh]**	$\mathbf{E_{PV}}$ **[kWh]**	**PV self-consumption [-]**	**Total costs [€]**	$\mathbf{E_{grid}}$ **[kWh]**
Scenario 1	5.125	6.311	0.8121	26.89	116.5
Scenario 2	5.125	6.311	0.8121	27.04	116.5
Scenario 3	6.311	6.311	1	26.78	113.8
Scenario 4	6.311	6.311	1	26.78	113.8
Scenario 5	6.311	6.311	1	25.19	114.4
Scenario 6	6.311	6.311	1	25.20	113.8
min $\mathbf{E_{grid}}$	6.311	6.311	1	26.78	113.8

Table 5.9: Results of the scenarios with 6 EVs and λ_{PV_t} = 0 €/kWh.

	$\mathbf{E_{PV\text{-}EV}}$ **[kWh]**	$\mathbf{E_{PV}}$ **[kWh]**	**PV self-consumption [-]**	**Total costs [€]**	$\mathbf{E_{grid}}$ **[kWh]**
Scenario 1	5.125	6.311	0.8121	26.27	116.5
Scenario 2	5.125	6.311	0.8121	26.43	116.5
Scenario 3	6.311	6.311	1	26.16	113.8
Scenario 4	6.311	6.311	1	26.16	113.8
Scenario 5	6.311	6.311	1	24.62	114.4
Scenario 6	6.311	6.311	1	24.58	113.8
min $\mathbf{E_{grid}}$	6.311	6.311	1	26.16	113.8

5.3. Additional case studies - Dynamic grid price and dynamic FIT

As energy storage devices, e.g. batteries, are becoming less expensive rapidly, as was established in the literature review, these may be used to support further penetration of PV by charging the batteries during the day and discharging them at night. However, as with every commodity, there needs to be a financial incentive to store it and the method to subsequently store it should be inexpensive, so that the aforementioned financial incentive is not immediately wasted. As can be concluded from the previous sections, a flat FIT does not provide such an incentive. Such a financial incentive could however be to implement a dynamic FIT, e.g. 90% of the dynamic grid price, thus $\lambda_{\mathrm{FIT}_t} = 0.9 \cdot \lambda_{\mathrm{G2V}_t}$ [84]. Since λ_{G2V_t} is correlated to demand, λ_{FIT_t} will also be and therefore, in case of high demand, it will be preferable to feed energy into the grid. It is likely that this form of electricity pricing will be the future and therefore it is important to study the behavior of the proposed EMS with such a price mechanism, and compare it to uncontrolled charging with an identical price mechansim. Further, as stated before, peak demand and irradiance do not have substantial coincidence, hence inexpensive or free energy produced by a PV system needs to be stored in order to feed it into the grid when λ_{FIT_t} has increased. Evidently, such a process, e.g. V2G, is accompanied by additional charging and discharging losses, as well as additional degradation of the battery and thus requires careful consideration regarding its viability. As stated before, a degradation cost of 0.038 €/kWh was used in the previous sections, justified by the fact that capacity loss due to V2G was less than half of capacity loss due to driving cycles. However, if one were to concoct a case study with higher battery degradation costs, this would merely decrease the likelihood of V2G viability.

The additional case studies are both performed using the PV profile with high irradiation, without marginal costs for PV energy and with 4 and 6 EVs, i.e. one and two charging points. The reason for this is understandable as these case studies include the best conditions to induce potential V2G processes and therefore provide a clear guideline to the feasibility of V2G as a concept. In addition, these case studies are selected due to the fact that they are comparable to studies found in literature, such as in [4, 41, 84, 85]. Furthermore, an uncontrolled charging policy in combination with dynamic purchase tariff and dynamic FIT is also examined, so as to ascertain the full potential of the proposed EMS and put its results into perspective. The results for the case study with 4 EVs and an uncontrolled charging policy are presented in figs. 5.41 and A.137 to A.140, whereas the results with 4 EVs controlled by the EMS are presented in figs. 5.42 and A.141 to A.144. Further, results of the uncontrolled charging policy in combination with two charging points are presented in figs. 5.43 and A.145 to A.148, while results of the EMS are presented in figs. 5.44 and A.149 to A.152. In addition, the numerical results are presented in table 5.10.

First, it can be seen from the uncontrolled charging policy, presented in fig. 5.41, that power withdrawal from the grid and the dynamic tariffs show a similar trend, i.e. downwards, during the first half of the day. This is caused by the fact that power drawn from the grid during the morning is most significant, while the price is significant as well, due to the typical peak in demand that occurs during the morning. As irradiance increases, less power from the grid is required but simultaneously, grid price decrease as demand decreases similarly. Continuing through the day, the EVs finish charging exactly when FIT is at its lowest point and feeding in power at this time is therefore generating less revenue. Later, the FIT increases while the amount of power decreases as sunset approaches. Therefore it can be concluded that the disadvantage of the uncontrolled charging policy is even greater than in case of a flat tariff, since power withdrawal from the grid and grid price tend to show similar trend. This can be clearly seen when looking at fig. 5.42, where several interesting details can be noticed. First, power withdrawal from the grid is clearly shifted to the afternoon, similar as during scenario 5 and 6. However, due to the dynamic FIT, the EMS is motivated to feed a surplus of PV power into the grid during periods with high FIT and thus aiding to alleviate stress on the grid. Furthermore, it can be seen that there is no V2G process initiated during the entire day. The reason for this is evident since there is basically only one possibility for V2G, which is during the second peak in FIT, i.e. early evening. However, prior to that there is a valley period in terms of grid price and consequently FIT. During that period it is preferable to draw power from the grid in order to supplement produced PV power but due to limited span of the valley period, it is not possible to draw additional power to feed back at a later point in time. Moreover, the peak in grid price and FIT during the morning motivate the EMS to feed produced PV power back immediately rather than early evening, since this is far more efficient and without battery degradation cost. The numerical results presented in table 5.10 clearly show the improvements due to the EMS. Self-consumption is increased and energy exchange with the grid is reduced accordingly, while not maximized and minimized, as was shown in previous scenarios. The reason for this is the active contribution of the EMS to peak shaving. Moreover, the charging cost are reduced by a notable 118.44% when compared to uncontrolled charging. It should be noted that charging costs have been turned into a profit for the aggregated system, which proves the effectiveness of the EMS and its potential to increase sustainability.

The second case in which an uncontrolled charging policy is applied, is with 6 EVs, i.e. two charging points. The resulting power allocation is presented in fig. 5.43, from which a similar pattern as with one charging point arises. Power withdrawal decreases as PV power generation increases, while the purchase tariff decreases as well. However, an additional issue arises in this case, since there is no cooperation between the two charging points. This implies that when the second charging point is done charging, which is sooner than the first charging point, it feeds its generated PV power into the grid for a relatively low FIT rather than aiding the other charging point. This is also the reason that in the aforementioned figure, power is drawn from the grid while feeding PV power to the grid. While it is true that this is not possible for one charging point due to the fact that the converter cannot conduct in both directions simultaneously, this graph depicts the total power exchange and the aforementioned constraint therefore remains satisfied. If then the optimal power allocation due to the EMS, presented in fig. 5.44, is examined, similarities between this case and the case with one charging point are evident. However, it should be noted that it was established above that the present setting would allow for autonomous operation, but due to the high FIT in the morning it is more profitable to feed PV power into the grid, while drawing relatively cheap power from the grid during the afternoon. This behavior is also preferable for utilities, as demand is shaved and becomes less fluctuant. Furthermore, the EMS has proven that under these circumstances, V2G does contribute to the optimal solution. This is possible due to the fact that the EV involved in V2G, EV 6, is parked at the second charging point, which is the charging point that is occupied for 50%. Hence, the specific EV can be charged beyond its energy requirement because more time is available for the charging process, after which it can participate in V2G during the early evening when the FIT has risen considerably. It should be noted however, that the contribution in terms of energy appears to be minimal, due to the fact that the difference between λ_{FIT_t} and λ_{G2V_t} ought to be substantial before it becomes profitable. In addition and as noted before, increasing λ_{deg} would decrease the likelihood of V2G occurring in the optimal charging strategy. Furthermore, table 5.10 shows that self-consumption has decreased and consequently energy exchange with the grid increased, similar as in the previous case. Therefore, a similar reasoning regarding the benefit of this holds. Finally, in terms of profit increase the EMS shows a remarkable result. Whereas the uncontrolled charging policy leads to a profit of €1.47, the EMS manages to increase this to €7.74, or an increase of 427.45%, caused mainly by the lack of cooperation and the inability to shift demand away from the peak in purchase tariff.

A final remark should be made regarding the remaining case studies, as preliminary results showed that the EMS could not prove that including V2G would lead to optimality.

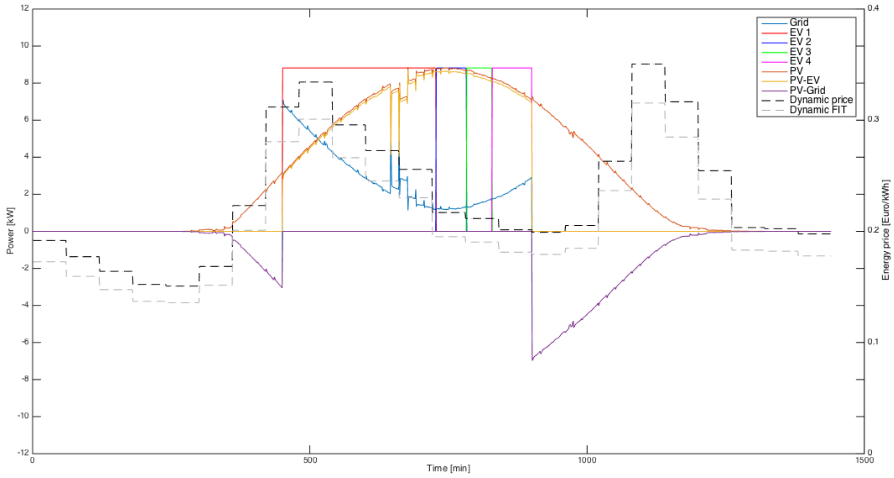

Figure 5.41: Power allocation with a dynamic FIT, 4 EVs, λ_{PV_t} = 0 €/kWh, uncontrolled charging.

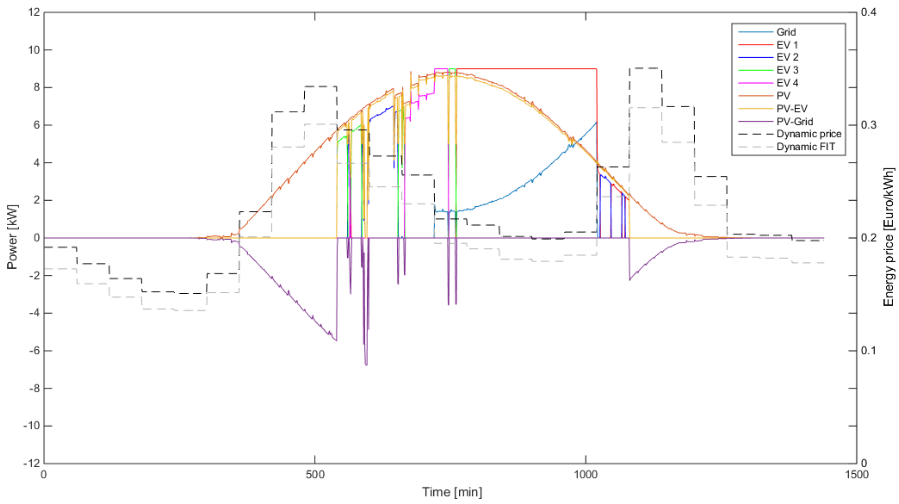

Figure 5.42: Power allocation with a dynamic FIT, 4 EVs, λ_{PV_t} = 0 €/kWh.

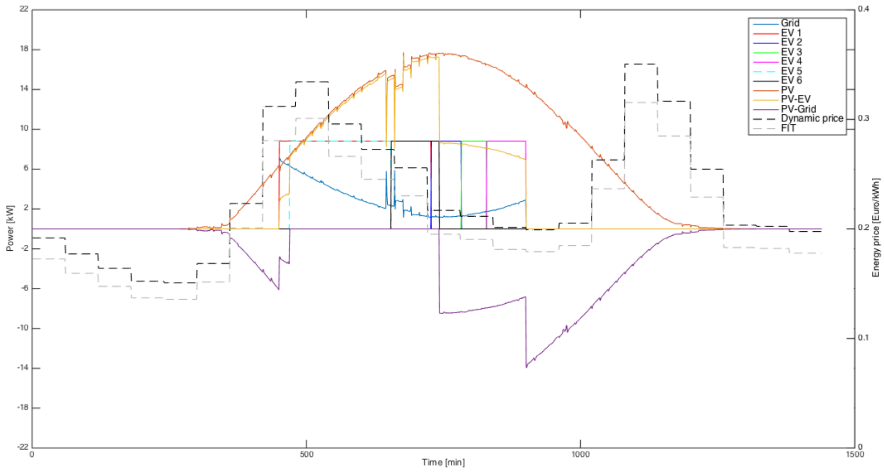

Figure 5.43: Power allocation with a dynamic FIT, 6 EVs and λ_{PV_t} = 0 €/kWh, uncontrolled charging.

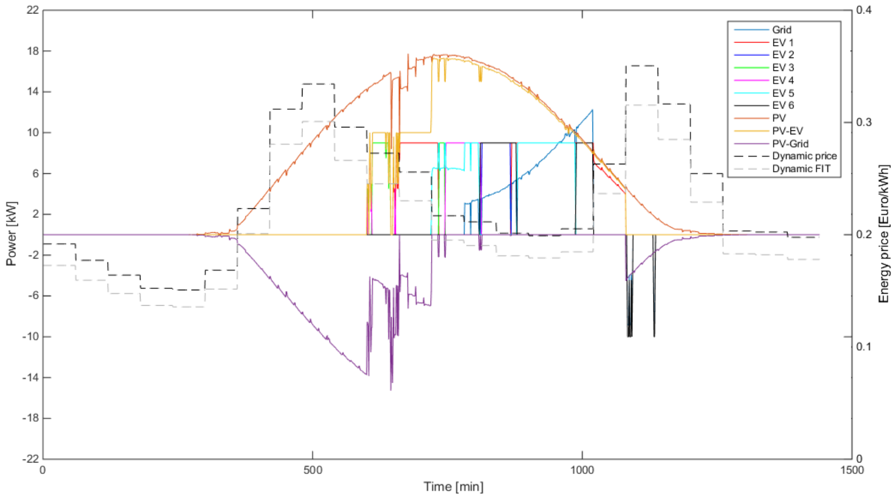

Figure 5.44: Power allocation with a dynamic FIT, 6 EVs and λ_{PV_t} = 0 €/kWh.

Table 5.10: Results of the additional scenarios with dynamic FIT and λ_{PV_t} = 0 €/kWh.

	$E_{PV\text{-}EV}$ [kWh]	E_{PV} [kWh]	PV self-consumption [-]	Total costs [€]	E_{grid} [kWh]
Uncontrolled charging - 4 EVs	53.56	72.72	0.7365	2.181	39.61
Energy management system - 4 EVs	59.93	72.72	0.8241	-0.4022	27.07
Uncontrolled charging - 6 EVs	84.40	145.4	0.5804	-1.468	94.24
Energy management system - 6 EVs	96.45	145.4	0.6632	-7.743	75.20

5.4. Conclusion

Throughout this section the EMS has proved to be able to reduce charging costs, impact on the grid and grid dependency. The tables 5.2 and 5.3 showed that PV self-consumption increased with more than 20% in case of one charging point to the maximum achievable with the exception of scenario 5, where the high FIT decreased self-consumption. Therefore, it can be concluded that minimizing charging costs implies maximizing PV self-consumption, under the condition that $\lambda_{G2V_t} > \lambda_{FIT_t}$. Additionally, it can be concluded that a high FIT in combination with a dynamic tariff will motivate the EMS to feed a surplus of PV power into the grid during peak hours, while drawing power from the grid during off-peak hours and therefore aiding in peak shaving. This behavior was not seen in case of a low FIT, due to the fact that it is less profitable to do so and increasing self-consumption is preferred. When one charging point, flat tariffs, i.e. scenario 3 and 4, and marginal costs for PV energy were taken into consideration, costs were reduced by 3.56% and 23.49%, respectively, when compared to uncontrolled charging. A dynamic tariff, i.e. scenario 5 and 6, for purchasing energy from the grid allowed the EMS to postpone charging until the price had significantly lowered and consequently reduce costs further. The reduction amounted to 4.28% for scenario 5 and 1.94% for scenario 6, where it is important to note that these are additional reductions, i.e. the cost reduction in scenario 5 is compared to that of scenario 3.

An important remark needs to be made regarding the marginal costs of PV energy, λ_{PV_t}. During the literature review no study in the research area of "Optimization of power flows in smart grids" was found to include marginal costs of PV energy, possibly due to the assumption that these are sunk costs. Although it is the belief of the author that this does not properly reflect reality, all scenarios were also considered in an extra case study, i.e. when λ_{PV_t} = 0 €/kWh. The reason for this decision is simple: to be able to make a fair comparison between the results attained during this thesis and other scientific work. As a result from excluding these marginal costs, self-consumption remained the same since it had already reached it limit and could therefore not be further improved. However, the EMS showed additional improvements in terms of cost reduction, as was shown in table 5.3. More specifically, with $\lambda_{\mathrm{G2V}_t} = \lambda_{\mathrm{FIT}_t}$ = 0.23 €/kWh, i.e. scenario 3, the EMS reduced charging costs by 35.30% when compared to scenario 1. When the FIT was lowered to 0.09 €/kWh, i.e. scenario 4, the EMS realized a considerable reduction of 72.75%. Imposing a dynamic tariff, i.e. scenario 5 and 6, showed that costs could be even further reduced by 58.13% and 17.02% when compared to scenario 3 and 4, respectively.

The next step was to assess how the EMS behaved when a second charging point was included that was occupied for 50%, of which the results were presented in tables 5.4 and 5.5. The aim of this particular case study was to ascertain to which extent the EMS allowed cooperation between the charging points in case of a surplus of PV energy, a likely event e.g. during summer or holiday periods. The uncontrolled charging processes in scenario 1 and 2 showed that there is no cooperation, leading to the conclusion that a workplace with large EV fleet would increase stress on the grid significantly though high demand in the morning and overproduction during the afternoon, and it was noted these results can be extrapolated to the number of charging points.

During the following scenarios a similar pattern arose as was the case with one charging point, where self-consumption increased with almost 25% to 82.56%, although the maximum achievable 83.27% self-consumption was not attained. This was due to the specific charging process that occurred when the objective was to minimize energy exchange with the grid, in which the EMS decided to temporarily store energy in one EV, so that is could later charge another EV at the first charging point. In terms of cost the latter did not prove to be optimal and as a consequence, less energy produced by the PV system was used in the subsequent scenarios. Furthermore, it was expected that the cost reduction would be higher, owing to the fact that there is twice as much PV energy production and less demand. When marginal costs for PV were considered, this resulted in a cost reduction of 6.97% and 32.19% for scenario 3 and 4, respectively. Imposing a dynamic grid tariff led to further reduction of charging costs by the EMS in scenario 5 when compared to scenario 3, more specifically by 6.86%. Comparable to the case with one charging point, this specific pricing mechanism showed increase in energy exchange with the grid. However, lowering the FIT in scenario 6 meant that there was no further improvement possible, when compared to scenario 4. This was mainly due to the fact that the system was able to work autonomously during scenario 4 and was therefore independent of fluctuations in grid price.

Excluding marginal costs allowed the EMS to increase profit by 10.50% in scenario 3, when compared to scenario 1. Furthermore, lowering the FIT to 0.09 €/kWh, i.e. scenario 4, resulted in a substantial reduction of 171.43% when compared to scenario 2. The latter implies that charging costs incurred in scenario 2 were turned around into a profit, a similar result as in scenario 4 when marginal costs of PV were excluded and one charging point was examined. In addition, the EMS proved, in combination with the price mechanism in scenario 5, to further increase profit by 8.37%, although again with an increase of energy exchanged with the grid. Similarly, scenario 6 did not show an improvement when compared to scenario 4 due to the fact that the system was already independent of grid price.

During winter, the low level of irradiation proved to be challenging for the EMS, clearly due to the fact that energy requirements were mainly met by drawing power from the grid. In addition, total parking time and PV power output showed maximum overlap. These facts ensured that the difference between including marginal costs for PV, λ_{PV_t}, or not made little difference in terms of percentual cost reduction, which was presented in tables 5.6 to 5.9. Nevertheless, in case of one charging point the EMS proved to reduce charging costs by 0.39% when $\lambda_{\mathrm{G2V}_t} = \lambda_{\mathrm{FIT}_t} = 0.23$ €/kWh, i.e. scenario 3, when compared to scenario 1, while utilizing all energy produced by the PV system versus 96.26% during uncontrolled charging. Therefore, reducing λ_{FIT_t} to 0.09 €/kWh, i.e. scenario 4, did not make a difference in terms of absolute charging costs, since self-consumption was 100%, however, costs were reduced by 0.49% when compared to scenario 2 due to the fact that self-consumption was not 100% during uncontrolled charging. Similarly as during summer, the price mechanism in scenario 5 motivated the EMS to draw power from the grid when the price was relatively low. In comparison to scenario 3 however, charging costs were further reduced by 2.80%. Finally, low FIT in combination with dynamic grid tariff, i.e. scenario 6, motivated the EMS to postpone charging until the price was relatively low, whereas the EMS did not have this stimulus when a flat grid tariff was imposed, e.g. scenario 4. This resulted in a cost reduction of 2.78% when compared to scenario 4.

The case study with two charging points showed little difference between including or excluding λ_{PV_t}, similarly as when one charging point was considered. Furthermore, since there was no cooperation between the charging points during uncontrolled charging, self-consumption decreased to 81.21%. By allowing the charging points to collaborate, the EMS achieved 100% self-consumption. In case of scenario 3, this resulted in a cost reduction of 0.41% when compared to scenario 1. Similarly as with one charging point, the absolute charging costs incurred in scenario 3 and 4 were the same, owing to the fact that self-consumption was 100%. However, when scenario 4 was compared to scenario 2, the cost reduction achieved with the reduced FIT was slightly higher: 0.99%. Replacing constant λ_{G2V_t} with a dynamic variant, i.e. scenario 5, showed a further reduction in charging costs of 5.90% when compared to scenario 3. In addition, comparing results of scenario 6 with scenario 4 showed a further reduction of 5.88%.

From the aforementioned results, some interesting conclusions can be drawn. First, the proposed EMS proved that it was able to reduce charging costs while optimally utilizing PV power under various circumstances. This leads to the conclusion that the EMS is robust and able to improve the aforementioned aspects for nearly any situation. For example, one situation where it would not be able to improve them is when there would be no PV output and the current price mechanism applicable in The Netherlands, i.e. netting (scenario 1), is implemented, since in that case it does not matter when charging occurs. However, although dynamic tariffs are currently being experimented with in The Netherlands, when such pricing mechanisms come into effect it will allow the EMS to show further improvements in terms of cost reduction and the manner in which energy is consumed in general. In addition, the presented model has the clear advantage that it is able to forecast solar power output, consequently anticipate on future inputs and act accordingly. Therefore, the EMS is predictive rather than reactive, which has several benefits. For example, even though it may be more profitable to sell PV power to the grid at time t, e.g. because the FIT is relatively high, the EMS forecasted low solar power output at $t + k$ and therefore decides it is favorable to charge the EV with inexpensive or free PV power at time t. Furthermore, rather than being a purely abstract model, without too many modifications the EMS has the potential to be utilized in practice.

Second, as stated before, the proposed EMS proved to optimally utilize PV power while the objective was to decrease costs. This implied significant stress reduction on the grid, an important issue due to the threats large scale uncontrolled charging of EVs pose such as overloading [24], increase of emissions [93] and blackouts [57]. Furthermore, implementing a dynamic tariff that represents correlation between peak demand and price could reduce these threats further. Additionally, if a dynamic FIT were to be implemented, it was shown that by temporarily storing PV energy in the EVs, these could be included in the energy market and assist to alleviate peak demand. Therefore, it can be concluded that the proposed EMS can aid through shifting load away from peak demand and offering support during peak demand. Taking the aforementioned and the characteristics of a smart grid, presented in section 2.3, into consideration, it can be said that the model will transform unintelligent charging stations to smart and sustainable ones that can cooperate with each other.

Continuing with the third conclusion that is more specific to the examined scenarios, it was observed that during all case studies the cost reduction during scenario 4 is significantly larger than scenario 3, in which the only difference was the height of the FIT. The reason for this is the fact that costs during scenario 1 and 2 could only be reduced by feeding the surplus of PV power back to the grid. While the FIT was 0.23 €/kWh, this still resulted in significant revenues, however, when the FIT was decreased in scenario 2, charging costs increased. In addition, during the latter scenario PV energy was still fed into the grid, even though the FIT was lower than the marginal cost because it could not curtail PV power and thus effectively adding to the costs rather than reducing them. Therefore, the relative gain achieved by the EMS will increase in significance with decreasing FIT. A similar reasoning holds when marginal costs for PV were not taken into account, although uncontrolled charging with low FIT still yielded revenue in that case. This result is important since FITs are being reduced while RESs mature, e.g. as is currently the case in Germany.

Fourth, the combination of a dynamic tariff and high FIT, i.e. scenario 5, proved to aid in peak shaving. This was because the EMS anticipated on a low electricity price during the afternoon and could therefore sell a surplus of PV power during the morning. Lowering the FIT, i.e. scenario 6, showed that the EMS could reduce costs further in addition to maximizing self-consumption and decreasing energy exchange with the grid. This is an important result since increasing penetration of EVs into the vehicle fleet could pose serious threats to the main grid, as stated before. Therefore, if a smart energy management system is implemented and the retailer imposes a dynamic tariff, it could shift demand from peak hours. Additional case studies were examined to ascertain the possibilities of both a dynamic purchase tariff and FIT, which is a likely future scenario. It was shown that uncontrolled charging in combination with such a price mechanism proved to be substantially disadvantageous for the charging costs, since the EMS draws a significant amount of power from the grid during peak price, whereas it feeds power into the grid when the FIT is relatively low. Since the charging pattern remains the same regardless of the price mechanism, here too it mainly adds to peak demand during morning. Both these characteristics are considered to be negative and the EMS showed significant improvements with both one and two charging points. More specifically, charging costs were reduced by 118.44% in case of one charging point, while actively contributing to peak shaving. However, the most notable result was in case of two charging points, where the profit was increased with 427.45%. The main reasons for this result was the lack of cooperation and the inability to shift demand away from the peak in purchase tariff during the uncontrolled charging policy.

Fifth, the final row in tables 5.2 to 5.9 showed the maximum achievable self-consumption by minimizing energy exchange with the grid. This was important to ascertain because only then a conclusion could be drawn as to what extent the EMS would improve self-consumption when compared to uncontrolled charging. Consequently, it can be concluded that the EMS in combination with the price mechanisms in scenario 3, 4 and 6 maximize PV self-consumption in case of one charging point and approach the maximum in case of two charging points. Additionally, as stated before, a dynamic grid tariff will, besides maximizing PV self-consumption, shift load from peak demand to off-peak hours during the afternoon.

One of the concepts under investigation during this thesis is the viability of V2G. It has been proven by the proposed model that V2G led to an optimal solution, albeit in a best-case scenario. In case one would consider higher battery degradation costs, lower irradiation or a single, fully occupied charging point, including V2G will not lead to the optimal solution. However, V2V showed potential, especially in case of low irradiation because the EMS anticipated low λ_{G2V_t} later during the day and discharged an EV at the semi-occupied charging point to charge another EV at the fully occupied charging point. Later in the afternoon, there would be enough time for the former EV to charge with relatively inexpensive grid power until the required SOC. Taking into account the aforementioned, battery packs need to decrease further in price until V2G becomes truly profitable. As stated before, it can be concluded that the EMS in combination with a dynamic grid tariff and a dynamic FIT will reduce both costs and stress on the grid significantly, by shifting demand to an off-peak period and feeding a potential surplus into grid during peak demand. Moreover, it is stressed that without forecasting capability, the EMS would not be able to anticipate on future solar power and act accordingly, reducing its effectiveness.

Moreover, to put the achievements of the proposed EMS into perspective, a few comparable studies a that have been discussed in the literature review are repeated briefly. For example, the study in [41] achieved a cost reduction of 8.4% on a daily basis while minimizing charging costs. This study was performed on a day with high irradiation while a dynamic grid tariff and dynamic FIT were imposed. Additionally, V2G was investigated but battery degradation costs were not incorporated.

Another example is the study performed in [4], in which a cost reduction of 23.80% was realized during a day with high irradiation, in which V2G, although without battery degradation costs, dynamic grid tariff and dynamic FIT were taken into account. Furthermore, the authors of [89] achieved a cost reduction of 2.12% during a day with high irradiation and including a dynamic tariff but without V2G, mainly due to the fact that the parking lot possessed its own battery bank for which battery degradation costs were taken into consideration.

The EMS proposed in [84] incorporated a dynamic grid tariff, as well as a dynamic FIT in combination with V2G and battery degradation costs. In addition, no RESs were implemented, however, cost reductions of 33%, 10% and 20% were realized for household, commercial and mixed usage, respectively. Finally, cost reductions of 15%, 10% and 10% were achieved for household, commercial and mixed usage, respectively, were achieved in [85], in which a dynamic grid tariff, as well as a dynamic FIT in combination with V2G and battery degradation costs were taken into account.

Therefore, in order to make a fair comparison with the aforementioned studies, the results attained during the additional case studies should be taken into consideration, in which both a dynamic grid tariff and FIT were imposed. In case of 4 EVs, this particular case study showed an improvement of 118.44% when compared to uncontrolled charging, implying that charging costs were turned into profit. When 6 EVs were considered, the proposed EMS proved it was able to increase profit by 427.45% when compared to uncontrolled charging in combination with a dynamic purchase tariff and dynamic FIT. From this it may be concluded that the EMS proposed in this thesis provides remarkable results.

6 Conclusion and potential applications of the EMS

The present chapter reflects on the results and, subsequently, the contributions of this thesis. In addition, conclusions will be drawn about the aforementioned results and recommendations for future work will be given to finalize this chapter.

6.1. Overview of thesis work

The purpose of this thesis was to design an EMS that would optimize power flows on a solar powered workplace parking lot with EVs present. The main objective of the optimization was to minimize charging costs, while increasing PV self-consumption and reducing stress on the grid, so that electrification of the transportation sector can be increased while avoiding both significant increase in peak demand and EV charging with non-renewable energy. In order to achieve this, constraints, decision variables and an objective function were identified, after which a mathematical framework was formulated that accommodated the foundation of the proposed mathematical optimization. Furthermore, due to the very nature of the optimization problem at hand and the specific constraints imposed on the system, it was decided to formulate the problem as MILP, as it has at least one advantage: although introducing binary or integer variables inherently cause non-convexity, MILP is a powerful method through which it remains possible to achieve global optimum. This was important, since other optimization methods such as PSO or GA cannot prove whether the solution is a local or global optimum. In addition, the tendency in scientific literature regarding optimization problems is to create an abstract model with the purpose of displaying improvements that can be realized over uncontrolled charging. In order to distinguish this thesis, it was deemed necessary that apart from the abstract model, the EMS would have real-life viability and therefore it was decided to extend its capabilities by bestowing on it a predictive rather than reactive feature, i.e. by enabling it to forecast PV power. To this end, the Box-Jenkins approach was applied to identify the appropriate time-series model from the ARIMA processes, after which its parameters were estimated and finally it was subjected to various statistical tests. Moreover, the performance of the EMS was examined on the basis of scenarios in which several price mechanisms were entertained, after which results were analyzed and finally put into perspective with existing scientific results. The optimization problem was modeled in GAMS, whereas the solar irradiance was modeled and forecasted using Matlab. The EMS was then simulated in Matlab.

6.2. Results and conclusions

Solar power forecasting

As stated in the previous section, it was considered necessary for the EMS to be able to forecast PV power for that would allow it to predict and act accordingly rather than react. Although uncertainties remain, even with the addition of forecasting capabilities, better informed decisions regarding power allocation can be made. In addition, this allowed the proposed EMS to transform from merely an abstract model to a practical tool. Since the ARIMA process uses time-series to predict future behavior, the forecast horizon was set to fifteen minutes, which decreased the error significantly. The forecast for a day with high irradiation is presented in fig. 6.1, where a coefficient of determination, R^2, of 0.986 and RMSE of 0.395 kW were achieved. Furthermore, a similar approach was taken in case of a day with low irradiation, of which the forecast is presented in fig. 6.2. R^2 and RMSE amounted to 0.970 and 0.0429 kW, respectively. These statistics were considered to be satisfactory.

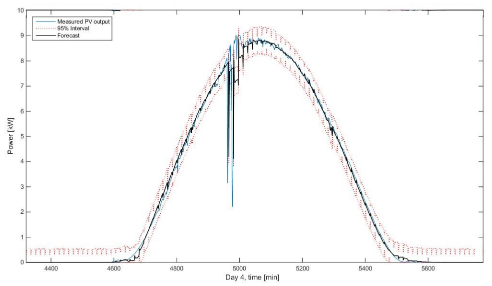

Figure 6.1: Forecast of PV power for a day with high irradiation.

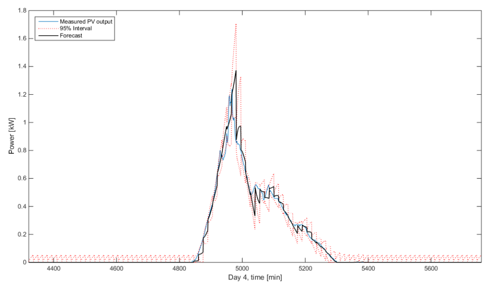

Figure 6.2: Forecast of PV power for a day with low irradiation.

Energy management system

Having established the mathematical framework in chapter 3 and input parameters in chapter 4, simulations could be run according to the established scenarios. Promising results were attained with respect to the reduction of costs, impact on the grid and grid dependency. It was shown that the EMS was able to significantly improve the aforementioned aspects during each case study except for two cases. First, imposing a dynamic purchase tariff in combination with a high FIT would reduce costs substantially, but showed to have detrimental effects in terms of energy exchange with the grid. Second, although still beneficial, during days with extreme low PV energy production improvements were less substantial. The reason for this was twofold although in fact these were intertwined, namely that the achieved self-consumption during uncontrolled charging (96.26%) was already high and PV production covered a mere 4.79 - 5.96% of energy demand by the EVs, depending on the number of charging points. Therefore, little improvement was possible in terms of self-consumption, meaning that more or less the same amount of energy had to be drawn from the grid. Nevertheless, results were still promising and a brief overview is given here, where it should be noted that the spread in the results are due to the specific scenario under consideration:

- Low PV energy production:
  - One charging point:
    - ◇ When taking marginal cost for PV, λ_{PV_t}, into consideration, in comparison to uncontrolled charging, the charging costs were reduced by 0.39 - 0.49% in case of flat tariffs and further reduced with 2.78 - 2.80% in case of a dynamic purchase tariff.
    - ◇ Eliminating λ_{PV_t} led to cost reductions of 0.40 - 0.50% in case flat tariffs were imposed. Introducing a dynamic purchase tariff led to further cost reductions of 2.83 - 2.86%.
  - Two charging points:
    - ◇ Including λ_{PV_t} led to cost reductions between 0.41 and 0.99% in case of flat tariffs and this was further reduced by 5.88 - 5.90% when a dynamic purchase tariff was introduced.
    - ◇ Excluding λ_{PV_t} led to 0.42 - 1.02% less charging costs, while a dynamic purchase tariff allowed the EMS to reduce costs further by 5.89 - 6.05%.
- High PV energy production:
  - One charging point:
    - ◇ While λ_{PV_t} was included, costs were reduced by 3.56 - 23.49% in case of flat tariffs, whereas further cost reductions of 1.94 - 12.23% were achieved when a dynamic purchase price was implemented.

    ◇ Omitting λ_{PV_t} enabled the EMS to reduce charging costs by 35.30 - 72.75% when flat tariffs were imposed and this was further reduced by 17.02 - 58.13% in case of a dynamic purchase tariff.
- Two charging points:
    ◇ Including λ_{PV_t} led to cost reductions between 6.97 and 32.19% in case of flat tariffs and this was further reduced by 0 - 6.86% when a dynamic purchase tariff was introduced.
    ◇ Eliminating λ_{PV_t} led to cost reductions of 10.50 - 171.43% in case flat tariffs were imposed. Introducing a dynamic purchase tariff led to further cost reductions of 0 - 8.37%.

From the aforementioned results it can be concluded that the proposed EMS will consistently improve in terms of cost reduction, impact on the grid and grid dependency. In fact, it is likely that it will always improve in terms of costs when compared to the status quo, except for the case when PV energy production would be zero and a flat tariff would be applicable. However, if in that scenario a dynamic tariff would be imposed, the EMS would again provide a significant improvement. Therefore, it can be stated that since it has shown to improve a worst-case scenario, the model is considered to be robust, although this does not imply that robust optimization has been carried out in this thesis.

Additionally, two extra scenarios were concocted where conditions were comparable as those in similar studies, in order to put the performance of the proposed EMS into perspective. Evidently, conditions were not identical and one should therefore exert carefulness when comparing results directly. Nevertheless, it was found that imposing both a dynamic purchase and feed-in tariff, while disregarding λ_{PV_t}, allowed the EMS to reduce costs by 118.44% and 427.45% for one and two charging points, respectively, when compared to uncontrolled charging. In addition to these notable results, the EMS aided the main electricity grid by feeding PV power during peak price, i.e. peak demand, and drawing power during valley price, i.e. valley demand, as can be seen in figs. 6.3 and 6.4. In comparison, cost reduction in similar studies ranged from 2.12 to 33.00%, emphasizing the fact the the proposed EMS provides excellent results.

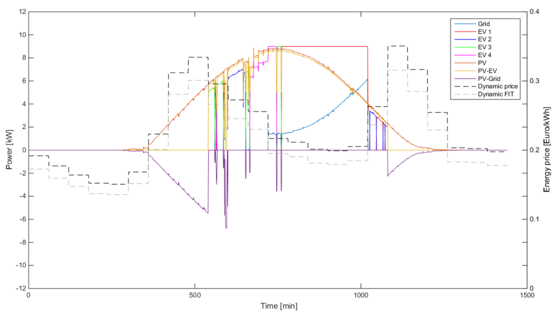

Figure 6.3: Power allocation with a dynamic FIT, 4 EVs, $\lambda_{PV_t} = 0$ €/kWh.

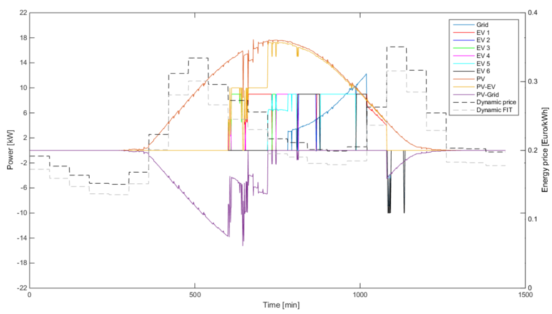

Figure 6.4: Power allocation with a dynamic FIT, 6 EVs, $\lambda_{PV_t} = 0$ €/kWh.

Furthermore, it was shown that V2G can lead to optimality, as can be seen in fig. 6.4. However, the circumstances under which this occurred and the limited extent of the V2G process led to the conclusion that for this concept to be profitable, battery prices need to decrease further.

Finally, arguably the most significant conclusion to be drawn based on the results presented throughout this thesis is the fact that the predictive EMS behaves in a logical and robust manner, i.e. it does what one could, and perhaps should, expect given a set of input parameters and does this consistently as well. Therefore, it is important to note that although the presented results are important, the EMS with its forecasting feature should be considered as the main contribution of this thesis.

6.3. Answering the research questions

Although the answers to the research questions, defined in section 1.2, have been implicitly answered in the previous sections, for the sake of clarity these are repeated and answered individually here.

- Which optimization technique should be used that is able to include the required constraints so that reality is modeled in a satisfactory manner?
  Considering the specific constraints to the present project, i.e. one EV was allowed to charge or discharge at time t at a charging point, and after having conducted a thorough literature study, it was found necessary to utilize binary variables that represent the on or off status of the charging/discharging process. In addition, as the mathematical program could be defined as a combination of linear constraints and objective function, it was possible to apply linear programming. Combining these characteristics, it was chosen to use mixed-integer linear programming, which is a powerful optimization method that can find the global optimum, even though the problem is non-convex due to the binary variables.

- Which available model should be utilized to forecast solar irradiance?
  Several methods and models exist to forecast solar irradiance. However, given the fact that the present project considered a solar carport, a model with high spatial resolution was required. In addition, for high accuracy the temporal resolution was one minute. After conducting the literature study, it became apparent that statistical models would perform best under these circumstances, after which the ARIMA class was selected as it showed greater potential in both spatial and temporal resolution, as was presented in fig. 2.3.

- As the forecast is made for a limited amount of time into the future, what methodology should be applied to provide the EMS with a predictive rather than reactive character?
  It was shown in section 4.1.1 that for larger forecast horizons, the standard deviation increases and consequently accuracy decreases. Therefore, if the EMS is to be used as a mean to anticipate on PV power generation and plan power allocation, accuracy needs to be guaranteed. Additionally, it was deemed not preferable to utilize a forecast horizon that was too short, since this would increase computational demand. Hence, a forecast horizon of fifteen minutes was selected and a flowchart depicting the functioning of the EMS was presented in fig. 3.2. The EMS feeds the latest PV power measurements into the ARIMA model and subsequently uses the forecast to make an optimal decision for the rest of the time period, based on the MILP model. Then, it skips fifteen minutes and repeats this process, thus ensuring high accuracy for the power allocation.

- To what extent can the proposed EMS decrease the grid dependency?
  Evidently, the answer to this question depends very much on the amount of power generated by the solar carport. For the scenario considering a high level or irradiation it was found that of the total energy demand, 93.23% could be supplied by the PV system while the EMS was implemented. In comparison, this was 71.68% during the uncontrolled charging policy, implying a significant increase. Since energy demand by the EVs was more than double the average demand by EVs in a similar setting [7], it can be concluded that the EMS can significantly reduce grid dependency but in the current state cannot work independently. Furthermore, in case a second charging point was added which was occupied for 50%, the EMS proved it was able to operate autonomously. Clearly, this was due to the surplus of generated power. During the subsequent case study, i.e. low irradiation, results were less notable, which could be expected since total energy production amounted to a mere 3.16 kWh. As a result, 95.60% of total energy demand had to be drawn from the grid, whereas this was 95.93% in case of the uncontrolled charging policy. Introducing a second charging station reduced the amount of energy that had to be drawn from the grid to 94.45% in case the EMS was implemented, a small reduction from 95.73% in case of the uncontrolled charging policy. Therefore, it can be concluded that during days with such low irradiation, grid dependency cannot significantly be reduced. Finally, it should be noted that one could further reduce grid dependency by increasing the size of the PV array. It was found that increasing the array with 30% would result in a 3.2% loss in energy yield due to the fact that the converter would not shut down in case of power surplus, but rather convert the amount of power it was rated for, i.e. 10 kW [14]. However, when the system produces less than what it is rated for, power output will be substantially more.

- What would be the cost benefit if this EMS is implemented, when compared to uncontrolled ("dumb") charging?
  From the perspective of the consumer, a reduction in overall costs is the main driver to transition from ICEs to EVs. More specifically, 48% of the consumers see sustainability as the main driver, whereas 71% view lower overall costs to be the most important driver [38]. This EMS was therefore designed to do both, to minimize charging costs while sustainability of the EVs is increased by charging these with locally

produced PV power. It has been shown in section 6.2 that in case of low PV power generation, charging costs have been reduced by 0.39 - 2.86% when one charging point was considered, while the reduction amounted to 0.41 - 6.05% in case of two charging points. Furthermore, during a day with high irradiation, the EMS achieved a cost reduction between 3.56 - 58.13% in case of one charging point and 6.86 - 8.37% when a second carport was introduced. Therefore it was concluded that the proposed EMS will always improve the status quo, i.e. an uncontrolled charging policy, in terms of charging costs, although the magnitude depends on irradiation and the price mechanism in place. In addition it should be noted that these cost reductions are direct, but it is important to realize that, in combination with a dynamic price mechanism, the EMS can reduce operational and capital expenditure for the main grid as well, since it can shift significant load due to EVs away from peak demand. Quantifying this benefit was outside the scope of the this thesis but might very well be worth investigating. Finally, additional case studies were performed in which both a dynamic purchase tariff and dynamic FIT were imposed, a scenario that is likely to occur in the future. It was shown that an uncontrolled charging policy with such a price mechanism had a detrimental effect on charging costs due to the similar trend in power withdrawal and price level. In case of one charging point, charging costs were reduced by 118.44%, whereas profit was increased by 427.45% in case of two charging points. The latter, notable, result was due to two drawbacks of the uncontrolled charging policy, i.e. the lack of cooperation and the inability to shift demand away from the peak in purchase tariff.

- To what extent can the proposed EMS alleviate stress on the grid that otherwise would occur due to uncontrolled charging?
  It has been shown that during a day with low irradiation, energy exchange with the grid was not significantly reduced due to the fact that 94.45 and 95.60% of the energy demand had to be drawn from the grid, in case of two and one charging points, respectively. Nevertheless, the EMS spread out the charging process and thus slightly shifted demand away from the morning peak, although there was no direct incentive to do so. In comparison, the uncontrolled charging policy EVs would start charging upon arrival, directly adding to morning peak demand. Imposing a dynamic tariff that relates price to demand however, showed that the EMS was very effective in shifting the EV charging process from peak to an off-peak period and consequently reducing stress on the grid significantly. Furthermore, in case of high irradiation, 93.23% of the energy demand could be supplied by the PV system, therefore already significantly alleviating stress on the grid. Similarly, a dynamic tariff would stimulate the EMS to draw the remaining required energy during the period when price, i.e. demand, was low. However, it should be noted that height of the FIT requires careful consideration, as a too high fixed FIT showed to have a detrimental effect on energy exchange with the grid. Finally, introducing both a dynamic purchase tariff and dynamic FIT motivated the EMS to not only shift demand away from peak period, but also to feed available PV power into the grid during peak demand.

- To what extent is vehicle-to-grid (V2G) a viable concept?
  Vehicle-to-grid is a promising concept that can aid in letting RESs penetrate further into the electricity generating mix, as it allows the EMS to temporarily store energy in EVs that can be fed back into the grid during peak demand. Nevertheless, three important notes should be made regarding its viability. First, which is specific to this project, is that charging time is scarce due to the fact that there are four EVs connected to a single charging point and charging power is limited to 10 kW. Consequently, charging an EV beyond its energy requirements is not achieved easily, especially if one requires that power to be generated by the PV system as much as possible since that would imply the largest price difference. It was shown in the previous chapter that V2G did occur in case a surplus of PV power was generated, an observation that is related to the subsequent and final point. Second, as long as there is no dynamic FIT, there is no incentive to temporarily store free PV power, as opposed to feeding it back immediately, which is accompanied with less losses. However, it was shown that vehicle-to-vehicle (V2V) did lead to optimality in case of low irradiation, due to the fact that drawing energy from the grid during peak price would be more expensive than drawing energy from another EV that can be charged at a later point in time, when the price has lowered. It should be noted that this is only possible in case of multiple charging points because it is not possible to charge/discharge multiple EVs parked at the same charging point. Finally, although V2G led to the optimal solution in a very specific case, the absolute amount was limited. The main reason for this was the battery degradation cost. Because of this, the difference between minimum purchase tariff and maximum FIT needs to be significant to overcome the additional losses, and therefore batteries first need to improve in terms of cycle life before V2G becomes viable.

6.4. Potential applications of the EMS

Evidently, the proposed EMS can be implemented at a solar powered parking lot of any size where it optimizes power flows with a certain objective, e.g. to minimize total charging costs. Nevertheless, the EMS is designed in such a way that, with minor changes, it can be deployed in different settings as well. Imagine for example an off-grid microgrid with battery storage that depends solely on its own sustainable energy production, and where costs are perhaps not of interest but careful planning, so as not to waste energy, even more so. In such a setting, the developed EMS can, especially due to its forecasting capabilities, take future energy production into account and make informed decisions regarding power allocation in order to e.g. minimize downtime or maximize stability of the microgrid.

An example in the built environment could be the inclusion of the office building to which the parking lot is linked. This building will have its own specific energy demand characteristics, such as servers and lighting, but besides acting as a load, it may additionally be capable of producing energy as well, e.g. through combined heat and power (CHP) or a rooftop PV system. In that case, the EMS could minimize cost or environmental impact by increasing self-consumption, similarly as investigated in this thesis. In addition, a penalty factor for non-supplied energy to the base load could be incorporated, in order to prevent blackouts. Finally, cooperation between such several offices will be possible and thus enabling the formation of a smart grid.

Finally, the EMS could be implemented on a grander scale including distributed generators (DGs) and loads, i.e. a smart grid, in which it can ensure stability of both the smart grid and utility grid. Throughout this thesis it became clear that the combination of the developed EMS with both a dynamic purchase tariff and dynamic FIT are powerful tools that can shift demand from peak hours and inject power into the grid during these peak. In this way, voltage fluctuations and consequently stress on the grid are reduced, decreasing both capital and operational expenditure.

Bibliography

[1] APX | Power Spot Exchange - Making Markets Work |. URL `https://www.apxgroup.com/`.

[2] ABB. Electric Vehicle Charging Infrastructure Terra 51 fast charging station. Technical report.

[3] A. Ahmad, T. N. Anderson, and T. T. Lie. Hourly global solar irradiation forecasting for New Zealand. *Solar Energy*, 122:1398–1408, 2015. ISSN 0038092X. doi: 10.1016/j.solener.2015.10.055. URL `http://dx.doi.org/10.1016/j.solener.2015.10.055`.

[4] P. Teimourzadeh Baboli, S. Bahramara, M. Parsa Moghaddam, and M. R. Haghifam. A mixed-integer linear model for optimal operation of hybrid AC-DC microgrid considering Renewable Energy Resources and PHEVs. *2015 IEEE Eindhoven PowerTech, PowerTech 2015*, 2015. doi: 10.1109/PTC.2015.7232507.

[5] Peder Bacher, Henrik Madsen, and Henrik Aalborg Nielsen. Online short-term solar power forecasting. *Solar Energy*, 83(10):1772–1783, 2009. ISSN 0038092X. doi: 10.1016/j.solener.2009.05.016.

[6] D Aaron R Barkhouse, Oki Gunawan, Tayfun Gokmen, Teodor K Todorov, and David B Mitzi. Device characteristics of a 10.1% hydrazine-processed Cu2ZnSn(Se,S)4 solar cell. *Progress in Photovoltaics: Research and Applications*, 20(1):6–11, 2012. ISSN 10627995. doi: 10.1002/pip.

[7] Islam Safak Bayram, Vahraz Zamani, Ryan Hanna, and Jan Kleissl. On the Evaluation of Plug-in Electric Vehicle Data of a Campus Charging Network. 2016.

[8] Mohamed Bin Shams, Shaker Haji, Ali Salman, Hussain Abdali, and Alaa Alsaffar. Time series analysis of Bahrain's first hybrid renewable energy system. *Energy*, 103:1–15, 2016. ISSN 03605442. doi: 10.1016/j.energy.2016.02.136. URL `http://www.sciencedirect.com/science/article/pii/S0360544216301980`.

[9] Tim Bollerslev. Generalized Autoregressive Conditional Heteroscedasticity. *Journal of Econometrics*, 31:307–327, 1986.

[10] Stefano Bracco, Federico Delfino, Fabio Pampararo, Michela Robba, and Mansueto Rossi. A dynamic optimization-based architecture for polygeneration microgrids with tri-generation, renewables, storage systems and electrical vehicles. *Energy Conversion and Management*, 96:511–520, 2015. ISSN 01968904. doi: 10.1016/j.enconman.2015.03.013.

[11] Alexander Brissette, Anderson Hoke, Joshua Traube, Fenglong Lu, and Dragan Maksimovizc. Study on the effect of solar irradiance intermittency mitigation on electric vehicle battery lifetime. *2013 1st IEEE Conference on Technologies for Sustainability (SusTech)*, pages 262–267, 2013. doi: 10.1109/SusTech.2013.6617331.

[12] Peter G. Bruce, Stefan a. Freunberger, Laurence J. Hardwick, and Jean-Marie Tarascon. Li–O2 and Li–S batteries with high energy storage. *Nature Materials*, 11(02):172–172, 2011. ISSN 1476-1122. doi: 10.1038/nmat3237.

[13] Gautham Ram Chandra Mouli, Mark Leendertse, Venugopal Prasanth, Pavol Bauer, and Sacha Silvester. Economic and environmental benefits of a solar powered smart EV charging station for workplaces in the Netherlands. In *2016 IEEE Transportation Electrification Conference & Expo (ITEC'16)*, 2016.

[14] G.R. Chandra Mouli, P. Bauer, and M. Zeman. System design for a solar powered electric vehicle charging station for workplaces. *Applied Energy*, 168:434–443, 2016. ISSN 03062619. doi: 10.1016/j.apenergy.2016.01.110.

[15] Chris Chatfield. *Time-Series Forecasting.* Chapman & Hall / CRC, Bath, 2000.

[16] Changsong Chen and Shanxu Duan. Optimal Integration of Plug-In Hybrid Electric Vehicles in Microgrids. *IEEE Transactions on Industrial Informatics*, 3203(c):1–1, 2014. ISSN 1551-3203. doi: 10.1109/TII.2014.2322822.

[17] Qifang Chen, Nian Liu, Xinyi Lu, and Jianhua Zhang. A Heuristic Charging Strategy for Real-Time Operation of PV-based Charging Station for Electric Vehicles. (51277067):465–469, 2014.

[18] ComEd. Live Prices | ComEd's Hourly Pricing Program. URL `https://hourlypricing.comed.com/live-prices/`.

[19] Compendium voor de Leefomgeving. Emissies broeikasgassen, 1990-2014. Technical report, Compendium voor de Leefomgeving, 2014.

[20] Seth a. Cutler, Brian Schmalberger, and Cecil Rivers. An intelligent solar ecosystem with electric vehicles. *2012 IEEE International Electric Vehicle Conference, IEVC 2012*, 2012. doi: 10.1109/IEVC.2012.6183168.

[21] Paul Denholm, Michael Kuss, and Robert M. Margolis. Co-benefits of large scale plug-in hybrid electric vehicle and solar PV deployment. *Journal of Power Sources*, 236:350–356, 2013. ISSN 03787753. doi: 10.1016/j.jpowsour.2012.10.007.

[22] Maimouna Diagne, Mathieu David, Philippe Lauret, John Boland, and Nicolas Schmutz. Review of solar irradiance forecasting methods and a proposition for small-scale insular grids. *Renewable and Sustainable Energy Reviews*, 27:65–76, 2013. ISSN 13640321. doi: 10.1016/j.rser.2013.06.042.

[23] Paul Eugen Dziadek, Wilhelm Feucht, Anton Mittnacht, Hans Georg Kula, and Heinz Frank. Eco-friendly application of EVs for home-to-work and home-to-education transports. *Proceedings of the IEEE International Conference on Industrial Technology*, pages 705–709, 2013. doi: 10.1109/ICIT.2013.6505758.

[24] Jan Willem Eising, Tom van Onna, and Floortje Alkemade. Towards smart grids: Identifying the risks that arise from the integration of energy and transport supply chains. *Applied Energy*, 123(2014):448–455, 2014. ISSN 03062619. doi: 10.1016/j.apenergy.2013.12.017.

[25] Amany El-Zonkoly. Intelligent energy management of optimally located renewable energy systems incorporating PHEV. *Energy Conversion and Management*, 84:427–435, 2014. ISSN 01968904. doi: 10.1016/j.enconman.2014.04.050.

[26] Amgad Elgowainy, Aymeric Rousseau, Michael Wang, Mark Ruth, Dave Andress, Jake Ward, Fred Joseck, Tien Nguyen, and Sujit Das. Cost of ownership and well-to-wheels carbon emissions/oil use of alternative fuels and advanced light-duty vehicle technologies. *Energy for Sustainable Development*, 17(6):626–641, 2013. ISSN 09730826. doi: 10.1016/j.esd.2013.09.001.

[27] Robert F. Engle. Autoregressive Conditional Heteroscedasticity with Estimates of the Variance of United Kingdom Inflation. *Econometrica*, 50(4):987–1008, 1982.

[28] EPRI/NRDC. Environmental Assessment of Plug-In Hybrid Electric Vehicles. Technical Report 1015325, 2007.

[29] Essent. Enkel- of dubbeltarief, wat past bij u? (Dutch). URL `https://www.essent.nl/content/particulier/producten/alle{_}energietarieven/enkeltarief{_}of{_}dubbeltarief/index.html`.

[30] ETP SmartGrids. European technology platform smart grids: strategic deployment document for Europe's electricity networks of the future. *European Commission*, page 69, 2010.

[31] European Commission | Joint Research Centre. Photovoltaic Geographical Information System. URL `http://re.jrc.ec.europa.eu/pvgis/apps4/pvest.php`.

[32] Fabrizio Fattori, Norma Anglani, and Giuseppe Muliere. Combining photovoltaic energy with electric vehicles, smart charging and vehicle-to-grid. *Solar Energy*, 110:438–451, 2014. ISSN 0038092X. doi: 10.1016/j.solener.2014.09.034.

[33] Farivar Fazelpour, Majid Vafaeipour, Omid Rahbari, and Marc a. Rosen. Intelligent optimization to integrate a plug-in hybrid electric vehicle smart parking lot with renewable energy resources and enhance grid characteristics. *Energy Conversion and Management*, 77:250–261, 2014. ISSN 01968904. doi: 10.1016/j.enconman.2013.09.006.

[34] L. Alfredo Fernandez-Jimenez, Andrés Muñoz-Jimenez, Alberto Falces, Montserrat Mendoza-Villena, Eduardo Garcia-Garrido, Pedro M. Lara-Santillan, Enrique Zorzano-Alba, and Pedro J. Zorzano-Santamaria. Short-term power forecasting system for photovoltaic plants. *Renewable Energy*, 44:311–317, 2012. ISSN 09601481. doi: 10.1016/j.renene.2012.01.108.

[35] Kacem Gairaa, Abdallah Khellaf, Youcef Messlem, and Farouk Chellali. Estimation of the daily global solar radiation based on Box–Jenkins and ANN models: A combined approach. *Renewable and Sustainable Energy Reviews*, 57:238–249, 2016. ISSN 13640321. doi: 10.1016/j.rser.2015.12.111. URL `http://www.sciencedirect.com/science/article/pii/S136403211501494X`.

[36] M. Ghofrani, A. Arabali, and M. Ghayekhloo. Optimal charging/discharging of grid-enabled electric vehicles for predictability enhancement of PV generation. *Electric Power Systems Research*, 117:134–142, 2014. ISSN 03787796. doi: 10.1016/j.epsr.2014.08.007.

[37] Yi Guo, Student Member, Jian Hu, and Wencong Su. Stochastic Optimization for Economic Operation of Plug-in Electric Vehicle Charging Stations at a Municipal Parking Deck Integrated with On-site Renewable Energy Generation. *Ieee Itec*, (1), 2014.

[38] Kalman Gyimesi and Ravi Viswanathan. The shift to electric vehicles. Technical Report June, IBM Institute for Business Value, 2013.

[39] Jayakrishnan Harikumaran. Sizing and Charge Control Strategies for a Grid-Connected Micro-grid with Electric Vehicles. Technical Report June, Technical University Delft, 2012.

[40] Fran Hoffart. Proper care extends Li-ion battery life. *Power Electronics Technology*, (April):24–28, 2008. ISSN 15402800.

[41] Masoud Honarmand, Alireza Zakariazadeh, and Shahram Jadid. Integrated scheduling of renewable generation and electric vehicles parking lot in a smart microgrid. *Energy Conversion and Management*, 86:745–755, 2014. ISSN 01968904. doi: 10.1016/j.enconman.2014.06.044.

[42] Ching-lai Hor, Simon J Watson Member, and Shanti Majithia. Daily Load Forecasting and Maximum Demand Estimation using ARIMA and GARCH. pages 11–16, 2006.

[43] Feiran Huang, Piampoom Sarikprueck, Yunzhi Cheng, and Wei-Jen Lee. Design Optimization of PHEV charging station. *Industrial & Commercial Power Systems Technical Conference (I&CPS), 2012 IEEE/IAS 48th*, pages 2–8, 2012. doi: 10.1109/ICPS.2012.6229606.

[44] Rui Huang, Tiana Huang, Rajit Gadh, and Na Li. Solar generation prediction using the ARMA model in a laboratory-level micro-grid. *2012 IEEE 3rd International Conference on Smart Grid Communications, SmartGridComm 2012*, (November):528–533, 2012. doi: 10.1109/SmartGridComm.2012.6486039.

[45] Idaho National Laboratory. Steady State Vehicle Charging Fact Sheet : 2015 Nissan Leaf. Technical report, 2015.

[46] Rich H. Inman, Hugo T.C. Pedro, and Carlos F.M. Coimbra. Solar forecasting methods for renewable energy integration. *Progress in Energy and Combustion Science*, 39(6):535–576, 2013. ISSN 03601285. doi: 10.1016/j.pecs.2013.06.002.

[47] Internation Renewable Energy Agency. Renewable Power Generation Costs in 2014. (January), 2015.

[48] International Energy Agency. Energy and climate change. *Preserving the global environment: the challenge of shared leadership*, 2015. ISSN 17505836. doi: 10.1016/j.ijggc.2012.01.005.

[49] International Energy Agency. Energy and Climate Change Study, Special Briefing for COP21. Technical report, International Energy Agency, 2015.

[50] IPCC. *Climate Change 2014: Synthesis Report. Contribution of Working Groups I, II and III to the Fifth Assessment Report of the Intergovernmental Panel on Climate Change*. 2014. ISBN 9789291691432.

[51] Monirul Islam, Saad Mekhilef, and Mahamudul Hasan. Single phase transformerless inverter topologies for grid-tied photovoltaic system: A review. *Renewable and Sustainable Energy Reviews*, 45:69–86, 2015. ISSN 13640321. doi: 10.1016/j.rser.2015.01.009. URL `http://dx.doi.org/10.1016/j.rser.2015.01.009`.

[52] ITRPV. International Technology Roadmap for Photovoltaic (ITRPV) 2014 Results. Technical Report April, ITRPV, 2015.

[53] Karel H. Jansen, Tim M. Brown, and G. Scott Samuelsen. Emissions impacts of plug-in hybrid electric vehicle deployment on the U.S. western grid. *Journal of Power Sources*, 195(16):5409–5416, 2010. ISSN 03787753. doi: 10.1016/j.jpowsour.2010.03.013.

[54] Linni Jian, Yanchong Zheng, Xinping Xiao, and C.C. Chan. Optimal scheduling for vehicle-to-grid operation with stochastic connection of plug-in electric vehicles to smart grid. *Applied Energy*, 146:150–161, 2015. ISSN 03062619. doi: 10.1016/j.apenergy.2015.02.030.

[55] H. G. J. Kamp. Besluit experimenten decentrale duurzame elektriciteitsopwekking, 2014.

[56] Koninklijk Nederlands Meteorologisch Instituut. Cesar Database, 2016. URL `http://www.cesar-database.nl/`.

[57] Preetika Kulshrestha, Lei Wang, Mo-yuen Chow, and Srdjan Lukic. Intelligent energy management system simulator for PHEVs at municipal parking deck in a smart grid environment. pages 1–6, 2009.

[58] D Lee and R Baldick. Limiting Ramp Rate of Wind Power Output using a Battery Based on the Variance Gamma Process. *... Conference on Renewable Energies and Power ...*, pages 1–6, 2012.

[59] Mark Leendertse. Solar powered charging station for electric cars- conductive and wireless inductive | TU Delft Repositories. Technical report, Technical University Delft, 2015. URL `http://repository.tudelft.nl/islandora/object/uuid{%}3A2fc5c66a-ae64-484d-a5df-9671f980cf8c?collection=education`.

[60] Yifan Li, Rakpong Kaewpuang, Ping Wang, Dusit Niyato, and Zhu Han. An energy efficient solution: Integrating Plug-In Hybrid Electric Vehicle in smart grid with renewable energy. *Proceedings of the 2012 IEEE Conference on Computer Communications Workshops*, pages 73–78, 2012. ISSN 0743166X. doi: 10.1109/INFCOMW.2012.6193522.

[61] Nian Liu, Qifang Chen, Jie Liu, Xinyi Lu, Peng Li, Jinyong Lei, and Jianhua Zhang. A Heuristic Operation Strategy for Commercial Building Microgrids Containing EVs and PV System. *IEEE Transactions on Industrial Electronics*, 62(4):2560–2570, 2015. ISSN 0278-0046. doi: 10.1109/TIE.2014.2364553.

[62] Alicja Lojowska. *Wind speed modeling*. PhD thesis, Technical University Delft, 2009.

[63] Tan Ma and O.a. Mohammed. Optimal Charging of Plug-in Electric Vehicles for a Car-Park Infrastructure. *IEEE Transactions on Industry Applications*, 50(4):2323–2330, 2014. ISSN 0093-9994. doi: 10.1109/TIA.2013.2296620.

[64] Siddhartha Mal, Arunabh Chattopadhyay, Albert Yang, and Rajit Gadh. Electric vehicle smart charging and vehicle-to-grid operation. *International Journal of Parallel, Emergent and Distributed Systems*, (December 2012):1–17, 2012. ISSN 1744-5760. doi: 10.1080/17445760.2012.663757.

[65] S Mesentean, W Feucht, a Mittnacht, and H Frank. Scheduling Methods for Smart Charging of Electric Bikes from a Grid-Connected Photovoltaic-System. *Computer Modeling and Simulation (EMS), 2011 Fifth UKSim European Symposium on*, pages 299–304, 2011. doi: 10.1109/EMS.2011.88.

[66] K Mets, T Verschueren, W Haerick, C Develder, and F De Turck. Optimizing smart energy control strategies for plug-in hybrid electric vehicle charging. *2010 IEEE/IFIP Network Operations and Management Symposium Workshops, NOMS 2010*, pages 293–299, 2010. doi: 10.1109/NOMSW.2010.5486561.

[67] MIT. Energy & Climate Outlook. Technical report, Massacusetts Institue of Technology, 2015.

[68] Francis Mwasilu, Jackson John Justo, Eun Kyung Kim, Ton Duc Do, and Jin Woo Jung. Electric vehicles and smart grid interaction: A review on vehicle to grid and renewable energy sources integration. *Renewable and Sustainable Energy Reviews*, 34:501–516, 2014. ISSN 13640321. doi: 10.1016/j.rser.2014.03.031.

[69] P.T.V.B. Narashima Kumar, Sajja Suryateja, Ganivada Naveen, Mukesh Singh, and Praveen Kumar. Smart Home Energy Management with integration of PV and storage facilities providing grid support. 6, 2013.

[70] NOS. Netbeheerders bepleiten: stroom soms gratis (Dutch). URL `http://nos.nl/artikel/2088653-netbeheerders-bepleiten-stroom-soms-gratis.html`.

[71] Björn Nykvist and Måns Nilsson. Rapidly falling costs of battery packs for electric vehicles. *Nature Climate Change*, 5(April):329—-332, 2015. ISSN 1758-678X. doi: 10.1038/nclimate2564.

[72] Miguel a. Ortega-Vazquez. Optimal scheduling of electric vehicle charging and vehicle-to-grid services at household level including battery degradation and price uncertainty. *IET Generation, Transmission & Distribution*, 8(6):1007–1016, 2014. ISSN 1751-8687. doi: 10.1049/iet-gtd.2013.0624.

[73] PBL. Trends in Global CO2 Emissions 2015 Report. Technical report, PBL Netherlands Environmental Assesment Agency, 2013.

[74] Hugo T C Pedro and Carlos F M Coimbra. Assessment of forecasting techniques for solar power production with no exogenous inputs. *Solar Energy*, 86(7):2017–2028, 2012. ISSN 0038-092X. doi: 10.1016/j.solener.2012.04.004.

[75] Scott B. Peterson, Jay Apt, and J.F. Whitacre. Lithium-ion battery cell degradation resulting from realistic vehicle and vehicle-to-grid utilization. *Journal of Power Sources*, 195(8):2385–2392, 2010. ISSN 03787753. doi: 10.1016/j.jpowsour.2009.10.010.

[76] V. Prema and K. Uma Rao. Development of statistical time series models for solar power prediction. *Renewable Energy*, 83:100–109, 2015. ISSN 09601481. doi: 10.1016/j.renene.2015.03.038.

[77] Qifang Chen, Nian Liu, Cheng Wang, and Jianhua Zhang. Optimal power utilizing strategy for PV-based EV charging stations considering Real-time price. *2014 IEEE Conference and Expo Transportation Electrification Asia-Pacific (ITEC Asia-Pacific)*, pages 1–6, 2014. doi: 10.1109/ITEC-AP.2014.6941123.

[78] Gordon Reikard. Predicting solar radiation at high resolutions: A comparison of time series forecasts. *Solar Energy*, 83(3):342–349, 2009. ISSN 0038092X. doi: 10.1016/j.solener.2008.08.007.

[79] REN21. Renewables 2014: Global Status Report - Key Findings. pages 1–13, 2014. doi: ISBN9783981593426.

[80] Rijksoverheid. Elektrisch Rijden in de versnelling Plan van Aanpak 2011-2015. *Publicaties*, page 22, 2011. URL `http://www.rijksoverheid.nl/documenten-en-publicaties/kamerstukken/2011/10/03/aanbiedingsbrief-green-deal.html`.

[81] Lena-Marie Ritte, Stefan Mischinger, Kai Strunz, and Johannes Eckstein. Modeling Photovoltaic Optimized Charging of Electric Vehicles. *2012 3rd IEEE PES Innovative Smart Grid Technologies Europe (ISGT Europe)*, pages 1–8, 2012. ISSN 2165-4816. doi: 10.1109/ISGTEurope.2012.6465792.

[82] RVO. Cijfers elektrisch vervoer | RVO.nl (Dutch). URL `http://www.rvo.nl/onderwerpen/duurzaam-ondernemen/energie-en-milieu-innovaties/elektrisch-rijden/stand-van-zaken/cijfers`.

[83] Ahmed Yousuf Saber and Ganesh Kumar Venayagamoorthy. Resource scheduling under uncertainty in a smart grid with renewables and plug-in vehicles. *IEEE Systems Journal*, 6(1):103–109, 2012. ISSN 19328184. doi: 10.1109/JSYST.2011.2163012.

[84] Pedro Sánchez-Martín, Guillermo Sánchez, and German Morales-España. Direct load control decision model for aggregated EV charging points. *IEEE Transactions on Power Systems*, 27(3):1577–1584, 2012. ISSN 08858950. doi: 10.1109/TPWRS.2011.2180546.

[85] Pedro Sanchez-Martin, Sara Lumbreras, and Antonio Alberdi-Alen. Stochastic Programming Applied to EV Charging Points for Energy and Reserve Service Markets. *IEEE Transactions on Power Systems*, PP (99):1–8, 2015. ISSN 0885-8950. doi: 10.1109/TPWRS.2015.2405755.

[86] G. Schwarz. Estimating the dimension of a model. *The Annals of Statistics*, 6(2):461–464, 1978. ISSN 0090-5364. doi: 10.1214/aos/1176344136.

[87] SMA. SUNNY TRIPOWER 60 The Best of Two Worlds. Technical report.

[88] João Soares, Hugo Morais, Tiago Sousa, Zita Vale, and Pedro Faria. Day-ahead resource scheduling including demand response for electric vehicles. *IEEE Transactions on Smart Grid*, 4(1):596–605, 2013. ISSN 19493053. doi: 10.1109/TSG.2012.2235865.

[89] W C Su, J H Wang, and J Roh. Stochastic Energy Scheduling in Microgrids With Intermittent Renewable Energy Resources. *Ieee Transactions on Smart Grid*, 5(4):1876–1883, 2014. doi: 10.1109/tsg.2013.2280645.

[90] Wencong Su and Mo-Yuen Chow. Investigating a large-scale PHEV/PEV parking deck in a smart grid environment. *2011 North American Power Symposium*, pages 1–6, 2011. doi: 10.1109/NAPS.2011.6024842.

[91] Wencong Su and Mo Yuen Chow. Computational intelligence-based energy management for a large-scale PHEV/PEV enabled municipal parking deck. *Applied Energy*, 96:171–182, 2012. ISSN 03062619. doi: 10.1016/j.apenergy.2011.11.088.

[92] Tesla. Daily Powerwall Home Battery. Technical report.

[93] Pinak Tulpule, Vincenzo Marano, Stephen Yurkovich, and Giorgio Rizzoni. Energy economic analysis of PV based charging station at workplace parking garage. *IEEE 2011 EnergyTech, ENERGYTECH 2011*, pages 1–6, 2011. doi: 10.1109/EnergyTech.2011.5948504.

[94] Pinak J. Tulpule, Vincenzo Marano, Stephen Yurkovich, and Giorgio Rizzoni. Economic and environmental impacts of a PV powered workplace parking garage charging station. *Applied Energy*, 108:323–332, 2013. ISSN 03062619. doi: 10.1016/j.apenergy.2013.02.068.

[95] UNEP. Emissions Gap Report. Technical report, United Nations Environment Program, 2015.

[96] U.S. Department of Energy (DOE). A System View of the Modern Grid. *Department of Energy - Office of Electricity Delivery and Energy Reliability*, (January):0–21, 2007.

[97] U.S. Energy Information Administration (EIA). How much carbon dioxide is produced per kilowatthour when generating electricity with fossil fuels? - FAQ - U.S. Energy Information Administration (EIA). URL `https://www.eia.gov/tools/faqs/faq.cfm?id=74{&}t=11`.

[98] Mart van der Kam and Wilfried van Sark. Smart charging of electric vehicles with photovoltaic power and vehicle-to-grid technology in a microgrid; a case study. *Applied Energy*, 152:20–30, 2015. ISSN 03062619. doi: 10.1016/j.apenergy.2015.04.092.

[99] Remco a. Verzijlbergh, Marija D Ilic, and Zofia Lukszo. The Role of Electric Vehicles on a Green Island. *North American Power Symposium (NAPS), 4-6 Aug. 2011*, pages 1–7. doi: 10.1109/NAPS.2011.6025199.

[100] Remco a. Verzijlbergh, Petra W. Heijnen, Stephan R. de Roode, Alexander Los, and Harm J.J. Jonker. Improved model output statistics of numerical weather prediction based irradiance forecasts for solar power applications. *Solar Energy*, 118:634–645, 2015. ISSN 0038092X. doi: 10.1016/j.solener.2015.06.005.

[101] H Wirth. Recent facts about photovoltaics in Germany. *Fraunhofer ISE*, page 92, 2015.

[102] WMO. Greenhouse Gas Bulletin. Technical report, World Meteorological Organization, 2015.

[103] K. Yoshimi, M. Osawa, D. Yamashita, T. Niimura, R. Yokoyama, T. Masuda, H. Kondou, and T. Hirota. Practical storage and utilization of household photovoltaic energy by electric vehicle battery. *2012 IEEE PES Innovative Smart Grid Technologies, ISGT 2012*, pages 1–8, 2012. doi: 10.1109/ISGT.2012.6175688.

[104] Pengcheng You, Zaiyue Yang, and Mo-yuen Chow. Optimal Cooperative Charging Strategy for a Smart Charging Station of Electric Vehicles. pages 1–11, 2015.

[105] Pei Zhang, Fuwu Yan, and Changqing Du. A comprehensive analysis of energy management strategies for hybrid electric vehicles based on bibliometrics. *Renewable and Sustainable Energy Reviews*, 48(205): 88–104, 2015. ISSN 13640321. doi: 10.1016/j.rser.2015.03.093.

[106] Sheng Shui Zhang. The effect of the charging protocol on the cycle life of a Li-ion battery. *Journal of Power Sources*, 161(2):1385–1391, 2006. ISSN 03787753. doi: 10.1016/j.jpowsour.2006.06.040.

[107] Hongwei Zhu Ã, Jinquan Wei, Kunlin Wang, Dehai Wu, Ahmad Y. Al-Hasan, Pietro P. Altermatt, Tobias Kiesewetter, Klaus Ellmer, Helmut Tributsch, Harry a Atwater, Albert Polman, Pierre-Luc T Boudreault, Ahmed Najari, Mario Leclerc, K R Catchpole, B C Century, and Hongwei Zhu. The history of solar. Technical report, 2011.

Nomenclature

Italic letters are used for denoting variables and indexes, whereas regular letters denote parameters and sets.

Symbols

α_i	ARCH parameters for i=1 ... q.
β_i	GARCH parameters i=1 ... p.
γ_l	Autocovariance function for lag l.
γ_0	Autocovariance function for $l = 0$.
ϵ_t	White noise during time period t with zero mean and variance σ_t^2.
η_{ch}	EV charging efficiency [-].
η_{dis}	EV discharging efficiency [-].
η_{inv}	Inverter efficiency [-].
η_{MPPT}	DC-DC converter efficiency [-].
θ_j	Moving average parameters for j=1 ... q.
Θ	Seasonal moving average parameter.
λ_{deg}	Degradation costs of EV's battery [€/kWh].
λ_{G2V_t}	Marginal buying price of utility energy during time period t [€/kWh].
λ_{FIT_t}	Marginal selling price of utility energy during time period t [€/kWh].
$\lambda_{\text{PV-EV}_t}$	Marginal price of PV energy when sold to an EV during time period t [€/kWh].
$\lambda_{\text{PV-grid}_t}$	Marginal price of PV energy when sold to the grid during time period t [€/kWh].
μ	Mean.
ρ_l	Autocorrelation function for lag l.
σ_t	Standard deviation during time period t.
σ_t^2	Variance at time t.
ϕ_i	Autoregressive parameters for i=1 ... p.
Φ	Seasonal autoregressive parameter.
C_{ch}	Charging costs [€].
$D_{i,c,t}^{\text{ch},+}$	Positive difference between on and off state of binary variable $u_{i,c,t}$ [-].
$D_{i,c,t}^{\text{ch},-}$	Negative difference between on and off state of binary variable $u_{i,c,t}$ [-].
$D_{i,c,t}^{\text{dis},+}$	Positive difference between on and off state of binary variable $v_{i,c,t}$ [-].
$D_{i,c,t}^{\text{dis},-}$	Negative difference between on and off state of binary variable $v_{i,c,t}$ [-].

$\mathrm{E}_{\mathrm{grid}}$	Energy exchange with the grid [kWh].
$EC_{i,c,t}$	Energy content of the battery of the ith EV at the cth charging point during time period t [kWh].
$\mathrm{EC}_{i,c}^{\mathrm{arrival}}$	Energy content of the ith EV at the cth charging point upon arrival [kWh].
$\mathrm{EC}_{i,c}^{\mathrm{departure}}$	Energy content of the ith EV at the cth charging point upon departure [kWh].
$\mathrm{EC}_{i,c}^{\mathrm{max}}$	Maximum energy content of the ith EV at the cth charging point for all time periods t [kWh].
$\mathrm{N}^{\mathrm{max}}$	Maximum initiations of charging and discharging process [-].
$P_{\mathrm{V2G}_{i,c,t}}$	Power transfer from the ith EV at the cth charging point during time period t [kW].
$P_{\mathrm{ch}_{i,c,t}}$	Power transfer to the ith EV at the cth charging point during time period t [kW].
$P_{\mathrm{grid}^{+}_{i,c,t}}$	Power transfer from the grid to the ith EV at the cth charging point during time period t [kW].
$P_{\mathrm{grid}^{-}_{i,c,t}}$	Power transfer to the grid from the ith EV at the cth charging point during time period t [kW].
$P_{\mathrm{PV\text{-}EV}_{i,c,t}}$	Power transfer from the PV system to the ith EV at the cth charging point during time period t [kW].
$P_{\mathrm{PV\text{-}grid}_t}$	Power transfer from the PV system to the grid during time period t [kW].
$\mathrm{P}_{\mathrm{grid}_{i,c}}^{+,\mathrm{max}}$	Maximum power transfer from the grid to the ith EV at the cth charging point [kW].
$\mathrm{P}_{\mathrm{grid}_{i,c}}^{-,\mathrm{max}}$	Maximum power transfer to the grid to the ith EV at the cth charging point [kW].
$\mathrm{P}_{\mathrm{ch}_{i,c}}^{\mathrm{max}}$	Maximum power transfer to the ith EV at the cth charging point [kW].
$\mathrm{P}_{\mathrm{V2G}_{i,c}}^{\mathrm{max}}$	Maximum power transfer from the ith EV at the cth charging point [kW].
$\mathrm{P}_{\mathrm{PV}_t}^{\mathrm{max}}$	Maximum PV power during time period t [kW].
$\mathrm{R}_{\mathrm{dis}}$	Revenues from discharging [€].
TC	Total costs incurred from the charging/discharging process [€].
$s_{i,c,t}$	Binary variable that prevents feeding power into the grid while drawing power from the grid [-].
$u_{i,c,t}$	Binary variable that determines whether the ith EV at the cth charging point during time period t is available for charging (1) or not (0) [-].
$v_{i,c,t}$	Binary variable that determines whether the ith EV at the cth charging point during time period t is discharging (1) or not (0) [-].

Appendices

A

Detailed insight into the charging processes

A.1. Summer

A.1.1. One charging point - four EVs

Scenario 1 and 2

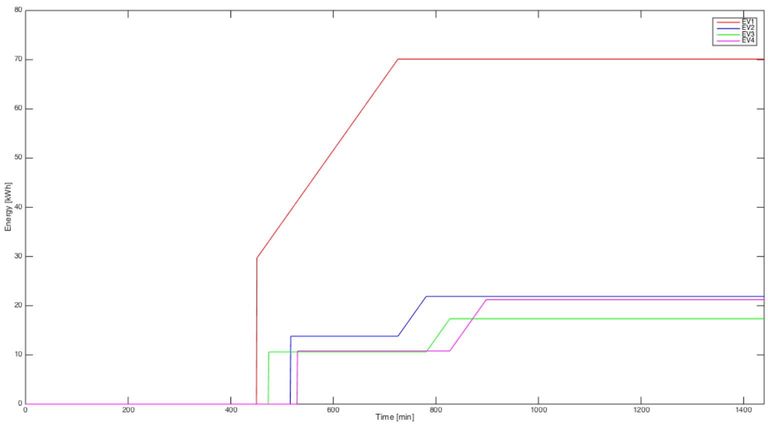

Figure A.1: Energy content during uncontrolled charging of 4 EVs with λ_{PV_t} = 0.097 €/kWh.

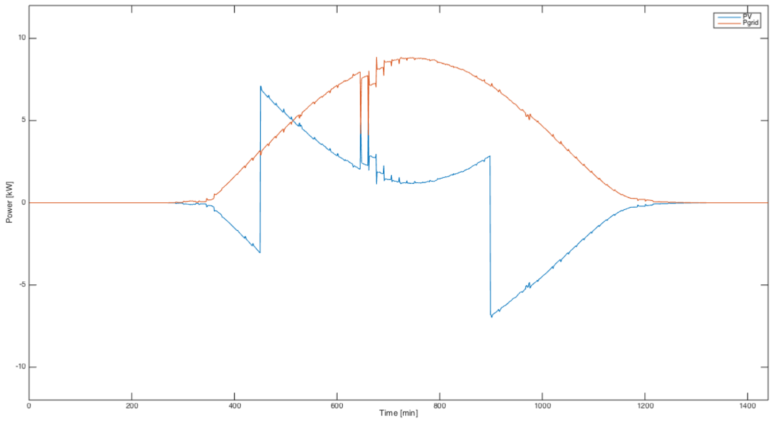

Figure A.2: Power allocation during uncontrolled charging of 4 EVs with λ_{PV_t} = 0.097 €/kWh, plotted without EVs.

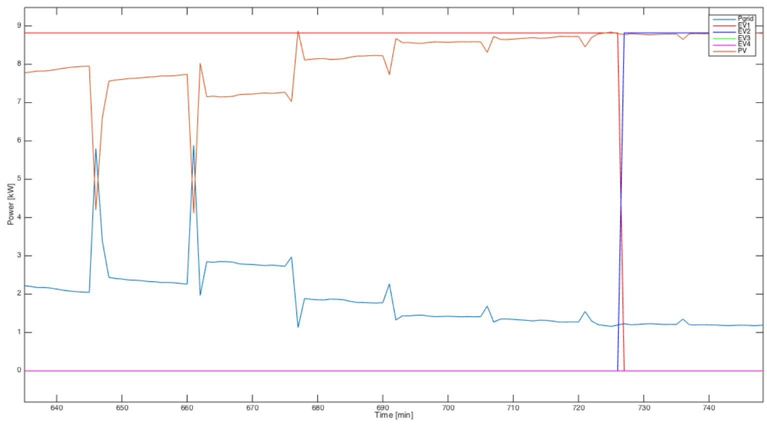

Figure A.3: Power allocation during uncontrolled charging of 4 EVs with λ_{PV_t} = 0.097 €/kWh, zoom in.

Scenario 3

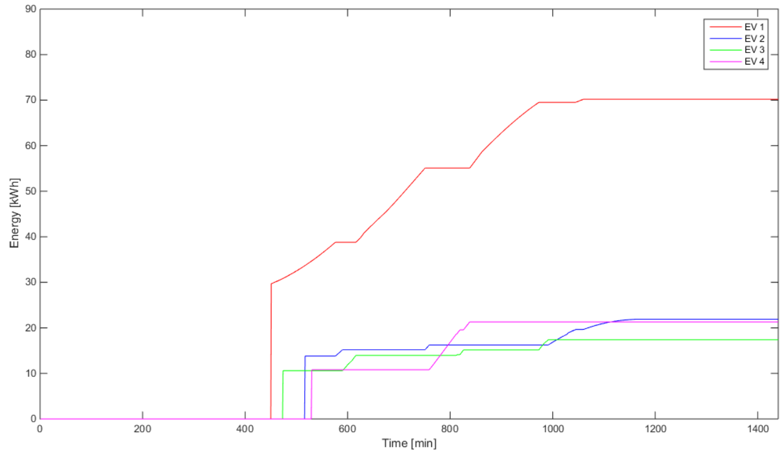

Figure A.4: Energy content during scenario 3 of 4 EVs with λ_{PV_t} = 0.097 €/kWh.

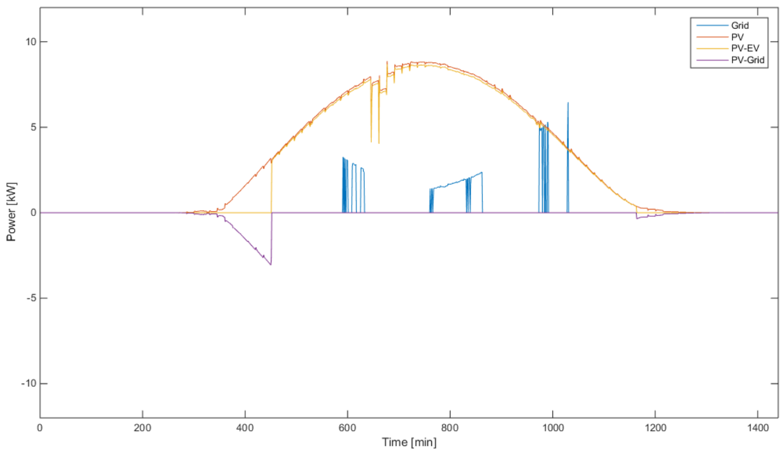

Figure A.5: Power allocation during scenario 3 of 4 EVs with λ_{PV_t} = 0.097 €/kWh, plotted without EVs.

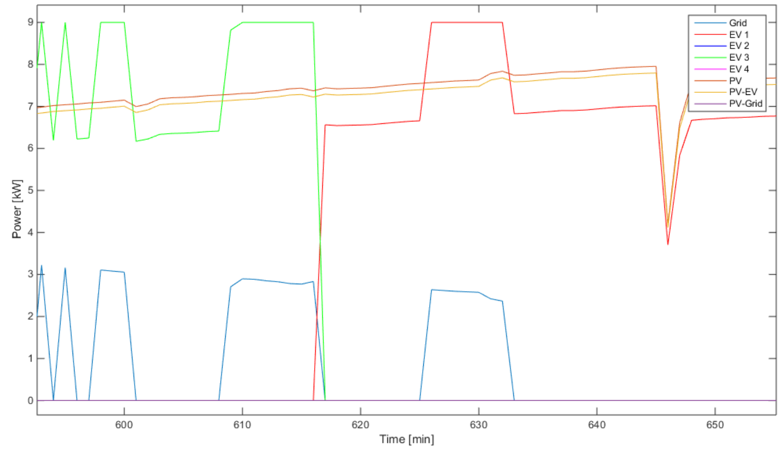

Figure A.6: Power allocation during scenario 3 of 4 EVs with λ_{PV_t} = 0.097 €/kWh, zoom in.

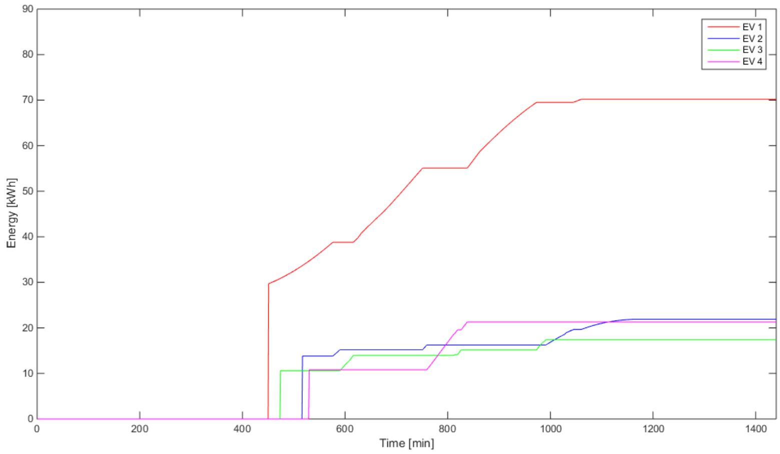

Figure A.7: Energy content during scenario 3 of 4 EVs with λ_{PV_t} = 0 €/kWh.

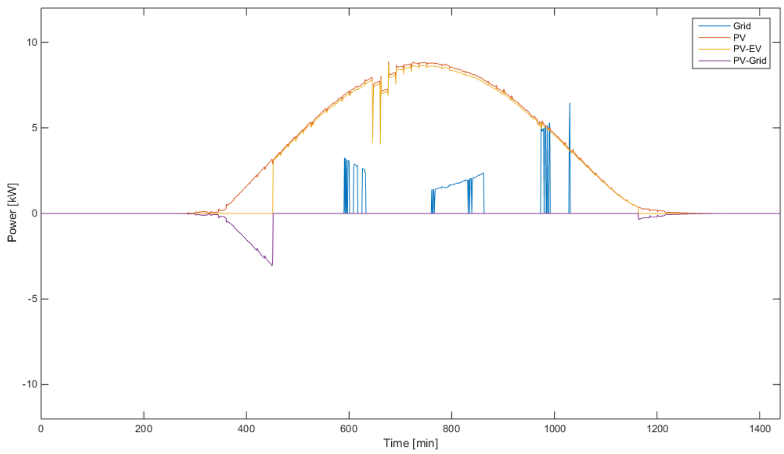

Figure A.8: Power allocation during scenario 3 of 4 EVs with λ_{PV_t} = 0 €/kWh, plotted without EVs.

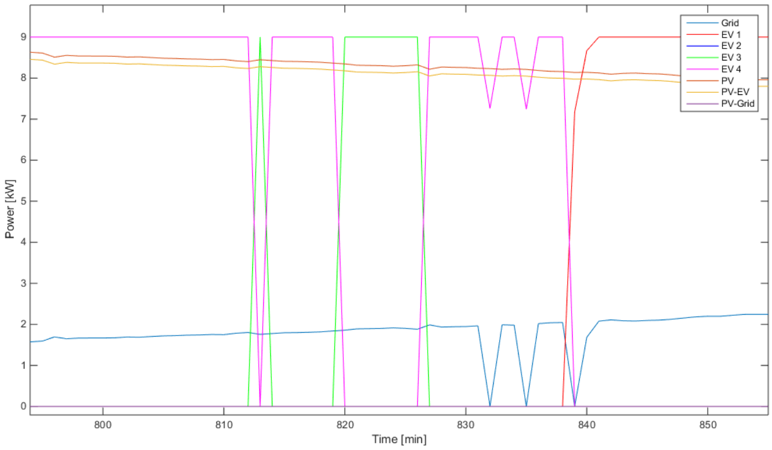

Figure A.9: Power allocation during scenario 3 of 4 EVs with λ_{PV_t} = 0 €/kWh, zoom in.

Scenario 4

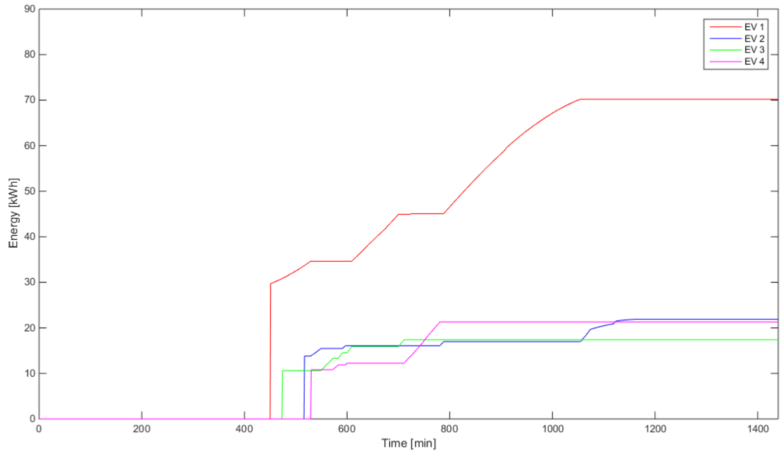

Figure A.10: Energy content during scenario 4 of 4 EVs with λ_{PV_t} = 0.097 €/kWh.

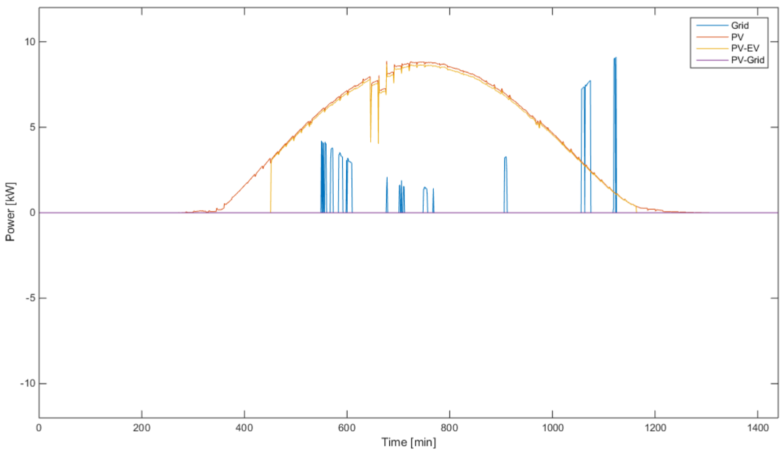

Figure A.11: Power allocation during scenario 4 of 4 EVs with λ_{PV_t} = 0.097 €/kWh, plotted without EVs.

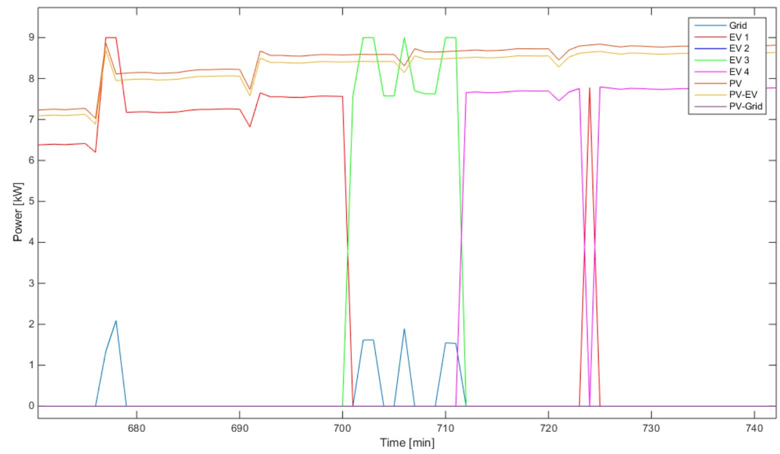

Figure A.12: Power allocation during scenario 4 of 4 EVs with λ_{PV_t} = 0.097 €/kWh, zoom in.

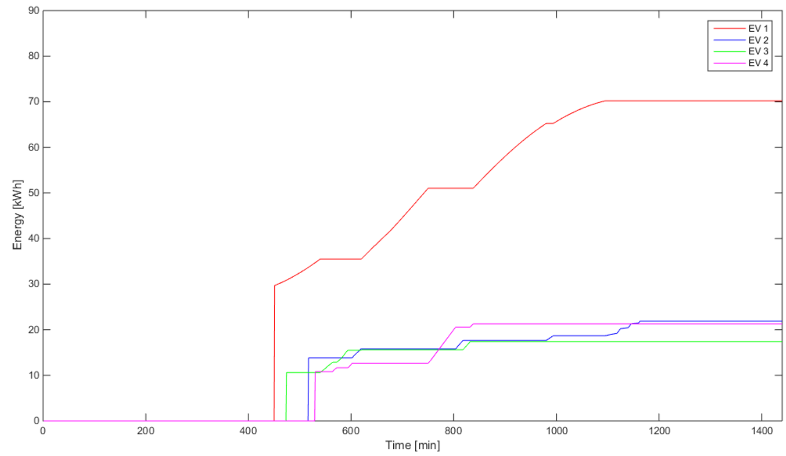

Figure A.13: Energy content during scenario 4 of 4 EVs with λ_{PV_t} = 0 €/kWh.

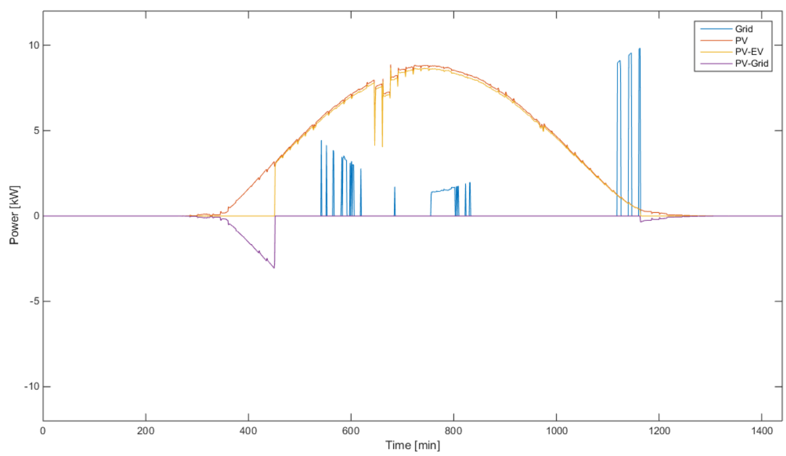

Figure A.14: Power allocation during scenario 4 of 4 EVs with λ_{PV_t} = 0 €/kWh, plotted without EVs.

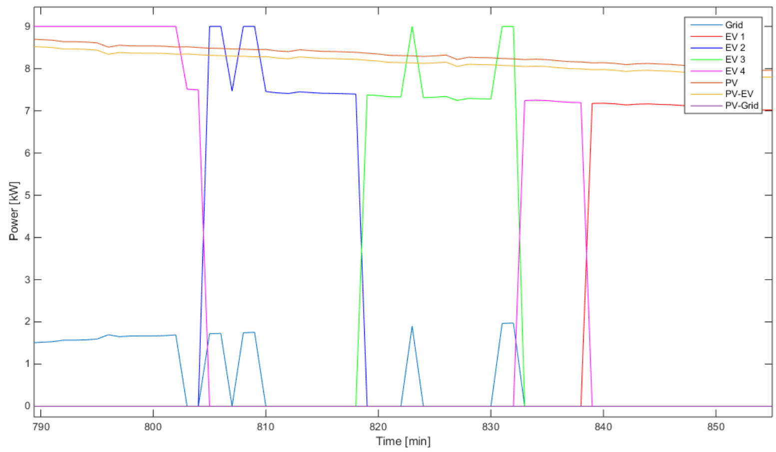

Figure A.15: Power allocation during scenario 4 of 4 EVs with λ_{PV_t} = 0 €/kWh, zoom in.

Scenario 5

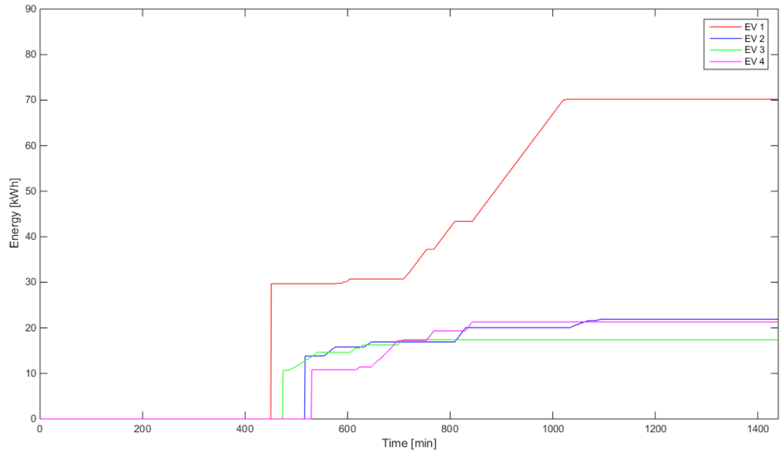

Figure A.16: Energy content during scenario 5 of 4 EVs with λ_{PV_t} = 0.097 €/kWh.

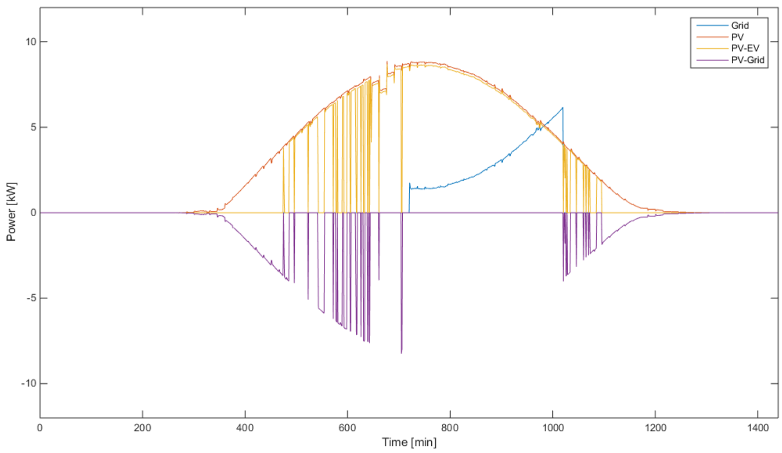

Figure A.17: Power allocation during scenario 5 of 4 EVs with λ_{PV_t} = 0.097 €/kWh, plotted without EVs or price.

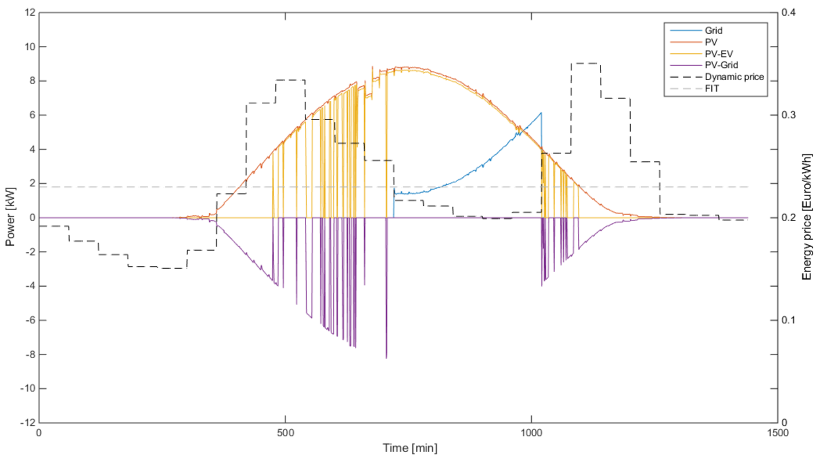

Figure A.18: Power allocation during scenario 5 of 4 EVs with λ_{PV_t} = 0.097 €/kWh, plotted without EVs.

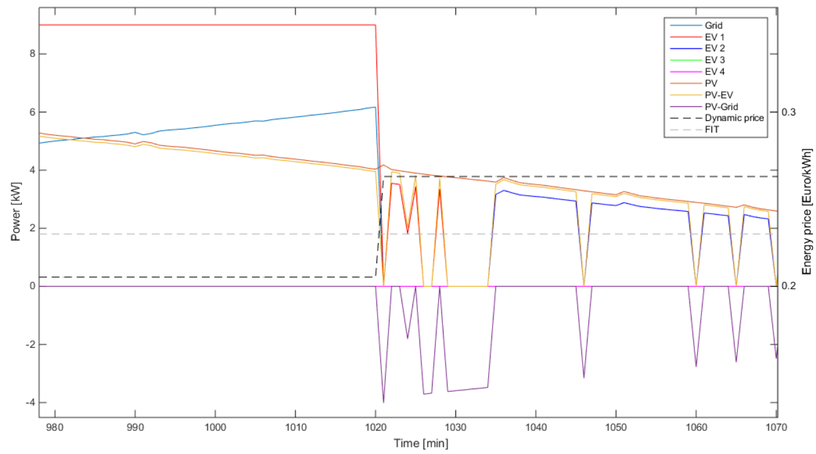

Figure A.19: Power allocation during scenario 5 of 4 EVs with λ_{PV_t} = 0.097 €/kWh, zoom in.

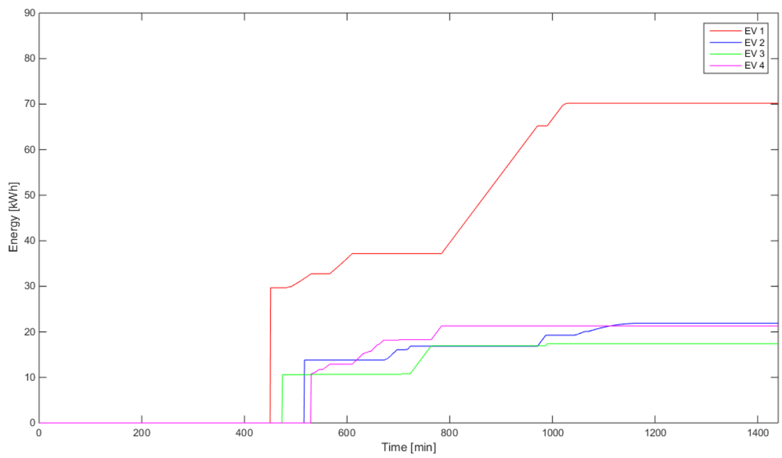

Figure A.20: Energy content during scenario 5 of 4 EVs with λ_{PV_t} = 0 €/kWh.

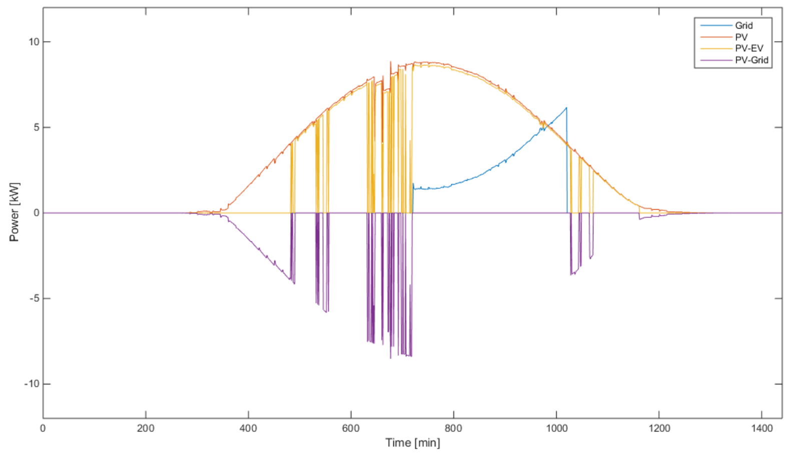

Figure A.21: Power allocation during scenario 5 of 4 EVs with λ_{PV_t} = 0 €/kWh, plotted without EVs or price.

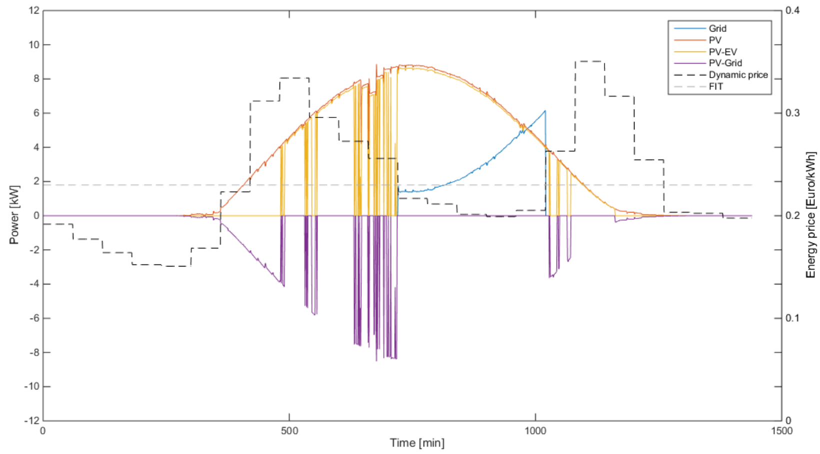

Figure A.22: Power allocation during scenario 5 of 4 EVs with λ_{PV_t} = 0 €/kWh, plotted without EVs.

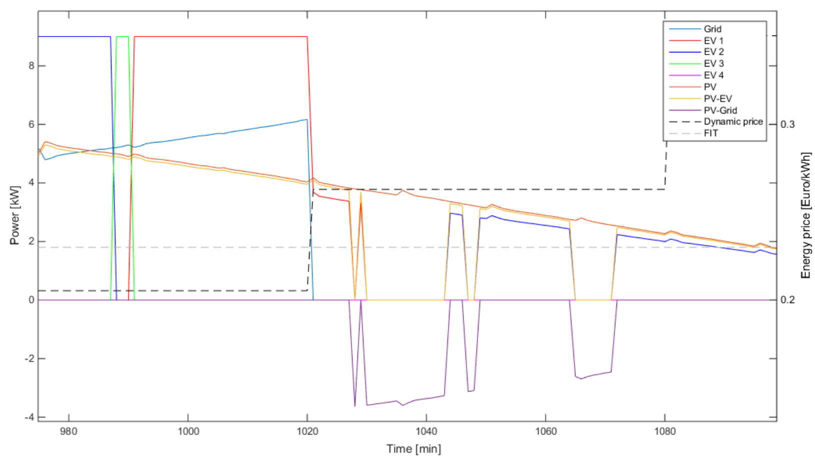

Figure A.23: Power allocation during scenario 5 of 4 EVs with λ_{PV_t} = 0 €/kWh, zoom in.

Scenario 6

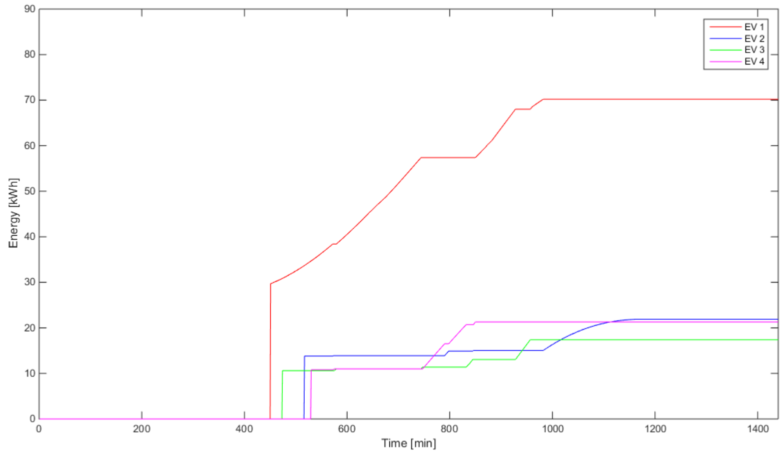

Figure A.24: Energy content during scenario 6 of 4 EVs with λ_{PV_t} = 0.097 €/kWh.

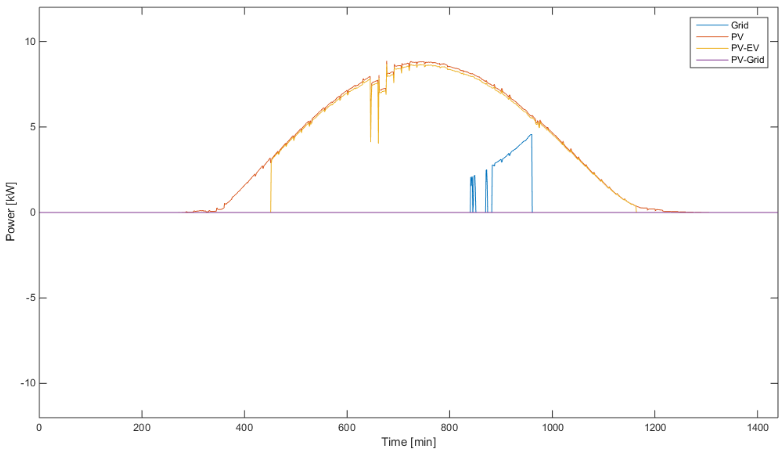

Figure A.25: Power allocation during scenario 6 of 4 EVs with λ_{PV_t} = 0.097 €/kWh, plotted without EVs or price.

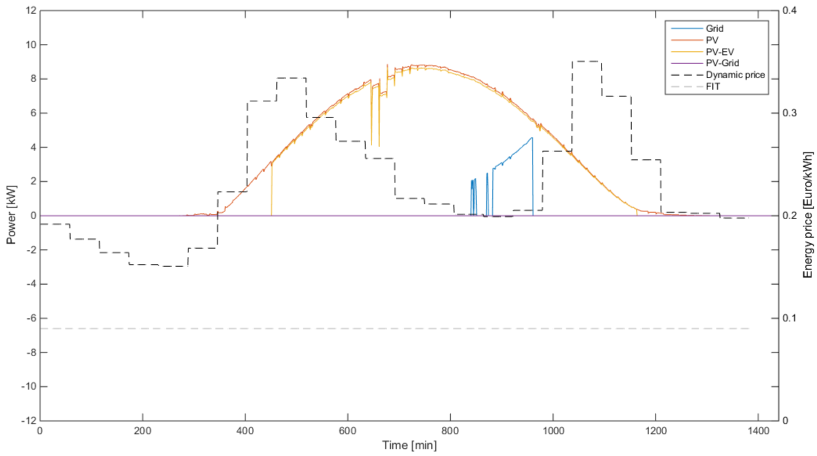

Figure A.26: Power allocation during scenario 6 of 4 EVs with λ_{PV_t} = 0.097 €/kWh, plotted without EVs.

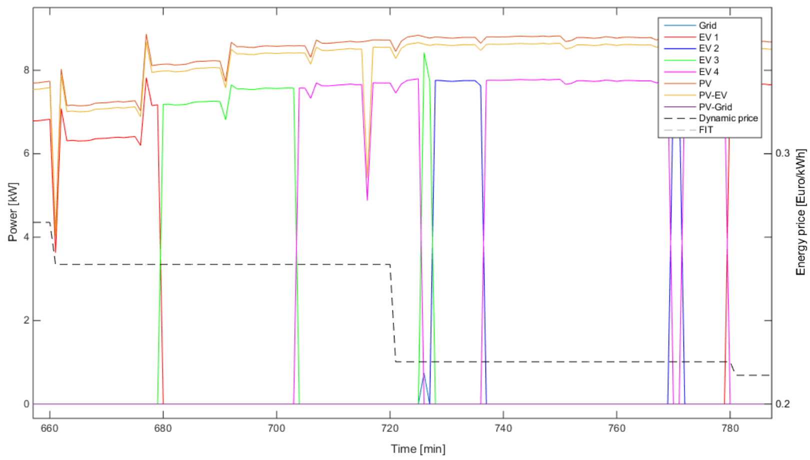

Figure A.27: Power allocation during scenario 6 of 4 EVs with λ_{PV_t} = 0.097 €/kWh, zoom in.

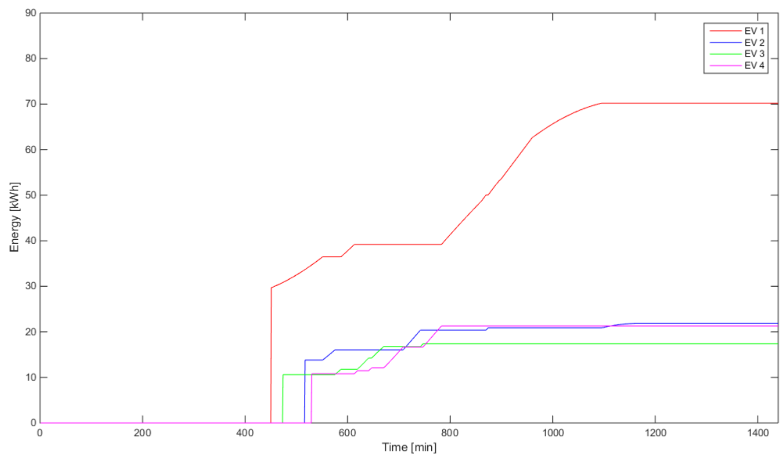

Figure A.28: Energy content during scenario 6 of 4 EVs with λ_{PV_t} = 0 €/kWh.

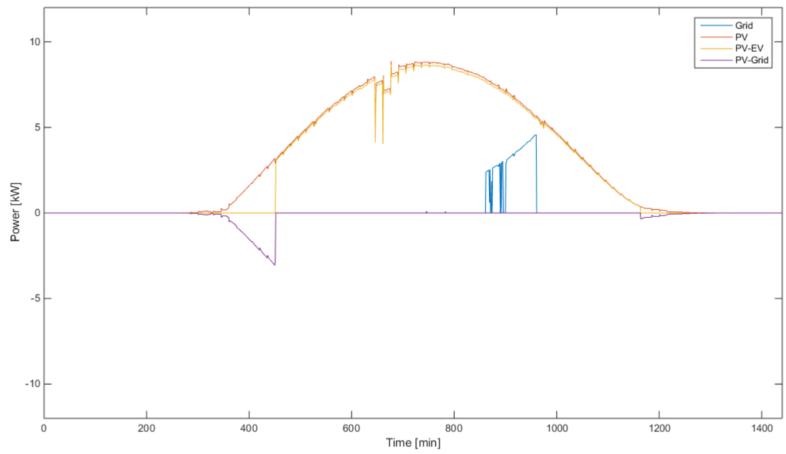

Figure A.29: Power allocation during scenario 6 of 4 EVs with λ_{PV_t} = 0 €/kWh, plotted without EVs or price.

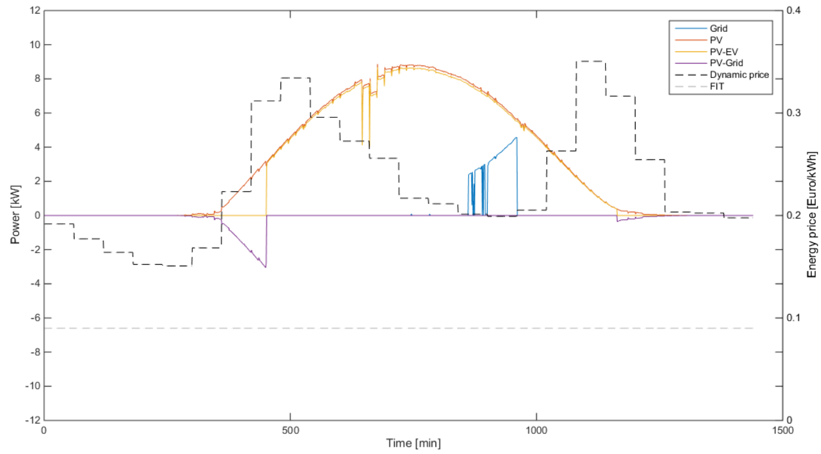

Figure A.30: Power allocation during scenario 6 of 4 EVs with λ_{PV_t} = 0 €/kWh, plotted without EVs.

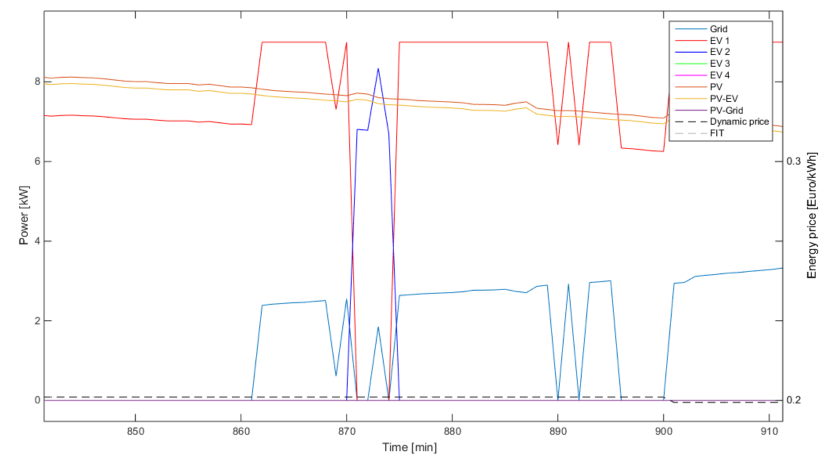

Figure A.31: Power allocation during scenario 6 of 4 EVs with λ_{PV_t} = 0 €/kWh, zoom in.

Minimize energy exchange with the grid

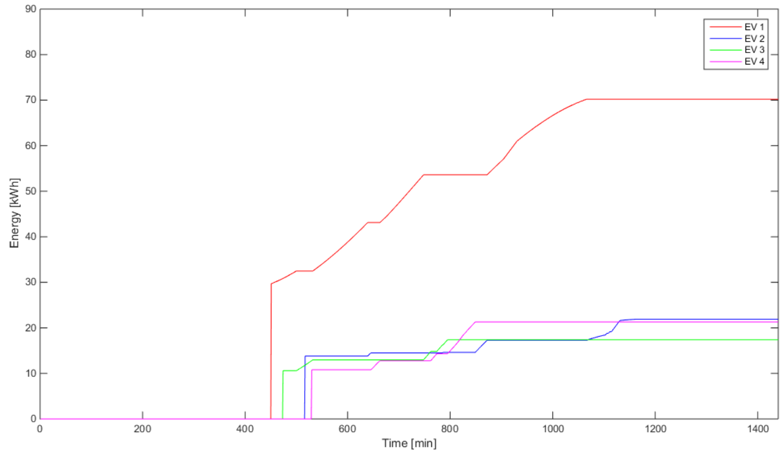

Figure A.32: Energy content of 4 EVs during minimization of energy exchange with grid.

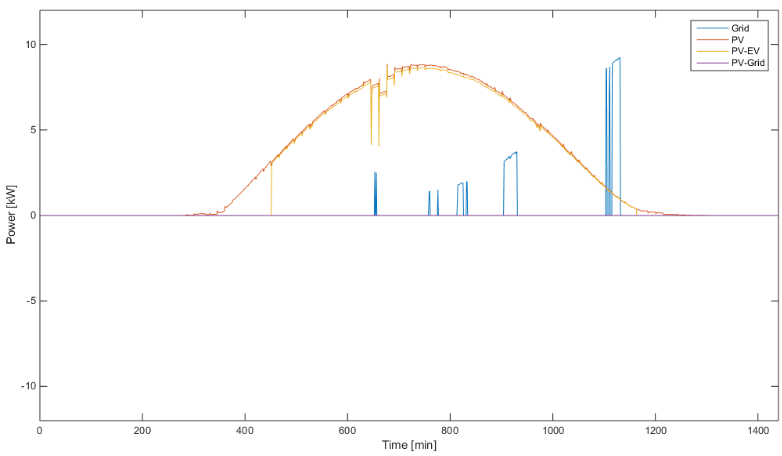

Figure A.33: Power allocation during minimization of energy exchange with grid, plotted without EVs.

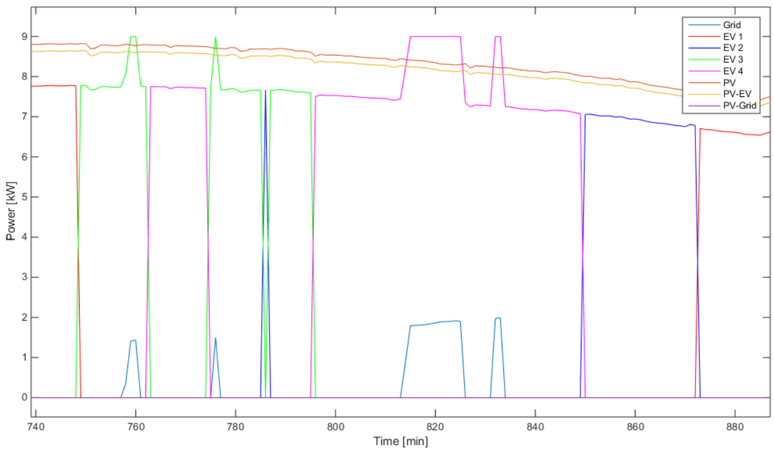

Figure A.34: Power allocation during minimization of energy exchange with grid, zoom in.

A.1.2. Two charging points - six EVs
Scenario 1 and 2

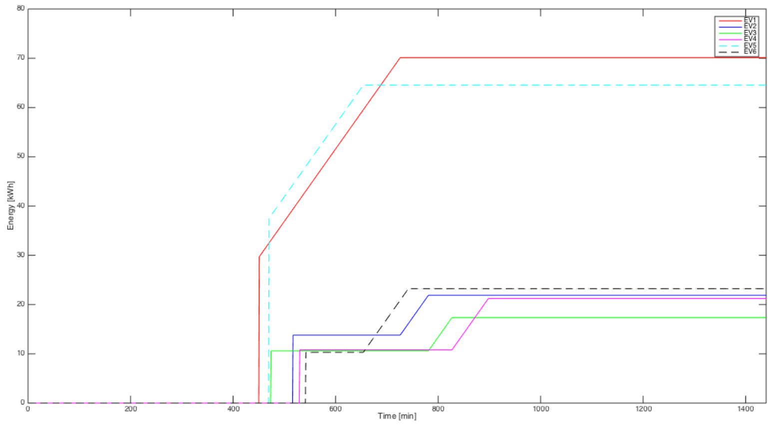

Figure A.35: Energy content during uncontrolled charging of 6 EVs with λ_{PV_t} = 0.097 €/kWh.

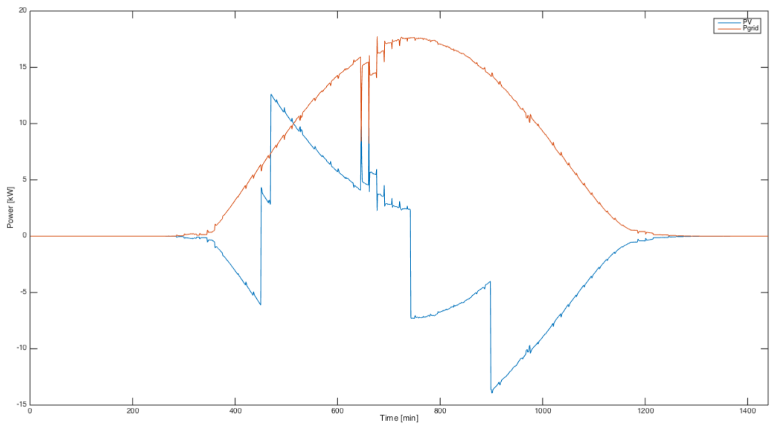

Figure A.36: Power allocation during uncontrolled charging of 6 EVs with λ_{PV_t} = 0.097 €/kWh, plotted without EVs.

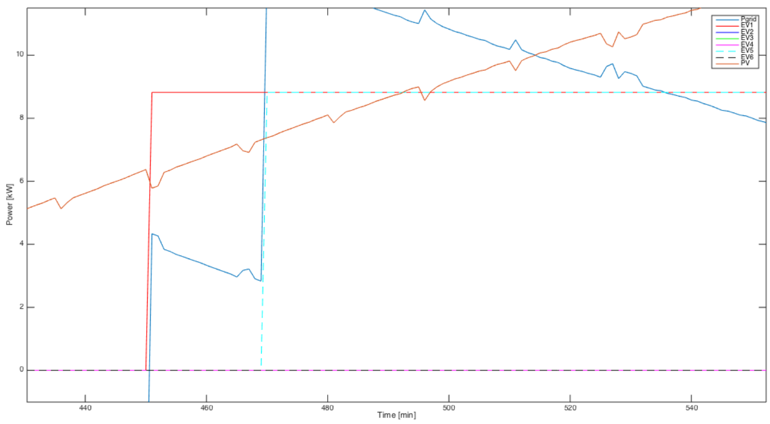

Figure A.37: Power allocation during uncontrolled charging of 6 EVs with λ_{PV_t} = 0.097 €/kWh, zoom in.

Scenario 3

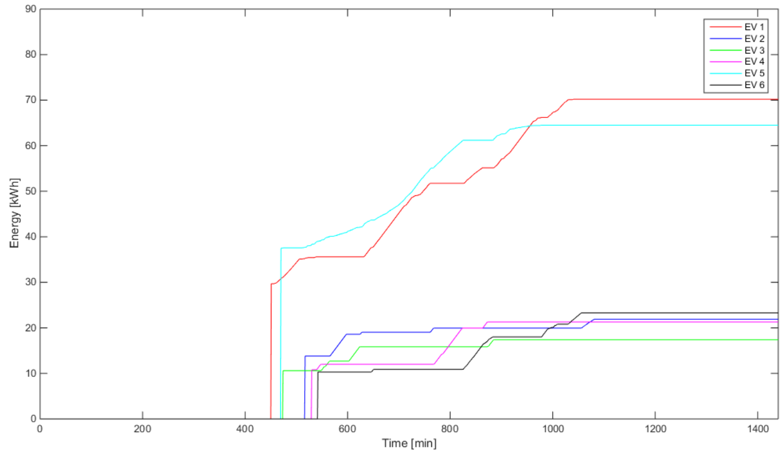

Figure A.38: Energy content during scenario 3 of 6 EVs with λ_{PV_t} = 0.097 €/kWh.

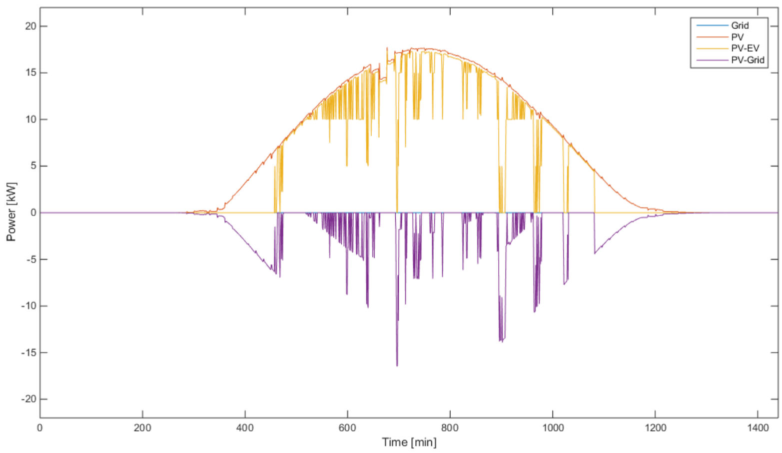

Figure A.39: Power allocation during scenario 3 of 6 EVs with λ_{PV_t} = 0.097 €/kWh, plotted without EVs.

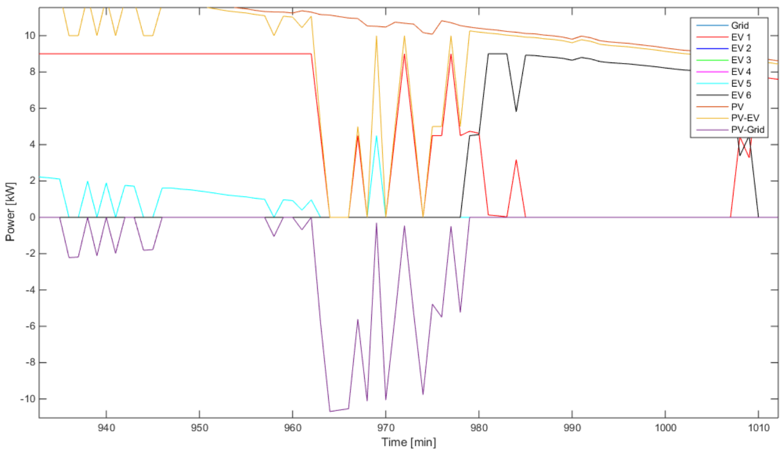

Figure A.40: Power allocation during scenario 3 of 6 EVs with λ_{PV_t} = 0.097 €/kWh, zoom in.

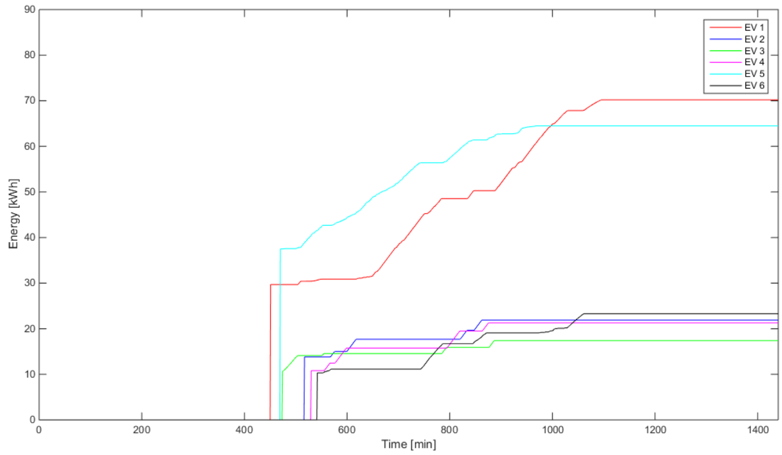

Figure A.41: Energy content during scenario 3 of 6 EVs with λ_{PV_t} = 0 €/kWh.

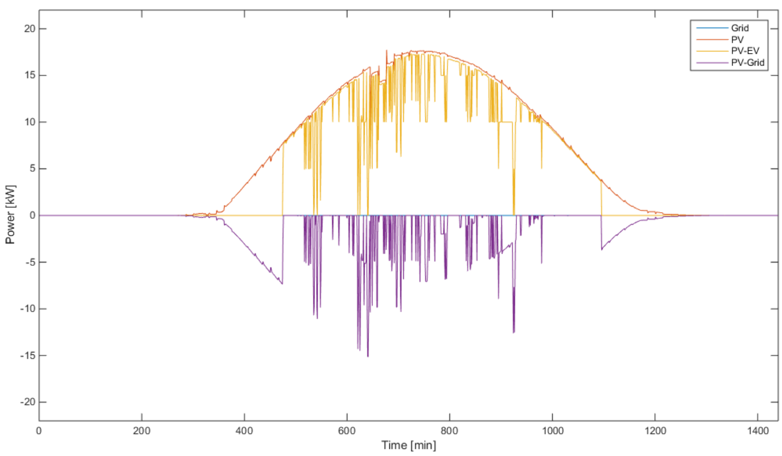

Figure A.42: Power allocation during scenario 3 of 6 EVs with λ_{PV_t} = 0 €/kWh, plotted without EVs.

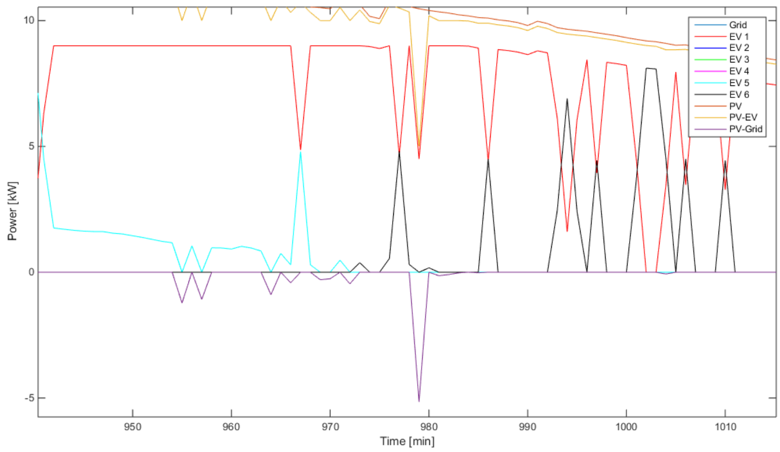

Figure A.43: Power allocation during scenario 3 of 6 EVs with λ_{PV_t} = 0 €/kWh, zoom in.

Scenario 4

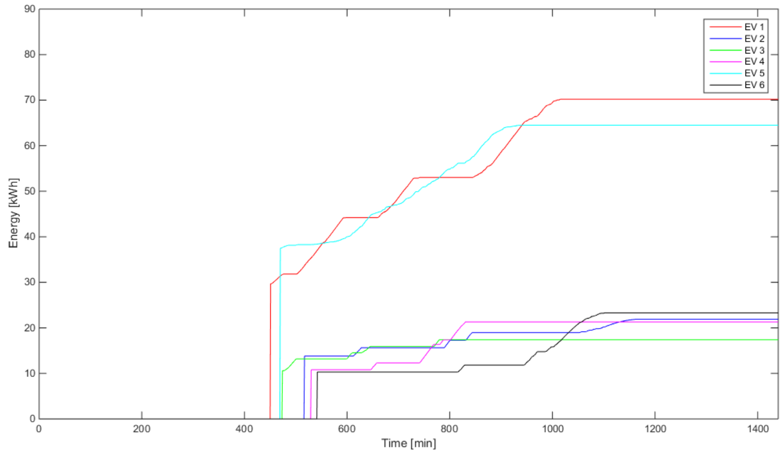

Figure A.44: Energy content during scenario 4 of 6 EVs with λ_{PV_t} = 0.097 €/kWh.

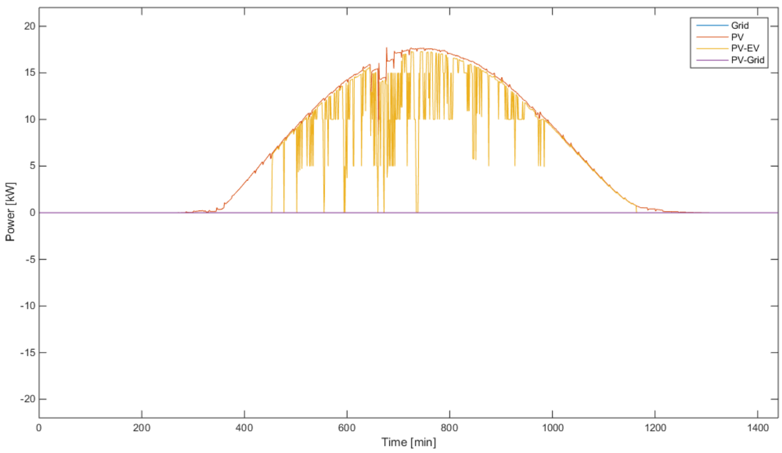

Figure A.45: Power allocation during scenario 4 of 6 EVs with λ_{PV_t} = 0.097 €/kWh, plotted without EVs.

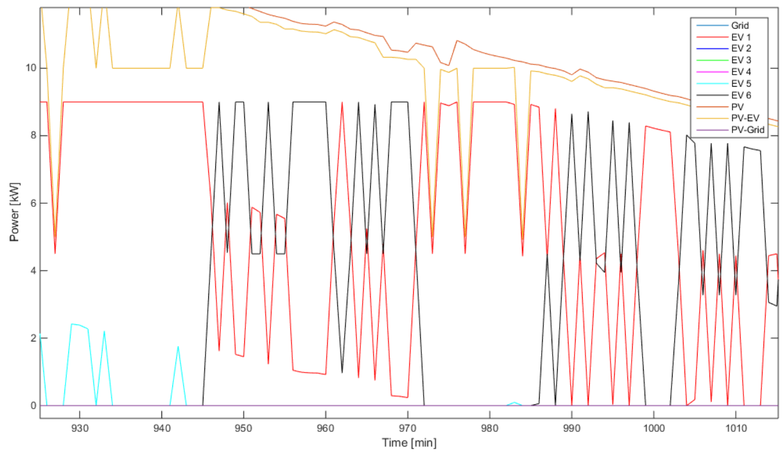

Figure A.46: Power allocation during scenario 4 of 6 EVs with λ_{PV_t} = 0.097 €/kWh, zoom in.

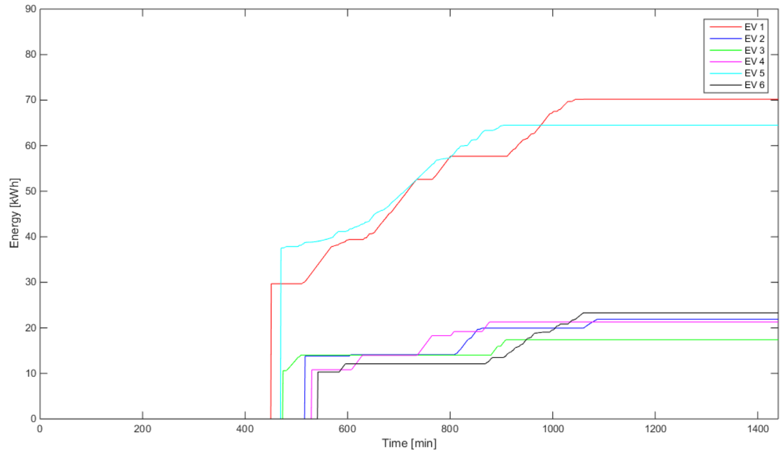

Figure A.47: Energy content during scenario 4 of 6 EVs with λ_{PV_t} = 0 €/kWh.

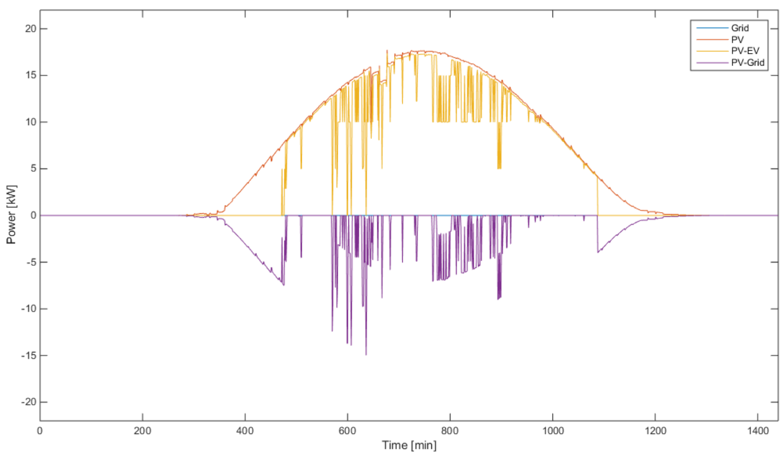

Figure A.48: Power allocation during scenario 4 of 6 EVs with λ_{PV_t} = 0 €/kWh, plotted without EVs.

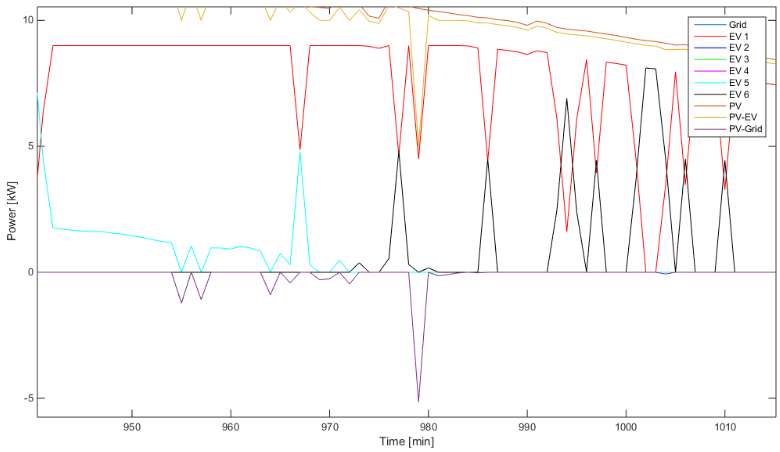

Figure A.49: Power allocation during scenario 4 of 6 EVs with λ_{PV_t} = 0 €/kWh, zoom in.

Scenario 5

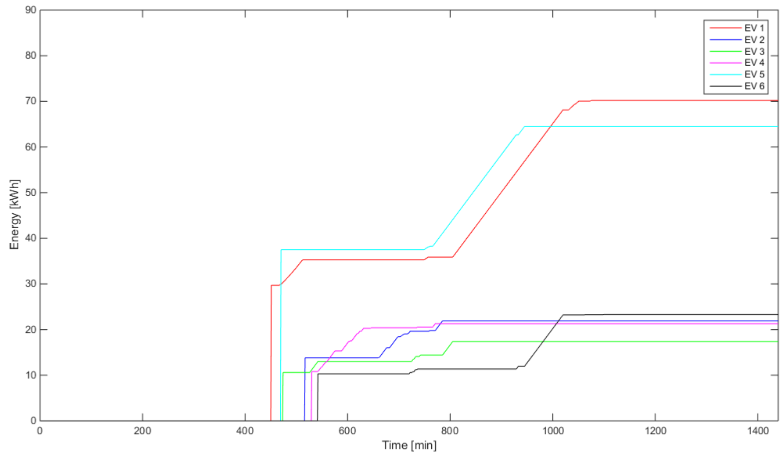

Figure A.50: Energy content during scenario 5 of 6 EVs with λ_{PV_t} = 0.097 €/kWh.

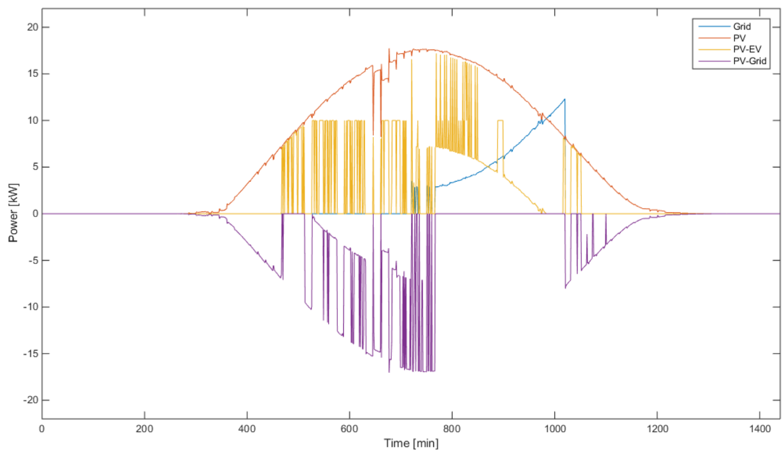

Figure A.51: Power allocation during scenario 5 of 6 EVs with λ_{PV_t} = 0.097 €/kWh, plotted without EVs or price.

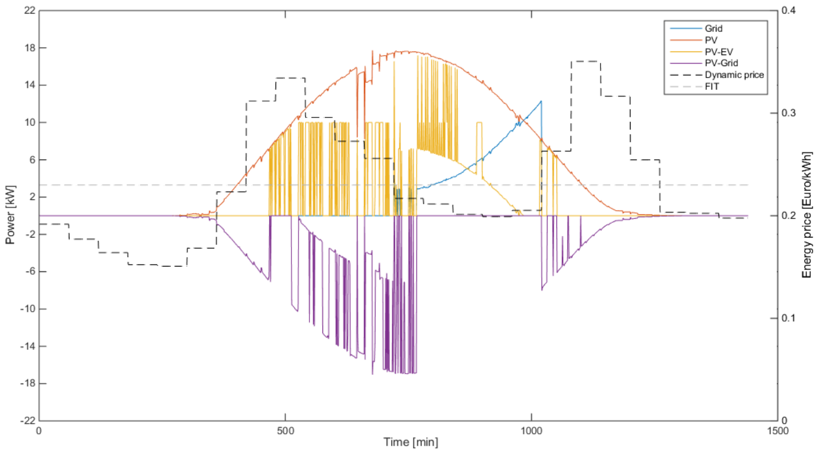

Figure A.52: Power allocation during scenario 5 of 6 EVs with λ_{PV_t} = 0.097 €/kWh, plotted without EVs.

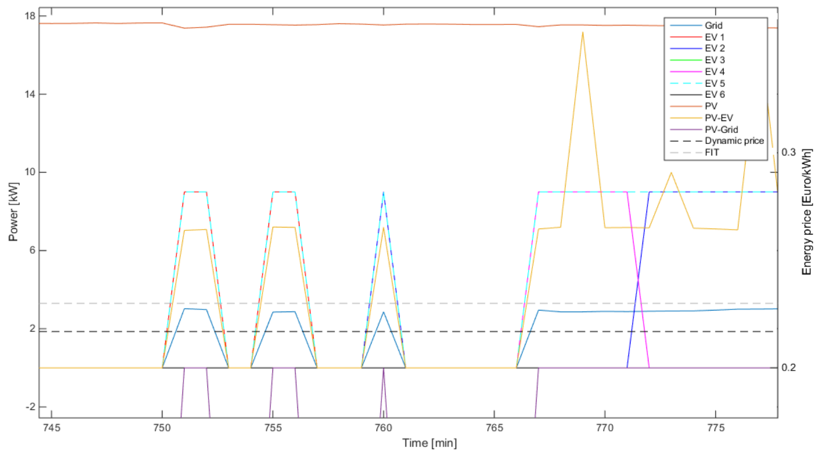

Figure A.53: Power allocation during scenario 5 of 6 EVs with λ_{PV_t} = 0.097 €/kWh, zoom in.

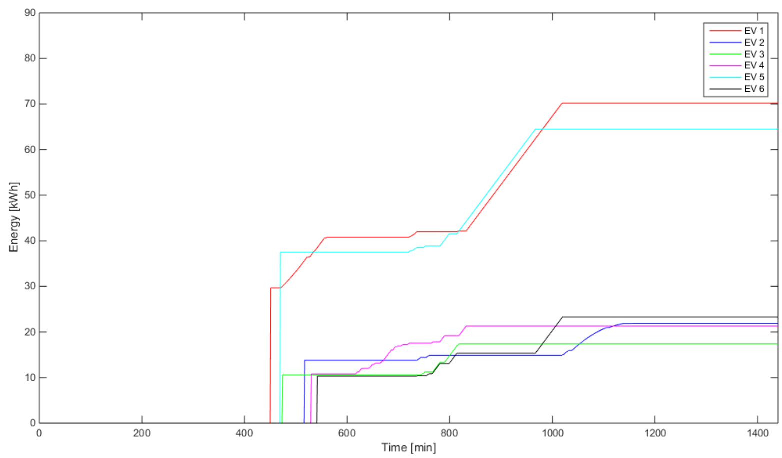

Figure A.54: Energy content during scenario 5 of 6 EVs with λ_{PV_t} = 0 €/kWh.

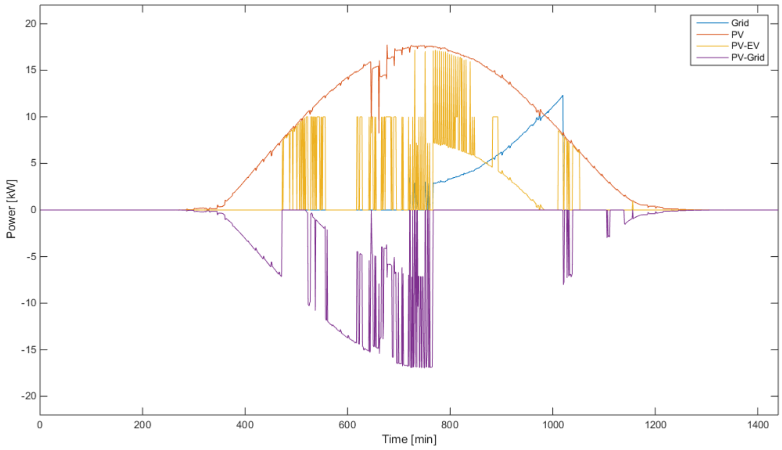

Figure A.55: Power allocation during scenario 5 of 6 EVs with λ_{PV_t} = 0 €/kWh, plotted without EVs or price.

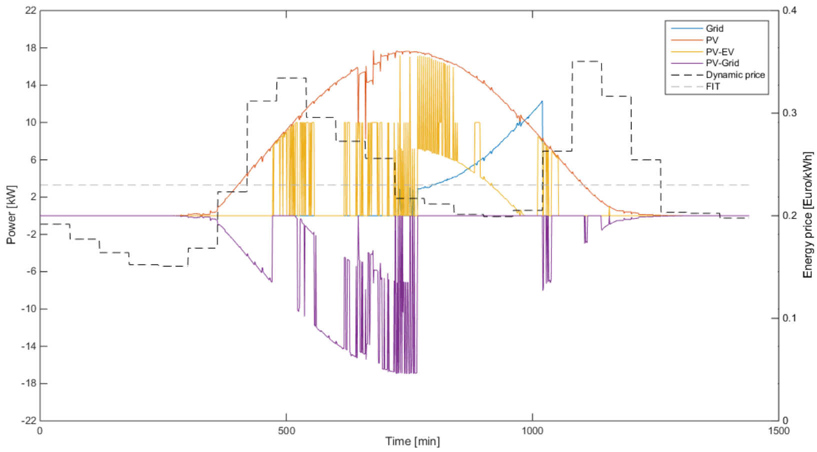

Figure A.56: Power allocation during scenario 5 of 6 EVs with λ_{PV_t} = 0 €/kWh, plotted without EVs.

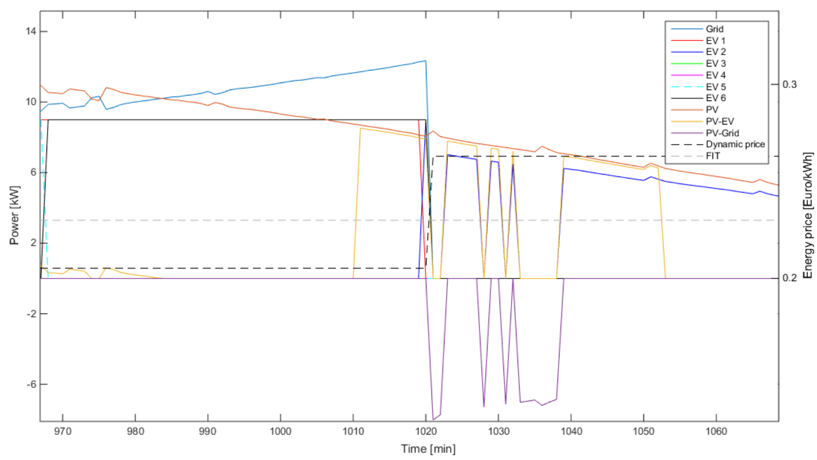

Figure A.57: Power allocation during scenario 5 of 6 EVs with λ_{PV_t} = 0 €/kWh, zoom in.

Scenario 6

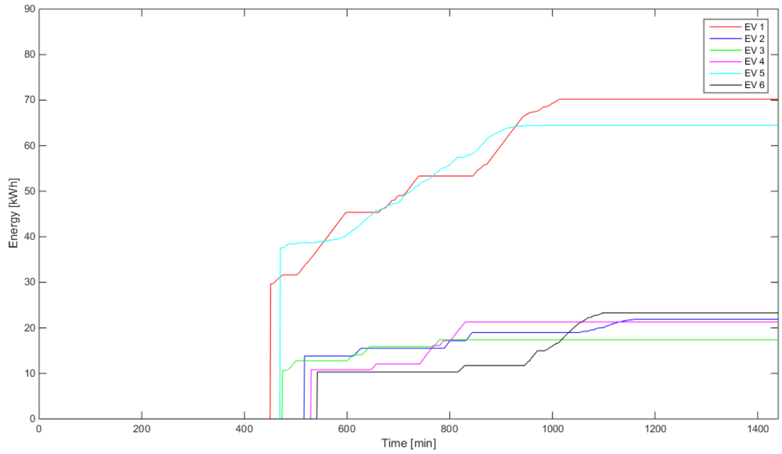

Figure A.58: Energy content during scenario 6 of 6 EVs with λ_{PV_t} = 0.097 €/kWh.

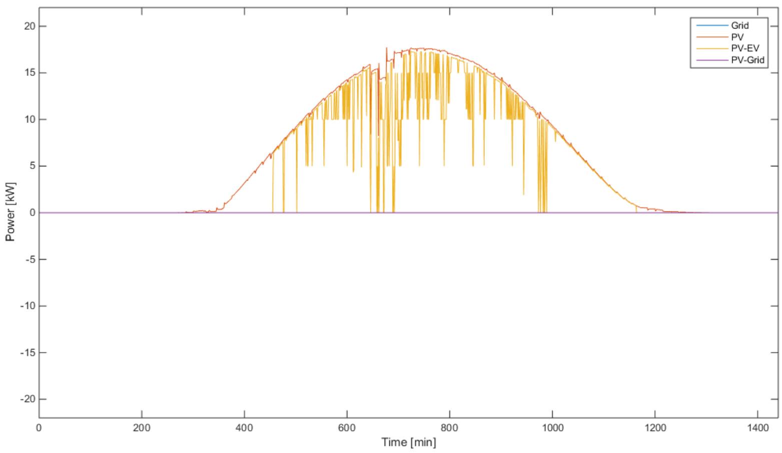

Figure A.59: Power allocation during scenario 6 of 6 EVs with λ_{PV_t} = 0.097 €/kWh, plotted without EVs or price.

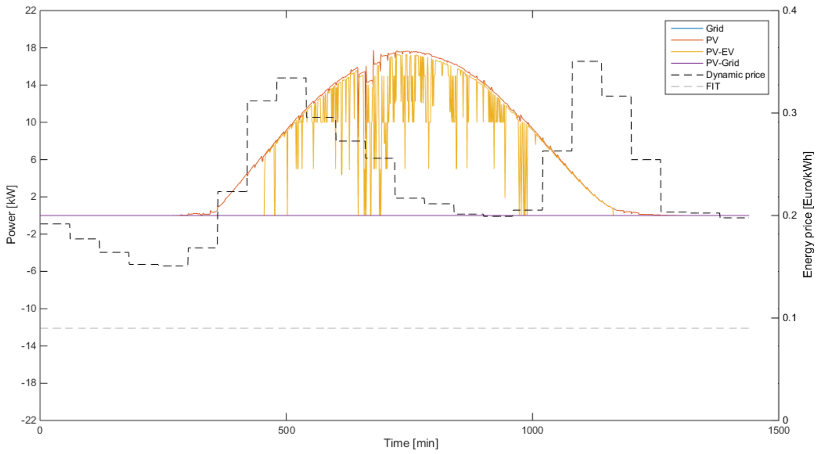

Figure A.60: Power allocation during scenario 6 of 6 EVs with λ_{PV_t} = 0.097 €/kWh, plotted without EVs.

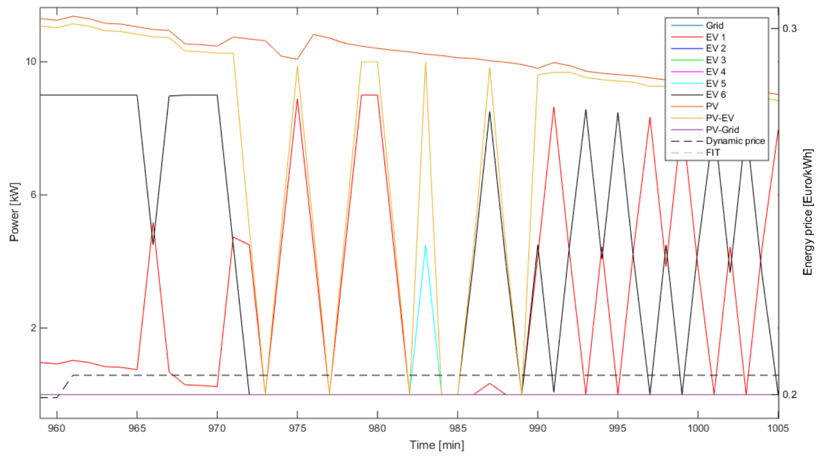

Figure A.61: Power allocation during scenario 6 of 6 EVs with λ_{PV_t} = 0.097 €/kWh, zoom in.

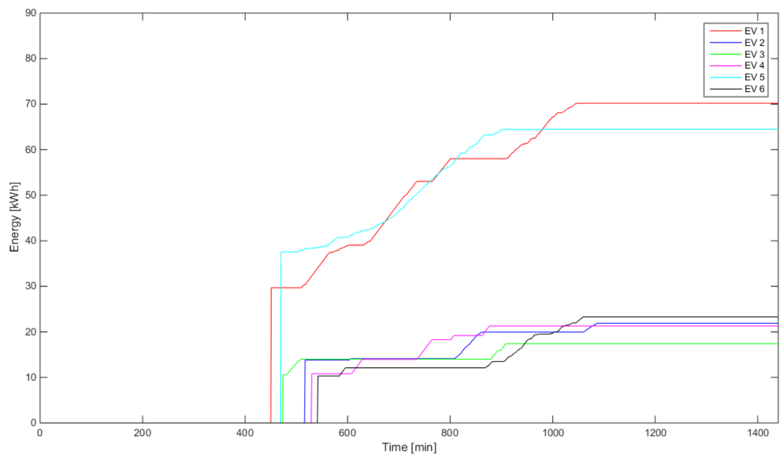

Figure A.62: Energy content during scenario 6 of 6 EVs with λ_{PV_t} = 0 €/kWh.

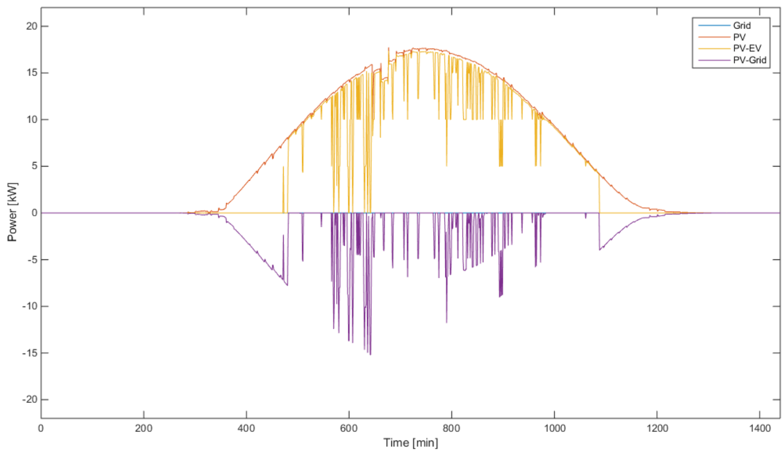

Figure A.63: Power allocation during scenario 6 of 6 EVs with λ_{PV_t} = 0 €/kWh, plotted without EVs or price.

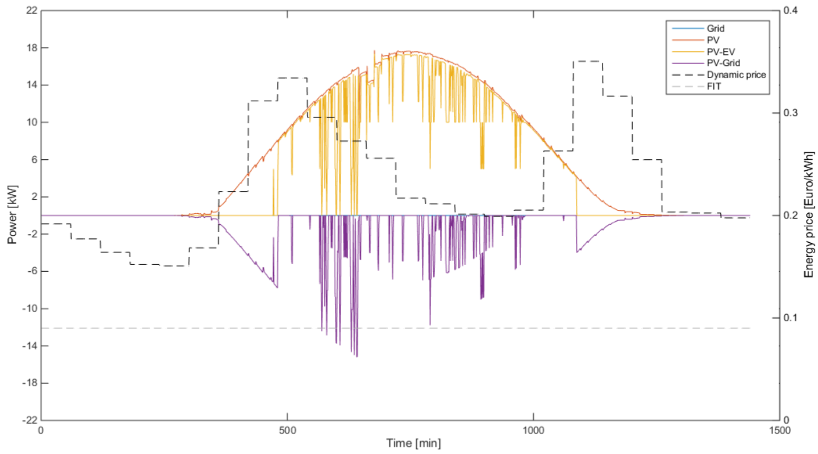

Figure A.64: Power allocation during scenario 6 of 6 EVs with λ_{PV_t} = 0 €/kWh, plotted without EVs.

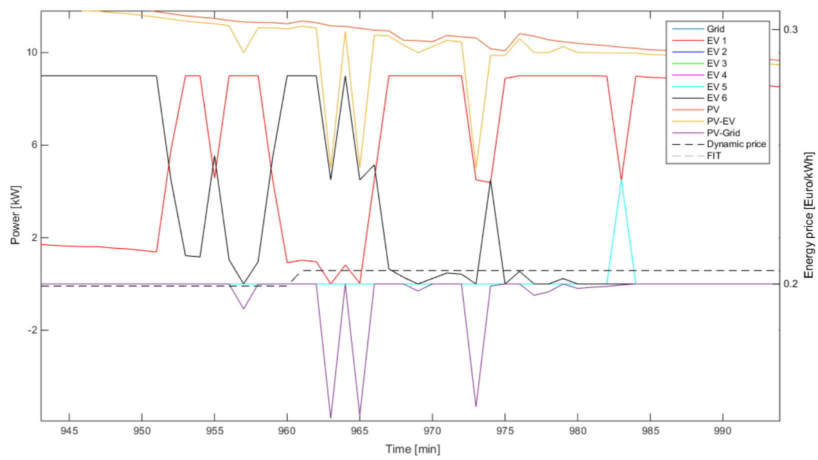

Figure A.65: Power allocation during scenario 6 of 6 EVs with λ_{PV_t} = 0 €/kWh, zoom in.

Minimize energy exchange with the grid

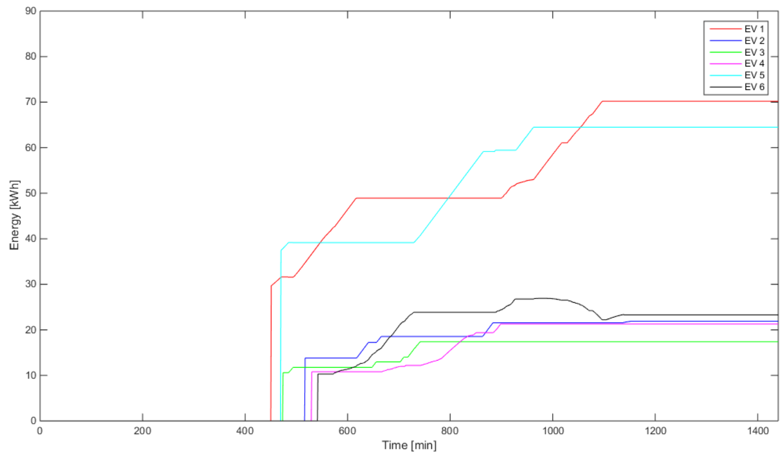

Figure A.66: Energy content of 6 EVs during minimization of energy exchange with grid.

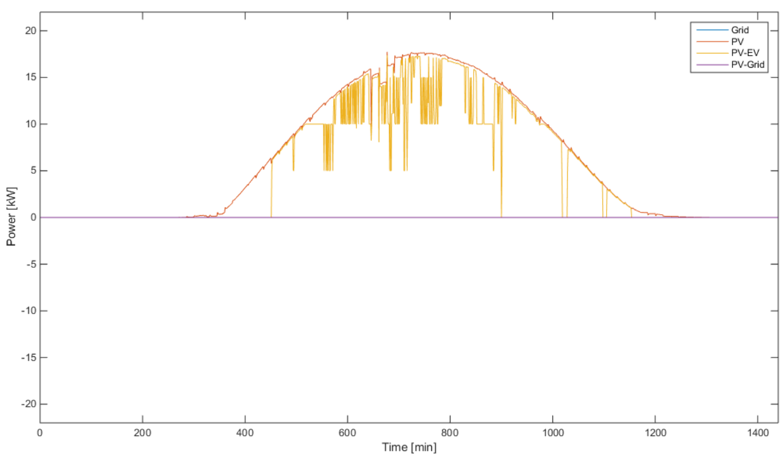

Figure A.67: Power allocation during minimization of energy exchange with grid, plotted without EVs.

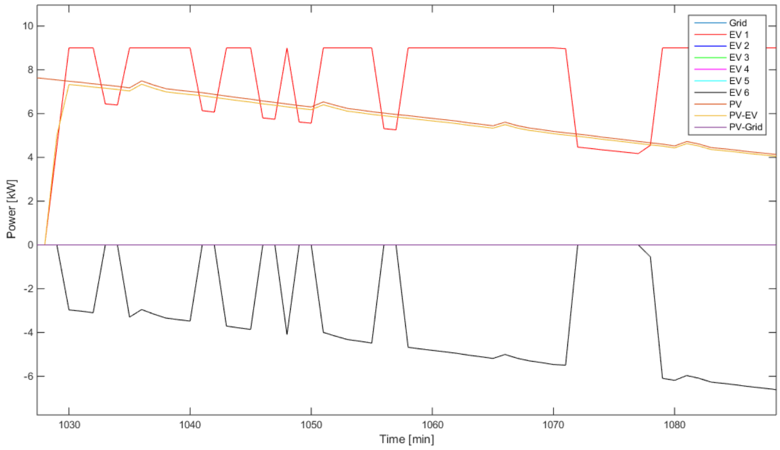

Figure A.68: Power allocation during minimization of energy exchange with grid, zoom in.

A.2. Winter

A.2.1. One charging point - four EVs

Scenario 1 and 2

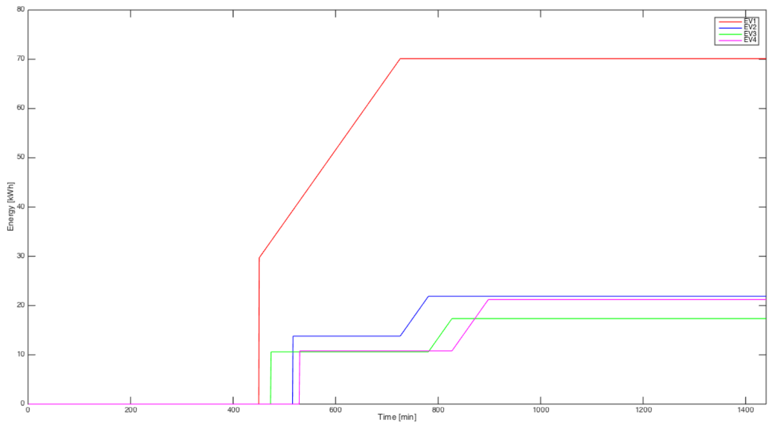

Figure A.69: Energy content during uncontrolled charging of 4 EVs with λ_{PV_t} = 0.097 €/kWh.

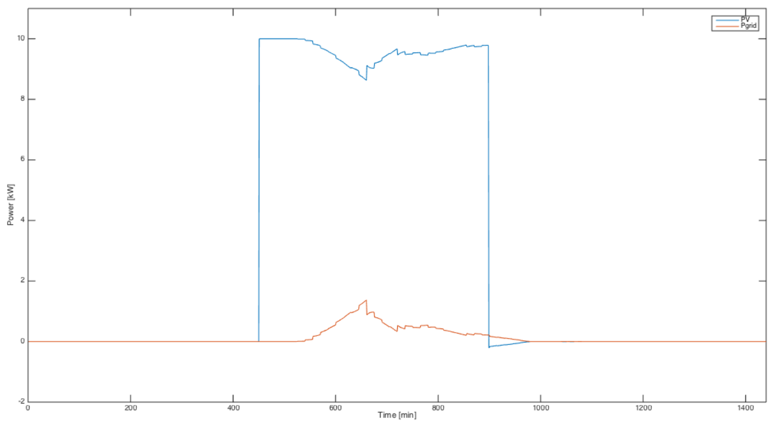

Figure A.70: Power allocation during uncontrolled charging of 4 EVs with λ_{PV_t} = 0.097 €/kWh, plotted without EVs.

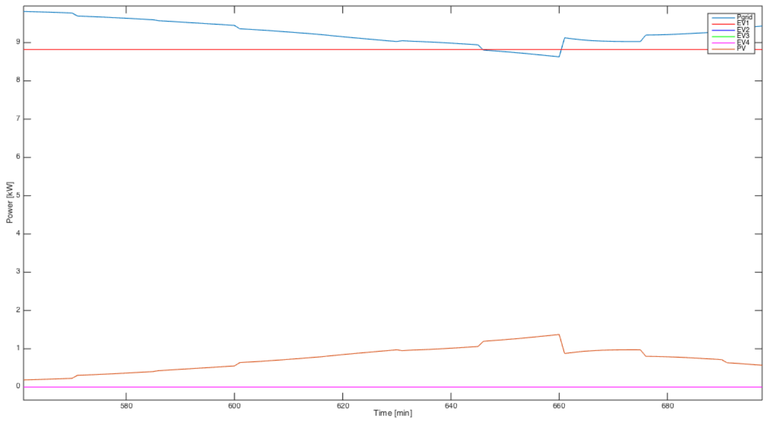

Figure A.71: Power allocation during uncontrolled charging of 4 EVs with λ_{PV_t} = 0.097 €/kWh, zoom in.

Scenario 3

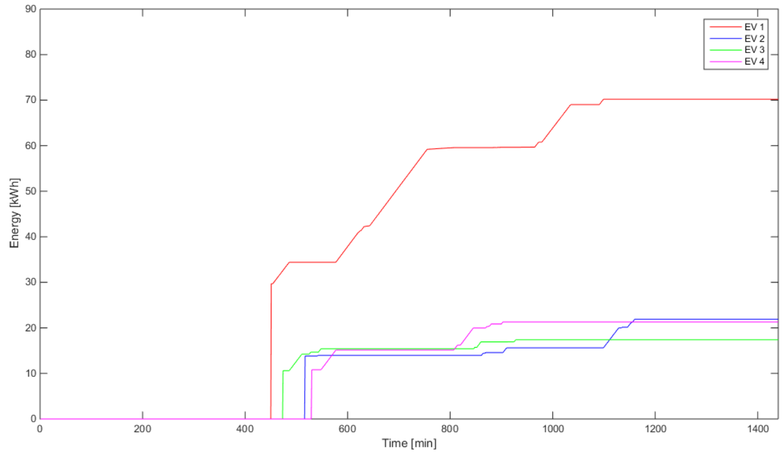

Figure A.72: Energy content during scenario 3 of 4 EVs with λ_{PV_t} = 0.097 €/kWh.

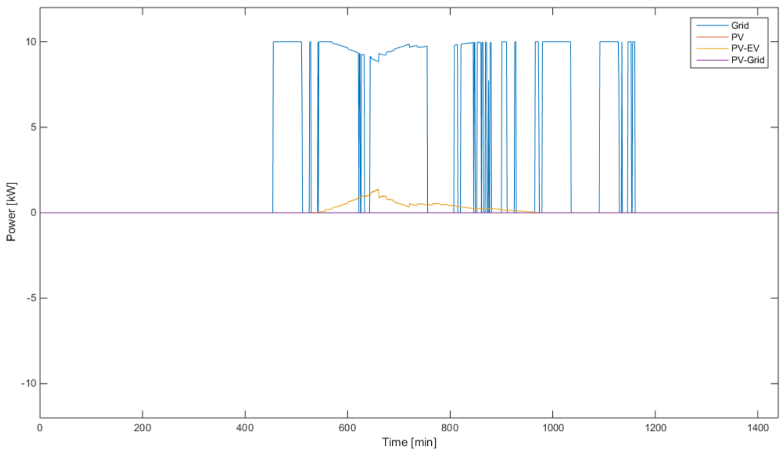

Figure A.73: Power allocation during scenario 3 of 4 EVs with λ_{PV_t} = 0.097 €/kWh, plotted without EVs.

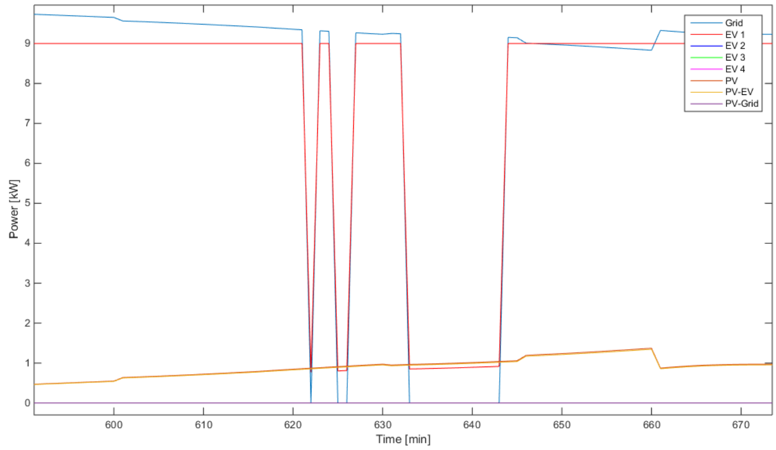

Figure A.74: Power allocation during scenario 3 of 4 EVs with λ_{PV_t} = 0.097 €/kWh, zoom in.

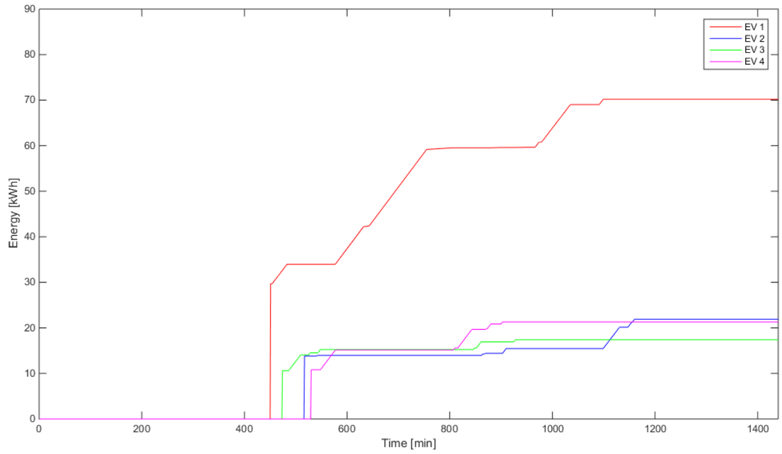

Figure A.75: Energy content during scenario 3 of 4 EVs with λ_{PV_t} = 0 €/kWh.

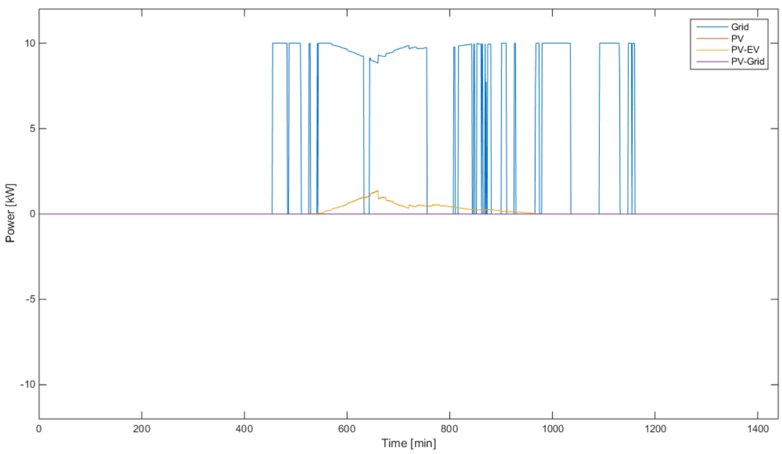

Figure A.76: Power allocation during scenario 3 of 4 EVs with λ_{PV_t} = 0 €/kWh, plotted without EVs.

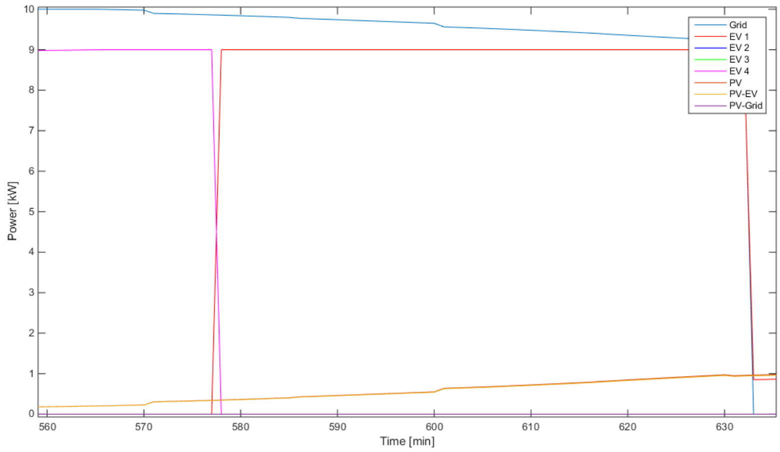

Figure A.77: Power allocation during scenario 3 of 4 EVs with λ_{PV_t} = 0 €/kWh, zoom in.

Scenario 4

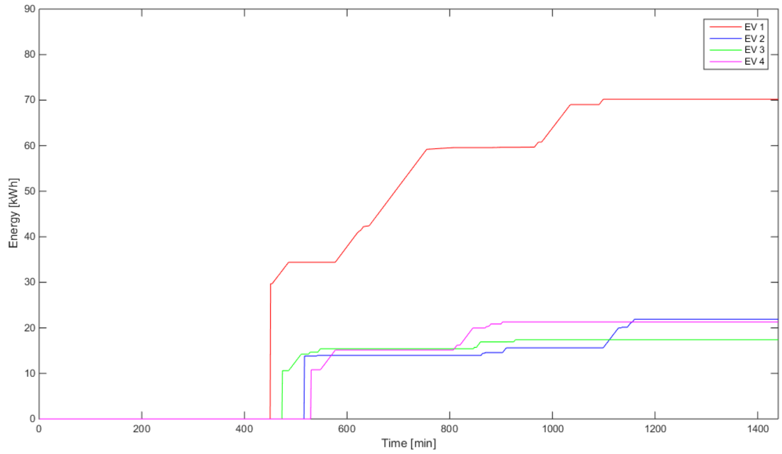

Figure A.78: Energy content during scenario 4 of 4 EVs with λ_{PV_t} = 0.097 €/kWh.

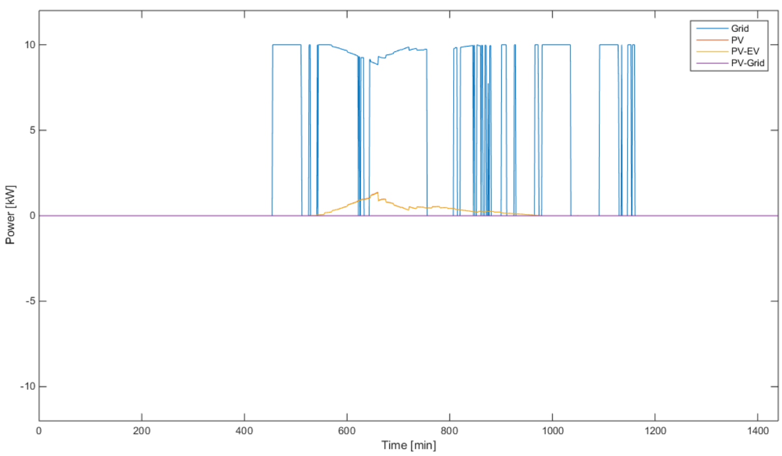

Figure A.79: Power allocation during scenario 4 of 4 EVs with λ_{PV_t} = 0.097 €/kWh, plotted without EVs.

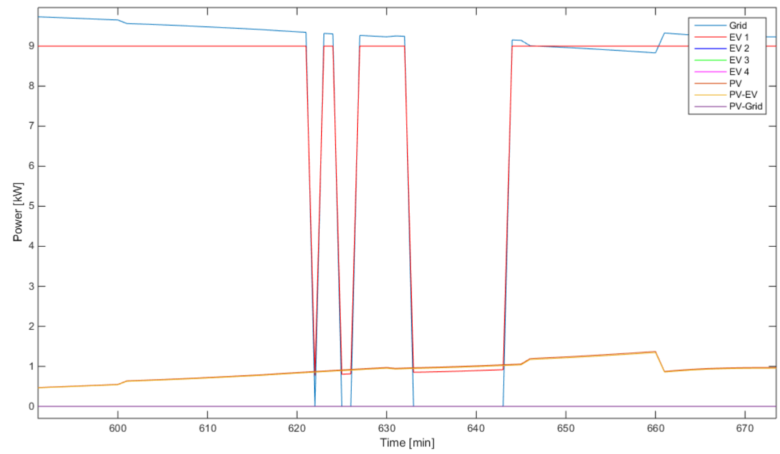

Figure A.80: Power allocation during scenario 4 of 4 EVs with λ_{PV_t} = 0.097 €/kWh, zoom in.

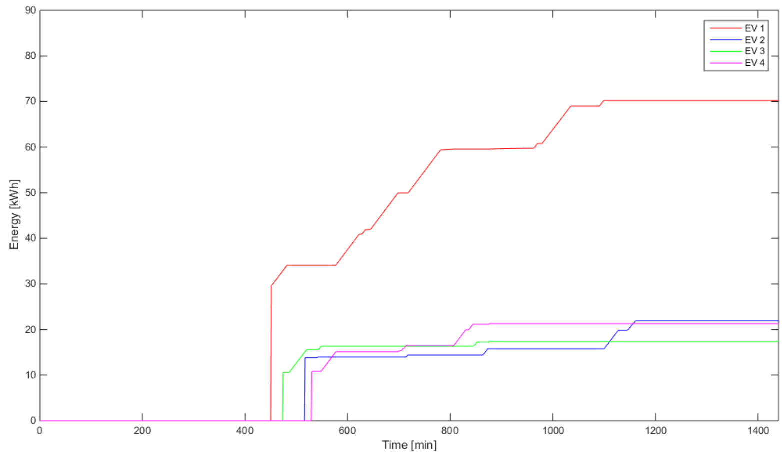

Figure A.81: Energy content during scenario 4 of 4 EVs with λ_{PV_t} = 0 €/kWh.

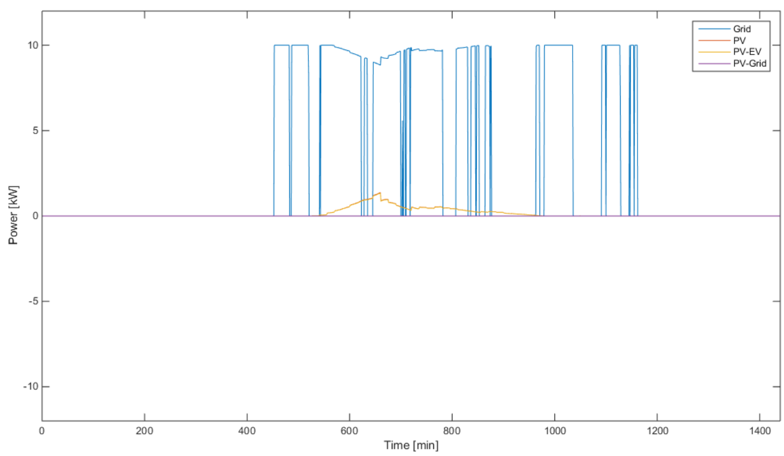

Figure A.82: Power allocation during scenario 4 of 4 EVs with λ_{PV_t} = 0 €/kWh, plotted without EVs.

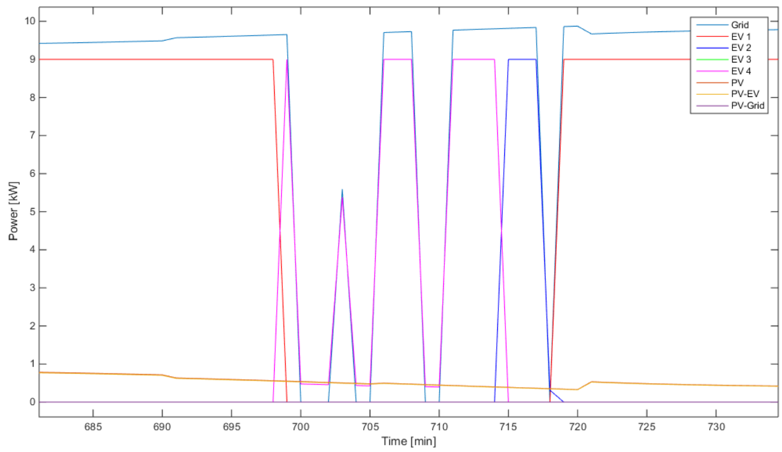

Figure A.83: Power allocation during scenario 4 of 4 EVs with λ_{PV_t} = 0 €/kWh, zoom in.

Scenario 5

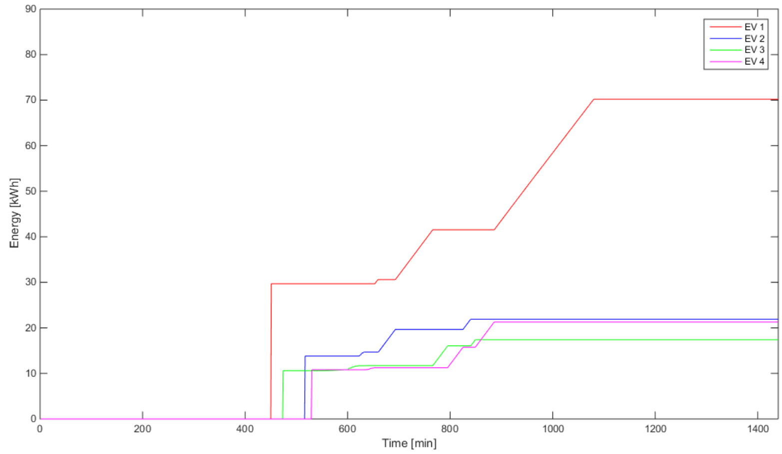

Figure A.84: Energy content during scenario 5 of 4 EVs with λ_{PV_t} = 0.097 €/kWh.

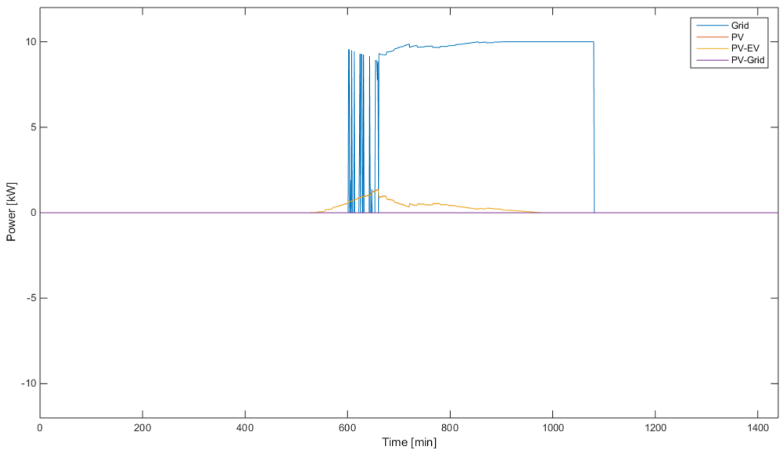

Figure A.85: Power allocation during scenario 5 of 4 EVs with λ_{PV_t} = 0.097 €/kWh, plotted without EVs or price.

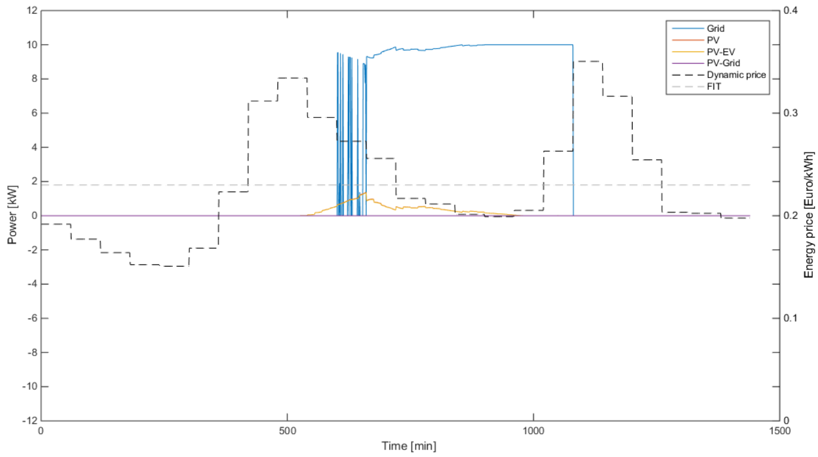

Figure A.86: Power allocation during scenario 5 of 4 EVs with λ_{PV_t} = 0.097 €/kWh, plotted without EVs.

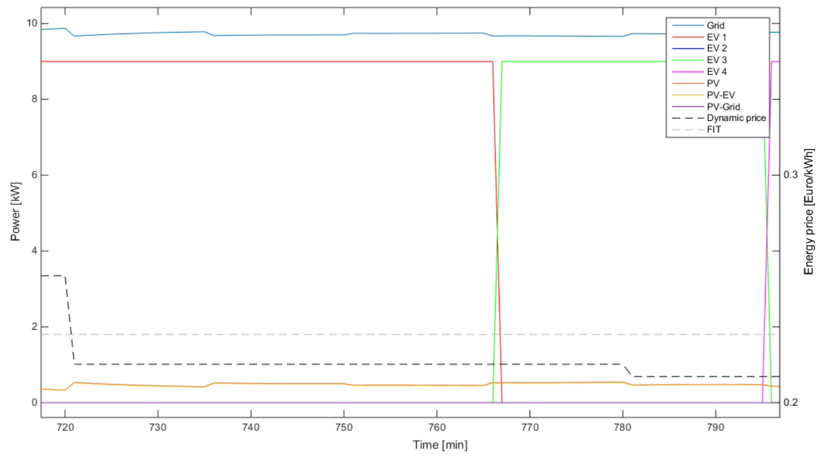

Figure A.87: Power allocation during scenario 5 of 4 EVs with λ_{PV_t} = 0.097 €/kWh, zoom in.

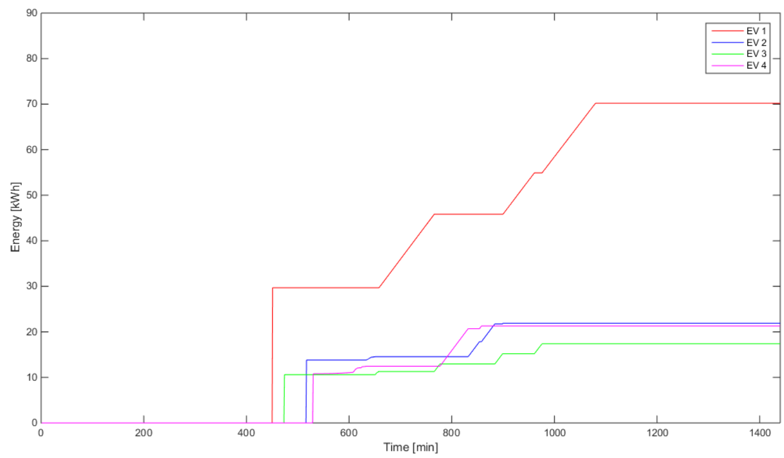

Figure A.88: Energy content during scenario 5 of 4 EVs with λ_{PV_t} = 0 €/kWh.

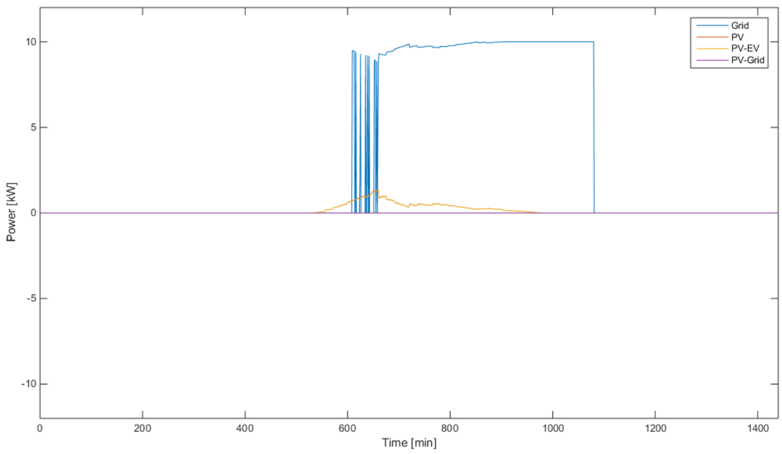

Figure A.89: Power allocation during scenario 5 of 4 EVs with λ_{PV_t} = 0 €/kWh, plotted without EVs or price.

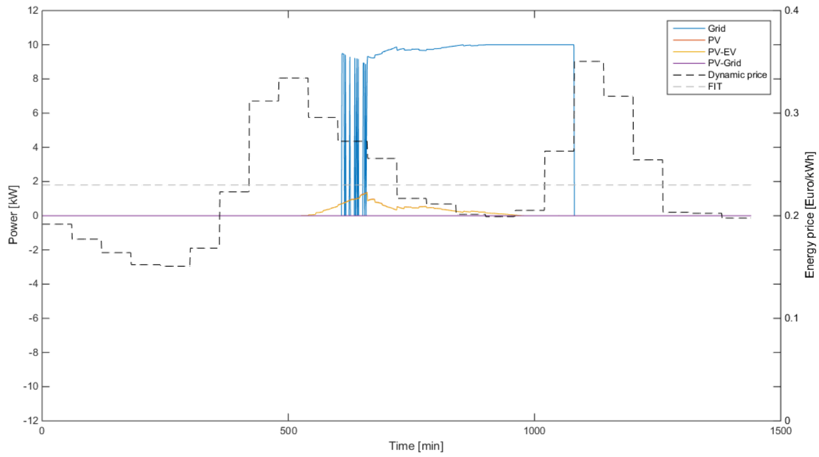

Figure A.90: Power allocation during scenario 5 of 4 EVs with λ_{PV_t} = 0 €/kWh, plotted without EVs.

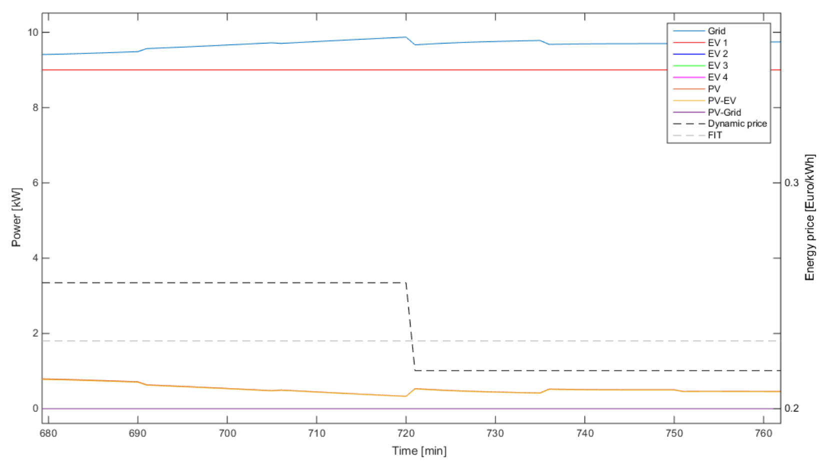

Figure A.91: Power allocation during scenario 5 of 4 EVs with λ_{PV_t} = 0 €/kWh, zoom in.

Scenario 6

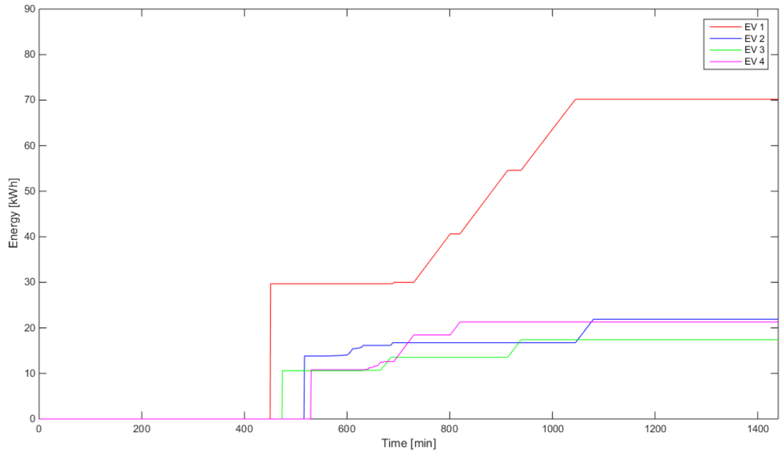

Figure A.92: Energy content during scenario 6 of 4 EVs with λ_{PV_t} = 0.097 €/kWh.

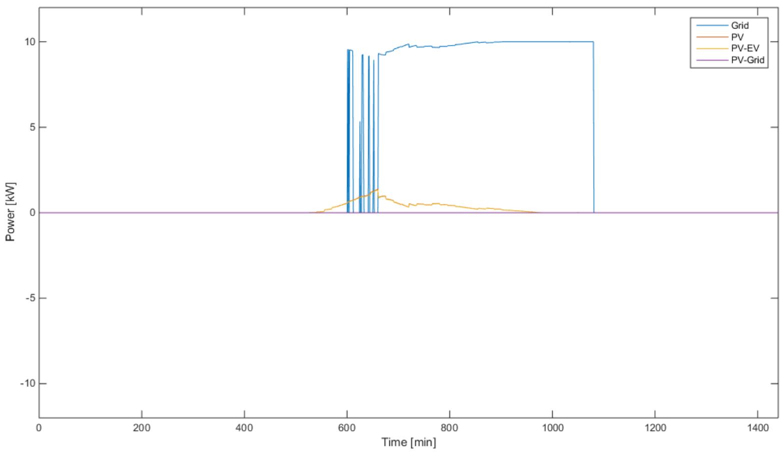

Figure A.93: Power allocation during scenario 6 of 4 EVs with λ_{PV_t} = 0.097 €/kWh, plotted without EVs or price.

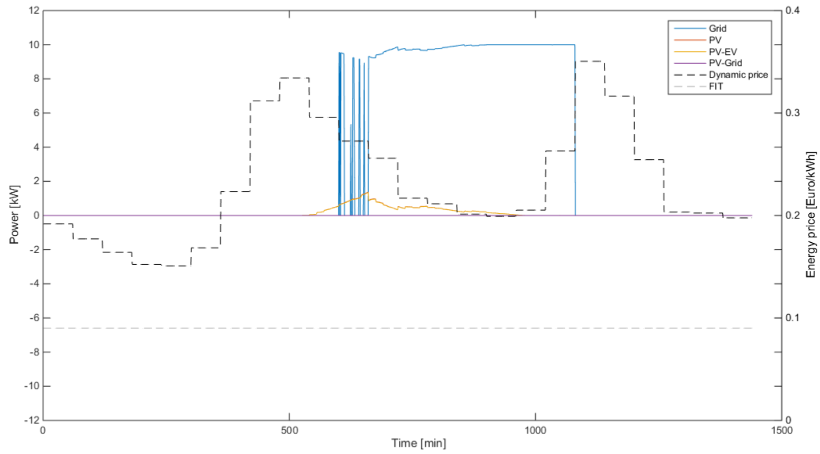

Figure A.94: Power allocation during scenario 6 of 4 EVs with λ_{PV_t} = 0.097 €/kWh, plotted without EVs.

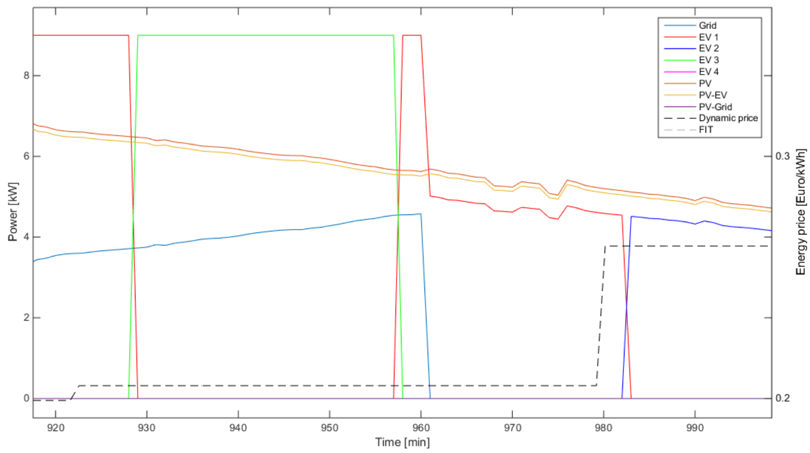

Figure A.95: Power allocation during scenario 6 of 4 EVs with λ_{PV_t} = 0.097 €/kWh, zoom in.

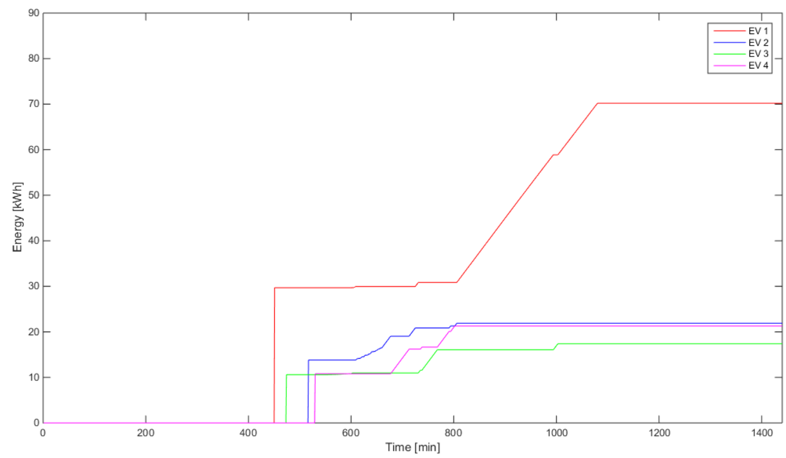

Figure A.96: Energy content during scenario 6 of 4 EVs with λ_{PV_t} = 0 €/kWh.

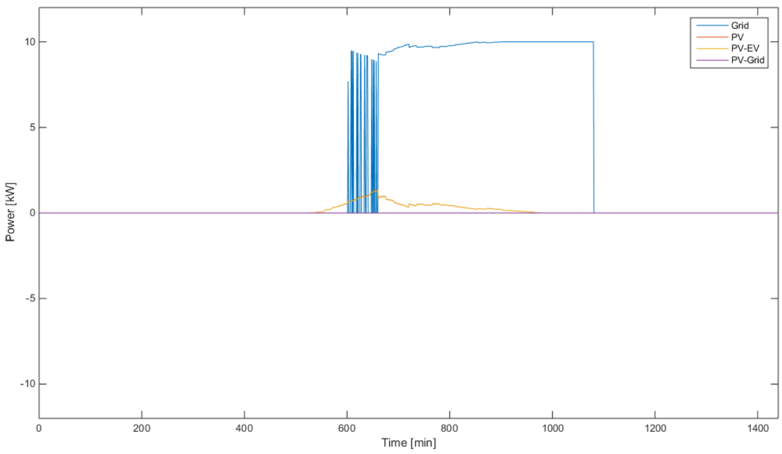

Figure A.97: Power allocation during scenario 6 of 4 EVs with λ_{PV_t} = 0 €/kWh, plotted without EVs or price.

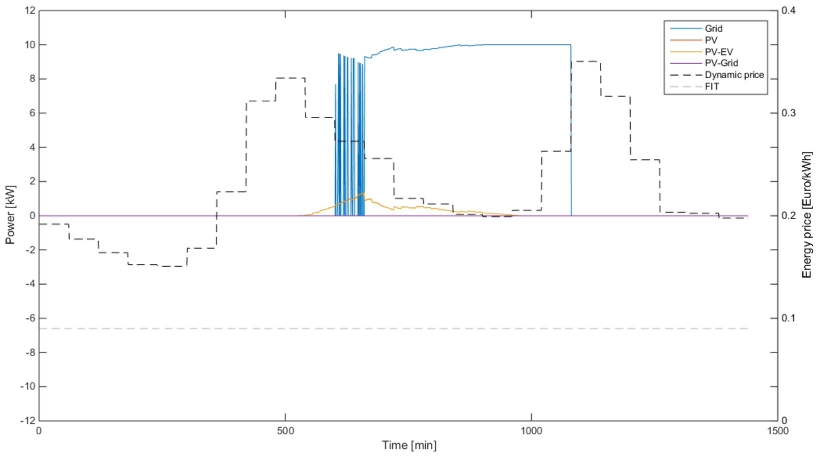

Figure A.98: Power allocation during scenario 6 of 4 EVs with λ_{PV_t} = 0 €/kWh, plotted without EVs.

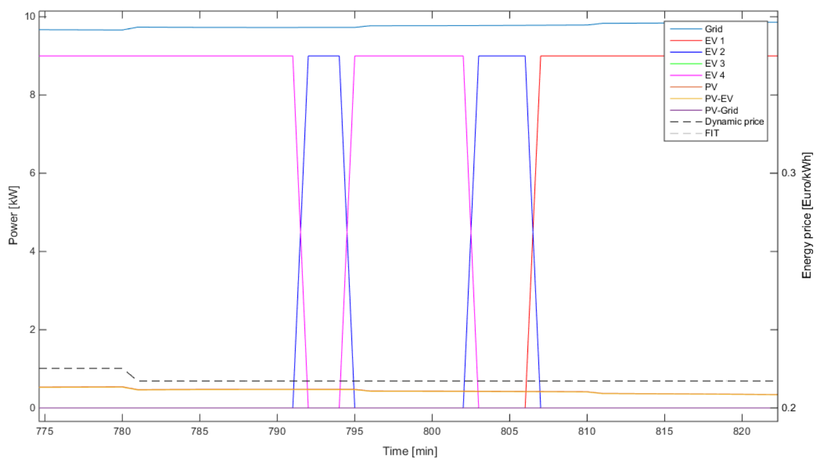

Figure A.99: Power allocation during scenario 6 of 4 EVs with λ_{PV_t} = 0 €/kWh, zoom in.

Minimize energy exchange with the grid

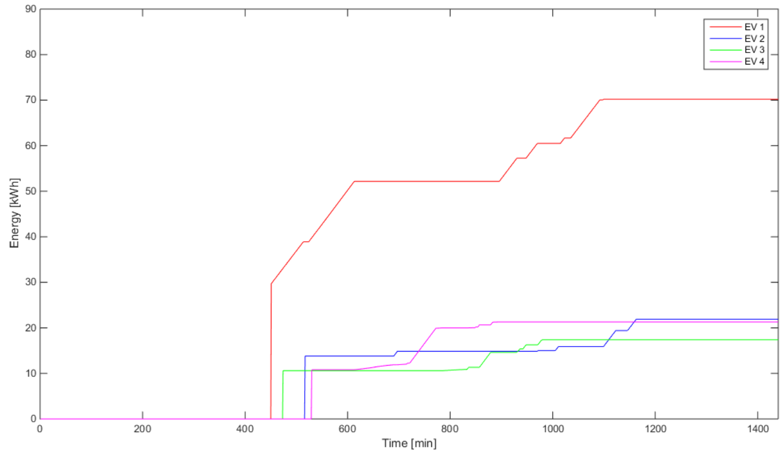

Figure A.100: Energy content of 4 EVs during minimization of energy exchange with grid.

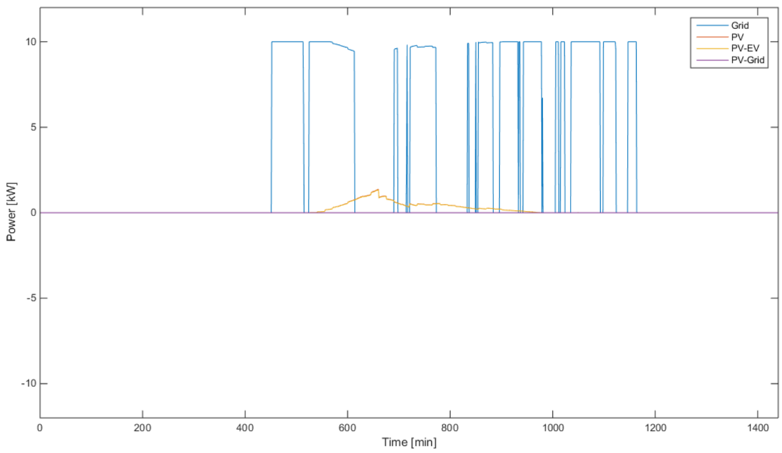

Figure A.101: Power allocation during minimization of energy exchange with grid, plotted without EVs.

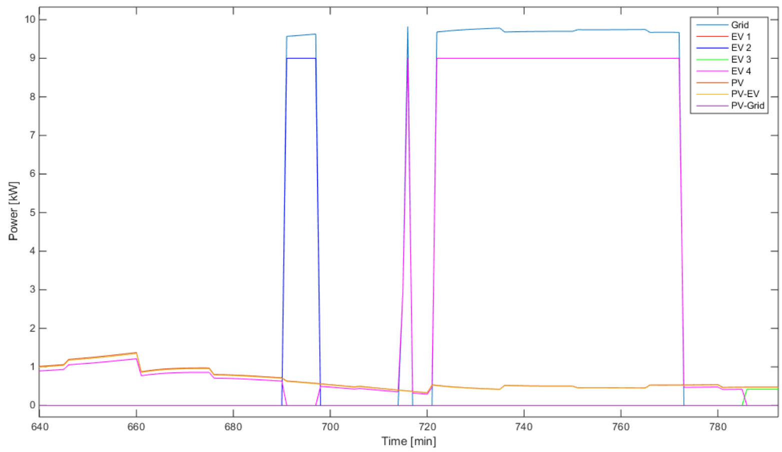

Figure A.102: Power allocation during minimization of energy exchange with grid, zoom in.

A.2.2. Two charging points - six EVs
Scenario 1 and 2

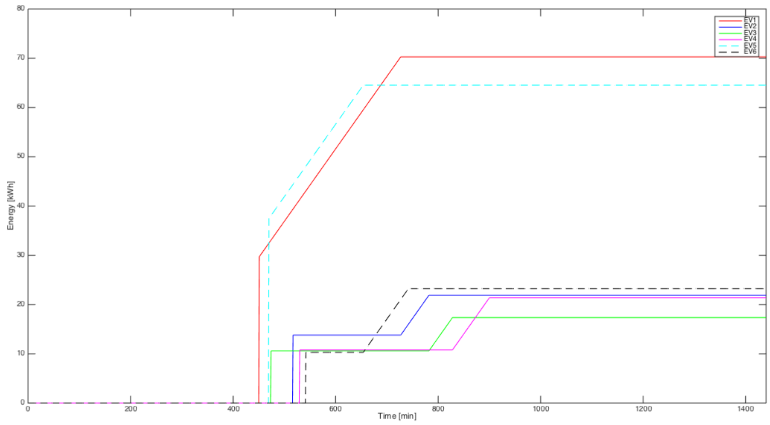

Figure A.103: Energy content during uncontrolled charging of 6 EVs with λ_{PV_t} = 0.097 €/kWh.

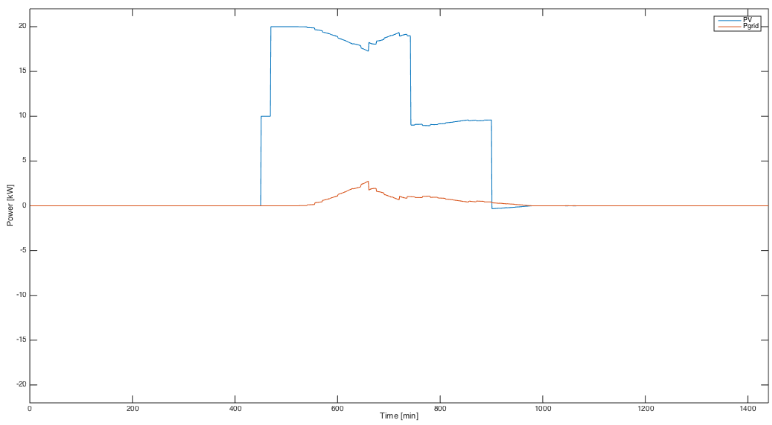

Figure A.104: Power allocation during uncontrolled charging of 6 EVs with λ_{PV_t} = 0.097 €/kWh, plotted without EVs.

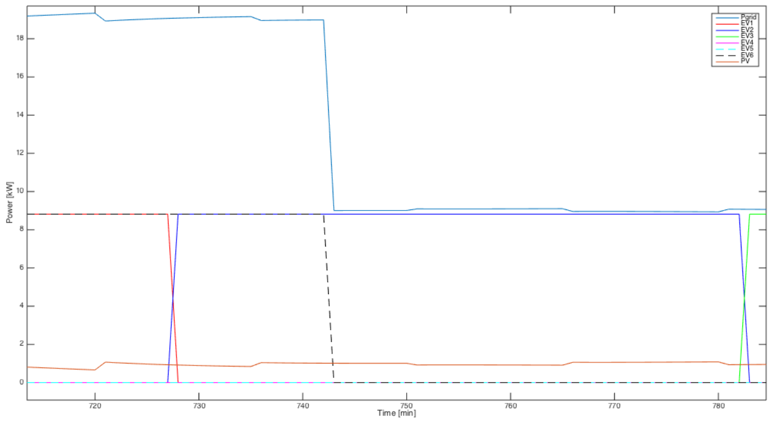

Figure A.105: Power allocation during uncontrolled charging of 6 EVs with λ_{PV_t} = 0.097 €/kWh, zoom in.

Scenario 3

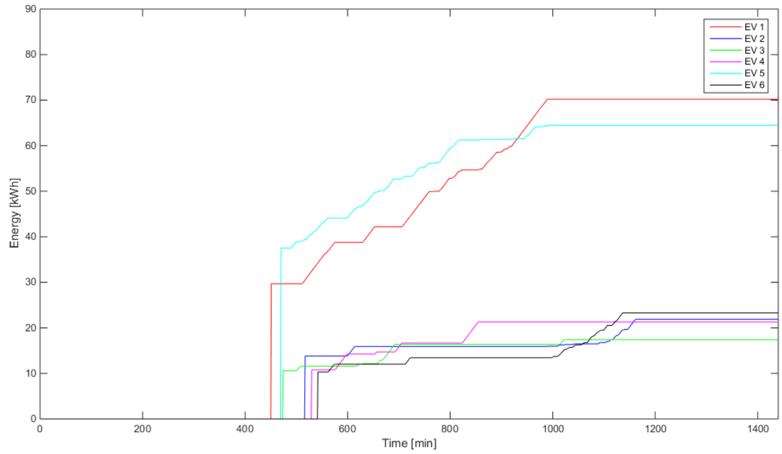

Figure A.106: Energy content during scenario 3 of 6 EVs with λ_{PV_t} = 0.097 €/kWh.

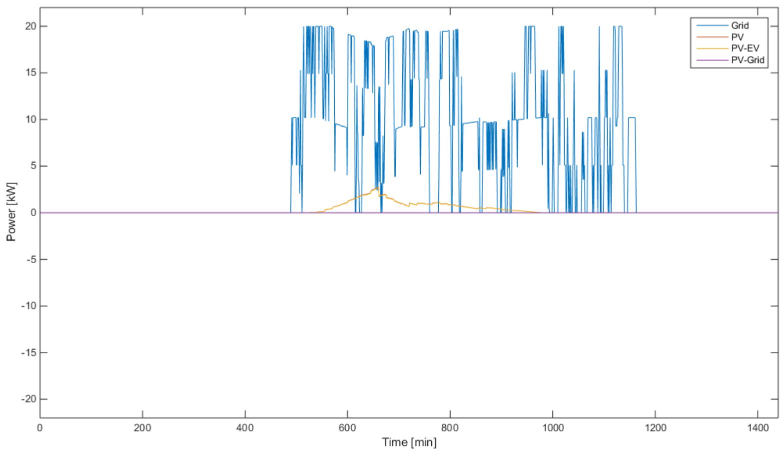

Figure A.107: Power allocation during scenario 3 of 6 EVs with λ_{PV_t} = 0.097 €/kWh, plotted without EVs.

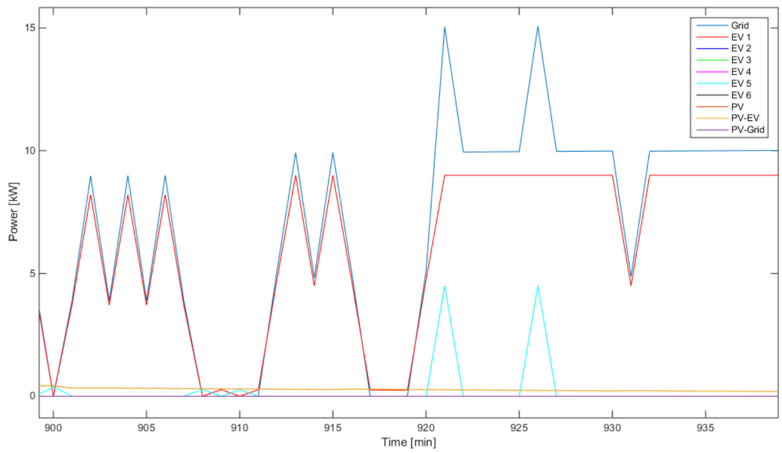

Figure A.108: Power allocation during scenario 3 of 6 EVs with λ_{PV_t} = 0.097 €/kWh, zoom in.

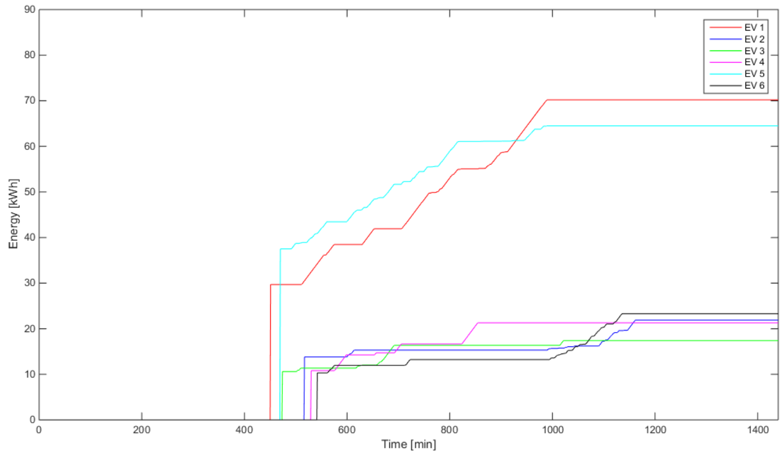

Figure A.109: Energy content during scenario 3 of 6 EVs with λ_{PV_t} = 0 €/kWh.

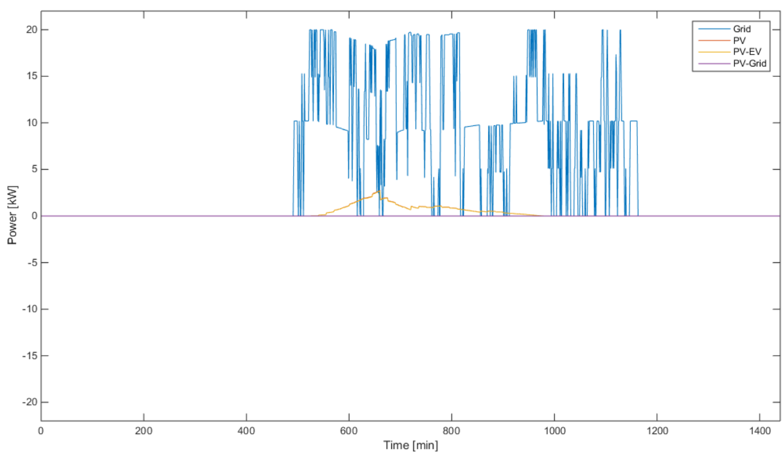

Figure A.110: Power allocation during scenario 3 of 6 EVs with λ_{PV_t} = 0 €/kWh, plotted without EVs.

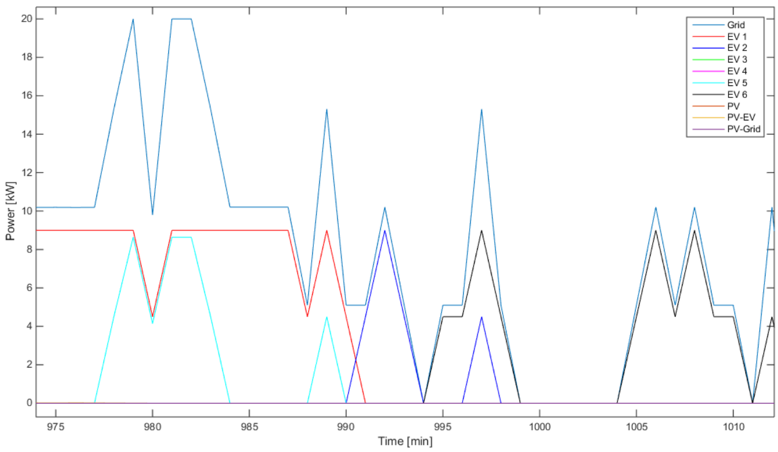

Figure A.111: Power allocation during scenario 3 of 6 EVs with λ_{PV_t} = 0 €/kWh, zoom in.

Scenario 4

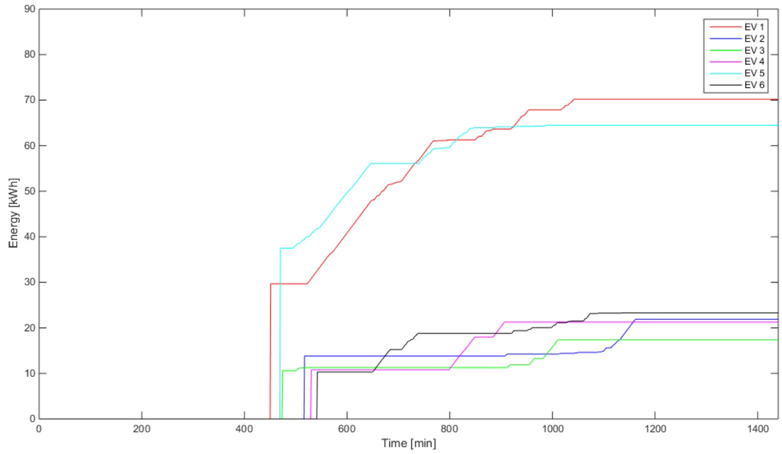

Figure A.112: Energy content during scenario 4 of 6 EVs with λ_{PV_t} = 0.097 €/kWh.

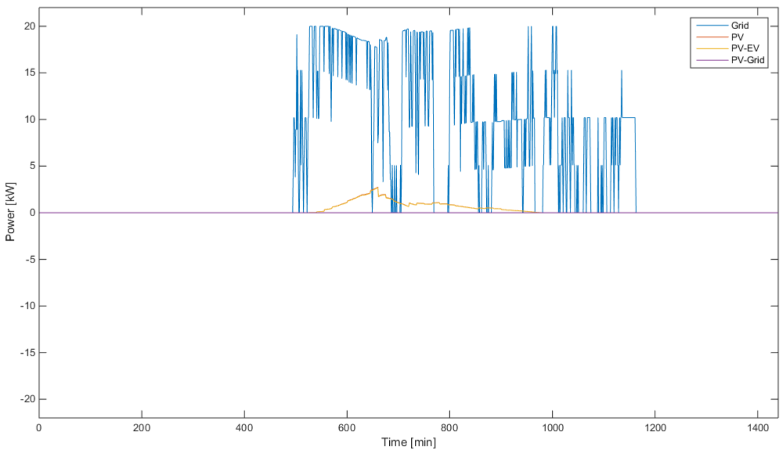

Figure A.113: Power allocation during scenario 4 of 6 EVs with λ_{PV_t} = 0.097 €/kWh, plotted without EVs.

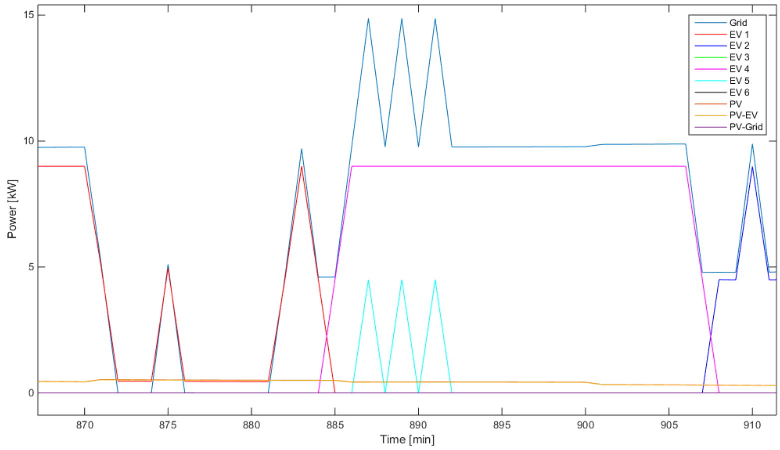

Figure A.114: Power allocation during scenario 4 of 6 EVs with λ_{PV_t} = 0.097 €/kWh, zoom in.

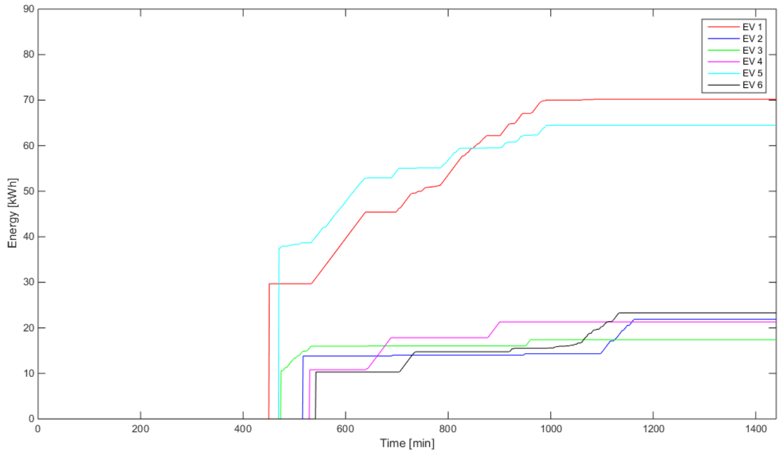

Figure A.115: Energy content during scenario 4 of 6 EVs with λ_{PV_t} = 0 €/kWh.

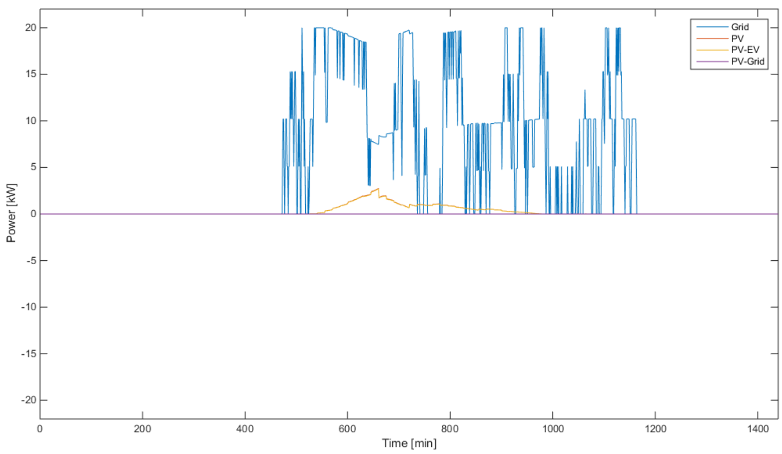

Figure A.116: Power allocation during scenario 4 of 6 EVs with λ_{PV_t} = 0 €/kWh, plotted without EVs.

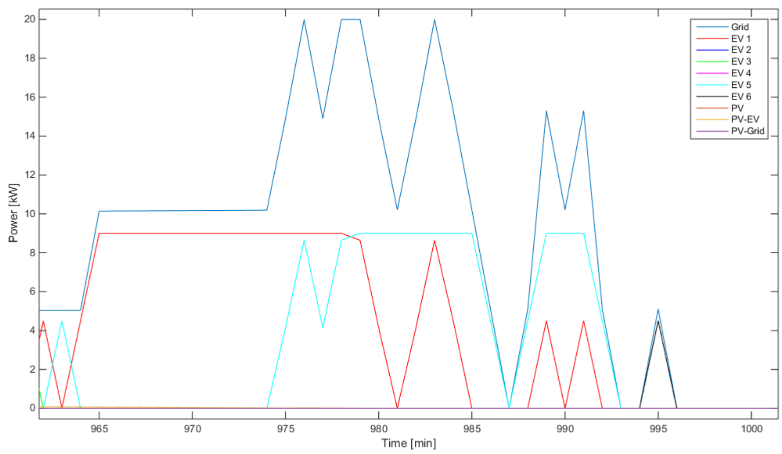

Figure A.117: Power allocation during scenario 4 of 6 EVs with λ_{PV_t} = 0 €/kWh, zoom in.

Scenario 5

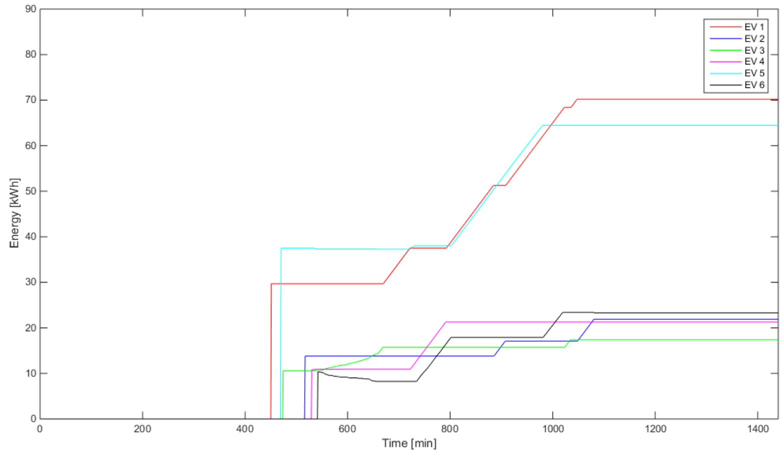

Figure A.118: Energy content during scenario 5 of 6 EVs with λ_{PV_t} = 0.097 €/kWh.

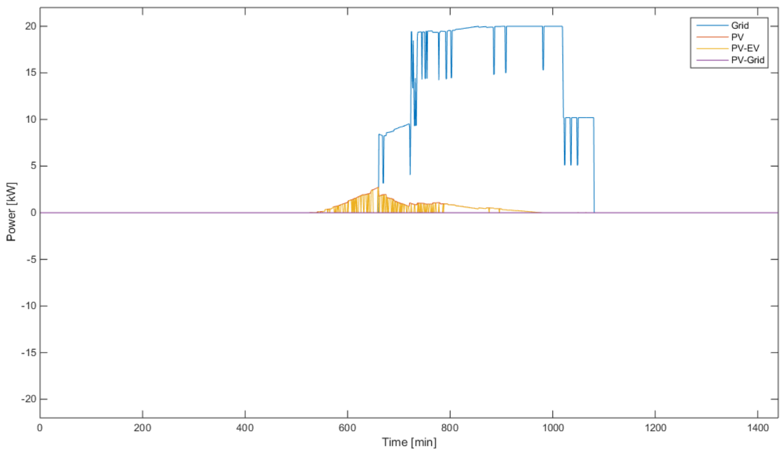

Figure A.119: Power allocation during scenario 5 of 6 EVs with λ_{PV_t} = 0.097 €/kWh, plotted without EVs or price.

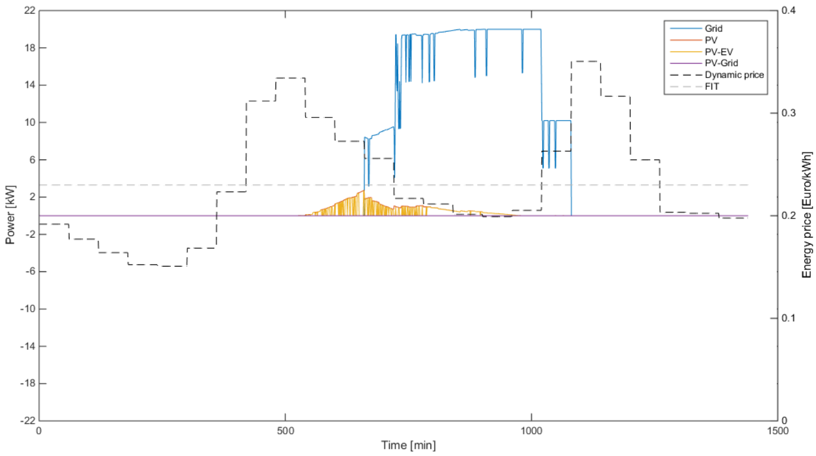

Figure A.120: Power allocation during scenario 5 of 6 EVs with λ_{PV_t} = 0.097 €/kWh, plotted without EVs.

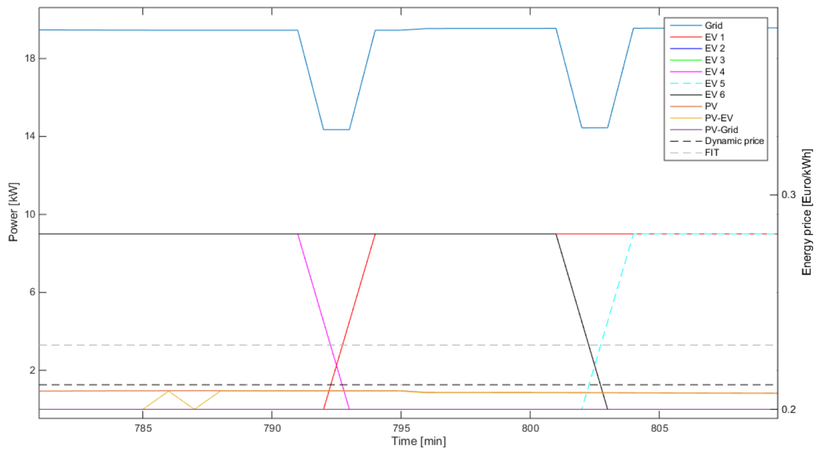

Figure A.121: Power allocation during scenario 5 of 6 EVs with λ_{PV_t} = 0.097 €/kWh, zoom in.

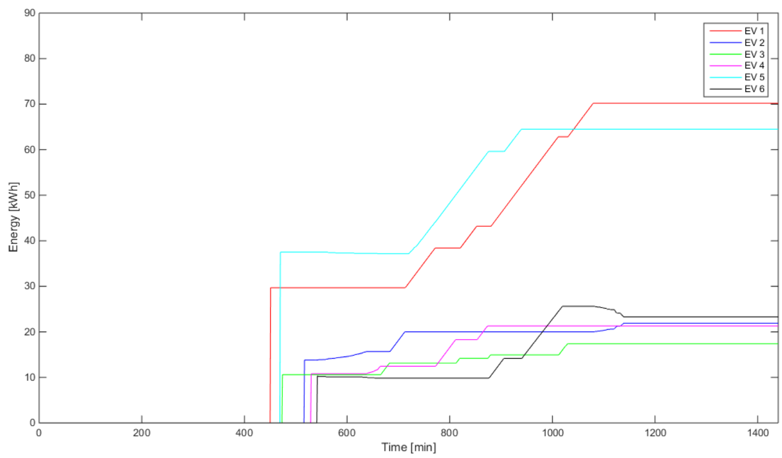

Figure A.122: Energy content during scenario 5 of 6 EVs with λ_{PV_t} = 0 €/kWh.

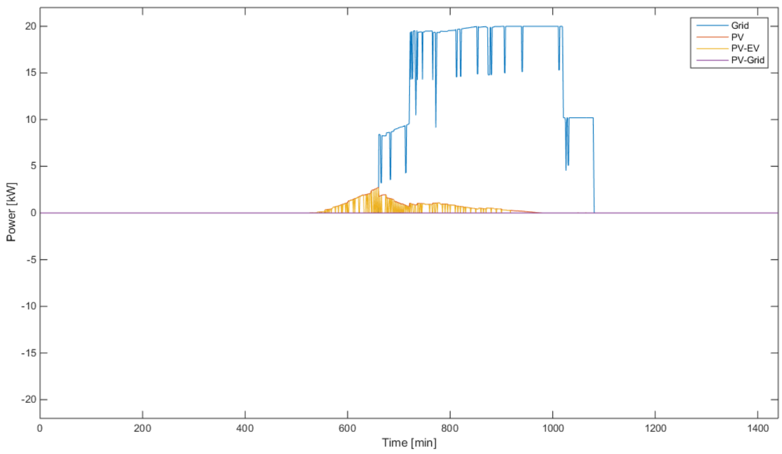

Figure A.123: Power allocation during scenario 5 of 6 EVs with λ_{PV_t} = 0 €/kWh, plotted without EVs or price.

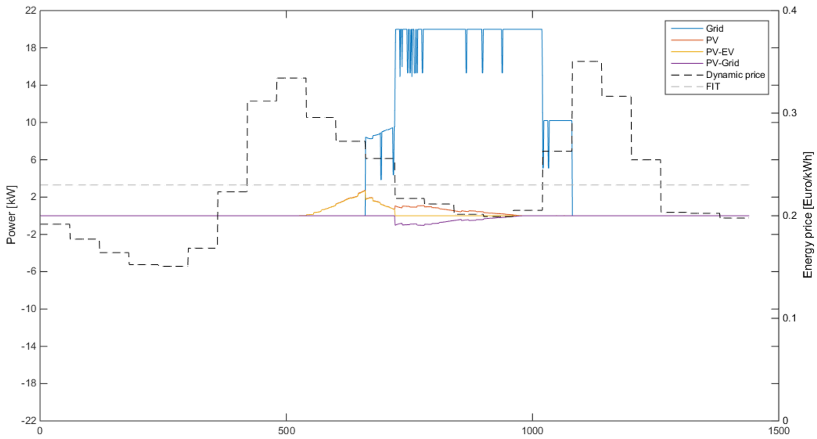

Figure A.124: Power allocation during scenario 5 of 6 EVs with λ_{PV_t} = 0 €/kWh, plotted without EVs.

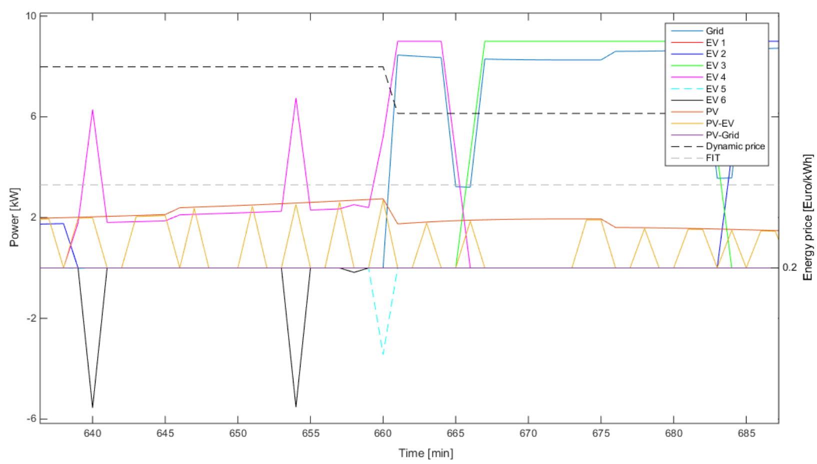

Figure A.125: Power allocation during scenario 5 of 6 EVs with λ_{PV_t} = 0 €/kWh, zoom in.

Scenario 6

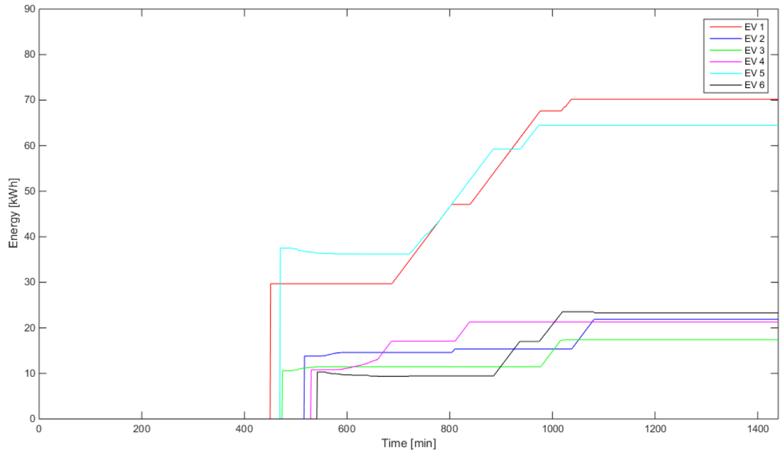

Figure A.126: Energy content during scenario 6 of 6 EVs with λ_{PV_t} = 0.097 €/kWh.

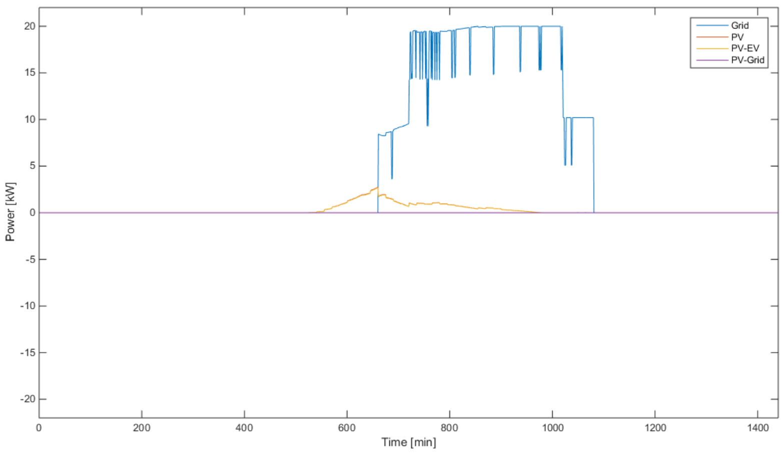

Figure A.127: Power allocation during scenario 6 of 6 EVs with λ_{PV_t} = 0.097 €/kWh, plotted without EVs or price.

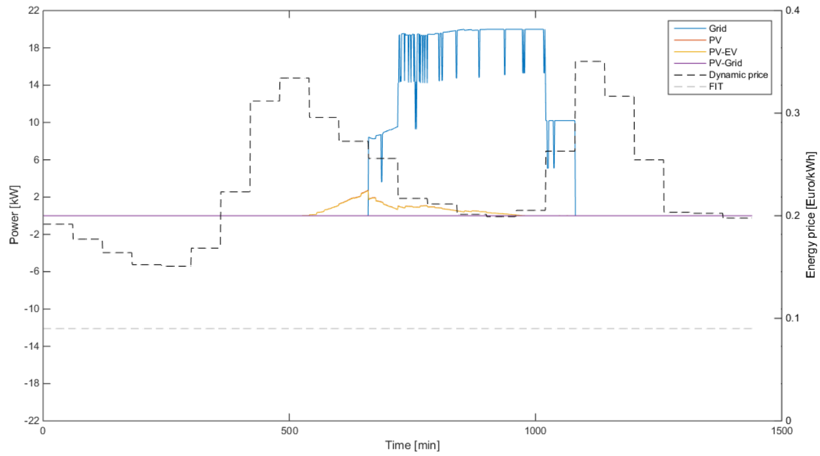

Figure A.128: Power allocation during scenario 6 of 6 EVs with λ_{PV_t} = 0.097 €/kWh, plotted without EVs.

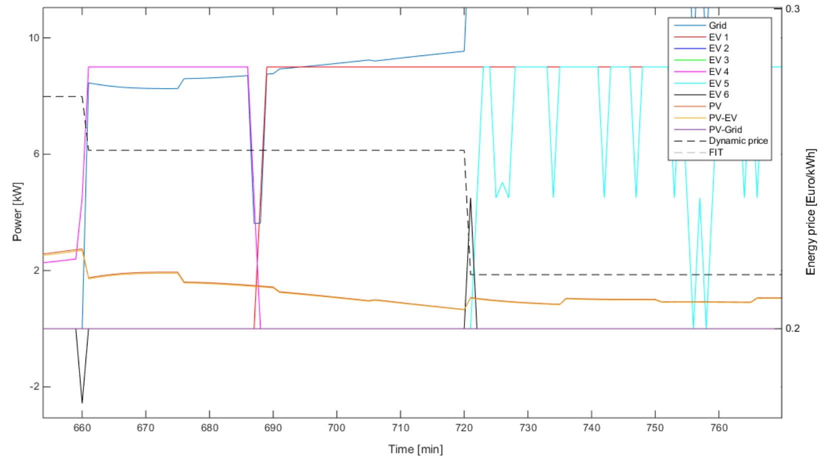

Figure A.129: Power allocation during scenario 6 of 6 EVs with λ_{PV_t} = 0.097 €/kWh, zoom in.

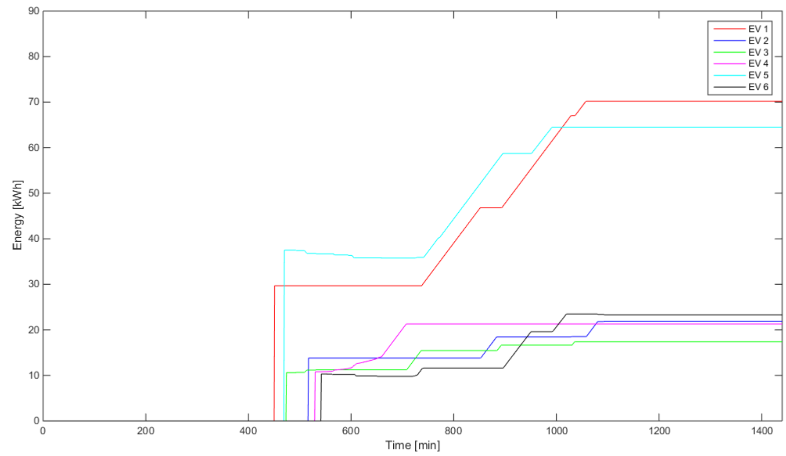

Figure A.130: Energy content during scenario 6 of 6 EVs with λ_{PV_t} = 0 €/kWh.

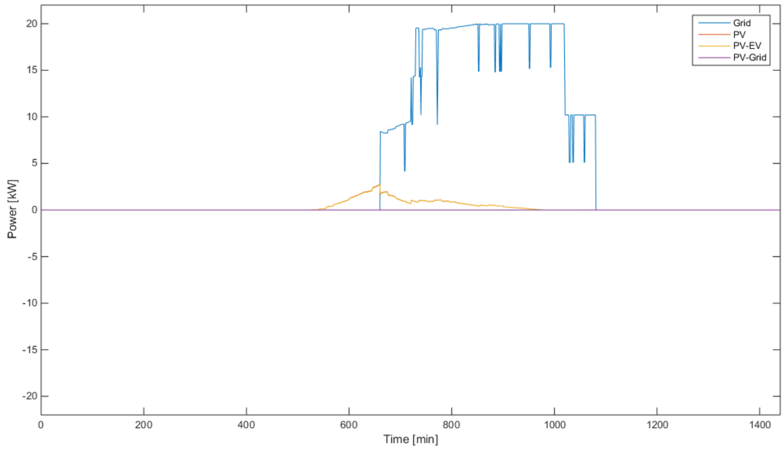

Figure A.131: Power allocation during scenario 6 of 6 EVs with λ_{PV_t} = 0 €/kWh, plotted without EVs or price.

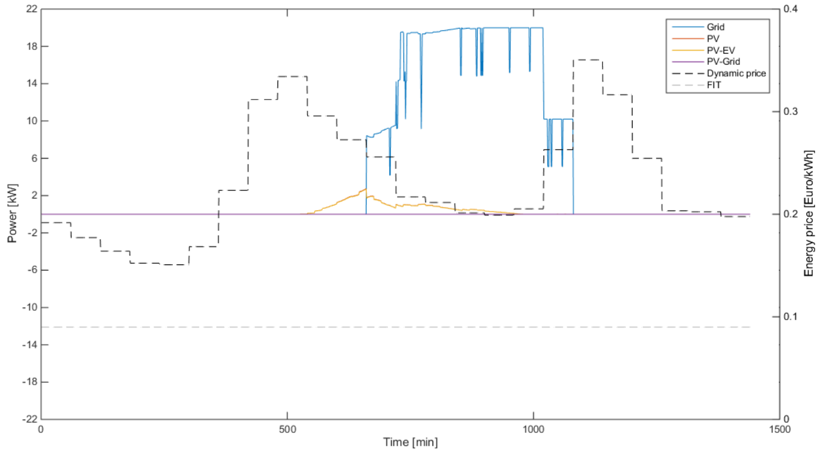

Figure A.132: Power allocation during scenario 6 of 6 EVs with λ_{PV_t} = 0 €/kWh, plotted without EVs.

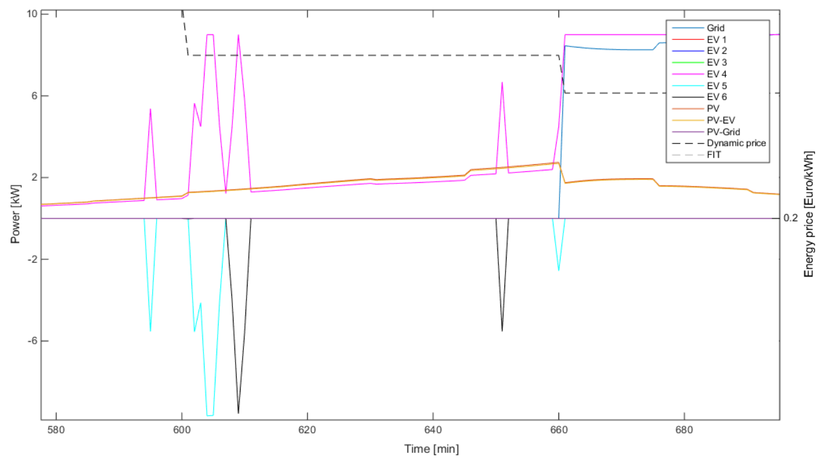

Figure A.133: Power allocation during scenario 6 of 6 EVs with λ_{PV_t} = 0 €/kWh, zoom in.

Minimize energy exchange with the grid

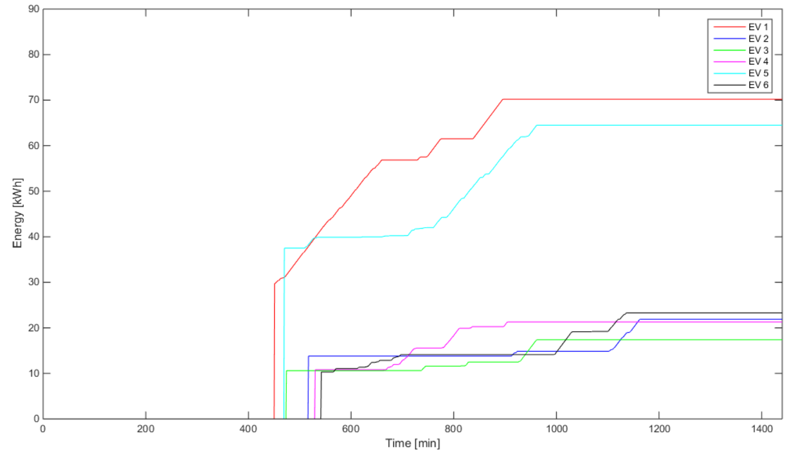

Figure A.134: Energy content of 6 EVs during minimization of energy exchange with grid.

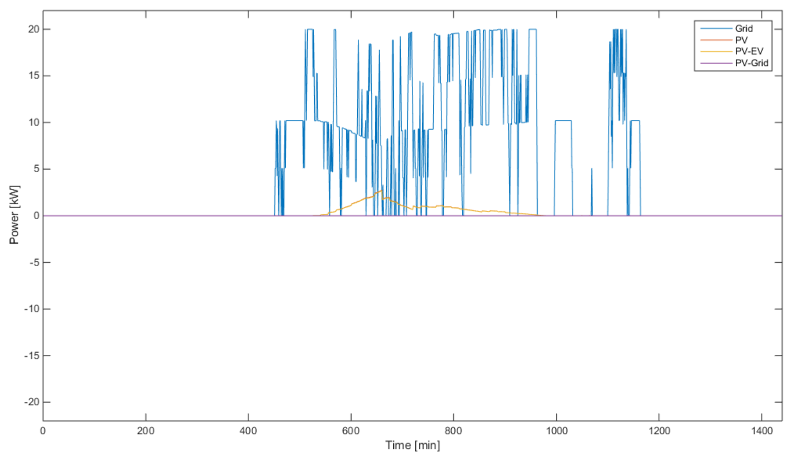

Figure A.135: Power allocation during minimization of energy exchange with grid, plotted without EVs.

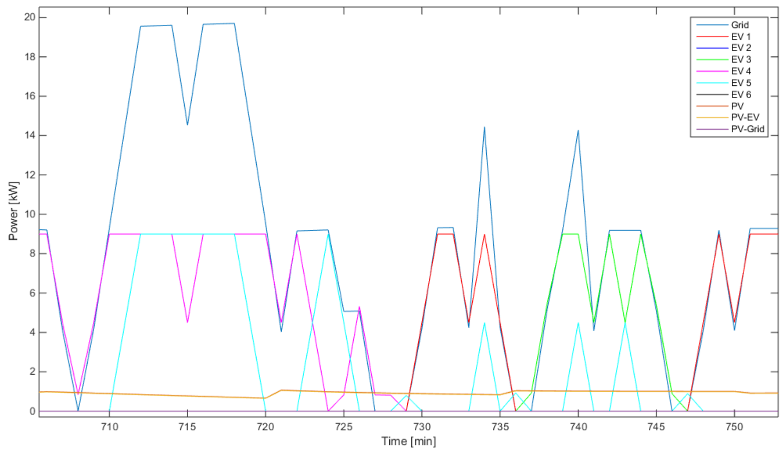

Figure A.136: Power allocation during minimization of energy exchange with grid, zoom in.

A.2.3. Additional case studies - Dynamic grid price and dynamic FIT

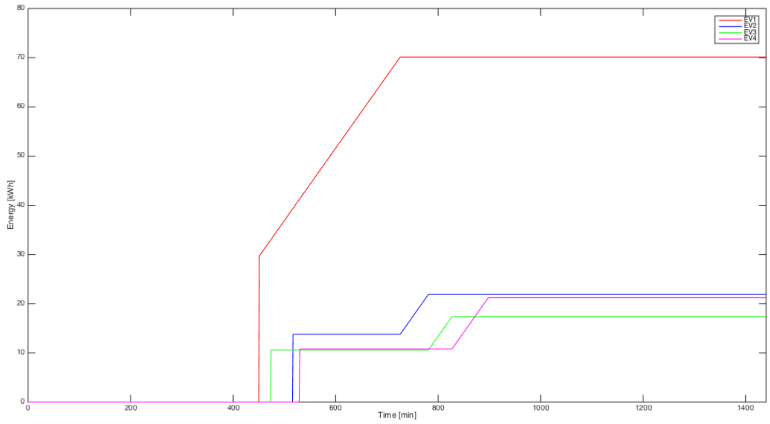

Figure A.137: Energy content with a dynamic FIT, 4 EVs and λ_{PV_t} = 0 €/kWh, uncontrolled charging.

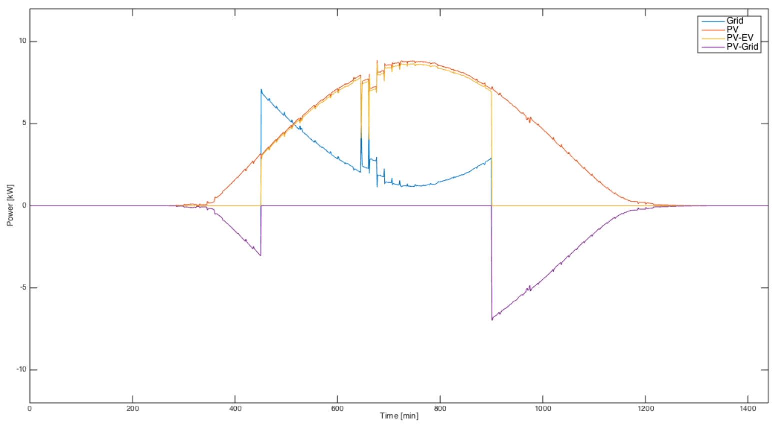

Figure A.138: Power allocation with a dynamic FIT, 4 EVs and λ_{PV_t} = 0 €/kWh, plotted without EVs or price, uncontrolled charging.

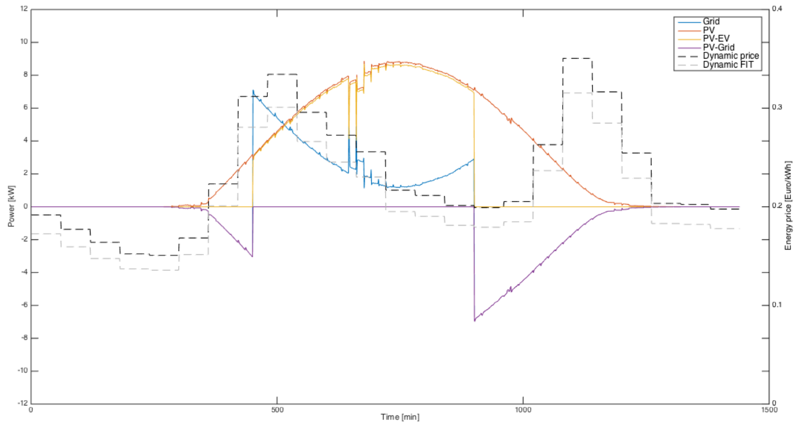

Figure A.139: Power allocation with a dynamic FIT, 4 EVs and λ_{PV_t} = 0 €/kWh, plotted without EVs, uncontrolled charging.

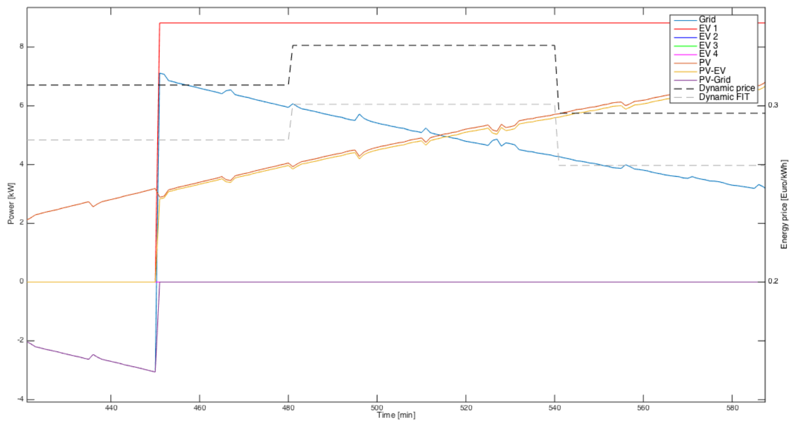

Figure A.140: Power allocation with a dynamic FIT, 4 EVs and λ_{PV_t} = 0 €/kWh, zoom in, uncontrolled charging.

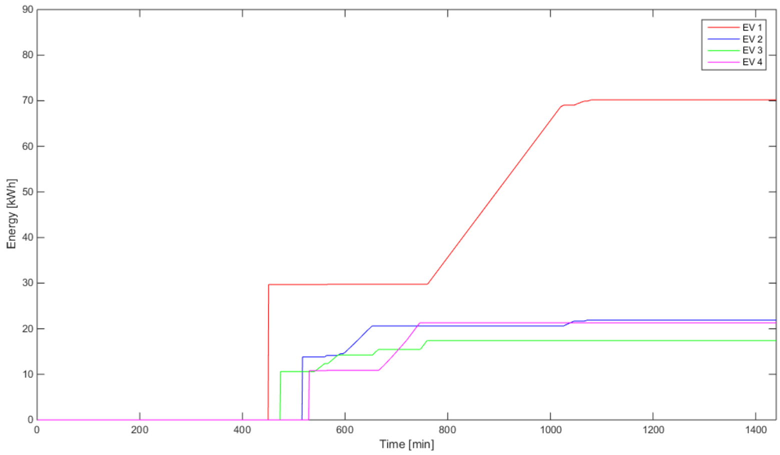

Figure A.141: Energy content with a dynamic FIT, 4 EVs and λ_{PV_t} = 0 €/kWh.

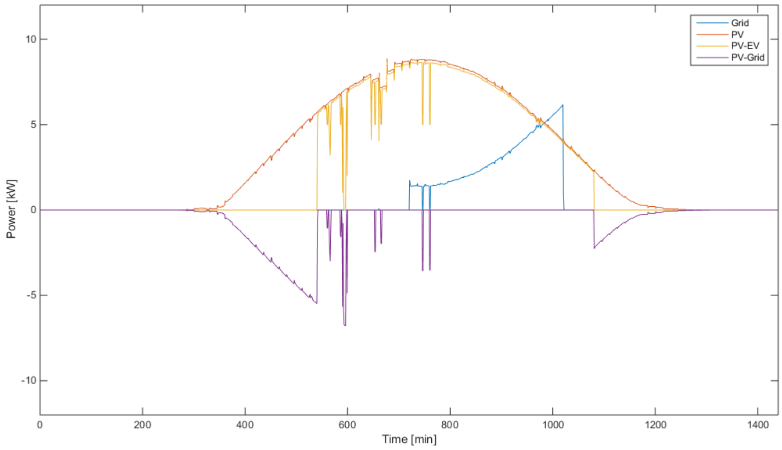

Figure A.142: Power allocation with a dynamic FIT, 4 EVs and λ_{PV_t} = 0 €/kWh, plotted without EVs or price.

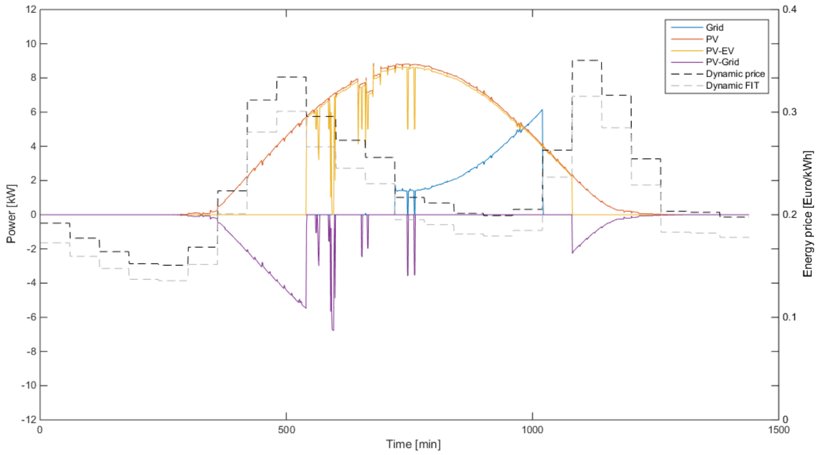

Figure A.143: Power allocation with a dynamic FIT, 4 EVs and λ_{PV_t} = 0 €/kWh, plotted without EVs.

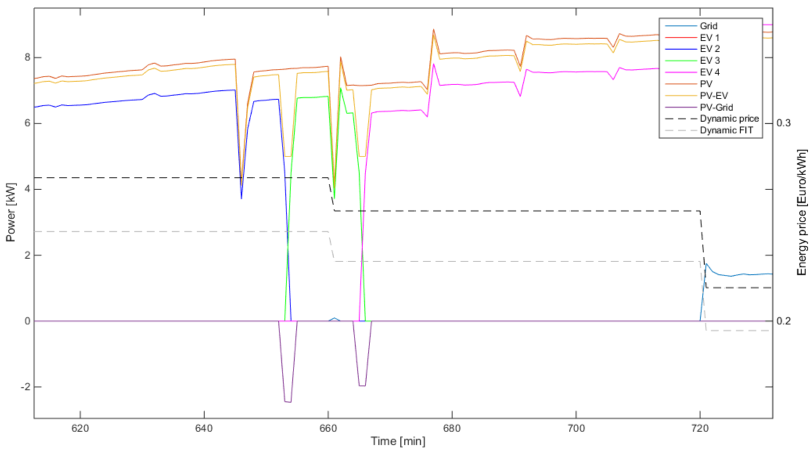

Figure A.144: Power allocation with a dynamic FIT, 4 EVs and λ_{PV_t} = 0 €/kWh, zoom in.

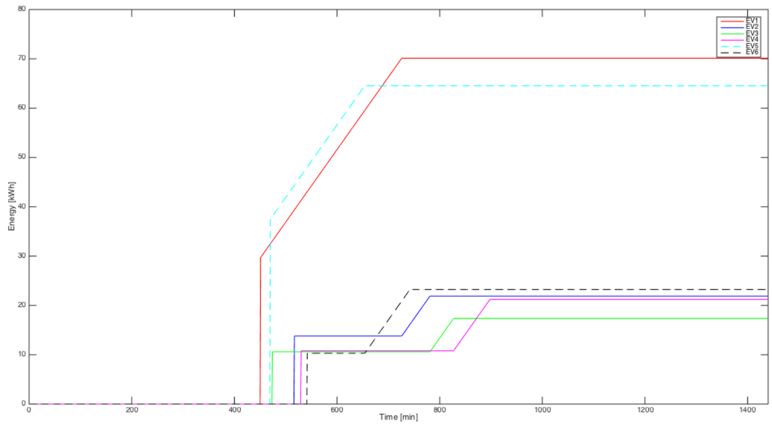

Figure A.145: Energy content with a dynamic FIT, 6 EVs and λ_{PV_t} = 0 €/kWh, uncontrolled charging.

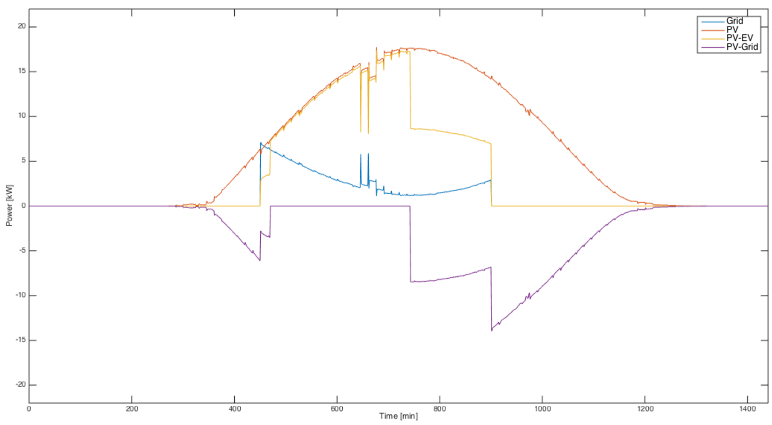

Figure A.146: Power allocation with a dynamic FIT, 6 EVs and λ_{PV_t} = 0 €/kWh, plotted without EVs or price, uncontrolled charging.

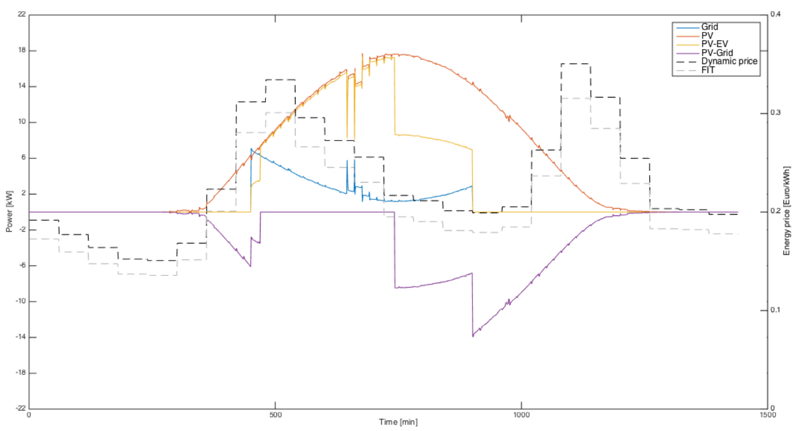

Figure A.147: Power allocation with a dynamic FIT, 6 EVs and λ_{PV_t} = 0 €/kWh, plotted without EVs, uncontrolled charging.

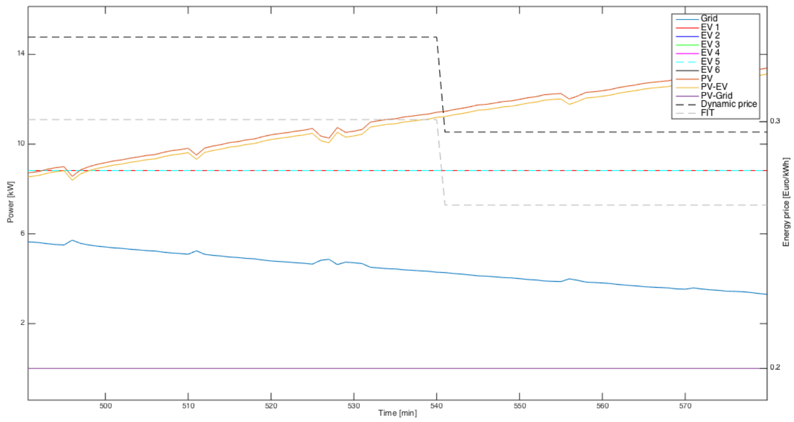

Figure A.148: Power allocation with a dynamic FIT, 6 EVs and λ_{PV_t} = 0 €/kWh, zoom in, uncontrolled charging.

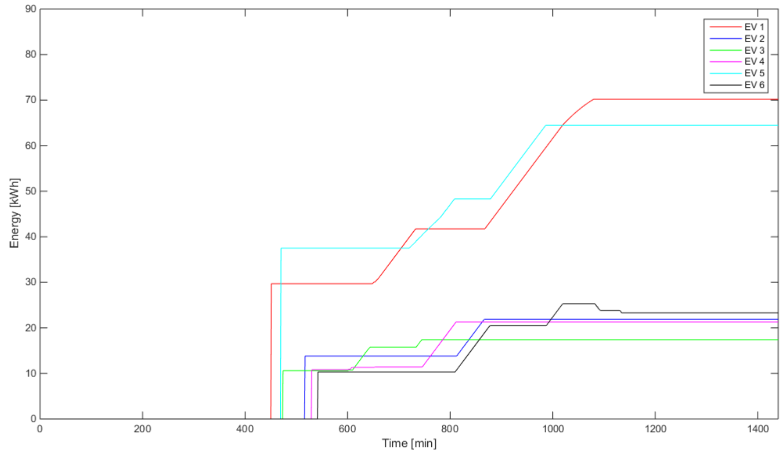

Figure A.149: Energy content with a dynamic FIT, 6 EVs and λ_{PV_t} = 0 €/kWh.

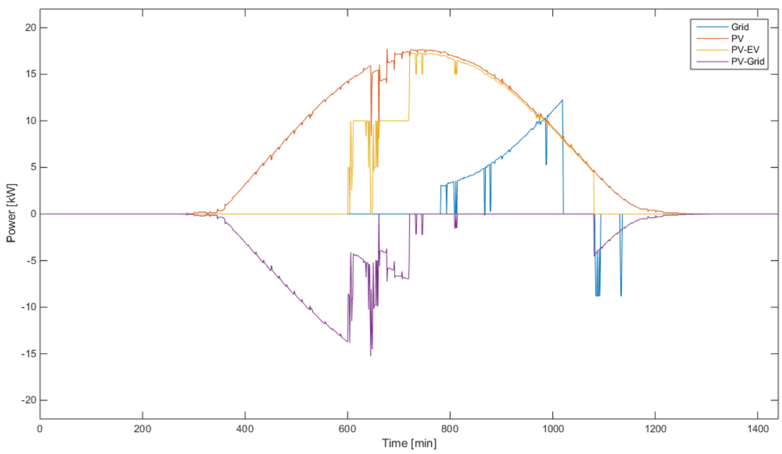

Figure A.150: Power allocation with a dynamic FIT, 6 EVs and λ_{PV_t} = 0 €/kWh, plotted without EVs or price.

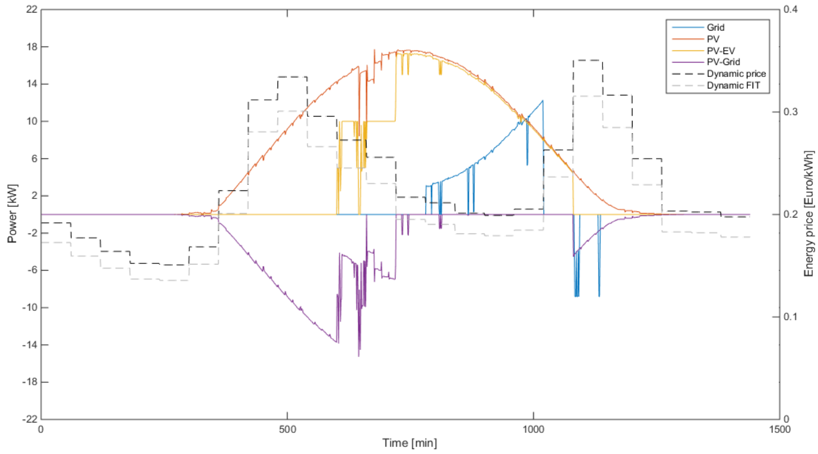

Figure A.151: Power allocation with a dynamic FIT, 6 EVs and λ_{PV_t} = 0 €/kWh, plotted without EVs.

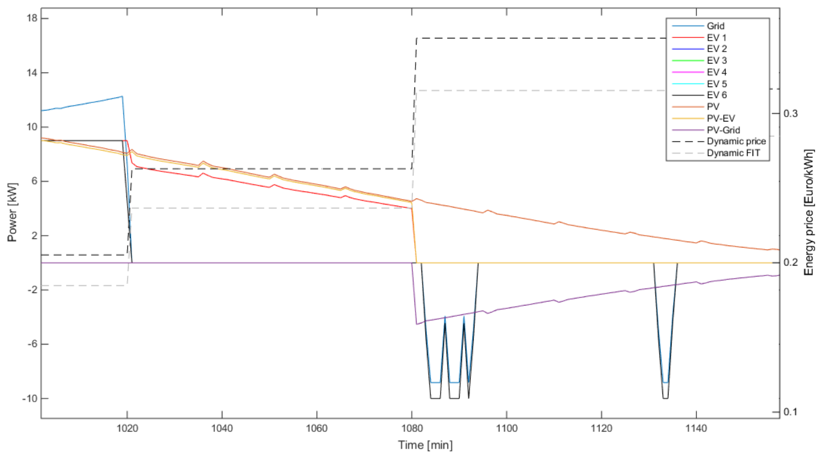

Figure A.152: Power allocation with a dynamic FIT, 6 EVs and λ_{PV_t} = 0 €/kWh, zoom in.

B

IEEE paper